Title
Activation mechanisms of SWI2/SNF2 family ATP-dependent Chromatin Remodeling Enzymes

Author
Gamarra, Nathan Ian

Publication Date
2020

Peer reviewed|Thesis/dissertation

Activation mechanisms of SWI2/SNF2 family ATP-dependent Chromatin Remodeling Enzymes

by
Nathan Gamarra

DISSERTATION
Submitted in partial satisfaction of the requirements for degree of
DOCTOR OF PHILOSOPHY

in

Biochemistry and Molecular Biology

in the

GRADUATE DIVISION
of the
UNIVERSITY OF CALIFORNIA, SAN FRANCISCO

Approved:

DocuSigned by:
EE2E6D32EE3043B...
Geeta Narlikar
Chair

DocuSigned by:
John Gross
DocuSigned by:
David Morgan
AAC13F29657E472...
John Gross
David Morgan

Committee Members

Acknowledgements

I dedicate this thesis to the countless outstanding people who have made it possible and especially the following individuals:

To my advisor, Geeta Narlikar, who has been an important role model personally and professionally and especially for showing me that doing great science goes hand in hand with having fun.

To Alok who has become a close and important friend during my time in the Narlikar Lab.

To my thesis committee members: David Morgan and John Gross. For fun scientific discussions and encouragement along the way.

To my mentor in the lab, Coral, who introduced me to the lab and is a close friend.

To all of my labmates in the Narlikar lab who made every day in the lab fun and intellectually stimulating.

To all of the rotation students that I have mentored in the lab, who gave me valuable opportunities to share in the joy of learning and discovery.

To the Agard lab, and especially Daniel, Klim, Miguel, and Andrew for introducing me to the best of UCSF during my first rotation and for being great friends and colleagues.

To the members of "Seagull Meat" and "Steak Club" and especially its core members: Joe, Daniel, Adam, Andrew, and Miguel. For fun nights dominating at pub trivia and enjoying great cuts of meat.

To my TETRAD classmate friends, and especially members of "the posse": Jonathan, Johnny, Emma, Terri, and Bettie. For many fun Friday nights and a particularly memorable trip to Point Reyes.

To Joseph Lobel, my roommate and close friend during graduate school. For being a great and caring person.

To Johnny Rodriguez, for being a friend and mentor during my early years in science and encouraging me to come to UCSF.

To the Tsai Lab at UC Irvine and especially Jesus Barajas, for introducing me to the joys of protein biochemistry and molecular structure.

To Stanford biochemistry and the Herschlag laboratory, for a fateful summer that introduced me to molecular mechanism that set me on a course toward this thesis.

To the UC Irvine Minority Sciences Program, and especially Dr. Luis Mota-Bravo and Dr. Marlene de la Cruz. For introducing me to science as a career and supporting me in discovering my passion in life.

To Sarah, my best friend and my partner for 10 years and untold more. For loving me for who I am and supporting me in pursuing my dreams, even if it means moving 400 miles.

To my parents, Monica and Igor, and my brother, Loren. For supporting and encouraging me throughout my life and shaping me into the person I am today. Without them, none of this would be possible.

Acknkowledgement of previously published work

Chapters 2 and 3 were published in the following articles:

N. Gamarra, S.L. Johnson, M.J. Trnka, A.L. Burlingame, G.J. Narlikar, The nucleosomal acidic patch relieves auto-inhibition by the ISWI remodeler SNF2h, ELife. 7 (2018) e35322. https://doi.org/10.7554/elife.35322.

J.P. Armache*, N. Gamarra*, S.L. Johnson, J.D. Leonard, S. Wu, G.J. Narlikar, Y. Cheng, Cryo-EM structures of remodeler-nucleosome intermediates suggest allosteric control through the nucleosome, ELife. 8 (2019) e46057. https://doi.org/10.7554/eLife.46057.

*Contributed equally

Activation mechanisms of SWI2/SNF2 family ATP-dependent Chromatin Remodeling Enzymes

by

Nathan Gamarra

Abstract

Eukaryotic genomes are packaged into chromatin: a highly heterogeneous structure composed of nucleic acids and proteins. This packaging controls access to DNA sequences and, as a result plays a critical role in nearly all genomic processes. The primary molecular structure of chromatin is the nucleosome: ~147 bp of DNA wrapped around a core of histone proteins. Both the location and status of nucleosomes in the genome are critical for the proper packaging of chromatin. As a result, cells have evolved several sophisticated molecular machines to disrupt or modify nucleosomes to achieve specific packaging states. A critical member of these machines are the SWI2/SNF2 superfamily of ATP-dependent chromatin remodeling enzymes, which are DNA translocases that harness the energy of ATP hydrolysis to physically disrupt nucleosomes. Because of their central role in control nucleosome structure throughout the genome, remodelers play roles in virtually all DNA-dependent process, but the precise mechanisms of how remodelers disrupt nucleosomes and how this disruption is coupled to other molecular events remains very poorly understood. In this thesis we focus on understanding the remodeling mechanisms of two subfamilies of SWI2/SNF2 remodelers that slide nucleosomes: INO80 and ISWI. To understand how these and other SWI2/SNF2 ATP-dependent remodelers might cooperate with nuclear machinery to enable biological

processes, we first review our broad understanding of remodeling mechanism as it compares to another molecular motor that disrupts nucleosomes: RNA polymerase. We then speculate on how these two distinct families cooperate to accomplish transcription on chromatin templates. After this, we set out to uncover elements of nucleosome that control remodeler activity and identify a conserved surface of the nucleosome known as the acidic patch that is required to activate both ISWI and INO80 family remodelers. Using a combination of biochemical and biophysical assays, we show that this surface activates remodeling by these two families after they bind the nucleosome. For the ISWI remodeler SNF2h, the acidic patch activates remodeling by serving as a landing pad for the binding of autoinhibitory domains while INO80 uses a separate mechanism. We then solve the near-atomic CryoEM structure of SNF2h bound to the nucleosome. Unexpectedly, we find that SNF2h binding in an activated state asymmetrically distorts the histone core of the nucleosome and that this may be important in regulating the activity of the enzyme. Finally, we test the hypothesis that by measuring remodeling activity of nucleosomes with site-specific restraints in the histone core. We find that specifically restraining histone dynamics in locations across all 4 histone proteins inhibits SNF2h-mediated nucleosome sliding. Taken together, these results suggest that remodelers rely on the structure and dynamics of both the DNA and protein components of the nucleosome to accomplish their activities.

Table of Contents

List of Figures

List of Tables

Chapter 1: Introduction

Abstract

Packaging of the eukaryotic genome into chromatin places fundamental physical constraints on transcription. Clarifying how transcription operates within these constraints is essential to understand how eukaryotic gene expression programs are established and maintained. Here we review what is known about the mechanisms of transcription on chromatin templates. Current models indicate that transcription through chromatin is accomplished by the combination of an inherent nucleosome disrupting activity of RNA polymerase and the action of ATP-dependent chromatin remodeling motors. Collaboration between these two types of molecular motors is proposed to occur at all stages of transcription through diverse mechanisms. Further investigation of how these two motors combine their basic activities is essential to clarify the interdependent relationship between genome structure and transcription.

Introduction

Elucidating the mechanisms of eukaryotic transcription is a major pursuit with deep implications for understanding the regulation of cellular states, development, and disease. Transcription in eukaryotes occurs in the context of chromatin: the crowded and highly regulated structures that package DNA. The fundamental unit of chromatin is the nucleosome: a highly stable structure, which wraps 145-147 bp of DNA around an octamer of histone proteins[1,2]. Because of the tight DNA wrapping and high stability of nucleosomes, chromatin presents a major barrier to transcription by RNA polymerases (Pols)[3]. Indeed, transcription by bacterial RNA polymerase and eukaryotic RNA Pol II is greatly inhibited on nucleosomal templates in vitro at physiological salt concentrations[4,5]. Furthermore, several factors which directly reshape chromatin

structure, including ATP-dependent chromatin remodeling enzymes, also regulate transcription in vitro and in vivo[6,7]. These findings have shaped a view of nucleosomes as generic repressors of transcription, with their regulated disruption enabling transcription.

However, several findings challenge this simple view of the role of nucleosomes and more generally, chromatin structure in transcription. In contrast to Pol II, Pol III and bacteriophage SP6 Pols are only modestly inhibited on nucleosome-containing templates at physiological salt[8,9]. Furthermore, transcription by these polymerases does not necessarily involve nucleosome eviction [8,9]. These observations suggest that transcription need not be incompatible with the presence of nucleosomes. Additionally, at slightly higher salt concentrations, Pol II efficiently transcribes through nucleosomes with only the loss of a single H2A/H2B dimer[4]. However, some sub-nucleosome particles, which physically occlude less DNA, inhibit transcription when compared to a complete nucleosome[10]. Finally, it has been shown that transcriptionally silenced regions can be accessible to digestion by nucleases and further that nucleosome plasticity promotes formation of transcriptionally repressed heterochromatin [11,12]. Together these results shape a more nuanced view of the role of chromatin in transcription as a dynamic platform that has coevolved with RNA polymerase and other nuclear proteins to enable complex, tightly regulated gene expression programs.

Key to understanding how transcription operates on chromatin is a thorough understanding of how chromatin structure is reorganized. The SWI2/SNF2 superfamily of ATP-dependent chromatin remodeling enzymes play an essential role in facilitating DNA-based processes (including transcription) by directly reshaping chromatin at the level of individual nucleosomes[6,7]. Like eukaryotic RNA polymerase, remodelers are large,

multi-subunit molecular machines which carry out complex and highly regulated reactions. Compared to RNA polymerase, our understanding of the basic mechanisms of remodelers is less mature. Even less understood is how remodeler activity is coordinated with RNA polymerases and other factors to both faithfully regulate transcription while maintaining genome architecture. However, recent structures of both remodelers and RNA polymerase with nucleosomes, together with prior biochemical data allow for developing models for how these motors collaborate.

In this review we first briefly summarize our current understanding of the core process of transcription and its regulation by elongation factors. We then discuss how this basic process is influenced by the presence of chromatin. Specifically, we focus on how the molecular motor at the heart of transcription, RNA polymerase, may accomplish its activity despite the physical constraints of the nucleosome. This is both due to an inherent chromatin remodeling capability of RNA polymerase and due to its collaboration with other factors including remodelers. We further compare our understanding of the chromatin remodeling activity of RNA polymerase to that of ATP-dependent chromatin remodelers and highlight open questions. Finally, we review how these ATP-dependent chromatin remodelers and RNA polymerases might collaborate.

The nucleosome: beyond a barrier

Although transcription by all three eukaryotic RNA polymerases on chromatin templates is generally inhibited, the nature and strength of this barrier varies. This depends not only on properties of the polymerase and its associated factors but also the structural properties of the nucleosome itself. Since the detailed structure of the canonical nucleosome was solved, a wealth of biophysical studies have shed light on the

core physical properties of the nucleosome, which provide insights into how molecular motors disrupt its structure (Figure 1.1) [13].

The canonical nucleosome is an ~0.2 MDa complex and contains bound to DNA an octamer of histone proteins : 2 copies each of histones H2A, H2B, H3, and H4 (Figure 1.1B). Each histone possesses both a structured domain, which folds cooperatively with the other histones to form a globular core, and unstructured tails[2]. Histones assemble in a stepwise fashion on DNA with an H3/H4 tetramer first depositing followed by two heterodimers of H2A/H2B. DNA wraps around the symmetric globular core ~1.7 times with the unstructured tails projecting out of the core[1]. This wrapping is stabilized by electrostatic contacts between basic residues in the histone core and the DNA phosphodiester backbone. With an average pI of ~11, histone proteins are very basic, facilitating their interaction with DNA [14]. However, a key acidic surface on H2A/H2B, known as the acidic patch, plays an important role as a recognition surface for many chromatin proteins (Figure 1.1A)[15]. Additionally, wrapping of DNA around the nucleosome introduces a single negative supercoil constrained over the length of the nucleosomal DNA[16]. Topological changes in the DNA are important for the stability of nucleosomes as octamer assembly on positively supercoiled DNA templates is disfavored[17]. Correspondingly, subjecting nucleosomal DNA to torsional stress from positive supercoiling reduces nucleosome stability[18].

The nucleosome is thermodynamically a very stable structure. In vitro nucleosomes remain intact under physiological salt concentrations at low micromolar concentrations even when heated to temperatures as high as 65 ºC [19]. At the same time, however, several dynamic transitions can be observed in nucleosomes without the addition of other factors (Figure 1.1C). DNA near the entry/exit (SHL±7) can transiently peel off the surface off the histone octamer exposing the underlying DNA[20,21]. The

histone H2A/H2B dimer can also associate with this unpeeled DNA and undock from the histone core[22]. Electron cryo-microscopy (cryo-EM) structures suggest that such dynamic changes involve intermediates with subtle conformational changes in the histone octamer[23]. Reversible dissociation of the H2A/H2B dimer also occurs and can result in stable sub-nuclesome structures, which wrap less DNA than a full nucleosome[24]. Additionally, it is proposed that the unstructured histone tails may associate with nucleosomal DNA influencing its exposure and dynamics[25,26]. Finally, nucleosomes have also been observed to spontaneously reposition along DNA in a process known as nucleosome sliding[27]. Molecular dynamics simulations suggest that subtle local changes in DNA twist could allow the resetting of histone-DNA contacts around the octamer by ~1bp increments[28]. CryoEM studies combined with histone-histone crosslinking suggest that dynamic rearrangements in histone conformation also facilitate nucleosome sliding[29].

The intrinsic properties of the nucleosome can be modulated by several factors. Sequences that can accommodate the DNA deformations associated with nucleosome formation promote nucleosome stability. Such sequences are often associated with AT dinucleotides at sites where the minor groove of DNA faces the histone octamer and GC dinucleotides at sites where the major groove of DNA faces the histone octamer[30]. This is because AT and GC dinucleotides favor compression of the minor and major grooves respectively, which occurs upon interaction with the histone octamer[31]. In contrast. continuous poly dA:dT tracts seen at some promoters disfavor nucleosome stability[32]. In addition to DNA sequence, post-translational modifications on histones can influence the structure, dynamics, and stability of the nucleosome[33]. Acetylation of histone tails has small effects on DNA unpeeling and histone tail accessibility, while phosphorylation and acetylation of the H3 core may have more substantial

effects[33,34]. Several variant histones also exist and can be incorporated into the nucleosome, which alter nucleosome properties. For example, histone H2Az is an H2A variant that is is particularly enriched at the +1 nucleosome relative to the transcription start site (TSS)[35]. H2Az-containing nucleosomes are less stable to mechanical stress, which may facilitate transcription elongation (discussed further below)[36].

Transcription through nucleosomes

RNA polymerase: a nucleotide dependent chromatin remodeler

In order to understand how RNA polymerase negotiates nucleosome structure, an understanding of the basic structure and mechanism of RNA polymerase is required. Transcription in Eukaryotes is carried out by one of three large (~0.5-1 MDa) multisubunit RNA Polymerases: Pol I, II, and III (Figure 1.2A)[37,38]. Most protein coding genes are transcribed by RNA Pol II. In contrast Pol I and III mostly transcribe noncoding genes, with rRNA being transcribed by Pol I and 5S rRNA, tRNA and other small RNAs being transcribed by PolIII. All three polymerases contain a core of 10 polymerase-specific subunits that share structural homology to prokaryotic multisubunit RNA polymerases[37]. This structure resembles a “claw” with three pincers called the “clamp”, “lobe”, and “jaw” that surround the DNA (Figure 1.2A). The clamp and jaw specifically engage the downstream DNA and feed it into the catalytic center [37]. In addition to these core subunits, the three polymerases also possess a flexible heterodimeric “stalk module” that binds to the core clamp module. The stalk module can make interactions with transcriptional regulators and the nascent RNA. Though considered part of the core polymerase, under certain circumstances the stalk module may need to dissociate during transcription by Pol II with consequences on RNA processing[39,40].

While many structural aspects are shared across all three eukaryotic RNA polymerases there are some key differences. The largest subunit of Pol II contains a repetitive extension at its C-terminus called the CTD, which is phosphorylated or dephosphorylated in specific patterns at different stages of transcription to help recruit transcriptional regulators[41]. Pol I and III utilize specific lobe-binding (LB) modules, which resemble the elongation factor TFIIF[37]. The LB module binds to the core subunits A12.2 in Pol I and C11 in Pol III. These core subunits contain domains that resemble the elongation factor TFIIS that is typically used by po and stimulate elongation using a similar mechanism[42]. Pol III also uniquely contains a heterotrimeric module that assists in transcription initiation[43].

To enable efficient elongation, RNA polymerase must function as a processive molecular motor, efficiently translocating along DNA. Several single-molecule studies have helped uncover the mechanical properties of RNA polymerases. Pol II can transcribe against forces of up to ~6.5 pN while Pol I can withstand somewhat higher forces (~9.5 pN)[44]. Translocation is thought to function through a brownian ratchet mechanism, where the polymerase can freely diffuse one-dimensionally along DNA forward or backward relative to the 3′ end of the nascent RNA (Figure 1.2B)[45]. The irreversible incorporation of a complementary ribonucleotide provides the energy to bias forward translocation. Despite such a mechanism for directionality, pausing and backtracking of the polymerase is frequent and often rate-limiting[45]. Pausing locations are influenced by properties of the DNA sequence being transcribed, the secondary structure of the nascent RNA, and by barriers such as nucleosomes[45,46]. To overcome pausing, elongation factors have evolved that physically associate with polymerase and prevent or resolve backtracked pauses. TFIIS, in particular, resolves backtracking by catalyzing the

endonucleolytic cleavage of the extruded 3′-end of the nascent RNA (Figure 1.2B). This resets the polymerase at the pause location and allows further rounds of elongation.

The unwinding of DNA by RNA polymerases generates torsional stress and is a major source of DNA supercoiling throughout the genome[47]. Transcription generates negative torsional stress upstream, which is expected to stabilize nucleosomes, and positive stress downstream of the polymerase, which is expected to destabilize nucleosomes (Figure 1.2B). If unresolved, torsional stress can hinder both the continued elongation and the stability of the chromatin template[48]. As a result, relief of DNA supercoiling by topoisomerases plays an important role in continued transcription and maintenance of chromatin structure[48,49]. Additionally, stable RNA:DNA hybrids formed between the nascent RNA and the DNA upstream of the polymerase, known as R-loops, may also play a role in absorbing negative torsional stress (Figure 1.2B)[47].

Eukaryotic RNA polymerases have been long appreciated as remodelers of nucleosome structure[50]. Early experiments of transcription on short nucleosome-containing templates suggested two mechanisms of remodeling linked to the type of polymerase transcribing. Transcription by Pol III is only modestly inhibited at physiological salt concentration and transfers intact histone octamers largely in cis upstream of its original position[9]. Like Pol III, nucleosomes also present only a modest barrier to transcription to Pol I under physiological conditions, although nucleosome transfer activity has not yet been reported[51]. In contrast, Pol II is almost completely inhibited at physiological salt concentrations[4]. At slightly higher salt concentrations, which loosens histone DNA-contacts, Pol II is able to more efficiently transcribe through the nucleosome with the dissociation of a single H2A/H2B dimer and without net change in nucleosome position[4,52]. This matches well with in vivo observations that H2A/H2B dimers are more readily exchanged at active genes than H3/H4[53]. Interestingly, E. coli

RNA polymerase transcribes through nucleosomes with very similar properties as Pol II suggesting that the chromatin remodeling properties of multisubunit polymerases may be ancestral to the evolution of nucleosome-based genome organization[5].

More recent experiments suggest that the mechanisms of Pol II and III may fundamentally be more similar than different. On longer DNA templates, Pol II transfers nucleosomes in cis upstream of its original location[54,55]. Apparent nucleosome transfer intermediates with Pol II have been visualized using atomic force microscopy and CryoEM[55,56]. Also, with TFIIF and TFIIS, Pol II more efficiently transcribes through nucleosomes raising the possibility that the TFIIF-like LB module or the TFIIS-like domains in the lobes of Pol I and III are responsible for their higher efficiency[57]. Indeed, deletion of the LB modules or the TFIIS-like domain from Pol I reduces its ability to transcribe through a nucleosome[58]. In light of these observations, it might be more useful to think of the Pol III and Pol II mechanisms as two potential pathways of nucleosome disruption that might be taken by eukaryotic polymerases (Figure 1.2C).

Of the three polymerases, the mechanism of transcription through chromatin is most understood for Pol II. Analyses of the pause sites within the nucleosome provide some clues for how this polymerase remodels nucleosomes[10,59]. At low salt concentrations, Pol II is predominantly paused at the entry side of the nucleosome, suggesting that the tight wrapping of the nucleosome blocks transcription. At higher salt concentrations, Pol II pause sites progressively invade further into the nucleosome up until just before the dyad. Pol II paused prior to the nucleosome dyad exposes entry DNA to cleavage by restriction enzymes[10]. Together, these results suggest that entry of Pol II into the nucleosome is associated with unpeeling of nucleosomal DNA at the entry side. Optical trapping experiments combined with kinetic modeling have supported the notion that RNA polymerase takes advantage of

spontaneous DNA breathing in order to enter and ratchet through the nucleosome[34,54]. Strangely, however, hexasomes lacking a single H2A/H2B dimer at the entry side, and thus unwrapped, are transcribed less-efficiently than full nucleosomes[10]. This suggests that the entry side dimer may be important in establishing intermediates required for passage through the nucleosome. In contrast, hexasomes lacking a dimer on the nucleosome exit side are transcribed more efficiently than nucleosomes and are disassembled by Pol II passage (Figure 1.2D)[10]. Hexasomes, produced by Pol II passage are more efficiently transcribed than nucleosomes, suggesting that Pol II preferentially displaces the exit side dimer[60].

Raising salt concentration or adding elongation factors shifts the location of Pol II pauses further into the nucleosome up until SHL -2/-1 [59]. Beyond this location, few nucleosome-dependent pause sites are observed. This suggests that entering the nucleosome represents a greater barrier than exiting the nucleosomes. Interestingly, Pol II pausing in vivo is enriched right before the nucleosome dyad, further suggesting that specifically transiting through the dyad may be the dominant barrier to elongation[59]. Consistent with this idea, mutating a histone-DNA contact near the dyad both reduces pausing near the dyad and improves transcription efficiency[34,61]. What structural changes are necessary to allow Pol II to pass through the dyad? Since removal of the exit side dimer facilitates passage of Pol II, transiting beyond the dyad may also involve unpeeling of DNA from the exit side. Consistent with this possibility, increasing the length of DNA exiting the nucleosome, which promotes DNA breathing, allows Pol II to progress deeper into the nucleosome[62]. Pol II progression may allosterically loosen histone-DNA contacts ahead of the polymerase. Indeed, Pol II arrested near SHL -2 shows increased restriction site accessibility downstream of the polymerase near SHL+1[10]. Additionally, DNA sequences near SHL+2 appear to influence the ability of polymerase to transit.

Interestingly, sequences that promote pol II passage do not necessarily destabilize nucleosomes. These observations suggest that Pol II passage may require the formation of a specific sequence-dependent intermediate to pass beyond the dyad.

Recent high resolution CryoEM snapshots of Pol II transcribing on nucleosomal templates provide new clarity to earlier biochemical observations[56,63–65]. As Pol II initially approaches the nucleosome, DNA at the entry site unpeels from the octamer consistent with biochemical and biophysical observations[56,63]. In this initial encounter the lobe and clamp regions of the core make additional contacts with nucleosomal DNA at the dyad [63]. Further progression peels more entry side DNA from the surface of the octamer. Once Pol II reaches SHL-1, the lobe region of Pol II makes contact with the H2A/H2B dimer, providing an explanation for the retention of the entry side dimer. Major pause sites internal to the nucleosome are immediately adjacent to histone-DNA contacts, suggesting that breaking these contacts is required for further progression. Pol II translocation also involves rotation of the core structure relative to the nucleosome core. It is unclear if steric constraints imposed by the rotation of Pol II also limits its progression. Some reconstructions of the SHL -1 pause revealed the presence of a foreign DNA wrapping around the unpeeled region of the octamer, which may represent a histone transfer intermediate. Consistent with this, close inspection of the raw Cryo-EM micrographs show evidence for nucleosomes invading this complex[56].

Regulation of RNA polymerase-mediated nucleosome remodeling

Several features of nucleosome structure play an important role in controlling elongation through the nucleosome. As already mentioned, DNA sequence can influence RNA polymerase progression through the nucleosome[59]. Histone tails repress the ability of Pol II to transit through the nucleosome largely through their effect on restricting

DNA breathing[34,66]. Several post translational modifications of the histone proteins play positive roles in Pol II passage. Acetylation of histone tails improves Pol II passage by modestly increasing DNA breathing[34]. Histone modifications may also directly affect core histone-DNA interactions. Poly ADP-ribosylation of histones, which is associated with elongation, appears to globally loosen histone-DNA contacts[67]. Importantly, not all transcription-associated histone modifications play a direct role in the progression of Pol II through the nucleosome, as has been suggested for H3K4 trimethylation[68]. Instead, these may regulate transcription by impacting higher order chromatin organization or the recruitment of additional regulators. The incorporation of certain histone variants can also facilitate passage through the nucleosome (as discussed later).

As mentioned before, elongation factors promote the progression of polymerases through the nucleosome. Pol II-nucleosome structures suggest that transcription intermediates can accommodate association of several elongation factors including NELF, Paf1, and TFIIS[63]. Transcription of nucleosome-containing templates with Pol II and elongation factors both shifts pause sites deeper into the nucleosome and improves overall transit efficiency. CryoEM structures of Pol II-nucleosome intermediates with the elongation factors Spt4/5 and Elf1 has also suggested that elongation factors may directly assist in the stabilization of Pol II intermediates through contacts with the histones. Spt4/5 and Elf1 cooperatively promote Pol II passage both by affecting the orientation of the Pol II clamp on the nucleosome and by direct contacts with the histone proteins[64,69]. Direct histone contacts may be a widespread mechanism of elongation factors on the nucleosome. Indeed, contacts between Paf1 and the H2A/H2B acidic patch have been detected and the elongation factor Spt6 has been shown to have histone chaperone activity[70,71]. Interestingly, despite the higher fraction of complexes stalled at SHL-1, no octamer transfer intermediates were detected in their CryoEM

reconstructions[64]. It is possible that these factors bias elongation through a pathway that does not involve octamer transfer (Figure 1.2C).

In addition to specific elongation factors, general histone chaperones also play a key role in transcription, and particularly the H2A/H2B chaperone FACT (FAcilitates Chromatin Transcription). FACT improves elongation in vitro and its depletion in vivo produces major elongation defects by all three polymerases[51,72]. Including FACT alone with Pol II transcription reactions promotes passage through the nucleosome and the formation of hexasomes[72,73]. However, dissociation of the dimer is not required for FACT function as neither covalent crosslinking of the histone octamer, nor destabilization of the histone dimer-tetramer interface inhibits FACT-dependent stimulation[73]. This has led to a model that FACT assists with Pol II passage mainly by facilitating disruption of nucleosomal DNA. Consistent with this, cryoEM structures combined with Hydrogen-Deuterium exchange experiments suggest that FACT binds to the DNA-binding surface of H2A-H2B, promoting DNA unpeeling[74]. A recent cryoEM structure of FACT bound to a nucleosome with Pol II arrested at -4 shows FACT shifted one SHL downstream from the dyad[69]. As a result, it is possible that FACT interactions with the nucleosome may be highly dynamic and adapt in response to Pol II passage. Interestingly, a kinetic analysis of FACT-assisted elongation has suggested that FACT reduces barriers throughout the nucleosome, but particularly between SHL -5 and SHL+2[73]. FACT has also been implicated in the reassembly of nucleosome structure in the wake of Pol II passage[75]. This reassembly function may be linked to the action of other factors (such as remodelers with nucleosome assembly activity) or elongation-associated histone modifications (such as H2B ubiquitination)[76,77].On a sub-nucleosome, FACT adopts multiple conformations linked to the presence or absence of a second H2A-H2B dimer [74]. This may facilitate the displacement or retention of the dimer during Pol II progression. With Pol II, FACT

makes contact with the entry-side dimer, which may stabilize its retention during Pol II passage[69].

Finally, intrinsic properties of RNA polymerase and the nascent RNA may play an important role in remodeling nucleosome structure. Local changes in DNA topology mediated by RNA polymerase may influence passage through the nucleosome. Consistent with this possibility, DNA nicks within the nucleosome, which relax torsional stress, can both promote and inhibit transcription through the nucleosome depending on their location[78]. With prokaryotic polymerase, nicks between the entry side and SHL-3 inhibit passage, while nicks between SHL-3 and SHL+3 facilitate passage. Nicks near the entry side of the nucleosome likewise inhibit Pol II nucleosome passage[78]. This supports a role for local torsional stress in regulating Pol II passage through the nucleosome. Higher resolution Pol II-nucleosome structures are needed to visualize the detailed changes in DNA topology that accompany Pol II passage. Notably phosphorylation of the CTD does not appear to directly impact chromatin transcription[79]. However, association of factors with the CTD is likely to allosterically influence core polymerase properties (as has been proposed for during termination of transcription)[80]. Adjacent polymerases may also influence nucleosome remodeling properties. Transcription with tandem polymerases improves overall transcription efficiency through the nucleosome[60,81]. This is in part due to the remodeling activity of the leading polymerase but also due to prevention of backtracking of the leading polymerase by the trailing polymerase. Finally, nascent RNA can both positively and negatively impact transcription through the nucleosome through at least two types of mechanisms. Nascent RNA secondary structure can influence polymerase pausing and backtracking [34,46] and R-loops may contribute directly to remodeling of the nucleosome as they are expected to generally destabilize nucleosome structure[82,83].

ATP-dependent chromatin remodelers

Diverse activities mediated by diverse motors

Although able to produce many alterations to nucleosome structure, RNA polymerase is fundamentally limited in its remodeling capabilities. On the mechanistic side, this may reflect fundamental mechanical limitations imposed by the polymerase machinery. However, on the biological side, by being dependent on other factors RNA polymerases open themselves up for many regulatory possibilities. ATP-dependent chromatin remodelers are among the many factors that regulate RNA polymerase action on chromatin. Remodelers range in size from small single subunit motors to large multi-subunit complexes (Figure 1.3A)[6]. They are able to catalyze a wide range of activities including most spontaneous transitions seen with the nucleosome alone (Figure 1.1C). However, remodelers do not necessarily act as "heat", simply lowering the activation barrier to thermally inaccessible states[7]. This is because the irreversibility of ATP-hydrolysis allows structural changes produced by remodelers to be directional. For example, the SWR complex catalyzes the exchange of canonical H2A/H2B dimers with H2Az/H2B dimers but does not catalyze the opposite reaction (Figure 1.3B)[84]. Remodelers are also capable of creating stable non-canonical nucleosome structures not observed spontaneously. SWI/SNF-family remodelers catalyze the formation of stable structures called remosomes which contain an intact histone octamer but wrap ~30bp more DNA than canonical nucleosomes and with overall weaker histone-DNA contacts (Figure 1.3C)[85,86]. Some remodelers can also slide nucleosomes in order to displace DNA-bound proteins or other nucleosomes (Figure 1.3D/E)[87,88]. The wider range of transformations produced by remodelers when compared to RNA polymerase is likely

linked to their fundamental activity of DNA translocation, which, as we discuss below, is a highly flexible means of disrupting nucleosome structure.

Structures and mechanisms of ATP-dependent Chromatin Remodeling Enzymes

Common to all remodelers is the presence of a single subunit containing an ATP-hydrolyzing domain with homology to the yeast protein SNF2 from the SWI/SNF complex. Remodelers are further divided into families based on differences within this subunit[89]. These differences appear to determine the range of reactions catalyzed by the ATPase complexes. For example, complexes containing ISWI-family ATPases appear to only catalyze nucleosome sliding and nucleosome assembly, while SWI/SNF-family ATPase complexes catalyze a diverse range of reactions[7]. The ATPase domain of remodelers has two RecA-like lobes, which contact the phosphodiester backbone of DNA. ATP binding and hydrolysis occurs at the interface between the two lobes. Changes in the relative conformations of the RecA-like lobes driven by the ATPase cycle is proposed to power DNA translocation.

Biochemical and structural studies are highlighting both the commonalities and differences amongst remodelers in how they engage and transform nucleosomes. The ATPase domain of most remodelers associates with nucleosomal DNA at SHL±2 (Figure 1.3F), with the only exception so far being the INO80 complex, which associates at SHL±6. Interestingly, structures of a truncated SNF2 ATPase subunit from the SWI/SNF complex suggest that this protein can associate with the nucleosome at both SHL±2 and SHL±6 suggesting that additional interactions outside of the ATPase domain may determine where the ATPase binds to the nucleosome[90]. From either of these locations, DNA translocation along the phosphodiester backbone appears to power the breaking of histone-DNA contacts required for nucleosome remodeling. This is supported by the fact

that single-stranded DNA gaps at these locations, which prevent translocation along DNA also prevent remodeling[91–94]. Binding of the SWI2/SNF2 ATPase to the phosphodiester backbone of nucleosomal DNA at SHL±2 appears to amplify local deformations in the conformation of the DNA double helix caused by nucleosome formation (Figure 1.3F)[95]. Such effects may exert sufficient torsional stress to locally destabilize histone-DNA contacts. Indeed, on naked DNA several remodelers have been shown to generate negative superhelical torsion[96]. However, it is important to note that remodeling of nucleosomes assembled on non-specifically nicked DNA, which globally relaxes superhelical torsion, is not necessarily inhibited [97,98]. This indicates that large-scale generation of superhelical torsion throughout the nucleosome is not necessarily a core requirement for remodeling.

Despite these core similarities, how translocation by the ATPase domains of remodelers is harnessed to create specific remodeling outcomes is likely to differ substantially and many of the details remain unclear. Nucleosome sliding has been proposed to occur by the propagation of helical twist defects around the nucleosome in a manner similar to what has been proposed for uncatalyzed nucleosome sliding (Figure 1.3F)[28,99]. The resetting of histone-DNA contacts around the nucleosome may only require single translocation events. Indeed, fundamental ~1-2bp increments of translocation can be observed during nucleosome sliding catalyzed by multiple remodelers[100,101]. Larger-scale disruptions of nucleosome structure such as nucleosome disassembly or histone exchange, which by necessity involve more extensive breaking of histone-DNA contacts, are likely to require more units of translocation and additional remodeler-nucleosome contacts to stabilize intermediates. Histone exchange by the SWR complex relies on contacts between its noncatalytic subunit Swc6 and

flanking DNA to enable the loosening of contacts between the exiting H2A-H2B dimer and nucleosomal DNA[102].

Remodelers also rely on dynamics in specific regions of the histone octamer core. The requirement for dynamics has been inferred from the combination of structural studies using techniques such as NMR and cryo-EM and from functional studies where restraining histone dynamics using site-specific disulfide crosslinking inhibits remodeling activity[103–105]. However, the histone dynamics required for remodeling appear to vary considerably between different remodelers. For example, H3-H4 crosslinking inhibits remodeling by the ACF complex but does not affect remodeling by the INO80 complex[103]. The use of octamer dynamics by remodelers may be a major distinguishing feature of their remodeling mechanisms when compared to RNA polymerases. So far, restraining histone octamer dynamics by crosslinking only appears to modestly, if at all, affect polymerase passage through the nucleosome[51,73].

Outside of the core SNF2-related catalytic subunit, remodelers are frequently associated with several accessory proteins, which differ substantially between families (Figure 1.3A). These proteins often play integral roles in promoting or regulating the core activity of remodelers[106]. In the case of the SWI/SNF family BAF complex, several alternative complexes exist with different compositions each having different roles in promoting tissue specific gene expression[107]. Some subunits may also have additional catalytic activities including histone modifying or ATPase activity. For example, in addition to a remodeling ATPase, the NURD complex contains a histone deacetylase subunit and members of the INO80 family of remodelers contain the hetero-hexameric AAA+ ATPase Rvb1/2[108,109]. While the histone deacetylase subunit of NURD is thought to act in concert with the remodeling ATPase to de-acetylate nucleosomes, the Rvb1/Rvb2 ATPase in the INO80 complexes is thought to be involved in complex

assembly[110]. It is also possible that accessory subunits dynamically associate with the complex during a remodeling reaction. Some evidence for this possibility is suggested by ChIP-exo data, which has captured subcomplexes of INO80-family remodelers on chromatin[111].

Principles of regulation

The process of remodeling can be divided into three stages in a manner analogous to transcriptional regulation. Like RNA polymerase, to initiate their activity remodelers must first be recruited to their relevant genomic locations at the proper time. After finding its target nucleosome, remodelers must commit to their remodeling activity. In the case of some activities, such as nucleosome sliding, this not only involves the decision to activate remodeling but also a commitment to a particular direction for the activity. Finally, after disrupting nucleosome structure, remodelers must have a means to sense the formation of an appropriate product and terminate further activity.

How remodelers achieve genomic specificity is unclear but is likely to involve the cooperative recognition of several chromatin features in addition to recruitment to specific genomic sequences by sequence specific DNA binding factors. In some cases this may be achieved directly through subunits of the remodeling complex. Many remodelers contain histone reader domains in either the ATPase or accessory subunits which can recruit the remodeler to nucleosomes with a specific post translational modification state. For example, the SWR complex's accessory protein Bdf1 contains a bromodomain which recruits it to acetylated nucleosomes[112,113]. However, targeting of remodelers to specific loci may often depend on its interaction with other factors that provide specificity. Remodelers can directly associate with sequence-specific transcription factors or other reader-domain proteins (like HP1) to execute their function.

Recruitment can not only play an important role in selecting the appropriate nucleosome to disrupt, but also the directionality of activity. For example, transcription factor binding to the ISW2 complex helps set the direction of nucleosome sliding by this complex[114].

After associating with their target nucleosomes, remodelers must dynamically integrate information about their substrate nucleosome and chromatin context to decide whether to proceed with remodeling. To accomplish this, a common theme across remodelers is regulation through auto-inhibition. In the absence of their substrate, the ATPase subunit is held in an inactive conformation often through the interactions with specific autoinhibitory domains (Figure 1.3G)[115–117]. Binding to the appropriate nucleosome substrate can disrupt this inactive conformation. However, in some cases, even after binding the nucleosome, autoinhibitory domains may still prevent either ATP hydrolysis or the coupling of hydrolysis to remodeling[118,119]. Overcoming such auto-inhibition may require a post-binding conformational change that enables contacts between the complex and specific substrate cues (Figure 1.3G). Common stimulatory substrate cues include accessible extranucleosomal DNA, the N-terminal tail of histone H4, and the H2A-H2B acidic patch. Sensing of these cues can be accomplished by direct interaction of the ATPase subunit with each cue, as appears to be the case for ISWI-family remodelers. Alternatively, accessory subunits may also bind to these motifs and allosterically activate the ATPase domain. For example, the non-catalytic SMARCB1 subunit of BAF complexes contacts the acidic patch in order to activate remodeling[120]. Modification of substrate cues provides a simple but potent means to control remodeler activity both positively and negatively. For example, post translational modification of the acidic patch modestly reduces remodeling by ISWI-family remodelers[121].

Another interesting means of regulation is the association of multiple remodeling complexes to the same nucleosome. Because the nucleosome is two-fold

pseudosymmetric, two complexes can in principle engage the same superhelical location on opposite faces of the nucleosome. For example, processive nucleosome sliding by the ACF complex is promoted by the cooperative association of two active complexes to a single nucleosome[122]. It has been proposed that a coordinated conformational switch prevents a futile tug of war between the two motors on the nucleosome[123]. Coordinating this switch may be achieved in part through asymmetric allosteric conformational changes in the octamer core[124]. This behavior may not be unique to ACF as the INO80 complex has also been reported to cooperatively associate with and remodel single nucleosomes. It remains unclear what would result if two different remodeling complexes were to attempt to remodel the same nucleosome. Interestingly, the location of several different remodeling families frequently overlap in ChIP-seq datasets, though further study will be needed to assess actual co-occupancy[125].

The changes that specify termination of remodeling activity are very poorly understood. Loss of substrate cues directly associated with the remodeling reaction catalyzed might provide a means to directly communicate termination of remodeling. For example, H2Az-only containing nucleosomes do not stimulate ATP hydrolysis by SWR, likely because they lack a substrate cue unique to the L2 loop of canonical H2A which is recognized by the Swc5 subunit[126]. Alternatively, substrate cues may emerge after remodeling which inhibit further remodeling activity. Some ISWI-family remodelers have been demonstrated to bind adjacent nucleosomes in addition to its substrate nucleosome, which may control its activity[127,128]. Competition between remodelers and other proteins for binding substrate cues may also provide an important means for terminating remodeling. For example, the H2A/H2B acidic patch, which is a common substrate cue for remodelers, is both bound by many non-remodeler proteins and by nucleosomes in trans via the H4 N terminal tail[15].

Interface of remodelers and RNA polymerases at different stages of transcription

Regulation of promoter chromatin architecture

Chromatin remodelers play an integral role in creation of promoter chromatin architecture by all three polymerases. This involves first the creation of a nucleosome depleted region (NDR) where sequence-specific and general transcription factors can assemble followed by the precise positioning of nucleosomes upstream and downstream of the transcription start site. Creation of an NDR appears to be an obligate feature of transcription initiation, since binding of TBP to DNA, which is required for all three polymerases to initiate, is greatly inhibited in the presence of nucleosomes[129,130]. However, chromatin architecture at the promoter plays additional key roles in coordinating events during initiation. Precise positioning of both the +1 and -1 nucleosome has been implicated in the cooperative assembly of the pre-initiation complex for Pol II and III-dependent genes [131–134]. This positioning of the +1 nucleosome may also be particularly important for transcription start site choice at some Pol II-dependent genes[134].

Our best understanding of how nucleosome-positioning is achieved at promoters comes from several elegant studies of *S. cerevisiae* Pol II promoter architecture (Figure 1.4A). Using a library of genomic DNA, purified histones, remodelers, and/or transcription factors, nucleosome positioning at Pol II promoters has been faithfully reconstituted[135]. Careful analysis of positioning experiments with different combinations of remodelers has delineated at least two general pathways through which remodelers cooperate to create promoter architecture (Figure 1.4A). One pathway relies on the binding of sequence-specific transcription factors to create a barrier against which the +1 and -1 nucleosomes

are positioned by the ISW2 complex. The second pathway relies on solely the ability of the INO80 complex to sense local DNA topology associated with promoter-proximal sequences to position the +1 and -1 nucleosomes[135,136]. Changes in DNA topology associated with RNA polymerase loading may cooperate with remodelers in further refining promoter chromatin architecture. Interestingly, neither histone modifications nor histone tails appear to substantially influence +1 posiitioning by INO80 as native, recombinant, and tailless histones are roughly equally sufficient for +1 positioning[136].

The +1 nucleosome is also associated with an enrichment in the histone variant H2Az, particularly for poised or inducible genes[35,137]. This is thought to reduce the initial barrier to Pol II immediately after promoter escape. In cerevisiae, the SWR complex is recruited to the +1 nucleosome in a manner that depends heavily on its Swc2 subunit binding promoter-proximal DNA and to a lesser extent on Bdf1 binding histone acetylation (Figure 1.4B)[111,113,138]. It is currently unclear whether these features are sufficient to directly recruit SWR to its substrate nucleosomes, or whether SWR depends on other factors for its recruitment. The opposite exchange reaction has been proposed to be catalyzed by INO80, but this activity remains debated[94,139–141]. Recent live-cell imaging experiments suggest instead that Pol II transcription directly displaces H2Az[141]. Interestingly, H2Az is enriched on the promoter distal side of the +1 nucleosome, which may facilitate its displacement by polymerase[142].

After initiation, remodelers may also play a key direct role in recycling transcription factors bound at the promoters. SWI/SNF-family remodelers have been shown to displace nucleosomes and transcription factors from DNA by sliding nucleosomes through them. In *S. cerevisiae* wide NDRs are associated with a RSC-bound “fragile” nucleosome, which may be used to displace nucleosomes and recycle transcription factors (Figure 1.4C)[143]. Consistent with a role in transcription factor displacement, transient depletion

of a subunit of the RSC complex increases the dwell time on chromatin by the Ace1p transcription factor at the CUP1 promoter[144].

Remodelers also play a key role in preventing transcription initiation by occluding NDRs. When recruited by specific transcription factors, the remodeler ISW2 in cerevisiae occludes NDRs by repositioning promoter nucleosomes [145,146]. In mammals, Pol I transcription is repressed by positioning of promoter nucleosomes over the NDR via the NoRC complex[147]. Additionally, remodelers play a role in preventing cryptic transcription. Deletion of several remodelers involved in even nucleosome spacing downstream of the TSS leads to the widespread upregulation of cryptic antisense transcripts[148–150]. Widespread nucleosome spacing over ORFs may be a general mechanism to repress cryptic promoters, which if allowed to proceed into active gene bodies can lead to transcription conflicts and inhibition of elongation.

Elongation

After initiation, remodelers continue to play a key role in regulating the progression of polymerases through the gene body (Figure 1.5). Remodelers can, in principle, facilitate elongation by disassembling nucleosomes ahead of the polymerase completely or to hexasomes (Figure 1.5A). In vitro, inclusion of RSC and the H2A/H2B chaperone NAP1 in transcription reactions promotes the formation of a hexasome which improves transcription efficiency by Pol II[151]. Incorporation of histone variants that present a lower barrier to polymerase, like H2Az or the mammalian-specific variant H2A.B, has also been suggested to improve elongation (Figure 1.4C)[152]. Remodelers can also reposition nucleosomes off of sequences that present a high energetic barrier to nucleosomal passage (Figure 1.5B). Repositioning of nucleosomes off of a high barrier sequence by ISW2 in vitro has been demonstrated to improve elongation efficiency[153]. Finally,

remodelers may create stable conformational rearrangements in the nucleosome that facilitate Pol II passage (Figure 1.5C). The remosome produced by RSC could represent one such rearrangement[85,86]. Interestingly, RSC has recently been shown to not only be associated with promoter nucleosomes, but also with nucleosomes within the bodies of highly transcribed genes[154].

Alternatively, remodelers may facilitate transcription elongation by directly acting on the elongating Pol II-nucleosome complex (Figure 1.5D). CHD1 is a single-subunit chromatin remodeler that plays a major role in promoting elongation[69,155,156]. CHD1 possess a DNA-Binding Domain (DBD) which engages extranucleosomal DNA and sets the directionality of nucleosome sliding and an ATPase domain that engages at SHL+2[157]. While nucleosome sliding could account for its role in elongation, we propose that CHD1 may also more directly assist in the disruption of nucleosome structure as Pol II transits the nucleosome. Biochemical data has suggested that CHD1 engages extranucleosomal DNA beyond SHL+7 to direct the sliding reaction[157]. However, Cryo-EM and biochemical data have revealed that CHD1 can also engage extranucleosomal DNA near SHL -7 with its ATPase domain still bound at SHL+2[158–160]. In this conformation, the DBD unpeels DNA at SHL-7 from the octamer surface[159–161]. This stable unpeeling may facilitate the entry of Pol II into the nucleosome. Pol II passage through the dyad requires disruption of DNA near SHL+2 which could be enabled by CHD1's ATPase domain. As Pol II progresses through the nucleosome, it may displace the DBD from SHL-7, allowing interactions at SHL+7. Consistent with this, a structure with CHD1 bound to a Pol-II transcribed nucleosome arrested at SHL-4.5 suggest the DBD undocks from SHL-7 as Pol II enters the nucleosome [69]. Unlike many remodelers, CHD1 does not depend on the H2A/H2B acidic patch to activate remodeling, which could allow it to cooperate with Paf1 or FACT in facilitating Pol II passage[162]. Interestingly CHD1

can form a complex with both FACT and Paf1 and deletion of CHD1 suppresses FACT phenotypes[155,156,163]. Whether CHD1 can remain associated with the nucleosome during Pol II passage is not fully understood. Recent cryo-EM structures of Pol II-nucleosome complexes suggest that binding of CHD1 and FACT to a transcribed nucleosome is mutually exclusive[69]. However, additional conformational rearrangements in the remodeler not detected in the captured states and/or contacts with elongation factors could allow CHD1 to remain associated with the nucleosome during Pol II passage.

Finally, remodelers may also facilitate elongation by treating elongating polymerase as a substrate. The protein CSB (Cockayne Syndrome B or Rad26 in *S. cerevisiae*) possesses nucleosome sliding and disassembly activity but can also directly associate with RNA polymerase[164,165]. Recently it was shown that CSB stimulates transcription in an ATP-dependent manner that is separate from nucleosome sliding[166]. CSB accomplishes this by associating with DNA at the transcription bubble and the DNA immediately upstream of the polymerase and preventing backtracking. CSB activity promotes progression of Pol II through the nucleosome with either nucleosome survival or complete disassembly (Figure 1.5E). It is unclear whether this is a mechanism unique to CSB or whether other remodelers could also treat RNA polymerase as a substrate.

Transcriptional termination

Remodelers also play important roles in transcription termination by Pols I and II[167–169]. One general theme is the creation of accessible sites for termination factors to assemble at the 3′ end of ORFs. Near Pol II termination sites at coding genes is a nucleosome depleted region surrounded by an evenly spaced array of nucleosomes [132,170]. The 3′ NDR may allow the cleavage and polyadenylation factor (CPF) to access

and process the nascent RNA. Formation of the NDR may be due in part to DNA supercoiling ahead of the elongating polymerase[171]. However, in *S. cerevisiae* the NDR also relies on the action of RSC, ISW1, and CHD1 and depletion of these remodelers can also cause termination defects[169]. How remodelers are recruited to these sites is unclear but direct interactions between remodelers and CPF, as has been reported for the SWI/SNF complex, could be responsible[172].

Following termination sites, slowing elongating polymerase plays a key role in the process of termination as some mechanisms of Pol I and Pol II disassembly rely on kinetic competition between factors traveling along the nascent RNA transcript and further elongation[80]. For Pol I and Pol II coding transcription, termination can be achieved by the 5′-3′ exonuclease Rat1 which degrades the elongating transcript and, upon reaching the polymerase, displaces it from DNA. In contrast, Pol II noncoding transcripts are released by the RNA helicase Sen1. which translocates along the nascent transcript until it reaches and dissociates the elongating polymerase. Nucleosomes positioned by remodelers near the 3′ NFR may function as a roadblock to slow elongating polymerase to facilitate termination. Mutating histone-DNA contacts at the entry/exit sites of nucleosomes in *S. cerevisiae* results in widespread transcriptional termination defects and changes in pol II occupancy consistent with an increased elongation rate[173].

In addition to these regulated termination pathways, there also exist pathways for clearing polymerase when it is terminally stalled by various roadblocks within the gene body. This is particularly relevant when the polymerase encounters DNA lesions that cannot be traversed. In this case, the stalled polymerase is polyubiquitinated, displaced, and degraded by the proteasome[174]. INO80 has been shown to associate with the AAA+ ATPase Cdc48 and assist in the displacement of stalled Pol II in a manner that depends on INO80's ATPase activity and ubiquitination of Pol II[175]. However, it is

unclear whether INO80 assists in displacement through its nucleosome remodeling activity or through an undiscovered mechanism.

Outlook

Our understanding of the mechanisms of chromatin remodeling by both RNA polymerases and specialized ATP-dependent remodelers has advanced considerably in recent years. While new insights will continue to emerge from studying both of these motors' actions on chromatin in isolation, a major gap is how much the mechanism of remodeling by these two classes of motors is altered when both are associated with the same nucleosome. How and under what conditions do remodelers and polymerase directly synergize to disrupt chromatin structure? When their activities conflict, whose activity prevails and what determines who results as the "winner?" The continuing application of single molecule methodologies could be very useful as a means to assess what happens when these motors meet on a single nucleosome. R-loop's role in regulating chromatin structure and remodelers is also a rich area of investigation. Interestingly, it was recently suggested that INO80 associates with and promotes the resolution of R-loops in cancer cells[176].

Chromatin-based regulation of transcription also occurs on larger scales beyond that of the single nucleosomes scale. Although chromatin was initially proposed to form a regular higher-order structure, multiple lines of evidence have converged on a view that chromatin structure is far more heterogeneous than initially anticipated[177]. In particular, the finding that nucleosome arrays can form liquid-like condensates underscores the complex and dynamic nature of higher-levels of chromatin organization[178]. While we are beginning to appreciate the myriad ways such condensates can influence genome compartmentalization, the environments within condensates may also dramatically

influence both the properties and mechanisms of nuclear motors [179]. Further clarifying the range of packaging states adopted by chromatin, and clarifying which of their physico-chemical properties are compatible with transcription and chromatin remodeling are essential areas of investigation. Interestingly, the RNA polymerase CTD has been demonstrated to form liquid-like condensates, which may regulate Pol II's localization or activity [180]. Integrating insights from these disparate approaches holds immense promise toward our comprehensive understanding of the relationship between genome structure and transcription.

Figures

FIGURE 1

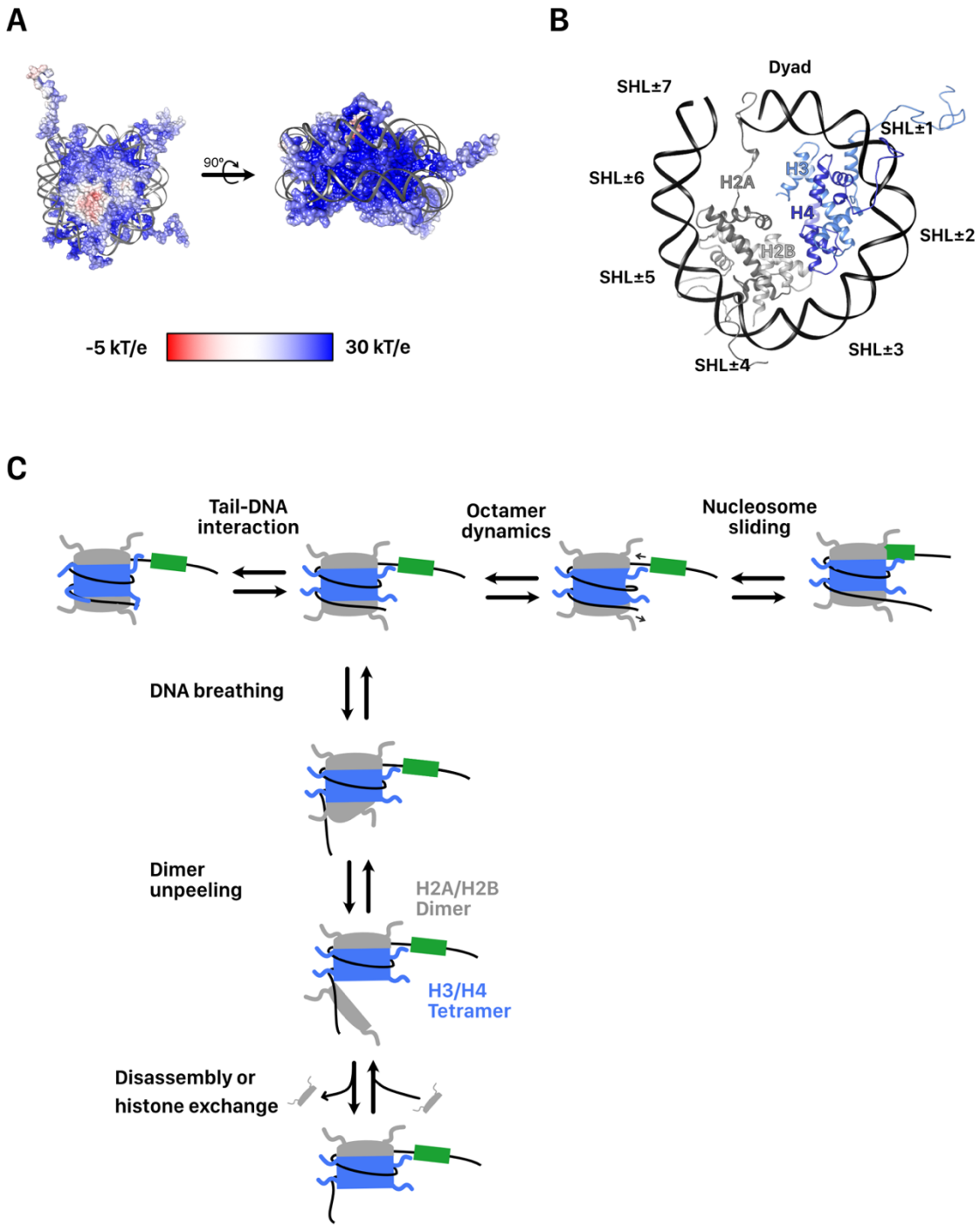

Figure 1.1 Core properties of the nucleosome
A. Nucleosome core particle with the surface of the histone octamer colored by charge. B. Ribbon diagram of one pseudosymmetrical half of the nucleosome. Locations of nucleosomal DNA are specified according to their SuperHelical Location (SHL) with each location being 10 bp from the dyad axis of symmetry. C. Dynamic states of a nucleosome in solution. Nucleosomes exist in equilibrium between many possible states. Transition between states may involve conformational changes in the histone octamer (e.g. during DNA breathing).

FIGURE 1.2

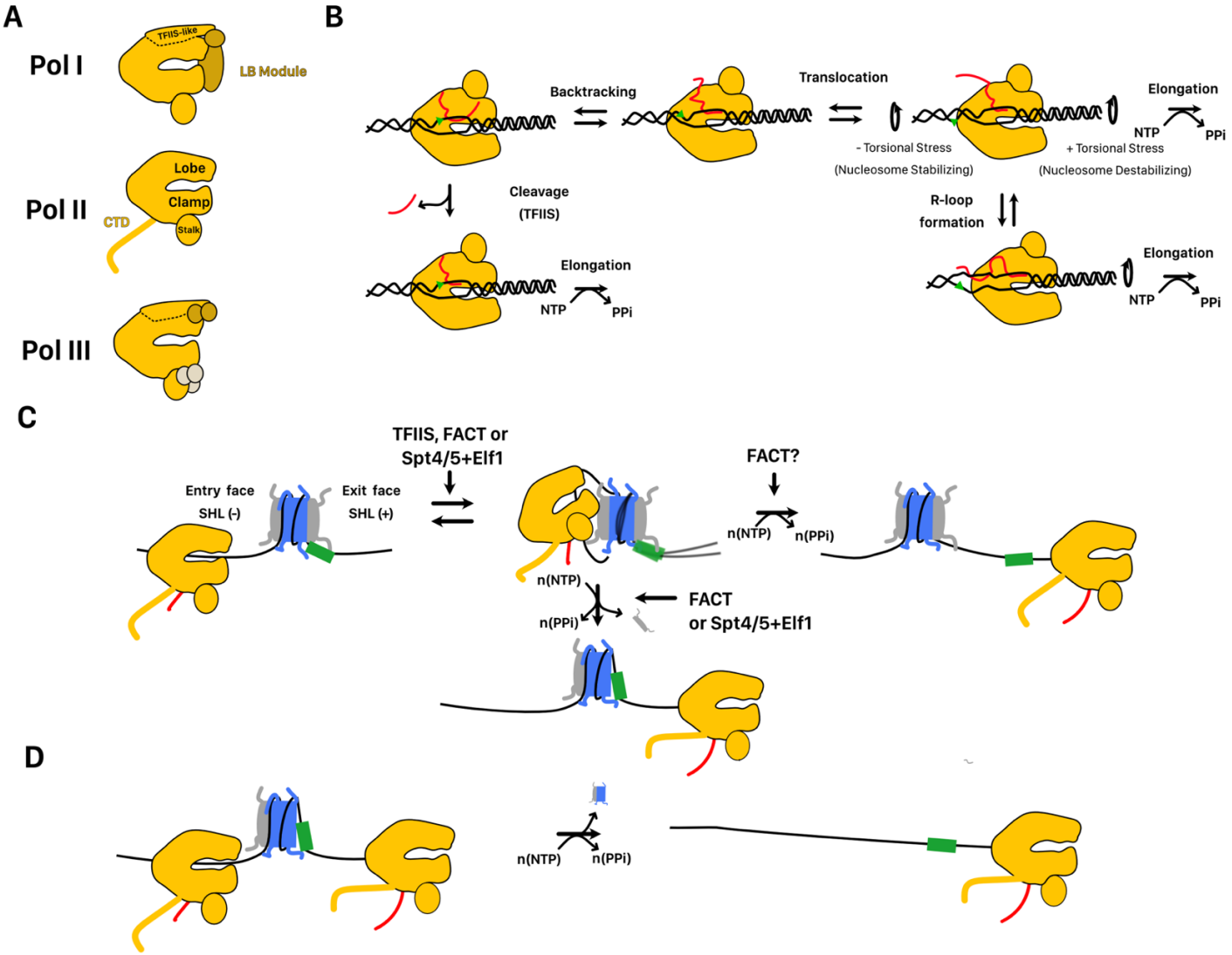
A
Pol I
TFIIS-like
LB Module
Pol II
Lobe
Clamp
CTD
Stalk
Pol III
B
Backtracking
Translocation
Elongation
NTP
PPi
- Torsional Stress
(Nucleosome Stabilizing)
+ Torsional Stress
(Nucleosome Destabilizing)
Cleavage
(TFIIS)
R-loop
formation
Elongation
NTP
PPi
C
TFIIS, FACT or
Spt4/5+Elf1
FACT?
Entry face
SHL (-)
Exit face
SHL (+)
n(NTP)
n(PPi)
n(NTP)
n(PPi)
FACT
or Spt4/5+Elf1
D
n(NTP)
n(PPi)

Figure 1.2 Mechanisms of nucleosome remodeling by RNA polymerases
A. Cartoon representations of the three eukaryotic RNA polymerases. The lobe, clamp, and stalk domains that are shared between all three polymerases are labeled on Pol II. The TFIIS like domain of the lobe and the LB module shared by Pol I and III are labeled on Pol I. Finally, the unique CTD of Pol II is also shown. B. Core mechanism of elongation shared by RNA polymerases. The green triangle is used as a reference point for polymerase translocation. Polymerase can either translocate 1 nt forward or pause and backtrack. DNA unwinding is associated with torsional stress ahead of and behind the transcription bubble. Stress behind the bubble can be absorbed by formation of a stable RNA-DNA hybrid called and R-Loop. Backtracked polymerase can be resolved by cleavage of the nascent transcript by TFIIS or the TFIIS-like domains of Pol I and III. Forward elongation is biased by irreversible incorporation of a complementary nucleotide. C. Mechanism of polymerase passage through the nucleosome. The green box is used as a reference location on the DNA. As polymerase translocates into the nucleosome core, it unpeels DNA at the entry side until it reaches the dyad. At the dyad further passage requires DNA unpeeling at the exit side and loosening of histone DNA contacts downstream of the dyad. Further passage is associated with either octamer transfer upstream of its current site or dissociation of an H2A/H2B dimer from the exit side. Elongation factors assist entrance into the nucleosome and may bias the outcome of Pol II passage. D. Additional passage of a hexasome by Pol II is associated with complete disassembly.

FIGURE 1.3

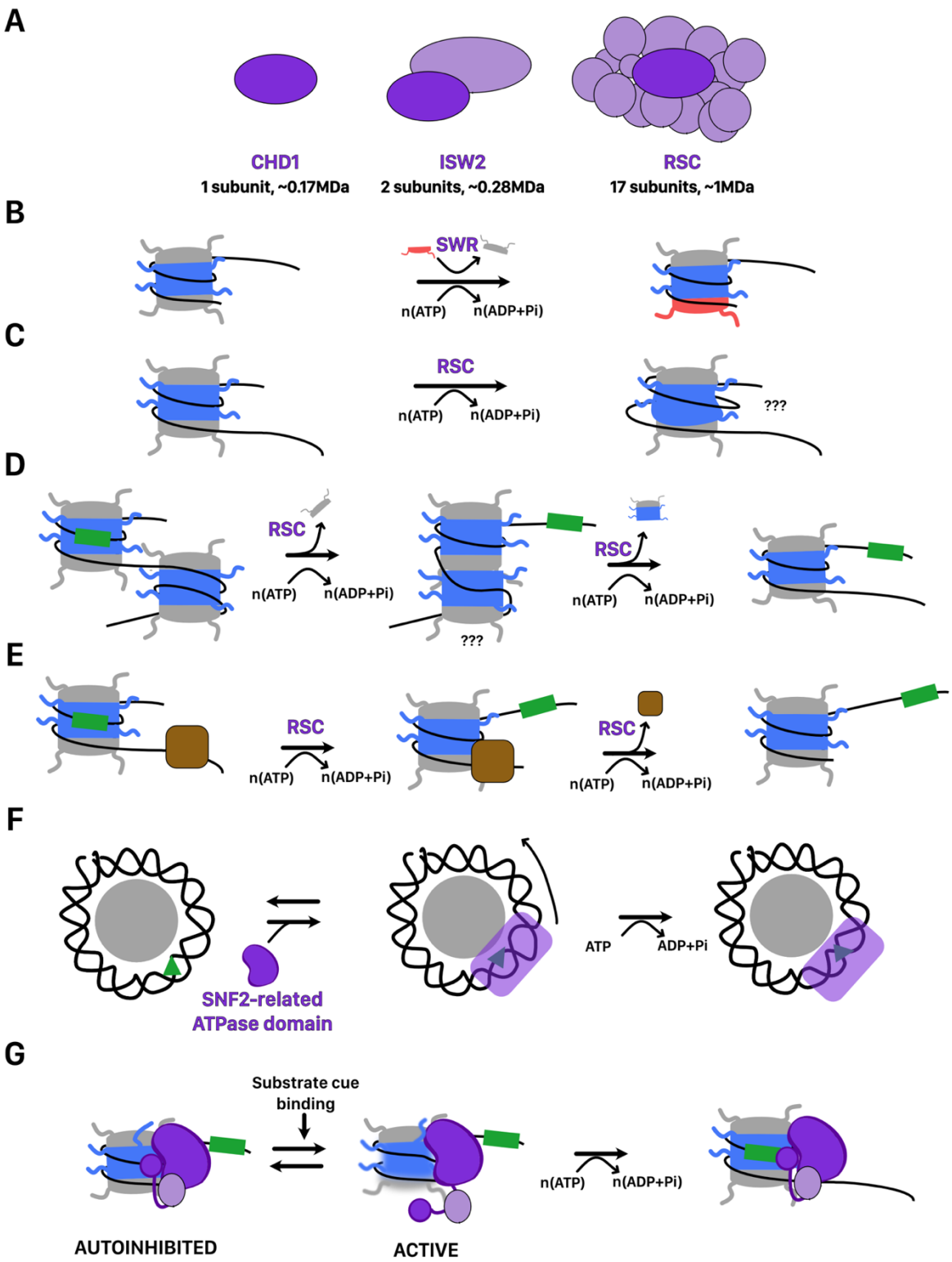
A
CHD1
1 subunit, ~0.17MDa
ISW2
2 subunits, ~0.28MDa
RSC
17 subunits, ~1MDa
B
SWR
n(ATP)
n(ADP+Pi)
C
RSC
n(ATP)
n(ADP+Pi)
???
D
RSC
n(ATP)
n(ADP+Pi)
???
RSC
n(ATP)
n(ADP+Pi)
E
RSC
n(ATP)
n(ADP+Pi)
RSC
n(ATP)
n(ADP+Pi)
F
SNF2-related
ATPase domain
ATP
ADP+Pi
G
Substrate cue
binding
n(ATP)
n(ADP+Pi)
AUTOINHIBITED
ACTIVE

Figure 1.3 Mechanisms of nucleosome remodeling by ATP-dependent chromatin remodelers

A. Cartoon representations of selected remodelers from *S. cerevisiae*. In dark purple is the ATP hydrolysing subunit. Remodelers range in size from the single subunit remodeler CHD1 to the mega dalton sized 17-subunit RSC complex. B. Directional histone exchange catalyzed by the SWR complex. H2A-H2B is exchanged for H2Az-H2B but not the reverse reaction. C. Remosome formation catalyzed by the RSC complex. The structure of remosomes is unclear but involves ~30bp of additional DNA wrapped around the core and looser histone-DNA contacts throughout the nucleosome. D. Nucleosome disassembly catalyzed by the RSC complex. RSC sliding of a nucleosome into an adjacent nucleosome causes its disassembly. This may involve an overlapping dinucleosome intermediate recently described. The green box is used as a reference location on the DNA. E. Transcription factor disruption by the RSC complex. RSC sliding of a nucleosome through a DNA-bound transcription factor causes its displacement. F. DNA translocation by SWI2/SNF2 family chromatin remodelers binding at SHL 2. The green triangle is used as a reference location on DNA. Binding at SHL2 stabilizes twist defects at that location, allowing breaking of histone DNA contacts. Binding, hydrolysis, and/or release of a nucleotide allows the resetting of histone-DNA contacts. Further rounds of translocation with additional contacts is expected to enable more complex activities, such as histone exchange. G. Regulation of remodeler activity by autoinhibitory domains. After binding the nucleosomes, remodelers are held inactive by contacts with autoinhibitory domains on either the ATP hydrolyzing subunit or accessory subunits. Contacts with substrate cues relieve this autoinhibition and allow remodeling activity. The active state may be associated with increased conformational dynamics in the histone octamer. The green box is used as a reference point on the DNA.

FIGURE 1.4

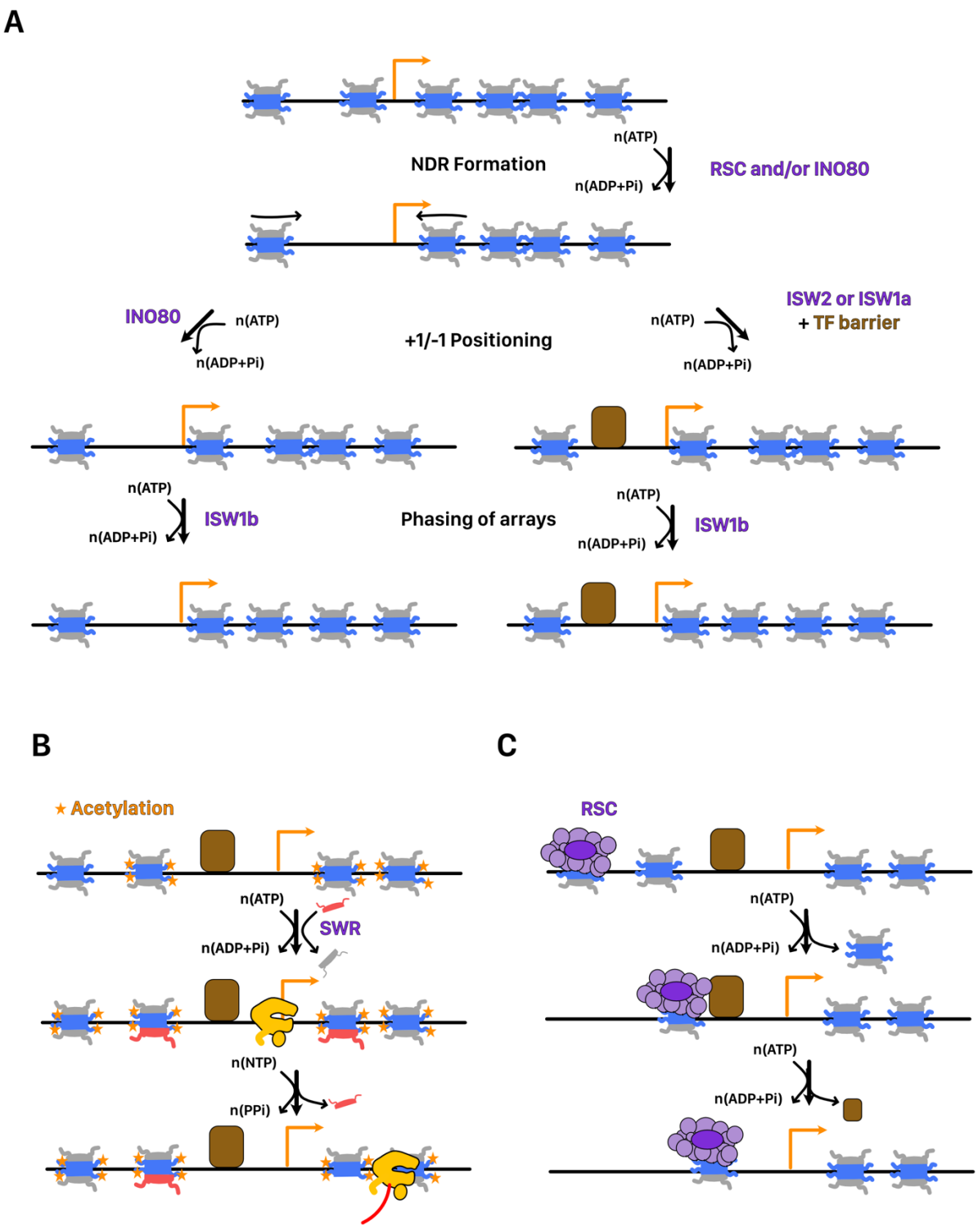
A
n(ATP)
NDR Formation
n(ADP+Pi)
RSC and/or INO80
INO80
n(ATP)
n(ADP+Pi)
+1/-1 Positioning
n(ATP)
n(ADP+Pi)
ISW2 or ISW1a
+ TF barrier
n(ATP)
n(ADP+Pi)
ISW1b
Phasing of arrays
n(ATP)
n(ADP+Pi)
ISW1b
B
Acetylation
n(ATP)
n(ADP+Pi)
SWR
n(NTP)
n(PPi)
C
RSC
n(ATP)
n(ADP+Pi)
n(ATP)
n(ADP+Pi)

Figure 1.4 Chromatin remodeling near the transcription start site
A. Two pathways for promoter chromatin architecture in *S. cerevisiae*. The NDR is first formed by the action of the RSC and/or INO80 complex recognizing sequence features near the promoter. The +1/-1 nucleosome is then positioned either by the INO80 complex using local DNA topology to position the nucleosome or by the ISW2 or ISW1a complexes positioning nucleosomes relative to a bound transcription factor. After establishment of the +1 nucleosome, ISW1b establishes a phased nucleosome array relative to the +1 nucleosome. B. Establishment of H2Az nucleosomes at the +1/-1 nucleosomes. SWR recognizes histone acetylation and possible promoter DNA sequences to exchange H2A with H2Az dimers. H2Az has a marked preference for incorporation on the promoter distal side of the nucleosome. Transcription by Pol II may disassemble H2Az containing nucleosomes during passage. C. RSC action at “fragile” nucleosome containing NDRs. RSC-bound “fragile” nucleosomes may be translocated to maintain a clear NDR or displace bound transcription factors.

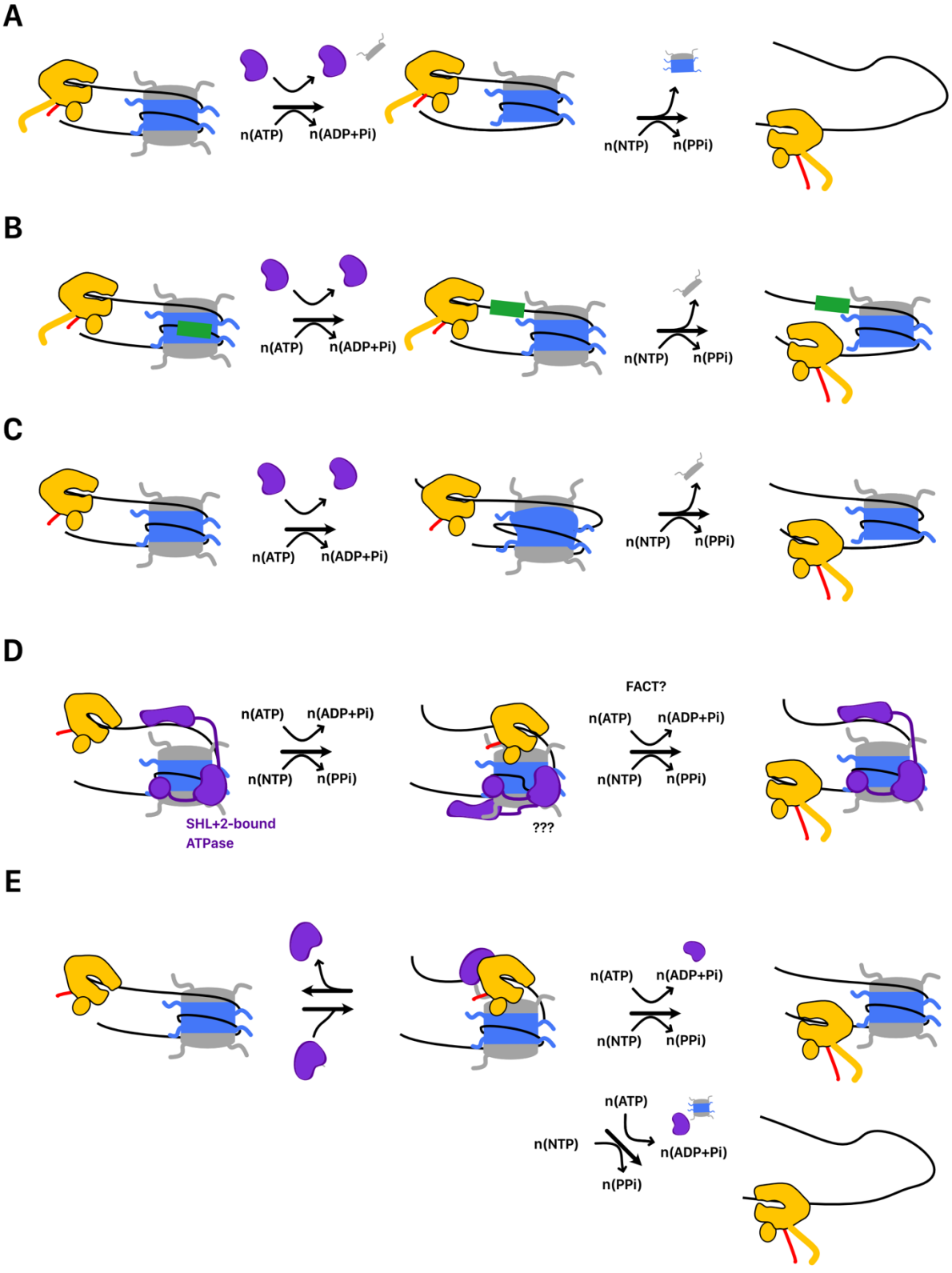
A
n(ATP)
n(ADP+Pi)
n(NTP)
n(PPi)
B
n(ATP)
n(ADP+Pi)
n(NTP)
n(PPi)
C
n(ATP)
n(ADP+Pi)
n(NTP)
n(PPi)
D
n(ATP)
n(ADP+Pi)
n(NTP)
n(PPi)
SHL+2-bound
ATPase
???
FACT?
n(ATP)
n(ADP+Pi)
n(NTP)
n(PPi)
E
n(ATP)
n(ADP+Pi)
n(NTP)
n(PPi)
n(ATP)
n(NTP)
n(ADP+Pi)
n(PPi)

Figure 1.5 Chromatin remodeling during elongation
Remodelers can promote Pol II passage by A. disassembling nuclesomes, B. translocating nucleosomes off of high-barrier sequences, or C. creating stable conformational rearrangements in nucleosome structure (e.g. remosomes). D. Speculative model for promotion of elongation. Binding of extranucleosomal DNA by CHD1's DNA binding domain stabilizes an unpeeled state that facilitates Pol II entry into the nucleosome. DNA translocation by the ATPase domain at SHL+2 may loosen histone DNA contacts needed to allow Pol II passage through the dyad. Contacts with FACT or other elongation factors (e.g. Paf1) may facilitate Pol II passage without CHD1 displacement. E. ATP-dependent elongation activity of CSB (Rad26). CSB binds Nucleosome-associated Pol II. Translocation of the DNA upstream of Pol II by CSB prevents backtracking and promotes passage through the nucleosome. This results in either nucleosome disassembly or full nucleosome survival.

References

[1] K. Luger, A.W. Mäder, R.K. Richmond, D.F. Sargent, T.J. Richmond, Crystal structure of the nucleosome core particle at 2.8 A resolution., Nature. 389 (1997) 251–260. https://doi.org/10.1038/38444.

[2] R.K. McGinty, S. Tan, Nucleosome Structure and Function, Chem Rev. 115 (2014) 2255–2273. https://doi.org/10.1021/cr500373h.

[3] M.G. Izban, D.S. Luse, Transcription on nucleosomal templates by RNA polymerase II in vitro: inhibition of elongation with enhancement of sequence-specific pausing., Gene Dev. 5 (1991) 683–696. https://doi.org/10.1101/gad.5.4.683.

[4] M.L. Kireeva, W. Walter, V. Tchernajenko, V. Bondarenko, M. Kashlev, V.M. Studitsky, Nucleosome Remodeling Induced by RNA Polymerase II Loss of the H2A/H2B Dimer during Transcription, Mol Cell. 9 (2002) 541–552. https://doi.org/10.1016/s1097-2765(02)00472-0.

[5] W. Walter, M.L. Kireeva, V.M. Studitsky, M. Kashlev, Bacterial Polymerase and Yeast Polymerase II Use Similar Mechanisms for Transcription through Nucleosomes, J Biol Chem. 278 (2003) 36148–36156. https://doi.org/10.1074/jbc.m305647200.

[6] C.R. Clapier, B.R. Cairns, The Biology of Chromatin Remodeling Complexes, Dx.Doi.Org. 78 (2009) 273–304. https://doi.org/10.1146/annurev.biochem.77.062706.153223.

[7] C.Y. Zhou, S.L. Johnson, N.I. Gamarra, G.J. Narlikar, Mechanisms of ATP-Dependent Chromatin Remodeling Motors, Annual Review of Biophysics. 45 (2016) 153–181. https://doi.org/10.1146/annurev-biophys-051013-022819.

[8] V.M. Studitsky, D.J. Clark, G. Felsenfeld, Overcoming a nucleosomal barrier to transcription, Cell. 83 (1995) 19–27. https://doi.org/10.1016/0092-8674(95)90230-9.

[9] V.M. Studitsky, G.A. Kassavetis, E.P. Geiduschek, G. Felsenfeld, Mechanism of Transcription Through the Nucleosome by Eukaryotic RNA Polymerase, Science. 278 (1997) 1960–1963. https://doi.org/10.1126/science.278.5345.1960.

[10] O.I. Kulaeva, D.A. Gaykalova, N.A. Pestov, V.V. Golovastov, D.G. Vassylyev, I. Artsimovitch, V.M. Studitsky, Mechanism of chromatin remodeling and recovery during passage of RNA polymerase II, Nat Struct Mol Biol. 16 (2009) 1272–1278. https://doi.org/10.1038/nsmb.1689.

[11] R.V. Chereji, P.R. Eriksson, J. Ocampo, H.K. Prajapati, D.J. Clark, Accessibility of promoter DNA is not the primary determinant of chromatin-mediated gene regulation, Genome Res. 29 (2019) 1985–1995. https://doi.org/10.1101/gr.249326.119.

[12] S. Sanulli, M.J. Trnka, V. Dharmarajan, R.W. Tibble, B.D. Pascal, A.L. Burlingame, P.R. Griffin, J.D. Gross, G.J. Narlikar, HP1 reshapes nucleosome core to promote phase separation of heterochromatin, Nature. 575 (2019) 390–394. https://doi.org/10.1038/s41586-019-1669-2.

[13] K. Zhou, G. Gaullier, K. Luger, Nucleosome structure and dynamics are coming of age, Nat Struct Mol Biol. 26 (2018) 3–13. https://doi.org/10.1038/s41594-018-0166-x.

[14] S.Y. Chung, W.E. Hill, P. Doty, Characterization of the histone core complex, Proc National Acad Sci. 75 (1978) 1680–1684. https://doi.org/10.1073/pnas.75.4.1680.

[15] R.K. McGinty, S. Tan, Recognition of the nucleosome by chromatin factors and enzymes., Current Opinion in Structural Biology. 37 (2016) 54–61. https://doi.org/10.1016/j.sbi.2015.11.014.

[16] T.J. Richmond, C.A. Davey, The structure of DNA in the nucleosome core., Nature. 423 (2003) 145–150. https://doi.org/10.1038/nature01595.

[17] D.J. Clark, G. Felsenfeld, Formation of nucleosomes on positively supercoiled DNA., Embo J. 10 (1991) 387–395. https://doi.org/10.1002/j.1460-2075.1991.tb07960.x.

[18] M.Y. Sheinin, M. Li, M. Soltani, K. Luger, M.D. Wang, Torque modulates nucleosome stability and facilitates H2A/H2B dimer loss, Nat Commun. 4 (2013) 2579. https://doi.org/10.1038/ncomms3579.

[19] H. Taguchi, N. Horikoshi, Y. Arimura, H. Kurumizaka, A method for evaluating nucleosome stability with a protein-binding fluorescent dye, Methods. 70 (2014) 119–126. https://doi.org/10.1016/j.ymeth.2014.08.019.

[20] K.J. Polach, J. Widom, Mechanism of protein access to specific DNA sequences in chromatin: a dynamic equilibrium model for gene regulation., Journal of Molecular Biology. 254 (1995) 130–149. https://doi.org/10.1006/jmbi.1995.0606.

[21] G. Li, M. Levitus, C. Bustamante, J. Widom, Rapid spontaneous accessibility of nucleosomal DNA., Nature Structural & Molecular Biology. 12 (2005) 46–53. https://doi.org/10.1038/nsmb869.

[22] V. Böhm, A.R. Hieb, A.J. Andrews, A. Gansen, A. Rocker, K. Tóth, K. Luger, J. Langowski, Nucleosome accessibility governed by the dimer/tetramer interface., Nucleic Acids Research. 39 (2011) 3093–3102. https://doi.org/10.1093/nar/gkq1279.

[23] S. Bilokapic, M. Strauss, M. Halic, Histone octamer rearranges to adapt to DNA unwrapping., Nature Structural & Molecular Biology. 25 (2018) 101–108. https://doi.org/10.1038/s41594-017-0005-5.

[24] Y. Arimura, H. Tachiwana, T. Oda, M. Sato, H. Kurumizaka, Structural analysis of the hexasome, lacking one histone H2A/H2B dimer from the conventional nucleosome., Biochemistry. 51 (2012) 3302–3309. https://doi.org/10.1021/bi300129b.

[25] K.J. Polach, P.T. Lowary, J. Widom, Effects of core histone tail domains on the equilibrium constants for dynamic DNA site accessibility in nucleosomes., Journal of Molecular Biology. 298 (2000) 211–223. https://doi.org/10.1006/jmbi.2000.3644.

[26] Z. Li, H. Kono, Distinct Roles of Histone H3 and H2A Tails in Nucleosome Stability, Sci Rep-Uk. 6 (2016) 31437. https://doi.org/10.1038/srep31437.

[27] A. Flaus, T. Owen-Hughes, Dynamic properties of nucleosomes during thermal and ATP-driven mobilization., Molecular and Cellular Biology. 23 (2003) 7767–7779. https://doi.org/10.1128/mcb.23.20.7767-7779.2003.

[28] G.B. Brandani, T. Niina, C. Tan, S. Takada, DNA sliding in nucleosomes via twist defect propagation revealed by molecular simulations, Nucleic Acids Res. 46 (2018) gky158-. https://doi.org/10.1093/nar/gky158.

[29] S. Bilokapic, M. Strauss, M. Halic, Structural rearrangements of the histone octamer translocate DNA., Nature Communications. 9 (2018) 1330. https://doi.org/10.1038/s41467-018-03677-z.

[30] P.T. Lowary, J. Widom, New DNA sequence rules for high affinity binding to histone octamer and sequence-directed nucleosome positioning., Journal of Molecular Biology. 276 (1998) 19–42. https://doi.org/10.1006/jmbi.1997.1494.

[31] B. Wu, K. Mohideen, D. Vasudevan, C.A. Davey, Structural Insight into the Sequence Dependence of Nucleosome Positioning, Structure. 18 (2010) 528–536. https://doi.org/10.1016/j.str.2010.01.015.

[32] E. Segal, J. Widom, Poly(dA:dT) tracts: major determinants of nucleosome organization, Current Opinion in Structural Biology. 19 (2009) 65–71. https://doi.org/10.1016/j.sbi.2009.01.004.

[33] G.D. Bowman, M.G. Poirier, Post-Translational Modifications of Histones That Influence Nucleosome Dynamics, Chem Rev. 115 (2015) 2274–2295. https://doi.org/10.1021/cr500350x.

[34] L. Bintu, T. Ishibashi, M. Dangkulwanich, Y.-Y. Wu, L. Lubkowska, M. Kashlev, C. Bustamante, Nucleosomal Elements that Control the Topography of the Barrier to Transcription, Cell. 151 (2012) 738–749. https://doi.org/10.1016/j.cell.2012.10.009.

[35] R.M. Raisner, P.D. Hartley, M.D. Meneghini, M.Z. Bao, C.L. Liu, S.L. Schreiber, O.J. Rando, H.D. Madhani, Histone Variant H2A.Z Marks the 5′ Ends of Both Active and

Inactive Genes in Euchromatin, Cell. 123 (2005) 233–248. https://doi.org/10.1016/j.cell.2005.10.002.

[36] S. Rudnizky, A. Bavly, O. Malik, L. Pnueli, P. Melamed, A. Kaplan, H2A.Z controls the stability and mobility of nucleosomes to regulate expression of the LH genes, Nat Commun. 7 (2016) 12958. https://doi.org/10.1038/ncomms12958.

[37] P. Cramer, K.-J. Armache, S. Baumli, S. Benkert, F. Brueckner, C. Buchen, G.E. Damsma, S. Dengl, S.R. Geiger, A.J. Jasiak, A. Jawhari, S. Jennebach, T. Kamenski, H. Kettenberger, C.-D. Kuhn, E. Lehmann, K. Leike, J.F. Sydow, A. Vannini, Structure of Eukaryotic RNA Polymerases, Annu Rev Biophys. 37 (2008) 337–352. https://doi.org/10.1146/annurev.biophys.37.032807.130008.

[38] R.G. Roeder, 50+ years of eukaryotic transcription: an expanding universe of factors and mechanisms, Nat Struct Mol Biol. 26 (2019) 783–791. https://doi.org/10.1038/s41594-019-0287-x.

[39] A.L. Mosley, G.O. Hunter, M.E. Sardiu, M. Smolle, J.L. Workman, L. Florens, M.P. Washburn, Quantitative Proteomics Demonstrates That the RNA Polymerase II Subunits Rpb4 and Rpb7 Dissociate during Transcriptional Elongation, Mol Cell Proteomics. 12 (2013) 1530–1538. https://doi.org/10.1074/mcp.m112.024034.

[40] L. Duek, O. Barkai, R. Elran, I. Adawi, M. Choder, Dissociation of Rpb4 from RNA polymerase II is important for yeast functionality, Plos One. 13 (2018) e0206161. https://doi.org/10.1371/journal.pone.0206161.

[41] J. Zaborowska, S. Egloff, S. Murphy, The pol II CTD: new twists in the tail, Nat Struct Mol Biol. 23 (2016) 771–777. https://doi.org/10.1038/nsmb.3285.

[42] W. Ruan, E. Lehmann, M. Thomm, D. Kostrewa, P. Cramer, Evolution of Two Modes of Intrinsic RNA Polymerase Transcript Cleavage, J Biol Chem. 286 (2011) 18701–18707. https://doi.org/10.1074/jbc.m111.222273.

[43] M.K. Vorländer, H. Khatter, R. Wetzel, W.J.H. Hagen, C.W. Müller, Molecular mechanism of promoter opening by RNA polymerase III, Nature. 553 (2018) 295–300. https://doi.org/10.1038/nature25440.

[44] A. Lisica, C. Engel, M. Jahnel, É. Roldán, E.A. Galburt, P. Cramer, S.W. Grill, Mechanisms of backtrack recovery by RNA polymerases I and II, Proc National Acad Sci. 113 (2016) 2946–2951. https://doi.org/10.1073/pnas.1517011113.

[45] E. Nudler, RNA Polymerase Backtracking in Gene Regulation and Genome Instability, Cell. 149 (2012) 1438–1445. https://doi.org/10.1016/j.cell.2012.06.003.

[46] M.L. Kireeva, B. Hancock, G.H. Cremona, W. Walter, V.M. Studitsky, M. Kashlev, Nature of the Nucleosomal Barrier to RNA Polymerase II, Mol Cell. 18 (2005) 97–108. https://doi.org/10.1016/j.molcel.2005.02.027.

[47] S. Corless, N. Gilbert, Effects of DNA supercoiling on chromatin architecture, Biophysical Rev. 8 (2016) 245–258. https://doi.org/10.1007/s12551-016-0210-1.

[48] S.S. Teves, S. Henikoff, Transcription-generated torsional stress destabilizes nucleosomes, Nat Struct Mol Biol. 21 (2014) 88–94. https://doi.org/10.1038/nsmb.2723.

[49] C. Naughton, N. Avlonitis, S. Corless, J.G. Prendergast, I.K. Mati, P.P. Eijk, S.L. Cockroft, M. Bradley, B. Ylstra, N. Gilbert, Transcription forms and remodels supercoiling domains unfolding large-scale chromatin structures, Nat Struct Mol Biol. 20 (2013) 387–395. https://doi.org/10.1038/nsmb.2509.

[50] V.M. Studitsky, W. Walter, M. Kireeva, M. Kashlev, G. Felsenfeld, Chromatin remodeling by RNA polymerases, Trends Biochem Sci. 29 (2004) 127–135. https://doi.org/10.1016/j.tibs.2004.01.003.

[51] J.L. Birch, B.C. Tan, K.I. Panov, T.B. Panova, J.S. Andersen, T.A. Owen-Hughes, J. Russell, S. Lee, J.C.B.M. Zomerdijk, FACT facilitates chromatin transcription by RNA polymerases I and III, Embo J. 28 (2009) 854–865. https://doi.org/10.1038/emboj.2009.33.

[52] O.I. Kulaeva, V.M. Studitsky, Mechanism of histone survival during transcription by RNA polymerase II, Transcription. 1 (2010) 85–88. https://doi.org/10.4161/trns.1.2.12519.

[53] C. Thiriet, J.J. Hayes, Replication-independent core histone dynamics at transcriptionally active loci in vivo, Gene Dev. 19 (2005) 677–682. https://doi.org/10.1101/gad.1265205.

[54] C. Hodges, L. Bintu, L. Lubkowska, M. Kashlev, C. Bustamante, Nucleosomal Fluctuations Govern the Transcription Dynamics of RNA Polymerase II, Science. 325 (2009) 626–628. https://doi.org/10.1126/science.1172926.

[55] L. Bintu, M. Kopaczynska, C. Hodges, L. Lubkowska, M. Kashlev, C. Bustamante, The elongation rate of RNA polymerase determines the fate of transcribed nucleosomes, Nat Struct Mol Biol. 18 (2011) 1394–1399. https://doi.org/10.1038/nsmb.2164.

[56] T. Kujirai, H. Ehara, Y. Fujino, M. Shirouzu, S. Sekine, H. Kurumizaka, Structural basis of the nucleosome transition during RNA polymerase II passage, Science. 362 (2018) 595–598. https://doi.org/10.1126/science.aau9904.

[57] M.G. Izban, D.S. Luse, Factor-stimulated RNA polymerase II transcribes at physiological elongation rates on naked DNA but very poorly on chromatin templates., J Biological Chem. 267 (1992) 13647–55.

[58] P.E. Merkl, M. Pilsl, T. Fremter, K. Schwank, C. Engel, G. Längst, P. Milkereit, J. Griesenbeck, H. Tschochner, RNA polymerase I (Pol I) passage through nucleosomes depends on Pol I subunits binding its lobe structure, J Biol Chem. 295 (2020) 4782–4795. https://doi.org/10.1074/jbc.ra119.011827.

[59] V.A. Bondarenko, L.M. Steele, A. Újvári, D.A. Gaykalova, O.I. Kulaeva, Y.S. Polikanov, D.S. Luse, V.M. Studitsky, Nucleosomes Can Form a Polar Barrier to Transcript Elongation by RNA Polymerase II, Mol Cell. 24 (2006) 469–479. https://doi.org/10.1016/j.molcel.2006.09.009.

[60] O.I. Kulaeva, F.-K. Hsieh, V.M. Studitsky, RNA polymerase complexes cooperate to relieve the nucleosomal barrier and evict histones, Proc National Acad Sci. 107 (2010) 11325–11330. https://doi.org/10.1073/pnas.1001148107.

[61] F. Hsieh, M. Fisher, A. Újvári, V.M. Studitsky, D.S. Luse, Histone Sin mutations promote nucleosome traversal and histone displacement by RNA polymerase II, Embo Rep. 11 (2010) 705–710. https://doi.org/10.1038/embor.2010.113.

[62] J.B. Crickard, J. Lee, T.-H. Lee, J.C. Reese, The elongation factor Spt4/5 regulates RNA polymerase II transcription through the nucleosome, Nucleic Acids Res. 45 (2017) gkx220-. https://doi.org/10.1093/nar/gkx220.

[63] L. Farnung, S.M. Vos, P. Cramer, Structure of transcribing RNA polymerase II-nucleosome complex, Nat Commun. 9 (2018) 5432. https://doi.org/10.1038/s41467-018-07870-y.

[64] H. Ehara, T. Kujirai, Y. Fujino, M. Shirouzu, H. Kurumizaka, S. Sekine, Structural insight into nucleosome transcription by RNA polymerase II with elongation factors, Science. 363 (2019) eaav8912. https://doi.org/10.1126/science.aav8912.

[65] T. Kujirai, H. Kurumizaka, Transcription through the nucleosome, Curr Opin Struc Biol. 61 (2020) 42–49. https://doi.org/10.1016/j.sbi.2019.10.007.

[66] A. Újvári, F.-K. Hsieh, S.W. Luse, V.M. Studitsky, D.S. Luse, Histone N-terminal Tails Interfere with Nucleosome Traversal by RNA Polymerase II, J Biol Chem. 283 (2008) 32236–32243. https://doi.org/10.1074/jbc.m806636200.

[67] R. Martinez-Zamudio, H.C. Ha, Histone ADP-Ribosylation Facilitates Gene Transcription by Directly Remodeling Nucleosomes, Mol Cell Biol. 32 (2012) 2490–2502. https://doi.org/10.1128/mcb.06667-11.

[68] R. Pavri, B. Zhu, G. Li, P. Trojer, S. Mandal, A. Shilatifard, D. Reinberg, Histone H2B Monoubiquitination Functions Cooperatively with FACT to Regulate Elongation by RNA Polymerase II, Cell. 125 (2006) 703–717. https://doi.org/10.1016/j.cell.2006.04.029.

[69] L. Farnung, M. Ochmann, M. Engehom, P. Cramer, Structural basis of nucleosome transcription mediated by Chd1 and FACT, BioRxiv. (2020). https://doi.org/10.1101/2020.11.30.403857.

[70] A. Bortvin, F. Winston, Evidence That Spt6p Controls Chromatin Structure by a Direct Interaction with Histones, Science. 272 (1996) 1473–1476. https://doi.org/10.1126/science.272.5267.1473.

[71] C.E. Cucinotta, A.E. Hildreth, B.M. McShane, M.K. Shirra, K.M. Arndt, The nucleosome acidic patch directly interacts with subunits of the Paf1 and FACT complexes and controls chromatin architecture in vivo, Nucleic Acids Research. 47 (2019) 8410–8423. https://doi.org/10.1093/nar/gkz549.

[72] R. Belotserkovskaya, S. Oh, V.A. Bondarenko, G. Orphanides, V.M. Studitsky, D. Reinberg, FACT facilitates transcription-dependent nucleosome alteration., Science (New York, N.Y.). 301 (2003) 1090–1093. https://doi.org/10.1126/science.1085703.

[73] F.-K. Hsieh, O.I. Kulaeva, S.S. Patel, P.N. Dyer, K. Luger, D. Reinberg, V.M. Studitsky, Histone chaperone FACT action during transcription through chromatin by RNA polymerase II, Proc National Acad Sci. 110 (2013) 7654–7659. https://doi.org/10.1073/pnas.1222198110.

[74] Y. Liu, K. Zhou, N. Zhang, H. Wei, Y.Z. Tan, Z. Zhang, B. Carragher, C.S. Potter, S. D'Arcy, K. Luger, FACT caught in the act of manipulating the nucleosome, Nature. 577 (2020) 426–431. https://doi.org/10.1038/s41586-019-1820-0.

[75] A. Jamai, A. Puglisi, M. Strubin, Histone Chaperone Spt16 Promotes Redeposition of the Original H3-H4 Histones Evicted by Elongating RNA Polymerase, Mol Cell. 35 (2009) 377–383. https://doi.org/10.1016/j.molcel.2009.07.001.

[76] J.-S. Lee, A.S. Garrett, K. Yen, Y.-H. Takahashi, D. Hu, J. Jackson, C. Seidel, B.F. Pugh, A. Shilatifard, Codependency of H2B monoubiquitination and nucleosome reassembly on Chd1, Gene Dev. 26 (2012) 914–919. https://doi.org/10.1101/gad.186841.112.

[77] C. Jeronimo, A. Angel, C. Poitras, P. Collin, J. Mellor, F. Robert, FACT is recruited to the +1 nucleosome of transcribed genes and spreads in a Chd1-dependent manner, Biorxiv. (2020) 2020.08.20.259960. https://doi.org/10.1101/2020.08.20.259960.

[78] N.A. Pestov, N.S. Gerasimova, O.I. Kulaeva, V.M. Studitsky, Structure of transcribed chromatin is a sensor of DNA damage, Sci Adv. 1 (2015) e1500021. https://doi.org/10.1126/sciadv.1500021.

[79] Y.V. Liu, D.J. Clark, V. Tchernajenko, M.E. Dahmus, V.M. Studitsky, Role of C-terminal domain phosphorylation in RNA polymerase II transcription through the nucleosome, Biopolymers. 68 (2003) 528–538. https://doi.org/10.1002/bip.10302.

[80] O. Porrua, M. Boudvillain, D. Libri, Transcription Termination: Variations on Common Themes, Trends Genet. 32 (2016) 508–522. https://doi.org/10.1016/j.tig.2016.05.007.

[81] J. Jin, L. Bai, D.S. Johnson, R.M. Fulbright, M.L. Kireeva, M. Kashlev, M.D. Wang, Synergistic action of RNA polymerases in overcoming the nucleosomal barrier, Nat Struct Mol Biol. 17 (2010) 745–752. https://doi.org/10.1038/nsmb.1798.

[82] K. Dunn, J.D. Griffith, The presence of RNA in a double helix inhibits its interaction with histone protein, Nucleic Acids Res. 8 (1980) 555–566. https://doi.org/10.1093/nar/8.3.555.

[83] T.G. Fazzio, Regulation of chromatin structure and cell fate by R-loops, Biochem Soc Symp. 7 (2016) 00–00. https://doi.org/10.1080/21541264.2016.1198298.

[84] E. Luk, A. Ranjan, P.C. FitzGerald, G. Mizuguchi, Y. Huang, D. Wei, C. Wu, Stepwise histone replacement by SWR1 requires dual activation with histone H2A.Z and canonical nucleosome., Cell. 143 (2010) 725–736. https://doi.org/10.1016/j.cell.2010.10.019.

[85] M.S. Shukla, S.H. Syed, F. Montel, C. Faivre-Moskalenko, J. Bednar, A. Travers, D. Angelov, S. Dimitrov, Remosomes: RSC generated non-mobilized particles with approximately 180 bp DNA loosely associated with the histone octamer, Proc National Acad Sci. 107 (2010) 1936–1941. https://doi.org/10.1073/pnas.0904497107.

[86] M.S. Shukla, S.H. Syed, R. Boopathi, E.B. Simon, S. Nahata, L. Ramos, D. Dalkara, C. Moskalenko, A. Travers, D. Angelov, S. Dimitrov, A. Hamiche, J. Bednar,

Generation of Remosomes by the SWI/SNF Chromatin Remodeler Family, Scientific Reports. 9 (2019) 14212. https://doi.org/10.1038/s41598-019-50572-8.

[87] M. Li, A. Hada, P. Sen, L. Olufemi, M.A. Hall, B.Y. Smith, S. Forth, J.N. McKnight, A. Patel, G.D. Bowman, B. Bartholomew, M.D. Wang, Dynamic regulation of transcription factors by nucleosome remodeling., ELife. 4 (2015). https://doi.org/10.7554/elife.06249.

[88] M.L. Dechassa, A. Sabri, S. Pondugula, S.R. Kassabov, N. Chatterjee, M.P. Kladde, B. Bartholomew, SWI/SNF has intrinsic nucleosome disassembly activity that is dependent on adjacent nucleosomes., Molecular Cell. 38 (2010) 590–602. https://doi.org/10.1016/j.molcel.2010.02.040.

[89] A. Flaus, D.M.A. Martin, G.J. Barton, T. Owen-Hughes, Identification of multiple distinct Snf2 subfamilies with conserved structural motifs., Nucleic Acids Research. 34 (2006) 2887–2905. https://doi.org/10.1093/nar/gkl295.

[90] X. Liu, M. Li, X. Xia, X. Li, Z. Chen, Mechanism of chromatin remodelling revealed by the Snf2-nucleosome structure, Nature. 544 (2017) 440–445. https://doi.org/10.1038/nature22036.

[91] A. Saha, J. Wittmeyer, B.R. Cairns, Chromatin remodeling by RSC involves ATP-dependent DNA translocation., Genes & Development. 16 (2002) 2120–2134. https://doi.org/10.1101/gad.995002.

[92] M. Zofall, J. Persinger, S.R. Kassabov, B. Bartholomew, Chromatin remodeling by ISW2 and SWI/SNF requires DNA translocation inside the nucleosome., Nature Structural & Molecular Biology. 13 (2006) 339–346. https://doi.org/10.1038/nsmb1071.

[93] A. Ranjan, F. Wang, G. Mizuguchi, D. Wei, Y. Huang, C. Wu, H2A histone-fold and DNA elements in nucleosome activate SWR1-mediated H2A.Z replacement in budding yeast., ELife. 4 (2015) e06845. https://doi.org/10.7554/elife.06845.

[94] S. Brahma, M.I. Udugama, J. Kim, A. Hada, S.K. Bhardwaj, S.G. Hailu, T.-H. Lee, B. Bartholomew, INO80 exchanges H2A.Z for H2A by translocating on DNA proximal to histone dimers., Nature Communications. 8 (2017) 15616. https://doi.org/10.1038/ncomms15616.

[95] M. Li, X. Xia, Y. Tian, Q. Jia, X. Liu, Y. Lu, M. Li, X. Li, Z. Chen, Mechanism of DNA translocation underlying chromatin remodelling by Snf2, Nature. 567 (2019) 409–413. https://doi.org/10.1038/s41586-019-1029-2.

[96] K. Havas, A. Flaus, M. Phelan, R. Kingston, P.A. Wade, D.M. Lilley, T. Owen-Hughes, Generation of superhelical torsion by ATP-dependent chromatin remodeling activities., Cell. 103 (2000) 1133–1142.

[97] G. Längst, P.B. Becker, ISWI Induces Nucleosome Sliding on Nicked DNA, Molecular Cell. 8 (2001) 1085–1092. https://doi.org/10.1016/s1097-2765(01)00397-5.

[98] S. Aoyagi, J.J. Hayes, hSWI/SNF-catalyzed nucleosome sliding does not occur solely via a twist-diffusion mechanism., Molecular and Cellular Biology. 22 (2002) 7484–7490. https://doi.org/10.1128/mcb.22.21.7484-7490.2002.

[99] J. Winger, I.M. Nodelman, R.F. Levendosky, G.D. Bowman, A twist defect mechanism for ATP-dependent translocation of nucleosomal DNA., ELife. 7 (2018) 391. https://doi.org/10.7554/elife.34100.

[100] S. Deindl, W.L. Hwang, S.K. Hota, T.R. Blosser, P. Prasad, B. Bartholomew, X. Zhuang, ISWI remodelers slide nucleosomes with coordinated multi-base-pair entry steps and single-base-pair exit steps., Cell. 152 (2013) 442–452. https://doi.org/10.1016/j.cell.2012.12.040.

[101] B.T. Harada, W.L. Hwang, S. Deindl, N. Chatterjee, B. Bartholomew, X. Zhuang, Stepwise nucleosome translocation by RSC remodeling complexes., ELife. 5 (2016) 3653. https://doi.org/10.7554/elife.10051.

[102] O. Willhoft, M. Ghoneim, C.-L. Lin, E.Y.D. Chua, M. Wilkinson, Y. Chaban, R. Ayala, E.A. McCormack, L. Ocloo, D.S. Rueda, D.B. Wigley, Structure and dynamics of the yeast SWR1-nucleosome complex, Science (New York, N.Y.). 362 (2018) eaat7716. https://doi.org/10.1126/science.aat7716.

[103] K.K. Sinha, J.D. Gross, G.J. Narlikar, Distortion of histone octamer core promotes nucleosome mobilization by a chromatin remodeler., Science (New York, N.Y.). 355 (2017) eaaa3761. https://doi.org/10.1126/science.aaa3761.

[104] J.P. Armache, N. Gamarra, S.L. Johnson, J.D. Leonard, S. Wu, G.J. Narlikar, Y. Cheng, Cryo-EM structures of remodeler-nucleosome intermediates suggest allosteric control through the nucleosome, ELife. 8 (2019) e46057. https://doi.org/10.7554/eLife.46057.

[105] N. Gamarra, G. Narlikar, Histone dynamics within the nucleosome octamer play a critical role in SNF2h-mediated nucleosome sliding, BioRxiv. (2020) 2020.03.13.992073. https://doi.org/10.1101/2020.03.13.992073.

[106] M. Oppikofer, T. Bai, Y. Gan, B. Haley, P. Liu, W. Sandoval, C. Ciferri, A.G. Cochran, Expansion of the ISWI chromatin remodeler family with new active complexes., EMBO Reports. 18 (2017) 1697–1706. https://doi.org/10.15252/embr.201744011.

[107] N. Mashtalir, A.R. D'Avino, B.C. Michel, J. Luo, J. Pan, J.E. Otto, H.J. Zullow, Z.M. McKenzie, R.L. Kubiak, R.St. Pierre, A.M. Valencia, S.J. Poynter, S.H. Cassel, J.A. Ranish, C. Kadoch, Modular Organization and Assembly of SWI/SNF Family Chromatin Remodeling Complexes, Cell. 175 (2018) 1272-1288.e20. https://doi.org/10.1016/j.cell.2018.09.032.

[108] Z.O. Jónsson, S.K. Dhar, G.J. Narlikar, R. Auty, N. Wagle, D. Pellman, R.E. Pratt, R. Kingston, A. Dutta, Rvb1p and Rvb2p are essential components of a chromatin remodeling complex that regulates transcription of over 5% of yeast genes., The Journal of Biological Chemistry. 276 (2001) 16279–16288. https://doi.org/10.1074/jbc.m011523200.

[109] H.F. Allen, P.A. Wade, T.G. Kutateladze, The NuRD architecture, Cell Mol Life Sci. 70 (2013) 3513–3524. https://doi.org/10.1007/s00018-012-1256-2.

[110] C.Y. Zhou, C.I. Stoddard, J.B. Johnston, M.J. Trnka, I. Echeverria, E. Palovcak, A. Sali, A.L. Burlingame, Y. Cheng, G.J. Narlikar, Regulation of Rvb1/Rvb2 by a Domain within the INO80 Chromatin Remodeling Complex Implicates the Yeast Rvbs as

Protein Assembly Chaperones., Cell Reports. 19 (2017) 2033–2044. https://doi.org/10.1016/j.celrep.2017.05.029.

[111] K. Yen, V. Vinayachandran, B.F. Pugh, SWR-C and INO80 chromatin remodelers recognize nucleosome-free regions near +1 nucleosomes., Cell. 154 (2013) 1246–1256. https://doi.org/10.1016/j.cell.2013.08.043.

[112] N.J. Krogan, M.-C. Keogh, N. Datta, C. Sawa, O.W. Ryan, H. Ding, R.A. Haw, J. Pootoolal, A. Tong, V. Canadien, D.P. Richards, X. Wu, A. Emili, T.R. Hughes, S. Buratowski, J.F. Greenblatt, A Snf2 Family ATPase Complex Required for Recruitment of the Histone H2A Variant Htz1, Mol Cell. 12 (2003) 1565–1576. https://doi.org/10.1016/s1097-2765(03)00497-0.

[113] M. Durant, B.F. Pugh, NuA4-Directed Chromatin Transactions throughout the Saccharomyces cerevisiae Genome ▿ †, Mol Cell Biol. 27 (2007) 5327–5335. https://doi.org/10.1128/mcb.00468-07.

[114] D.A. Donovan, J.G. Crandall, V.N. Truong, A.L. Vaaler, T.B. Bailey, D. Dinwiddie, L.E. McKnight, J.N. McKnight, Basis of Specificity for a Conserved and Promiscuous Chromatin Remodeling Protein, Biorxiv. (2020) 2020.05.25.115584. https://doi.org/10.1101/2020.05.25.115584.

[115] G. Hauk, J.N. McKnight, I.M. Nodelman, G.D. Bowman, The chromodomains of the Chd1 chromatin remodeler regulate DNA access to the ATPase motor., Molecular Cell. 39 (2010) 711–723. https://doi.org/10.1016/j.molcel.2010.08.012.

[116] X. Xia, X. Liu, T. Li, X. Fang, Z. Chen, Structure of chromatin remodeler Swi2/Snf2 in the resting state., Nature Structural & Molecular Biology. 23 (2016) 722–729. https://doi.org/10.1038/nsmb.3259.

[117] L. Yan, L. Wang, Y. Tian, X. Xia, Z. Chen, Structure and regulation of the chromatin remodeller ISWI, Nature. 540 (2016) 466–469. https://doi.org/10.1038/nature20590.

[118] C.R. Clapier, B.R. Cairns, Regulation of ISWI involves inhibitory modules antagonized by nucleosomal epitopes, Nature. 492 (2012) 280–284. https://doi.org/10.1038/nature11625.

[119] W.L. Hwang, S. Deindl, B.T. Harada, X. Zhuang, Histone H4 tail mediates allosteric regulation of nucleosome remodelling by linker DNA., Nature. 512 (2014) 213–217. https://doi.org/10.1038/nature13380.

[120] N. Mashtalir, H. Suzuki, D.P. Farrell, A. Sankar, J. Luo, M. Filipovski, A.R. D'Avino, R.St. Pierre, A.M. Valencia, T. Onikubo, R.G. Roeder, Y. Han, Y. He, J.A. Ranish, F. DiMaio, T. Walz, C. Kadoch, A Structural Model of the Endogenous Human BAF Complex Informs Disease Mechanisms, Cell. (2020). https://doi.org/10.1016/j.cell.2020.09.051.

[121] G.P. Dann, G.P. Liszczak, J.D. Bagert, M.M. Müller, U.T.T. Nguyen, F. Wojcik, Z.Z. Brown, J. Bos, T. Panchenko, R. Pihl, S.B. Pollock, K.L. Diehl, C.D. Allis, T.W. Muir, ISWI chromatin remodellers sense nucleosome modifications to determine substrate preference, Nature. 548 (2017) 607–611. https://doi.org/10.1038/nature23671.

[122] L.R. Racki, J.G. Yang, N. Naber, P.D. Partensky, A. Acevedo, T.J. Purcell, R. Cooke, Y. Cheng, G.J. Narlikar, The chromatin remodeller ACF acts as a dimeric motor to space nucleosomes., Nature. 462 (2009) 1016–1021. https://doi.org/10.1038/nature08621.

[123] J.D. Leonard, G.J. Narlikar, A Nucleotide-Driven Switch Regulates Flanking DNA Length Sensing by a Dimeric Chromatin Remodeler, Molecular Cell. (2015). https://doi.org/10.1016/j.molcel.2015.01.008.

[124] N. Gamarra, S.L. Johnson, M.J. Trnka, A.L. Burlingame, G.J. Narlikar, The nucleosomal acidic patch relieves auto-inhibition by the ISWI remodeler SNF2h, ELife. 7 (2018) e35322. https://doi.org/10.7554/elife.35322.

[125] S.A. Morris, S. Baek, M.-H. Sung, S. John, M. Wiench, T.A. Johnson, R.L. Schiltz, G.L. Hager, Overlapping chromatin-remodeling systems collaborate genome wide at dynamic chromatin transitions., Nature Structural & Molecular Biology. 21 (2014) 73–81. https://doi.org/10.1038/nsmb.2718.

[126] Y. Huang, L. Sun, L. Pierrakeas, L. Dai, L. Pan, E. Luk, Z. Zhou, Role of a DEF/Y motif in histone H2A-H2B recognition and nucleosome editing, Proceedings of the National Academy of Sciences. 117 (2020) 3543–3550. https://doi.org/10.1073/pnas.1914313117.

[127] K. Yamada, T.D. Frouws, B. Angst, D.J. Fitzgerald, C. DeLuca, K. Schimmele, D.F. Sargent, T.J. Richmond, Structure and mechanism of the chromatin remodelling factor ISW1a., Nature. 472 (2011) 448–453. https://doi.org/10.1038/nature09947.

[128] S.K. Bhardwaj, S.G. Hailu, L. Olufemi, S. Brahma, S. Kundu, S.K. Hota, J. Persinger, B. Bartholomew, Dinucleosome specificity and allosteric switch of the ISW1a ATP-dependent chromatin remodeler in transcription regulation, Nat Commun. 11 (2020) 5913. https://doi.org/10.1038/s41467-020-19700-1.

[129] A.N. Imbalzano, H. Kwon, M.R. Green, R.E. Kingston, Facilitated binding of TATA-binding protein to nucleosomal DNA., Nature. 370 (1994) 481–485. https://doi.org/10.1038/370481a0.

[130] K. Kramm, C. Engel, D. Grohmann, Transcription initiation factor TBP: old friend new questions, Biochem Soc T. 47 (2019) 411–423. https://doi.org/10.1042/bst20180623.

[131] X. Zhao, P.S. Pendergrast, N. Hernandez, A Positioned Nucleosome on the Human U6 Promoter Allows Recruitment of SNAPc by the Oct-1 POU Domain, Mol Cell. 7 (2001) 539–549. https://doi.org/10.1016/s1097-2765(01)00201-5.

[132] C. Jiang, B.F. Pugh, Nucleosome positioning and gene regulation: advances through genomics, Nat Rev Genet. 10 (2009) 161–172. https://doi.org/10.1038/nrg2522.

[133] Y. Kumar, P. Bhargava, A unique nucleosome arrangement, maintained actively by chromatin remodelers facilitates transcription of yeast tRNA genes, Bmc Genomics. 14 (2013) 402. https://doi.org/10.1186/1471-2164-14-402.

[134] W.K.M. Lai, B.F. Pugh, Genome-wide uniformity of human ‘open’ pre-initiation complexes, Genome Res. 27 (2017) 15–26. https://doi.org/10.1101/gr.210955.116.

[135] N. Krietenstein, M. Wal, S. Watanabe, B. Park, C.L. Peterson, B.F. Pugh, P. Korber, Genomic Nucleosome Organization Reconstituted with Pure Proteins, Cell. 167 (2016) 709-721.e12. https://doi.org/10.1016/j.cell.2016.09.045.

[136] E. Oberbeckmann, N. Krietenstein, V. Niebauer, Y. Wang, K. Schall, M. Moldt, T. Straub, R. Rohs, K.-P. Hopfner, P. Korber, S. Eustermann, Genome information processing by the INO80 chromatin remodeler positions nucleosomes, Biorxiv. (2020) 2020.11.03.366690. https://doi.org/10.1101/2020.11.03.366690.

[137] B. Guillemette, A.R. Bataille, N. Gévry, M. Adam, M. Blanchette, F. Robert, L. Gaudreau, Variant Histone H2A.Z Is Globally Localized to the Promoters of Inactive Yeast Genes and Regulates Nucleosome Positioning, Plos Biol. 3 (2005) e384. https://doi.org/10.1371/journal.pbio.0030384.

[138] A. Ranjan, G. Mizuguchi, P.C. FitzGerald, D. Wei, F. Wang, Y. Huang, E. Luk, C.L. Woodcock, C. Wu, Nucleosome-free region dominates histone acetylation in targeting SWR1 to promoters for H2A.Z replacement., Cell. 154 (2013) 1232–1245. https://doi.org/10.1016/j.cell.2013.08.005.

[139] M. Papamichos-Chronakis, S. Watanabe, O.J. Rando, C.L. Peterson, Global Regulation of H2A.Z Localization by the INO80 Chromatin-Remodeling Enzyme Is Essential for Genome Integrity, Cell. 144 (2011) 200–213.

[140] F. Wang, A. Ranjan, D. Wei, C. Wu, Comment on “A histone acetylation switch regulates H2A.Z deposition by the SWR-C remodeling enzyme,” Science. 353 (2016) 358–358. https://doi.org/10.1126/science.aad5921.

[141] A. Ranjan, V.Q. Nguyen, S. Liu, J. Wisniewski, J.M. Kim, X. Tang, G. Mizuguchi, E. Elalaoui, T.J. Nickels, V. Jou, B.P. English, Q. Zheng, E. Luk, L.D. Lavis, T. Lionnet, C. Wu, Live-cell single particle imaging reveals the role of RNA polymerase II in histone H2A.Z eviction, Elife. 9 (2020) e55667. https://doi.org/10.7554/elife.55667.

[142] H.S. Rhee, A.R. Bataille, L. Zhang, B.F. Pugh, Subnucleosomal Structures and Nucleosome Asymmetry across a Genome, Cell. 159 (2014) 1377–1388. https://doi.org/10.1016/j.cell.2014.10.054.

[143] S. Brahma, S. Henikoff, RSC-Associated Subnucleosomes Define MNase-Sensitive Promoters in Yeast, Mol Cell. 73 (2019) 238-249.e3. https://doi.org/10.1016/j.molcel.2018.10.046.

[144] G.D. Mehta, D.A. Ball, P.R. Eriksson, R.V. Chereji, D.J. Clark, J.G. McNally, T.S. Karpova, Single-Molecule Analysis Reveals Linked Cycles of RSC Chromatin Remodeling and Ace1p Transcription Factor Binding in Yeast, Mol Cell. 72 (2018) 875-887.e9. https://doi.org/10.1016/j.molcel.2018.09.009.

[145] J.P. Goldmark, T.G. Fazzio, P.W. Estep, G.M. Church, T. Tsukiyama, The Isw2 chromatin remodeling complex represses early meiotic genes upon recruitment by Ume6p., Cell. 103 (2000) 423–433. https://doi.org/10.1016/s0092-8674(00)00134-3.

[146] T.G. Fazzio, C. Kooperberg, J.P. Goldmark, C. Neal, R. Basom, J. Delrow, T. Tsukiyama, Widespread collaboration of Isw2 and Sin3-Rpd3 chromatin remodeling complexes in transcriptional repression., Molecular and Cellular Biology. 21 (2001) 6450–6460. https://doi.org/10.1128/mcb.21.19.6450-6460.2001.

[147] J. Li, G. Längst, I. Grummt, NoRC-dependent nucleosome positioning silences rRNA genes, The EMBO Journal. 25 (2006) 5735–5741. https://doi.org/10.1038/sj.emboj.7601454.

[148] I. Whitehouse, O.J. Rando, J. Delrow, T. Tsukiyama, Chromatin remodelling at promoters suppresses antisense transcription., Nature. 450 (2007) 1031–1035. https://doi.org/10.1038/nature06391.

[149] J. Pointner, J. Persson, P. Prasad, U. Norman-Axelsson, A. Strålfors, O. Khorosjutina, N. Krietenstein, J.P. Svensson, K. Ekwall, P. Korber, CHD1 remodelers regulate nucleosome spacing in vitro and align nucleosomal arrays over gene coding regions in S. pombe., The EMBO Journal. 31 (2012) 4388–4403. https://doi.org/10.1038/emboj.2012.289.

[150] B.P. Hennig, K. Bendrin, Y. Zhou, T. Fischer, Chd1 chromatin remodelers maintain nucleosome organization and repress cryptic transcription., EMBO Reports. 13 (2012) 997–1003. https://doi.org/10.1038/embor.2012.146.

[151] B.G. Kuryan, J. Kim, N.N.H. Tran, S.R. Lombardo, S. Venkatesh, J.L. Workman, M. Carey, Histone density is maintained during transcription mediated by the chromatin remodeler RSC and histone chaperone NAP1 in vitro, Proc National Acad Sci. 109 (2012) 1931–1936. https://doi.org/10.1073/pnas.1109994109.

[152] T.A. Soboleva, M. Nekrasov, D.P. Ryan, D.J. Tremethick, Histone variants at the transcription start-site, Trends Genet. 30 (2014) 199–209. https://doi.org/10.1016/j.tig.2014.03.002.

[153] D.A. Gaykalova, V. Nagarajavel, V.A. Bondarenko, B. Bartholomew, D.J. Clark, V.M. Studitsky, A polar barrier to transcription can be circumvented by remodeler-induced nucleosome translocation, Nucleic Acids Res. 39 (2011) 3520–3528. https://doi.org/10.1093/nar/gkq1273.

[154] E. Biernat, J. Kinney, K. Dunlap, C. Rizza, C.K. Govind, The RSC complex remodels nucleosomes in transcribed coding sequences and promotes transcription in Saccharomyces cerevisiae, BioRxiv. (2020) 2020.03.11.987974. https://doi.org/10.1101/2020.03.11.987974.

[155] N.J. Krogan, M. Kim, S.H. Ahn, G. Zhong, M.S. Kobor, G. Cagney, A. Emili, A. Shilatifard, S. Buratowski, J.F. Greenblatt, RNA Polymerase II Elongation Factors of Saccharomyces cerevisiae: a Targeted Proteomics Approach, Mol Cell Biol. 22 (2002) 6979–6992. https://doi.org/10.1128/mcb.22.20.6979-6992.2002.

[156] R. Simic, D.L. Lindstrom, H.G. Tran, K.L. Roinick, P.J. Costa, A.D. Johnson, G.A. Hartzog, K.M. Arndt, Chromatin remodeling protein Chd1 interacts with transcription elongation factors and localizes to transcribed genes, Embo J. 22 (2003) 1846–1856. https://doi.org/10.1093/emboj/cdg179.

[157] J.N. McKnight, K.R. Jenkins, I.M. Nodelman, T. Escobar, G.D. Bowman, Extranucleosomal DNA binding directs nucleosome sliding by Chd1., Molecular and Cellular Biology. 31 (2011) 4746–4759. https://doi.org/10.1128/mcb.05735-11.

[158] I.M. Nodelman, F. Bleichert, A. Patel, R. Ren, K.C. Horvath, J.M. Berger, G.D. Bowman, Interdomain Communication of the Chd1 Chromatin Remodeler across the DNA

Gyres of the Nucleosome, Molecular Cell. 0 (2017) 711–723. https://doi.org/10.1016/j.molcel.2016.12.011.

[159] L. Farnung, S.M. Vos, C. Wigge, P. Cramer, Nucleosome-Chd1 structure and implications for chromatin remodelling., Nature. 550 (2017) 539–542. https://doi.org/10.1038/nature24046.

[160] R. Sundaramoorthy, A.L. Hughes, H. El-Mkami, D.G. Norman, H. Ferreira, T. Owen-Hughes, Structure of the chromatin remodelling enzyme Chd1 bound to a ubiquitinylated nucleosome., ELife. 7 (2018) 977. https://doi.org/10.7554/elife.35720.

[161] J.M. Tokuda, R. Ren, R.F. Levendosky, R.J. Tay, M. Yan, L. Pollack, G.D. Bowman, The ATPase motor of the Chd1 chromatin remodeler stimulates DNA unwrapping from the nucleosome, Nucleic Acids Res. 46 (2018) gky206-. https://doi.org/10.1093/nar/gky206.

[162] R.F. Levendosky, A. Sabantsev, S. Deindl, G.D. Bowman, The Chd1 chromatin remodeler shifts hexasomes unidirectionally., ELife. 5 (2016) 3302. https://doi.org/10.7554/elife.21356.

[163] D. Biswas, R. Dutta-Biswas, D.J. Stillman, Chd1 and yFACT Act in Opposition in Regulating Transcription ▿ †, Mol Cell Biol. 27 (2007) 6279–6287. https://doi.org/10.1128/mcb.00978-07.

[164] W. Wang, J. Xu, O. Limbo, J. Fei, G.A. Kassavetis, J. Chong, J.T. Kadonaga, P. Russell, B. Li, D. Wang, Molecular basis of chromatin remodeling by Rhp26, a yeast

CSB ortholog, Proc National Acad Sci. 116 (2019) 201818163. https://doi.org/10.1073/pnas.1818163116.

[165] J. Xu, I. Lahiri, W. Wang, A. Wier, M.A. Cianfrocco, J. Chong, A.A. Hare, P.B. Dervan, F. DiMaio, A.E. Leschziner, D. Wang, Structural basis for the initiation of eukaryotic transcription-coupled DNA repair, Nature. 551 (2017) 653–657. https://doi.org/10.1038/nature24658.

[166] J. Xu, W. Wang, L. Xu, J.-Y. Chen, J. Chong, J. Oh, A.E. Leschziner, X.-D. Fu, D. Wang, Cockayne syndrome B protein acts as an ATP-dependent processivity factor that helps RNA polymerase II overcome nucleosome barriers, Proc National Acad Sci. 117 (2020) 25486–25493. https://doi.org/10.1073/pnas.2013379117.

[167] C. Alén, N.A. Kent, H.S. Jones, J. O'Sullivan, A. Aranda, N.J. Proudfoot, A Role for Chromatin Remodeling in Transcriptional Termination by RNA Polymerase II, Mol Cell. 10 (2002) 1441–1452. https://doi.org/10.1016/s1097-2765(02)00778-5.

[168] A. Németh, J. Perez-Fernandez, P. Merkl, S. Hamperl, J. Gerber, J. Griesenbeck, H. Tschochner, RNA polymerase I termination: Where is the end?, Biochimica Et Biophysica Acta Bba - Gene Regul Mech. 1829 (2013) 306–317. https://doi.org/10.1016/j.bbagrm.2012.10.007.

[169] J. Ocampo, R.V. Chereji, P.R. Eriksson, D.J. Clark, Contrasting roles of the RSC and ISW1/CHD1 chromatin remodelers in RNA polymerase II elongation and termination, Genome Res. 29 (2019) 407–417. https://doi.org/10.1101/gr.242032.118.

[170] N. Spies, C.B. Nielsen, R.A. Padgett, C.B. Burge, Biased Chromatin Signatures around Polyadenylation Sites and Exons, Mol Cell. 36 (2009) 245–254. https://doi.org/10.1016/j.molcel.2009.10.008.

[171] M. Durand-Dubief, J.P. Svensson, J. Persson, K. Ekwall, Topoisomerases, chromatin and transcription termination, Biochem Soc Symp. 2 (2011) 66–70. https://doi.org/10.4161/trns.2.2.14411.

[172] S. Yu, A. Jordán-Pla, A. Gañez-Zapater, S. Jain, A. Rolicka, A.-K. Östlund Farrants, N. Visa, SWI/SNF interacts with cleavage and polyadenylation factors and facilitates pre-mRNA 3′ end processing, Nucleic Acids Res. 46 (2018) gky438-. https://doi.org/10.1093/nar/gky438.

[173] A.E. Hildreth, M.A. Ellison, A.M. Francette, J.M. Seraly, L.M. Lotka, K.M. Arndt, The nucleosome DNA entry-exit site is important for transcription termination and prevention of pervasive transcription, Elife. 9 (2020) e57757. https://doi.org/10.7554/elife.57757.

[174] B.P. Somesh, J. Reid, W.-F. Liu, T.M.M. Søgaard, H. Erdjument-Bromage, P. Tempst, J.Q. Svejstrup, Multiple Mechanisms Confining RNA Polymerase II Ubiquitylation to Polymerases Undergoing Transcriptional Arrest, Cell. 121 (2005) 913–923. https://doi.org/10.1016/j.cell.2005.04.010.

[175] A. Lafon, S. Taranum, F. Pietrocola, F. Dingli, D. Loew, S. Brahma, B. Bartholomew, M. Papamichos-Chronakis, INO80 Chromatin Remodeler Facilitates Release of RNA Polymerase II from Chromatin for Ubiquitin-Mediated Proteasomal Degradation, Mol Cell. 60 (2015) 784–796. https://doi.org/10.1016/j.molcel.2015.10.028.

[176] L. Prendergast, U.L. McClurg, R. Hristova, R. Berlinguer-Palmini, S. Greener, K. Veitch, I. Hernandez, P. Pasero, D. Rico, J.M.G. Higgins, A. Gospodinov, M. Papamichos-Chronakis, Resolution of R-loops by INO80 promotes DNA replication and maintains cancer cell proliferation and viability, Nat Commun. 11 (2020) 4534. https://doi.org/10.1038/s41467-020-18306-x.

[177] K. Maeshima, S. Ide, M. Babokhov, Dynamic chromatin organization without the 30-nm fiber, Curr Opin Cell Biol. 58 (2019) 95–104. https://doi.org/10.1016/j.ceb.2019.02.003.

[178] B.A. Gibson, L.K. Doolittle, M.W.G. Schneider, L.E. Jensen, N. Gamarra, L. Henry, D.W. Gerlich, S. Redding, M.K. Rosen, Organization of Chromatin by Intrinsic and Regulated Phase Separation., Cell. 179 (2019) 470-484.e21. https://doi.org/10.1016/j.cell.2019.08.037.

[179] Y. Zhang, G.J. Narlikar, T.G. Kutateladze, Enzymatic Reactions inside Biological Condensates, J Mol Biol. (2020). https://doi.org/10.1016/j.jmb.2020.08.009.

[180] M. Boehning, C. Dugast-Darzacq, M. Rankovic, A.S. Hansen, T. Yu, H. Marie-Nelly, D.T. McSwiggen, G. Kokic, G.M. Dailey, P. Cramer, X. Darzacq, M. Zweckstetter, RNA polymerase II clustering through carboxy-terminal domain phase separation, Nat Struct Mol Biol. 25 (2018) 833–840. https://doi.org/10.1038/s41594-018-0112-y.

Chapter 2: The nucleosomal acidic patch relieves auto-inhibition by the ISWI remodeler SNF2h

Abstract

ISWI family chromatin remodeling motors use sophisticated autoinhibition mechanisms to control nucleosome sliding. Yet how the different autoinhibitory domains are regulated is not well understood. Here we show that an acidic patch formed by histones H2A and H2B of the nucleosome relieves the autoinhibition imposed by the AutoN and the NegC regions of the human ISWI remodeler SNF2h. Further, by single molecule FRET we show that the acidic patch helps control the distance travelled per translocation event. We propose a model in which the acidic patch activates SNF2h by providing a landing pad for the NegC and AutoN auto-inhibitory domains. Interestingly, the acidic patch also inhibits the INO80 complex, indicating that this substrate feature can regulate remodeling enzymes with substantially different mechanisms. We therefore hypothesize that regulating access to the acidic patch of the nucleosome plays a key role in coordinating the activities of different remodelers in the cell.

Introduction

Eukaryotic genomes are packaged into chromatin, enabling large amounts of DNA to fit into the spatial constraints of the nucleus. This packaging has long been appreciated as a passive barrier to DNA access by nuclear factors. The discovery that chromatin regulators play critical roles in virtually all nuclear processes has informed a more nuanced view of chromatin as a dynamic regulatory platform that coordinates access to the genetic material. The smallest unit of chromatin is the nucleosome, a DNA-protein complex composed of ~150bp of DNA wrapped around an octamer of histone proteins[1]. Nucleosomes can further interact with each other and with other factors to form higher-order structures[2]. Consequently, cells have evolved several sophisticated strategies to

regulate chromatin structure at the nucleosome level. These include the covalent modification of histone proteins and DNA, as well as non-covalent changes to the position or composition of nucleosomes at specific genomic loci. Many of the non-covalent transformations, ranging from sliding nucleosomes to the complete disassembly of the histone octamer, are catalyzed by ATP-dependent chromatin remodeling enzymes [3]. Underscoring their central role in chromatin regulation, remodeling enzymes play essential roles in many processes including transcription, DNA replication, and DNA repair[4–6]. How a relatively small number of remodeler types carry out such diverse regulatory functions remains an area of active research, not least because much remains unknown regarding remodeler mechanisms for substrate recognition and the coupling of that recognition to activity.

Chromatin remodelers are members of the SF2 superfamily of nucleic acid motors, which catalyze noncovalent changes to nucleic acid substrates[3]. Chromatin remodelers, however, are unique in that they specifically mobilize DNA in the context of the nucleosome, where DNA is tightly bound to histone proteins. Remodelers are further classified into families based on the domain architecture of their ATPase subunit. These families differ in their specific biochemical activities[3]. Substantial progress in our general understanding of remodeling mechanisms has been made by asking what elements of the nucleosome are important for remodeling in different families. For example, maximal remodeling by ISWI family remodelers, which primarily slide nucleosomes, requires DNA flanking the nucleosome and the N-terminal tail of histone H4 [7,8]. Conversely, maximal remodeling by SWI/SNF family remodelers, which carry out the most diverse set of changes to nucleosome structure, does not require these nucleosomal epitopes[9]. Less is known about how these substrate cues are recognized and mechanistically coupled to remodeling. Some important insights have come from

biochemical analyses and structures of remodelers in the absence of nucleosomes, which suggest that in the ground state, chromatin remodelers are held in an inactive conformation by family-specific autoinhibitory motifs [10–13]. Binding to specific nucleosomal epitopes is thought to relieve this autoinhibition via conformational changes in the remodeler, but the details of this process remain unclear.

At the same time, structures of several nucleosome-protein complexes are revealing that many of these proteins interact with a conserved acidic patch formed by histones H2A and H2B on the top surface of the nucleosome [14]. These proteins interact with the acidic patch using an “arginine anchor” which nestles into a pocket formed by the α1-2 helices of histone H2A [14]. It is therefore plausible that chromatin remodelers also recognize the acidic patch. Indeed recent work has indicated that mutating the acidic patch reduces the activity of ISWI, SWI/SNF and some CHD family remodeling enzymes[15]. To investigate the mechanistic role of the acidic patch in nucleosome remodeling by the ISWI family of enzymes we used a combination of ensemble and single molecule methods in the context of the human ISWI enzyme, SNF2h. We observe that interactions with the acidic patch activate SNF2h by relieving auto-inhibition mediated by two conserved domains of ISWI enzymes. Our results further suggest that contacts with the acidic patch helps control the distance the nucleosome is moved during translocation events. Finally we find that the acidic patch also stimulates the activity of the INO80 complex. Together, these results highlight the broad and essential role the acidic patch plays in chromatin regulation.

Results

The acidic patch of the nucleosome is important for nucleosome sliding by SNF2h

The human ISWI ATPase, SNF2h, preferentially slides nucleosomes toward longer flanking DNA [8]. As a consequence of this activity, SNF2h slides mononucleosomes towards the center of a DNA strand, an activity that can be detected by a native gel mobility assay[8]. Recent work has shown that mutating residues in the nucleosome acidic patch reduces the ability of SNF2h to expose nucleosomal DNA to restriction enzymes[15]. To investigate the mechanism by which such mutations affect the nucleosome sliding activity of SNF2h and to determine if these mutations affected SNF2h binding or catalysis, we first used a mutant H2A in which 4 key residues in the H2A acidic patch are replaced with alanines (E61A, E64A, D90A, and D92A) (Figure 2.1A). We call nucleosomes in which all four of these H2A residues have been mutated to alanines "APM" (acidic patch mutant) nucleosomes. Using a native gel mobility assay, we measured remodeling rates of wild type (WT) and APM mononucleosomes containing 60 bp of DNA flanking one end of the nucleosome (0/60) (Figure 2.1B). APM nucleosomes are centered substantially slower than WT nucleosomes under conditions where SNF2h is in excess of nucleosomes (Figure 2.1B and 2.1C). Since the acidic patch has been shown to be critical for nucleosome binding by several chromatin proteins, we expected the apparent $K_{m,}$ K_m^{app}, to be increased with APM nucleosomes. Interestingly however, K_m^{app} is affected substantially less by mutation of the acidic patch than the maximal rate constant for remodeling, k_{max} (Figure 2.1D, 61nM to 280 nM, corresponding to ~4.5-fold increased K_m^{app}, versus 2.5 min^{-1} to 0.012 min^{-1}, corresponding to ~200-fold reduced k_{max}). These results indicate that the acidic patch plays a larger role in regulating maximal nucleosome sliding activity than nucleosome binding. We also measured ATP hydrolysis under

conditions where nucleosomes are in excess of SNF2h. At saturating nucleosome concentrations, APM nucleosomes stimulate ATP hydrolysis 4-fold less than WT (Figure 2.1G, Figure 2.2). Together, these results imply that the acidic patch plays a critical role in coupling ATP hydrolysis to remodeling after the binding step.

To further investigate the importance of the acidic patch, we asked whether binding by another factor to the acidic patch could compete for nucleosome sliding by SNF2h. We used a peptide derived from the latency associated nuclear antigen (LANA) from Kaposi's sarcoma-associated herpesvirus that has previously been shown to interact directly with the acidic patch via an arginine anchor [16]. We carried out these experiments using sub-saturating concentrations of SNF2h. Under these conditions most of the nucleosomes are unbound, allowing direct competition between the LANA peptide and SNF2h for the acidic patch. The presence of the LANA peptide dramatically slows remodeling by SNF2h in a dose-dependent manner (~200-fold reduction in rate constant at 50μM LANA peptide), while a peptide with a mutant arginine anchor does not have a detectable inhibitory effect (Figures 2.1E and F). We measured a K_I of 1.2 μM for inhibition by the LANA peptide, within 5-fold of its published affinity for the nucleosome (Figure 2.1F) (Fang et al., 2016). These results indicate that remodeling by SNF2h requires an interaction with the acidic patch that is mutually exclusive with the binding of acidic patch interacting factors such as the LANA peptide. The results are also consistent with recent work showing that the LANA peptide can inhibit the restriction enzyme accessibility activity of the SNF2h containing complex, ACF [15].

We next investigated if the acidic patch residues act independently or cooperatively by measuring the effects of individual mutations. Interestingly, except for residue E64**,** all the single alanine mutants have comparable defects as the four point

mutants combined (Figure 2.3). This observation suggests that three of the four acidic patch residues tested here act cooperatively to promote sliding by SNF2h.

The AutoN and NegC regions of SNF2h cooperate with the acidic patch to enable maximal remodeling

We next investigated which regions of SNF2h might functionally interact with the acidic patch. In principle, these would include (i) regions that directly contact the acidic patch and (ii) regions that do not directly contact the acidic patch, but whose function is energetically coupled to the presence of the acidic patch.

To investigate regions that may directly contact the acidic patch we carried out cross-linking mass spectrometry using the zero-length, carbodiimide based reagent EDC. This method catalyzes the formation of new amide bonds between protein carboxylates, such as the side chains of aspartate and glutamate residues, and amino groups and is therefore well suited to probing electrostatic interactors of the acidic patch. Hundreds of high confidence cross-linked residue pairs were identified using this approach. To focus on mechanistically meaningful domain-domain interactions, we employed a semi-quantitative mass spectrometry method to compare the extent of SNF2h-nucleosome cross-linking in the presence of different nucleotides (Figure 2.4B). In previous work we have shown that ADP•BeF_x mimics an activated state of the SNF2h-nucleosome complex [17–19]. We therefore, focused on domain level interactions that were enriched at least two-fold in the presence of ADP•BeF_x relative to ADP.

Cross-links between the H4 tail and RecA lobe 2 of SNF2h are strongly enhanced in the ADP•BeF_x state (Figure 2.4B). This result is consistent with previous work showing that the H4 tail activates ISWI remodelers and promotes a restricted active site conformation in the presence of ADP•BeF_x [7,18,20]. We also found that the ADP•BeF_x

state promotes specific cross-links between the H2A/H2B acidic patch and lysines in the extended AutoN region, RecA lobe 1, the NegC region, and the DNA binding HAND-SANT-SLIDE (HSS) region of SNF2h (Figure 2.5). While cross-links between the acidic patch and the AutoN, HSS and NegC regions are compatible with structural constraints from previous studies, the cross-links with the RecA lobe 1 are not easily explained. Multiple studies of ISWI remodelers suggest that their RecA lobes bind at a location two DNA helical turns from the nucleosome dyad (SHL±2), quite far from the H2A/H2B acidic patch [21–24]. We hypothesize that the RecA-acidic patch cross-links arise from a population of higher-order SNF2h-nucleosome aggregates in our mass-spec samples and therefore focus below on cross-links to the remaining three regions.

To test the functional significance of cross-links to AutoN, we mutated the lysines that crosslink to the acidic patch in the ADP•BeF_x state. However, none of the mutants significantly altered remodeling by SNF2h (Figure 2.6). These results suggest that the lysines in the AutoN region are in proximity to the acidic patch but do not make mechanistically significant interactions. We speculated, however, that other residues in AutoN might make functional interactions with the acidic patch. Previous work has indicated that many nucleosome binding proteins recognize the acidic patch via arginine residues. Near the AutoN lysines that crosslink to the acidic patch resides a key autoinhibitory motif specific to ISWI family remodelers that contains two arginine residues (Figure 2.4 - 2.5, R142 and R144). Autoinhibition by these arginine residues is relieved by a basic patch on the H4 tail, a nucleosomal epitope essential for maximal remodeling by ISWI-family remodelers [10,25]. We tested whether R142 and R144 functionally cooperate with the acidic patch by generating a mutated version of SNF2h with the two critical arginines of AutoN mutated to alanine (2RA), and measured the remodeling activity of this mutant. Consistent with previous reports, 2RA SNF2h remodels WT nucleosomes ~2-fold

faster than WT SNF2h [10,13]. However, 2RA SNF2h remodels APM nucleosomes ~50-fold faster than WT SNF2h (Figure 2.4F). This corresponds to a ~25-fold reduced dependency on the acidic patch for remodeling with 2RA SNF2h (Figure 2.4F). The same trend was also seen by an ensemble FRET remodeling assay (Figure 2.7). Together, these data suggest that the acidic patch contributes to relief of autoinhibition by R142 and R144 in AutoN. Since arginine residues are known to mediate this interaction in other systems, binding of either of the two arginines in AutoN to the acidic patch could provide a physical explanation for acidic patch recognition. However, given that neither carbodiimide chemistry nor any other commonly used cross-linking chemistry labels arginine residues, we cannot determine whether R142 and R144 make direct contacts with the acidic patch based on our mass-spectrometry data. We were unable to observe detectable binding between an AutoN peptide containing the 2R residues and the nucleosomal acidic patch through pull down assays (data not shown), suggesting that either these residues do not physically interact with the acidic patch or the surrounding regions of the SNF2h protein are required for stable binding.

To investigate the functional significance of cross-links to the NegC region of SNF2h, we determined the effect of replacing a stretch of 32 residues in NegC with a flexible serine-glycine linker (mNegC). NegC is another autoinhibitory region of SNF2h that imposes flanking DNA length sensitivity on SNF2h by specifically slowing down remodeling of nucleosomes without flanking DNA [17]. Consistent with previous work, mNegC SNF2h slides WT 0/60 nucleosomes ~1.2-fold faster than WT SNF2h (Figures 2.4E and F) [17]. However, mNegC SNF2h slides APM nucleosomes ~100-fold faster than WT SNF2h (Figure 2.4F). As a result, sliding of APM nucleosomes by mNegC SNF2h is only ~2-fold slower than WT nucleosomes. Thus the mNegC mutation almost completely

rescues the defect of the acidic patch mutation. These results suggest that residues in NegC also link activation of nucleosome sliding to acidic patch recognition.

The third category of cross-links entailed lysine residues in the HSS regions. Mutants in these lysines greatly reduced remodeling and, in contrast to the 2RA and mNegC SNF2h mutants, did not rescue the defects caused by the acidic patch mutations (data not shown). It is possible that the defects caused by these lysine mutations reflect direct contacts between the HSS residues and the acidic patch. However, because the HSS also contacts flanking DNA, the reduction in sliding rate could also arise from defects in binding DNA.

To better understand which crosslinks are dependent on H2A acidic patch binding, we also performed SNF2h-nucleosome cross-linking reactions with ADP•BeF_x in the presence of the LANA peptide which competes for acidic patch binding (Figure 2.1E). Addition of the LANA peptide substantially reduced crosslinks between the H2A acidic patch and both AutoN and NegC (Figure 2.7). In contrast, crosslinks between the HSS and the acidic patch were less strongly affected by LANA addition (Figure 2.7). This suggests that HSS positioning near the acidic patch in the ADP•BeF_x state is not strictly dependent on direct binding to the region of the H2A acidic patch contacted by the LANA peptide. As a result, we cannot unambiguously interpret HSS-acidic patch crosslinks as reflecting mechanistically significant interactions. Together, these data suggest that acidic patch recognition is strongly linked to relief of autoinhibition by NegC and AutoN for nucleosome sliding by SNF2h. Furthermore, activation of SNF2h involves conformational changes that bring both of these autoinhibitory domains and the HSS in closer proximity to the acidic patch.

The acidic patch is required to promote the translocation phase of the SNF2h reaction

To gain additional insight into which steps in the remodeling cycle involve interaction with the acidic patch, we turned to a single-molecule FRET assay (smFRET; Figure 2.8A). This assay is analogous to the ensemble FRET remodeling assay described in Figure 2.9, in that the activity of SNF2h in sliding nucleosomes away from DNA ends increases the distance between a donor and acceptor dye pair, and thus decreases the measured FRET efficiency. However, with smFRET we can follow the remodeling of individual, surface-immobilized nucleosomes, and thereby gain insights into the activity of SNF2h reaction steps that are obscured in asynchronous, population-averaged ensemble assays.

smFRET has previously been used to study remodeling by several ISWI family members, as well as by remodeling complexes from the SWI/SNF and INO80 families [3,26–29]. A key insight revealed by these smFRET studies is that ISWI family remodelers do not slide nucleosomes in a continuous manner, such that FRET decreases linearly over time, but rather in a series of alternating phases: a “pause” phase, in which FRET (and therefore nucleosome position) remain constant, and a “translocation” phase, in which the nucleosome is moved relative to the DNA end. These repeating pause phases, which so far appear to be specific to ISWI, are essential to our understanding of the mechanism of action of ISWI remodelers, because the overall remodeling rates observed in ensemble assays are dominated by the durations of the pause phases, not the translocation rate itself. Moreover, substrate cues such as the H4 tail and flanking DNA have been shown to be sensed in the pause phase, not the translocation phase, for ISWI family remodelers [29]. That is, shorter flanking DNA or mutation of the H4 tail increases the durations of the pauses, thereby decreasing the overall remodeling rate, while having no effect on the

actual sliding rate of the nucleosome. These results suggest a separation of regulation and activity in ISWI remodelers: translocation events are regularly interrupted by pauses that allow for the periodic interrogation of substrate cues. This pausing behavior also explains the ability of ISWI remodelers such as ACF to keep nucleosomes centered: if the nucleosome is translocated off-center, the interruption of this translocation by a new pause can trigger translocation in the opposite direction, restoring the nucleosome to a centered position.

As shown in Figure 2.8B, we find that SNF2h alone, like the ACF complex and the yeast ISWI enzymes, shares this alternating pause and translocation behavior at the single-molecule level. We first wished to ascertain whether the acidic patch, like other nucleosomal epitopes recognized by ISWI remodelers, affects the regulatory pause phase. Because the rate of remodeling of APM nucleosomes by SNF2h is significantly slower (on the order of hours) than the rate of dye photobleaching (on the order of minutes; Figure 2.10B), we assembled nucleosomes with a single point mutation in the acidic patch (E64R nucleosomes). We used the E64R mutation rather than the E64A mutation because the defect caused by this mutation was better rescued by the 2RA mutation in SNF2h than the defect in E64A (Figure 2.3). The single-point mutation (E64R) is less deleterious than mutating all 4-acidic residues (APM), and SNF2h remodels E64R nucleosomes ~40-fold more slowly than WT nucleosomes as opposed to 200-fold more slowly with APM nucleosomes (Figure 2.3). However, this remodeling rate is still very slow relative to the timescales typically measured by smFRET, which posed two additional challenges: an increase in the number of noise events (dye blinking, intensity fluctuations, etc) per remodeling trajectory, and an increase in the amount of data to be analyzed. These challenges were addressed through the use of custom in-house smFRET analysis software (“Traces”, https://github.com/stephlj/Traces) [3,30] to streamline the analysis of

large data sets, and the adaptation of a computationally fast, versatile, open-source hidden Markov model (HMM) library called pyhsmm to quantify the durations of the pauses (see Methods).

As shown in the example trajectories in Figure 2.8C, remodeling of E64R nucleosomes by SNF2h proceeds through the same alternating pause and translocation phases as does remodeling of WT nucleosomes. However, the pauses are noticeably longer with E64R nucleosomes, by at least a factor of 2 (Figure 2.8D), indicating that the acidic patch epitope, like other substrate cues, is indeed sensed during the regulatory pause phase. We note that remodeling of E64R nucleosomes in ensemble assays is significantly slower than the photobleaching rate (Figure 2.10B), so that by smFRET we only detect the fraction of remodeling events that are faster than photobleaching. As a result, the remodeling rate obtained for the E64R nucleosomes by smFRET represents an upper bound on the true remodeling rate (i.e. the E64R nucleosomes appear to remodel faster by smFRET than by ensemble assays (Figure 2.10B).

Given the ability of the 2RA mutation of the AutoN motif to partially rescue remodeling defects in APM nucleosomes in ensemble assays (Figure 2.4C), we next asked whether this rescue is due to a restoration of wild-type pause durations. In agreement with our ensemble results (Figure 2.4C), 2RA SNF2h remodels WT nucleosomes slightly faster than SNF2h by reducing pause durations (Figure 2.8D). The reduction is minor (~1.3 fold), consistent with a previous smFRET study of the effect of the 2RA mutation on pause durations for the ACF complex [29]. Furthermore, 2RA rescues the deleterious effect of the E64R acidic patch mutation, by nearly restoring wild-type pause durations (Figure 2.8D). The effects of the E64R nucleosomal mutation and the 2RA SNF2h mutation on pause durations therefore mirror the effects on overall remodeling rates of APM nucleosomes: 2RA remodels E64R nucleosomes nearly as fast

as SNF2h remodels WT nucleosomes, but not as fast as 2RA remodels WT nucleosomes (Figure 2.3). These results are consistent with a model in which relief of autoinhibition of the AutoN motif of SNF2h through direct or indirect interactions with the acidic patch enable pause exit (that is, promote the translocation phase).

The example traces in Figure 2.8C suggest an additional defect in remodeling of E64R nucleosomes: a reduction in the distance the nucleosome is moved during each translocation event (which we called the step size). Note that after two translocation events, WT nucleosomes with SNF2h or 2RA are moved from ~0.95 FRET to ~0.4 FRET (Figure 2.8C top and second from bottom), whereas after two translocation events the nucleosome in the E64R/SNF2h example trace has moved from ~0.95 FRET to ~0.75 FRET. Step size, like pause duration, plays an important role in regulating ISWI remodeler activity: since the pause durations dominate the overall remodeling rate, a smaller step size, which means more pauses per unit distance that the nucleosome is translocated, will mean a significant reduction in the overall remodeling rate (as observed in ensemble assays).

Step sizes can be quantified by converting the change in FRET between subsequent pauses to a change in the number of base pairs of DNA between the Cy5-labeled DNA end and the edge of the nucleosome. We accomplish this conversion by means of a calibration curve, described previously [31]. Like other ISWI family remodelers, SNF2h moves WT nucleosomes with an initial large step (~8 bp) followed by a smaller (~5 bp) step (Figure 2.8E, Figure 2.11) [26,27]. However, SNF2h moves E64R nucleosomes a shorter distance in each translocation phase, as indicated by the leftward shift of the cumulative distributions in the red curves of Figure 3E, relative to the black curves (on average, E64R nucleosomes move about 6 bp in the first translocation and about 4 bp in the second (Figure 2.11). Mutation of AutoN has little effect on the step size

in the context of WT nucleosomes, but largely restores the step size in the context of E64R nucleosomes to that of SNF2h with WT nucleosomes (Figure 3E, magenta and blue curves). Given that ISWI family remodelers have been shown to translocate a nucleosome in elementary steps of 1-2 bp [27], our results suggest that with E64R nucleosomes, SNF2h takes fewer of these elementary steps in succession during the translocation phase, before entering a new pause phase.

The major contributions to the remodeling defects observed with SNF2h and APM nucleosomes can therefore be attributed to two effects: first, an increase in pause duration, and second, a decrease in the distance travelled per translocation event, meaning that there are more (and longer) pauses in APM remodeling reactions per unit distance that the nucleosome is moved. Both of these effects are rescued by the 2RA mutation of the AutoN motif of SNF2h. We propose that the acidic patch is important for relieving autoinhibition by AutoN and thereby promoting exit from the pause phase. Further, we propose that the acidic patch is also involved in keeping AutoN out of the active site until the nucleosome has been translocated to the full extent (~8 bp initially, ~5 bp subsequently) and a new pause phase is entered (Figure 2.13).

The acidic patch is used by both ISWI and INO80 complexes

The ISWI ATPase forms complexes with several accessory proteins that regulate its localization and activity [32–35]. ACF is one of the best studied of these complexes. ACF is a heterodimer of the ISWI ATPase subunit (SNF2h in humans) and the accessory subunit Acf1, and is implicated in gene repression, DNA replication, and DNA repair [36–38]. Biochemically, human ACF has the same core activity as SNF2h, but displays greater nucleosome affinity, enhanced sliding rates, and better kinetic discrimination of flanking DNA length [8,32]. Despite these similarities, recent evidence suggests that ACF has

some mechanistic differences from SNF2h on its own. For instance, in the context of ACF, AutoN regulates flanking DNA length sensing through interaction of an Acf1-specific domain called WAC [29]. SNF2h alone has no comparable domain. Furthermore, recent work has suggested that mutating the nucleosomal acidic patch causes a smaller defect in remodeling by ACF compared to SNF2h [15]. Given this difference, we asked whether ACF requires the acidic patch for remodeling beyond binding. At saturating concentrations of ACF, where binding does not contribute to the overall remodeling rate, ACF slides APM nucleosomes 10-fold more slowly than WT (Figure 2.12A), indicating that ACF also uses the acidic patch in a step after binding. However, consistent with previous work, ACF is less dependent on the acidic patch compared to SNF2h alone [15].

We next asked whether ISWI-family complexes uniquely use the acidic patch, or whether it is also used by other chromatin remodeling enzymes. Recently, it was shown that while some CHD family remodelers slide nucleosomes largely independent of the acidic patch, others are dependent on it [15,39]. It has been further shown that SWI/SNF family enzymes also require the acidic patch for maximal activity [15]. These observations raise the possibility that acidic patch is a feature used by most remodeling enzymes. To address this issue we determined if the acidic patch is required by yeast INO80, which is in a distinct family from the CHD, ISWI and SWI/SNF families. INO80, like ACF, slides nucleosomes preferentially in the direction of longer flanking DNA and can also create evenly spaced nucleosome arrays [40]. This sliding activity is thought to be important for positioning the +1 nucleosome at transcription start sites [41]. Interestingly, we find that INO80 slides APM nucleosomes ~200-fold more slowly than WT nucleosomes at saturating concentrations (Figure 2.12B). This result indicates that INO80 also uses the acidic patch post-binding, but is more dependent on the acidic patch than the ACF complex.

Discussion

In this study, we investigate the role of the highly conserved H2A acidic patch in chromatin remodeling by ISWI enzymes. We find that the acidic patch is used post-binding in order to activate remodeling by both INO80 and ISWI family remodelers. Furthermore, using a combination of ensemble and single molecule methods, we show that the acidic patch is used by SNF2h to relieve autoinhibition by the conserved AutoN and NegC motifs. Below we explore the mechanistic and regulatory implications of these results.

ATP-dependent chromatin remodeling enzymes carry out specialized reactions on a complex substrate. Understanding how recognition of this substrate is coupled to activity can provide a means to understanding common principles underlying ATP-dependent chromatin remodeling mechanisms. Owing to decades of study, ISWI enzymes provide a useful model system to address this question. On the basis of crosslinking and footprinting studies, the ATPase domain of ISWI enzymes is thought to bind and translocate DNA two helical turns from the nucleosomal dyad (SHL±2) [21–24]. Work from several groups has also shown that for ISWI remodelers, recognition of both the H4 tail and flanking DNA enhances remodeling activity post-binding [8,10,42]. While the mechanisms by which these nucleosome cues activate remodeling are not well understood, the ISWI domains that recognize these cues are known. The C-terminal HAND-SANT-SLIDE (HSS) domain mediates flanking DNA recognition, while the H4 tail appears to be directly recognized by the second RecA lobe within the ATPase domain [13,21]. The acidic patch resides on a surface near SHL±6, far from where the ATPase domain engages the nucleosome. How then might the acidic patch be recognized and used by ISWI remodelers?

Our results suggest that two known autoinhibitory regions of ISWI enzymes, the AutoN region and the NegC region, functionally interact with the acidic patch, because mutating these regions dramatically reduces the dependence of SNF2h on the acidic patch for sliding. This suggests that a large role of the acidic patch is to relieve autoinhibition by both AutoN and NegC. While we do not have evidence for a direct interaction between the acidic patch and the two arginines in AutoN, our cross-linking mass spectrometry data suggests that activation of the enzyme places residues within both AutoN and NegC near this location. Our smFRET work here and previous smFRET work suggests that the AutoN region inhibits the transition from the pause phase to the translocation phase [29]. It has been shown that flanking DNA and the H4 tail are both sensed in the pause phase[29]. Further, previous ensemble work has suggested that the NegC region inhibits the transition between a flanking DNA sensing state of SNF2h and a translocation competent state of SNF2h [17]. We therefore propose that the acidic patch helps promote the translocation competent state of SNF2h by providing an alternative binding site for NegC and AutoN (Figure 2.13).

In addition to an increase in pause durations with the acidic patch mutations, the amount of DNA translocated within a translocation phase is reduced compared to WT nucleosomes. We hypothesize that translocation is interrupted by premature reversion of the enzyme to the autoinhibited state in the absence of stabilizing interactions with the acidic patch (Figure 5). As a result, more pauses are encountered per distance translocated. Our results lead to a model in which the acidic patch provides a binding surface for NegC and AutoN that sequesters these regions from inhibiting SNF2h (Figure 2.13). Combined with previous work, our results underscore how the strong coupling of relief of autoinhibition to recognition of two conserved nucleosome cues (the H4 tail and the acidic patch) make this motor exquisitely specific for its complex substrate.

The acidic patch increases K_m^{app} for SNF2h by ~5-fold, suggesting that interactions with the acidic patch also stabilize SNF2h binding. Thus the acidic patch appears to be used in at least two distinct steps of the SNF2h remodeling reaction. What residues in SNF2h might be interacting with the acidic patch in these two steps? In contrast to the rescuing effects of AutoN mutations on maximal activity, AutoN mutations additively increase K_m^{app} beyond solely mutating the acidic patch (Figure 2.14). This suggests that AutoN and the acidic patch do not cooperate in the ground state. It is thus possible that different SNF2h domains contact the acidic patch in different steps of the remodeling reaction. The different set of cross-links observed between the acidic patch and SNF2h regions in the ADP vs. ADP•BeF_x state are consistent with such a possibility.

Based on previous work, we have hypothesized that SNF2h undergoes a large conformational change prior to adopting a translocation competent state that repositions the C-terminus from binding flanking DNA towards binding the nucleosome core [17]. Our crosslinking-MS data provides additional insights into the structural rearrangements that accompany enzyme activation. We find that crosslinks between the H2A/H2B acidic patch and the SANT domain increase in the ADP•BeF_x-bound state compared to the ADP-bound state (Figure 2.4B), consistent with the HSS binding to the nucleosome core. Interestingly, these crosslinks are not substantially reduced by LANA peptide binding, suggesting that the location of the HSS in the ADP•BeF_x-bound state is not strongly dependent on direct contacts with the residues contacted by the LANA peptide (Figure 2.7). This result raises the possibility that the SANT domain and LANA peptide occupy adjacent regions on the nucleosome core. The SANT domain may then cross-link to the acidic patch when these sites are transiently exposed due to dynamics in LANA peptide binding. In contrast, NegC and AutoN crosslinks to the acidic patch are substantially reduced by the LANA peptide, suggesting LANA binding directly or indirectly

displaces these regions from the nucleosome. Overall our results suggest that the key accessory regions of SNF2h namely, HSS, NegC and AutoN, are all positioned near the acidic patch in the activated state. In agreement with this observation, crosslinks between the C-terminus of SNF2h and NegC increase in the ADP•BeF_x state (Figure 2.4B). The close positioning of multiple SNF2h accessory domains near the acidic patch raises the possibility that contacts between accessory domains may play a role in promoting the translocation-competent state. While substantial future work would be needed to test this possibility, it is analogous to recent observations with the yeast CHD1 remodeling motor that contacts between its N-terminus and the C-terminal DNA binding domain regulate the sliding reaction [43].

Most chromatin remodeling ATPases also form large multi-subunit complexes, which regulate the activity and specificity of the remodeling reaction. Here we find that the human ISWI complex, ACF, requires the acidic patch for maximal activity but shows a ~20-fold smaller defect upon mutation of the acidic patch than observed with SNF2h alone. This result is qualitatively consistent with recent studies showing that the acidic patch has a smaller role in the activity of ACF vs. SNF2h [15]. Our results here provide a mechanistic framework for understanding these recent observations. In particular, our results suggest that the accessory protein Acf1 alters the mechanism of relief of autoinhibition by the acidic patch in a manner that makes the reaction less dependent on the acidic patch, perhaps by providing an alternative binding partner for the AutoN and NegC domains. Such a domain would be analogous to the WAC motif of Acf1, which provides an alternative binding partner for the H4 tail [29]. In contrast to ACF, we find that the yeast INO80 complex, a large multisubunit complex, is as dependent on the acidic patch for nucleosome sliding as the isolated SNF2h ATPase. Importantly, INO80 family remodelers are insensitive to the presence of the H4 tail and no AutoN-like or

NegC like motif has been identified in the ATPase subunit of INO80[40]. The acidic patch must then activate INO80 through a mechanism distinct from ISWI complexes. Determining how the acidic patch is used by INO80 ATPases, and what roles the ATPase and accessory subunits play in this mechanism, are important areas of future study.

Combined with previous results [15], our results suggest that several families of chromatin remodelers require the acidic patch for remodeling. However, it is possible that this surface is not a universal requirement for chromatin remodeling, as yeast CHD1 can remodel nucleosomes largely independent of the acidic patch [39]. CHD1 instead uses an unidentified aspect of the histone H2A/H2B dimer to promote remodeling [39]. Yeast CHD1 and ISWI family remodelers have been thought to share a common remodeling mechanism, as these families share biochemical activities, like nucleosome sliding and spacing, and substrate cues required for maximal remodeling activity, such as the H4 tail and flanking DNA [44,45]. However, the enormous difference in dependence on the acidic patch between yeast CHD1 and ISWI enzymes raise the possibility that these families remodel nucleosomes through distinct mechanisms [39]. Importantly, while yeast CHD1 shares domains with ISWI remodelers such as the SANT-SLIDE domains at the C-terminus and a version of the NegC region, called the C-terminal bridge [11,46], CHD family remodelers do not appear to possess an AutoN motif. Instead, remodelers like CHD1 have an N-terminal double chromodomain which has an analogous role as an autoinhibitiory domain that is relieved by H4 tail binding [11].

At a primary level, the requirement of the acidic patch provides a powerful means for remodelers to sense and respond to chromatin structure and nucleosome content. Thus, nucleosomes lacking histone H2A-H2B dimers or containing a modified acidic patch through histone variants or covalent modifications may be recognized and remodeled differently than canonical nucleosomes by different remodelers [15]. Consistent with this

possibility, nucleosomes containing histone H2Az, which have an extended acidic patch, are remodeled ~2-fold faster by ISWI complexes than canonical nucleosomes [47]. Analogously, recent work has shown that find that INO80 preferentially slides H2AZ nucleosomes over H2A nucleosomes [48]. Finally, given the growing list of factors that recognize the acidic patch, it is likely that remodelers and other chromatin binding proteins compete for access to the acidic patch. Indeed, binding by the LANA peptide to the acidic patch competes for remodeling by SNF2h. Sensitivity to the acidic patch could be a general mechanism to regulate the outcome of chromatin remodeling at loci where remodelers and other factors are jostling for access to their chromatin substrates.

Acknowledgements

We thank Matthew Johnson for help in developing Traces, adapting his physmm code to smFRET data analysis, and the statistical analysis of smFRET data. We thank Song Tan for the Histone H2A E61A, E64A, D90A, D92A expression plasmid, and Greg Bowman, Robert Levendosky, and Cynthia Wolberger for purified Histone H2A E64R and H2A D90R/E92A. We thank Sebastian Deindl for providing an implementation of the Kerssemakers step-finding algorithm [49] in Matlab. We thank Chari Noddings for help with the constitutive dimer experiments. We also thank Coral Zhou, Laura Hsieh, and Muryam Gourdet for INO80 purification, Julia Tretyakova for histone purification, Serena Sanuli for help generating some of the nucleosome substrates, and all members of the Narlikar Lab for helpful discussions. This work was supported by a grant from the NIH to G.J.N (R01GM073767), an NSF predoctoral fellowship to N.G., a Leukemia and Lymphoma Society Career Development Program Fellow award to S.J, and a grant from the Adelson Medical Research Foundation to A.L.B. The Thermo Scientific Fusion Lumos was funded by the UCSF Program for Breakthrough Biomedical Research (PBBR).

Appendix to Chapter 2

A constitutive dimer of SNF2h is equally sensitive to disruption of the acidic patch

SNF2h remodels nucleosomes most efficiently as a dimer with two protomers bound on opposing faces of the nucleosome [17,59]. As a result, mutation of the acidic patch may disrupt nucleosome sliding through disruption of SNF2h dimerization on the nucleosome. To test this possibility, we measured remodeling of mononucleosomes using a constitutive covalent dimer of SNF2h created with the SpyCatcher system used previously to investigate SNF2h remodeling. We found that WT-WT SNF2h remodeling was compromised ~100-fold with APM nucleosomes, which is a comparable effect as with WT SNF2h (Supplemental Figure 2.1). Saturating concentrations are achieved at ~10-fold lower concentrations on APM nucleosomes with WT-WT SNF2h when compared to unconnected SNF2h (Supplemental Figure 2.1), suggesting a higher affinity for APM nucleosomes. The higher affinity of WT-WT SNF2h for APM nucleosomes is consistent with connected SNF2h remodeling nucleosomes as an intramolecular dimer.

Disrupting autoinhibition in a single protomer of a SNF2h dimer retains length sensing and does not induce a tug-of-war between protomers

Relieving autoinhibition represents the rate limiting step of remodeling by SNF2h after binding [25-27,29]. Sensing of flanking DNA is enforced by autoinhibition as mutation of NegC, which prevents sliding on nucleosomes with short flanking DNAs, also compromises flanking DNA length sensing and, as a result, also compromises nucleosome centering [17]. Furthermore, it's been proposed that autoinhibition may help coordinate the two protomers in a SNF2h dimers to prevent a tug-of-war by preventing an opposing protomer from competing during sliding [17]. We wondered whether disrupting autoinhibition in a single protomer of a constitutive SNF2h dimer might create a tug-of-

war between protomers and/or disrupt nucleosome centering. Surprisingly, both WT-AutoN(2RA) and WT-mNegC SNF2h both remodel WT nucleosomes at comparable rates to WT-WT SNF2h and generate predominantly centered nucleosomes (Figure A1). Both of these mutatnts are likely to remodel as intramolecular dimers as saturating concentrations of SNF2h can be achieved at ~10-fold lower concentrations of enzyme than with monomeric SNF2h. It remains unclear how SNF2h coordinates remodeling between protomers. It is possible that for both WT-AutoN(2RA) or WT-mNegC SNF2h the mutant protomer preferentially associates with the nucleosome face with longer flanking DNA, reducing the need for the two protomers to have equal strength of autoinhibition. It is also possible that there are additional mechanisms to prevent a second protomer of SNF2h from competing with a sliding protomer, which may also be coupled to flanking DNA length. The sliding protomer may inhibit the competing protomer "in trans" through direct contacts with non-catalytic domains, or there may be allosteric coordination through conformational changes in the nucleosome (see Chapter 3).

Disrupting autoinhibition in a single protomer reduces dependence on the acidic patch

Relieving autoinhibition is the major function of the acidic patch. We wondered whether disruption of autoinhibition in a single protomer of a SNF2h dimer is sufficient to improve remodeling. Mutation of NegC or AutoN on a single protomer imrpoved remodeling ~10-fold on APM nucleosomes (Supplemental Figure 2.1). However, this effect is not identical to completely disrupting autoinhibition by these two domains as remodeling with these asymmetric mutants on APM nucleosomes is still respectively ~3-fold and ~6-fold slower than AutoN (2RA) and mNegC mutant monomeric SNF2h (Supplemental Figure 2.1). This suggests that disruption of auroinhibition in a single

protomer is sufficient to restore most, but not all, of the defect associated with APM nucleosomes. Preferential association of the mutant SNF2h protomer with the face of the nucleosome with longer flanking DNA could help explain the large effects associated with mutating a single protomer of a dimer and further characterization of the binding orientation of these constitutive dimers is necessary. Additionally, autoinhibition between the two protomers within a dimeric SNF2h nucleosome complex may also be coupled in a such a way that disruption of autoinhibition in one protomer compromises autoinhibition in the opposing protomer

Residues in the H2A acidic patch additively contribute to remodeling by INO80

Earlier we demonstrated that three residues in the H2A acidic patch act cooperatively to promote remodeling by SNF2h. We wondered if this might be the same for nucleosome sliding by INO80. To do this we measured remodeling of 0/80 nucleosomes with INO80, which maximally stimulate nucleosome sliding [31]. Specifically, we compared remodeling of WT nucleosomes to nucleosomes with different point mutants in the acidic patch. In contrast to SNF2h, mutating any of the residues of the acidic patch has effects that are intermediate to mutating all the residues (Supplemental Figure 2.2). This further supports the hypothesis that the acidic patch activates sliding by INO80 through a mechanism distinct from SNF2h.

Materials and Methods

Expression and purification of chromatin remodeling enzymes

SNF2h was purified from *E. coli* as described previously with minor modifications (Leonard and Narlikar, 2015). DNA was precipitated following cell lysis by addition of 5% w/v Polyethylenimine (P3143, Sigma-Aldrich, St. Louis, MO) pH 7.9 dropwise to a final concentration of 0.1% and clarified by centrifugation. Following Cobalt affinity purification, the 6xHis tag was cleaved overnight with TEV protease and dialysed into SEC Buffer. TEV-cleaved SNF2h was then purified by anion exchange chromatography using a HiTrap Q column and Size Exclusion Chromatography (GE Life Sciences, Pittsburgh, MA). SNF2h concentration was determined by SDS-PAGE with BSA protein standards and staining with SYPRO Red (Thermo Fisher, Waltham, MA).

Human ACF was expressed and purified recombinantly from Sf9 insect cells by FLAG immunoaffinity purification as described previously with minor modifications [50]. SNF2h-FLAG and Acf1 were expressed separately via infection with baculovirus. Nuclear extracts from each construct were generated and mixed together at a 10:1 Acf1:SNF2h-FLAG volume ratio to ensure full assembly of the complex. This mixture was then bound to FLAG M2-affinity resin (Sigma-Aldrich, St. Louis, MO), washed with increasing KCl concentrations, and eluted with buffer with 100mM KCl and 1mg/mL FLAG Peptide. ACF concentration was determined by SDS-PAGE with BSA standards and based on the intensity of the Acf1 band.

INO80 was purified by FLAG immunoprecipitation based on previously published methods [31,51]. Briefly, *S. cerevisae* with endogenously flag tagged INO80 was grown in YEPD at 30ºC to saturation. Cells were pelleted by centrifugation for 10 min at 5000 rpm, resuspended with buffer H0.3, and pelleted again. Pelleted cells were then extruded

through a 60mL syringe into liquid nitrogen to create “noodles”. Cell “noodles” were then lysed using a Tissue Lyser II (Qiagen, Hilden Germany) cooled in liquid nitrogen. Frozen lysate powder was resuspended in equal volume of H0.3 and spun in an SW28 rotor for 2 hr at 25,000 rpm at 4ºC. Clarified lysate was mixed with equal volume buffer H0.3 and applied to FLAG M2-affinity resin (1 mL bead slurry per 40 mL of cleared lysate) equilibrated with H0.3 and incubated for 3 hours at 4ºC. Resin was washed with 3x50 mL buffer H0.5 followed by 3x10 mL washes with buffer H0.1 and eluted with H0.1 supplemented with 1mg/mL FLAG peptide. Eluate was concentrated, aliquoted, flash frozen in liquid nitrogen, and stored at -80ºC. INO80 concentration was determined by SDS-PAGE with BSA standards, based on the intensity of the Ino80-flag band.

Nucleosome labeling and reconstitution

Recombinant *Xenopus laevis* histones were expressed and purified from *E. coli* as previously described [52]. Histone H2A E61A, E64A, D90A, D92A expression plasmid was a generous gift from the Tan lab at Penn State. Purified histone H2A E64R was provided by the Wolberger lab. Histone octamer was reconstituted as previously described [52,53], except for smFRET nucleosomes where a 2:1 unlabeled:labeled H3 mixture was used during octamer assembly to generate nucleosomes with mostly one H3 or neither H3 labeled. Histone H3 with a cysteine introduced at position 33 was labeled with either Cy3 (for smFRET) or Cy5 (for ensemble assays) prior to histone octamer assembly via cysteine-maleimide chemistry. Cy3-labeled (for ensemble assays) and Cyanine 5 SE-labeled and biotinylated DNAs (for smFRET) were generated by PCR with HPLC-purified, labeled primers (Cy5 primers: TriLink Biotechnologies, San Diego, CA; Cy3 and biotinylated primers: IDT, Coralville, IA) and purified by PAGE. The strong, synthetic 601 nucleosome positioning sequence [54] was used to assemble all nucleosomes in this study, with an arbitrary sequence for DNA flanking the 601 positioning sequence (Figure

2.15). These DNAs were assembled with either wild-type or APM octamers by salt gradient dialysis and purified by glycerol gradient centrifugation [53].

Native gel remodeling assay

All remodeling reactions were performed under single turnover conditions (enzyme in excess of nucleosomes). Reactions with SNF2h were performed at 20ºC with 20nM nucleosomes, 12.5mM HEPES pH 7.5, 2mM Tris pH 7.5, 70mM KCl, 5 mM ATP•$MgCl_2$, 3mM $MgCl_2$,0.02% NP40, and ~3%(v/v) glycerol. Reactions with ACF and INO80 were performed as above at 30ºC and with minor changes in buffer composition (ACF: 10 nM nucleosomes, 12.5 mM HEPES pH 7.9, 2 mM Tris pH 7.5, 60 mM KCl, 2 mM ATP•$MgCl_2$, 3 mM $MgCl_2$, 0.02% NP40, 0.3 mg/mL FLAG peptide, and ~9% glycerol; INO80: 40 mM Tris pH 7.5, 60 mM KCl, 2 mM ATP•$MgCl_2$, 1.1 mM $MgCl_2$, 0.02% NP40, 0.5 mg/mL FLAG peptide, and 1% glycerol). Reactions were started with addition of enzyme and time points were quenched with excess ADP and plasmid DNA. Time points were then resolved by native PAGE (6% acrylamide, 0.5XTBE) and scanned on a Typhoon variable mode imager (GE Life Sciences, Pittsburgh, PA) by scanning for fluorescent labels. Gels were then quantified by densitometry using ImageJ. The fraction of nucleosomes end-positioned (i.e. unremodeled) at a given time point was determined by the ratio of fast-migrating nucleosomes to the total nucleosome intensity. This was fit to a single exponential decay using Prism 6 (GraphPad, La Jolla, CA) (Equation 1),

$$y = (y_0 - p)\, e^{-k_{obs}\ t} + p \qquad (1)$$

where y_0 is the initial fraction end-positioned, k_{obs} is the observed rate constant, and p is the fraction end-positioned at plateau. Reactions in a given concentration series were fit constrained to a common y_0 and p. Concentration series were fit to a cooperative binding model (Equation 2),

$$k_{obs} = k_{max} \frac{X}{(K_m^{app})^h + X^h} \quad (2)$$

where *X* is the concentration of SNF2h, *h* is the hill coefficient, K_m^{app} is the apparent K_m, and k_{max} is the saturating rate constant. Competition assays were performed as described above with varying concentrations of LANA peptide and fit to a single exponential decay. This was then fit to a simple competition binding model (Equation 3),

$$k_{obs} = \frac{k_0}{1 + \frac{X}{K_I}} \quad (3)$$

where k_0 is the rate constant without peptide, *X* is the concentration of peptide, and K_I is the inhibition constant.

ATPase assay

ATPase reactions were performed under multiple turnover conditions (nucleosomes in excess of enzymes). Reactions were performed with 25nM SNF2h, 12.5mM HEPES pH 7.5, 2mM Tris pH 7.5, 70mM KCl, 7.5μM ATP•$MgCl_2$, 3mM $MgCl_2$,0.02% NP40, ~3%(v/v) glycerol, and trace amounts of γ-^{32}P-ATP. Reactions were started with addition of enzyme, and 2.5 μL time points were quenched with an equal volume of 50 mM Tris pH 7.5, 3% SDS, and 100 mM EDTA. Inorganic phosphate was resolved from ATP on a PEI-cellulose TLC plate (Select Scientific) with 0.5 M LiCl/1M formic acid mobile phase. Plates were dried, exposed to a phosphorscreen overnight, and scanned on a Typhoon variable mode imager. Rate constants were determined by fitting a line through the first 10% of inorganic phosphate generated using Prism.

Ensemble FRET remodeling assay

Ensemble FRET remodeling assays were performed under the same conditions as gel remodeling assays. Reactions were initiated by addition of enzyme and then measured in a K2 fluorometer (ISS) equipped with a 550 nm short pass excitation filter and a 535

nm long pass emission filter. Reactions were excited at 515 nm and emission was measured at 665 nm. The resulting curves were fit to a two-phase exponential decay (Equation 4),

$$y = p + (y_0 - p)(f_{fast}\ e^{-k_{fast}t}) + (1 - f_{fast})\ e^{-k_{slow}t}) \qquad (4)$$

where f_{fast} is the fraction in the fast phase and k_{fast} and k_{slow} are the remodeling rates of the fast and slow phase respectively.

Crosslinking mass spectrometry

Crosslinking mass spectrometry samples were prepared by incubating 72µg of mononucleosomes without flanking DNA at 9µM final concentration with 24µM SNF2h in buffer containing either ADP or ADP•BeF_x (15 mM HEPES pH 7.5, 140 mM KCl, 0.5mM ADP•Mg, 0.5mM $MgCl_2$, ±0.5mM BeFx 1:5 $BeCl_2$:NaF) for 10 min at 30ºC. The crosslinking reaction with the LANA peptide was performed the same as the ADP•BeFx condition with 30µM peptide added. The samples were then reacted with 1 mM EDC and 20 µM N-hydroxysulfosuccinimide (added as a 10x stock in water) for 60 minutes at room temperature. Crosslinking reactions were then quenched by adding 10 mM Tris pH 7.5 and samples were acetone precipitated and washed once with cold acetone. The pellet was resuspended in 8M Urea, 5 mM TCEP, 100 mM ammonium bicarbonate and heated at 56°C for 25 minutes, followed by alkylation with 10 mM iodoacetamide for 40 min at room temperature. The sample was diluted 5-fold with 100 mM ammonium bicarbonate and digested with 1:25 trypsin for 4 hours at 37°C followed by addition of a second aliquot of trypsin and overnight digestion.

Crosslinked peptides were desalted using 100 µl OMIX C18 tips (Agilent), fractionated by size-exclusion chromatography (SEC), and analyzed by LC-MS similarly to a previously described method [55]. Briefly, trypsin digests were acidified to 0.2% TFA, desalted, and run over a Superdex Peptide PC 3.2/300 SEC column (GE Healthcare). SEC

fractions eluting between 0.9 ml and 1.4 ml were dried and resuspended in 0.1% formic acid for LC-MS. Each fraction was separated over a 15 cm x 75 µm ID PepMap C18 column (Thermo) using a NanoAcquity UPLC system (Waters) and analyzed by a Fusion Lumos mass spectrometer (Thermo). Precursor ions were measured from 375-1500 m/z in the Orbitrap analyzer (resolution: 120,000; AGC: 4.0e5). Ions charged 3+ to 8+ were isolated in the quadrupole (selection window: 1.6 m/z units; dynamic exclusion window: 30 sec; MIPS Peptide filter enabled), fragmented by HCD (Normalized Collision Energy: 28%) and measured in the Orbitrap (resolution: 30,000; AGC; 5.0e4). The cycle time was set to 3 seconds.

Peaklists were generated using PAVA (UCSF) and searched for crosslinked peptides with Protein Prospector 5.19.22 [56] against a target database containing human SNF2h plus the four core histone sequences from *X. laevis* concatenated with a decoy database containing 10 randomized copies of each target sequence (total database size 55 sequences). Loss of the initiator methionine and carbamidomethylation of cysteine. Methionine oxidation, peptide N-terminal glutamine to pyroglutamate formation, acetylation at the protein N-terminus, and mis-annotation of the monoisotopic peak (1Da neutral loss) were treated as variable modifications. EDC was designated as a heterobifunctional crosslinking reagent with specificity of aspartate, glutamate, and the protein C-terminus on one side and lysine and the protein N-terminus on the other with a bridge mass corresponding to loss of H_2O. A mass modification range of 400-5000 Da was specified on these residues and 85 product ion peaks from the peaklist were used in the search. Precursor and product ion tolerances were 8 and 25 ppm respectively.

Crosslinked spectral matches (CSMs) were initially classified as in [55]. The dataset was then aggregated into unique crosslinked residue-pair level data with a corresponding spectral count value. Due to the prevalence of multiple, closely spaced

Asp and Glu residues in a typical tryptic peptide, site-localization of EDC crosslinks is more challenging than with homobifunctional lysine-directed reagents. To address this, when the site-localization was judged to be ambiguous, all possible residue-pairs were kept with an annotation noting the ambiguity. When calculating spectral counts, fractional spectral counts were assigned to these ambiguous site localizations so that a given spectrum was awarded exactly 1 spectral count. For instance, a product ion spectrum matching equally well to both K91.H4-D65.H2B or K91.H4-E68.H2B contributes 0.5 towards the spectral counts of each residue-pair. Decoy CSMs were retained throughout this aggregation and spectral counting process. A linear SVM model, built on five features of the Protein Prospector search output (score difference, % of product ion signals matched, precursor charge, rank of peptide 1, and rank of peptide 2) was constructed to sort crosslinked residue pairs into decoy and target classes. Crosslinked residue-pairs with an SVM score greater than 1, score difference greater than 5, and at least one spectral count are reported. The final residue-pair level data set is reported at specificity of 99.7% corresponding to 0.05% FDR. The number of unique crosslinks in the ADP condition was 974, while 1470 crosslinks were unique to the ADP•BeF_x condition and 707 crosslinks were common to both conditions.

To determine which protein domains are involved in SNF2h mediated nucleosome sliding, residue level crosslink spectral counts were aggregated into domain level counts. Each domain pair was assigned a minimum spectral count of 1 to avoid dividing by zero, and the log2 ratio of spectral counts for each domain pair in the ADP•BeFx condition to the ADP condition were calculated. Domain pairs with a Log2 ratio of exactly 0 were treated as NA values. The remaining data were normalized such that the median value was set at 0. Hence, most domain-domain interactions were assumed to not change substantially between conditions.

Histone protein sequences were taken from *Xenopus Laevis* Uniprot Entries (without the initiator methionine) and domains were defined as follows: H2A N-term tail: 1-16, H2A: 17-43, H2A Acidic Patch: 44-100, H2A C-term tail: 101-129; H2B tail: 1-34, H2B: 35-99, H2B Acidic Patch: 100-122; H3 tail: 1-44, H3: 45-135; H4 tail: 25-102.

The sequence of SNF2h was identical to the Human entry in Uniprot (O60264) with an additional two amino acids at the N-terminus to match the construct used. All residue numbers are therefore shifted from the Uniprot entry by 2 aa. SNF2h domains were defined as follows: Snf2h1: 1-83, AutoN: 84-160, Snf2h2: 161-183, RecA1: 184-402, RecA2: 403-641, NegC: 642-703, Snf2h4: 704-736, HAND: 737-839, SANT: 840-894, SLIDE: 895-1013, Snf2h5: 1014-1054.

Annotated Mass Spectra are available using MS-Viewer at: http://msviewer.ucsf.edu/prospector/cgi-bin/msform.cgi?form=msviewer

The ADP data set is accessed with search key: 2x0kr2kzq1
The ADP•BeFx data set is accessed with search key: fjamygr8pl
The ADP•BeFx in the presence of LANA peptide is accessed with search key: c5o2mcxwum.

Raw mass spectrometry data is available in the MassIVE repository at UCSD with accession key: MSV000082136

Single molecule FRET measurements.

smFRET experiments were performed as previously described in [31] with modifications to the reaction buffers as described below.

Sample preparation and imaging. Briefly, as in [31], quartz slides were PEGylated and then incubated with neutravidin (A2666, ThermoFisher Scientific, Waltham, MA) to mediate attachment of biotinylated nucleosomes. After removal of unbound neutravidin, biotinylated nucleosomes at 12.5 pM in a modified Wash Buffer (12 mM HEPES-KOH, pH

7.5 at 22°C, 60 mM KCl, 1.4 mM $MgCl_2$, 10% glycerol, 0.1 mM EDTA, 0.02% Igepal, 1% [w/v] glucose, and 0.1 mg/mL acetylated BSA) were added and incubated for 10 minutes. Unbound nucleosomes were removed by washing with Wash Buffer. All incubations and experiments were performed at 20°C. Nucleosomes were imaged on a custom-built prism-based TIRF setup.

Immediately prior to data acquisition, the sample chamber was flushed with a modified imaging buffer (53 mM HEPES-KOH, pH 7.5 at 22°C, 9.1 mM Tris-acetate, pH 7.5 at 22°C [contributed by the Trolox], 63 mM KCl, 1.41 mM $MgCl_2$, 10% glycerol, 0.1 mM EDTA, 0.02% Igepal, 1% [w/v] glucose, 0.1 mg/mL acetylated BSA, 2 mM Trolox [Sigma 238813, made as an 11 mM stock in Tris-acetate, pH'd to 7.5 with 1 M NaOH, and stored at 4°C], 0.03 mM β-mercaptoethanol, 2 U/µL catalase [=0.2 mg/mL; Sigma E3289], and 0.08 U/µL glucose oxidase [0.8 mg/mL, Sigma G2133; made with the catalase as a 100x stock in SPB, and stored at 4°C for not more than one week]). Images were collected using Micro-Manager (www.micro-manager.org, San Francisco, CA) [57] at 7.4 Hz, with an exposure time of 100 ms. To start each reaction, saturating enzyme (400 nM for WT nucleosomes; 2 µM for E64R nucleosomes) and saturating ATP (1 mM) in 300 µL imaging buffer were added via an automated syringe pump (J-KEM Scientific, St. Louis, MO).

Data analysis. The number of remodeling events per smFRET experiment was roughly an order of magnitude lower with E64R nucleosomes compared to WT nucleosomes, necessitating significantly larger data sets for the E64R nucleosomes compared to WT. To streamline the data analysis process with these data sets, as well as to improve the overall quality of the data, we made use of the custom in-house software we have developed for smFRET image analysis, called Traces, available for download at https://github.com/stephlj/Traces [30]. In addition, the long pauses exhibited by SNF2h remodeling E64R nucleosomes are subject to an increased number of artifacts, such as

dye blinking or slight fluctuations in the noise, which can complicate quantification of smFRET trajectories. We therefore used the python-based HMM library pyhsmm (https://github.com/mattjj/pyhsmm), which we adapted for the analysis of smFRET data as part of the Traces package, to quantify pause durations. This particular HMM package, which fits a discrete state HMM to each trajectory generated by Traces, enables a reduction in the likelihood of the HMM identifying artifacts as real transitions, and also reduces analysis time.

As described in Figure 2.10, and consistent with previous smFRET studies with nucleosomes [26,27,29], we observe two predominant clusters of FRET values, at 0.57 and 0.95 FRET, in the absence of remodeler. These FRET states correspond to two of the four populations of nucleosomes that result from mixing unlabeled H3 with Cy3-labeled H3 during octamer formation: some nucleosomes will have a Cy3 label on the H3 proximal to the Cy5-labeled DNA end, resulting in the higher FRET state, and some will have a Cy3 label on the H3 distal to the Cy5-labeled DNA end, resulting in the mid-FRET state. There will also be a population of nucleosomes with both H3 histones unlabeled, which show no FRET; and a population with both copies of H3 labeled, which are distinguishable by two-step photobleaching of the Cy3 dye, and are excluded from all analyses (i.e. both calibration curve data [31] and remodeling data). We also excluded any trajectories to which pyhsmm fit an initial FRET value lower than 0.775 FRET, since nucleosomes with distally labeled H3's do not provide as great a dynamic range for monitoring nucleosome remodeling. We excluded any part of a trajectory including and subsequent to backtracking events (where the nucleosome was moved away from the center, that is, where FRET increased instead of decreasing). Each data set (e.g., E64R/SNF2h) consists of at least 100 trajectories collated from at least 3 (typically 5 to 7) different experiments. All errors were bootstrapped over trajectories (that is, for each data set, the ≥100

trajectories were resampled with replacement, and reported values, such as the means of each pause duration, were recalculated for each bootstrapped sample). Reported errors are standard deviations of the bootstrapped values. A similar procedure was used to obtain the errors on the cdfs in Figure 2.8E and Figure 2.11; the shaded regions represent +/- the standard deviation of the set of bootstrapped cdfs.

Figures

FIGURE 2.1

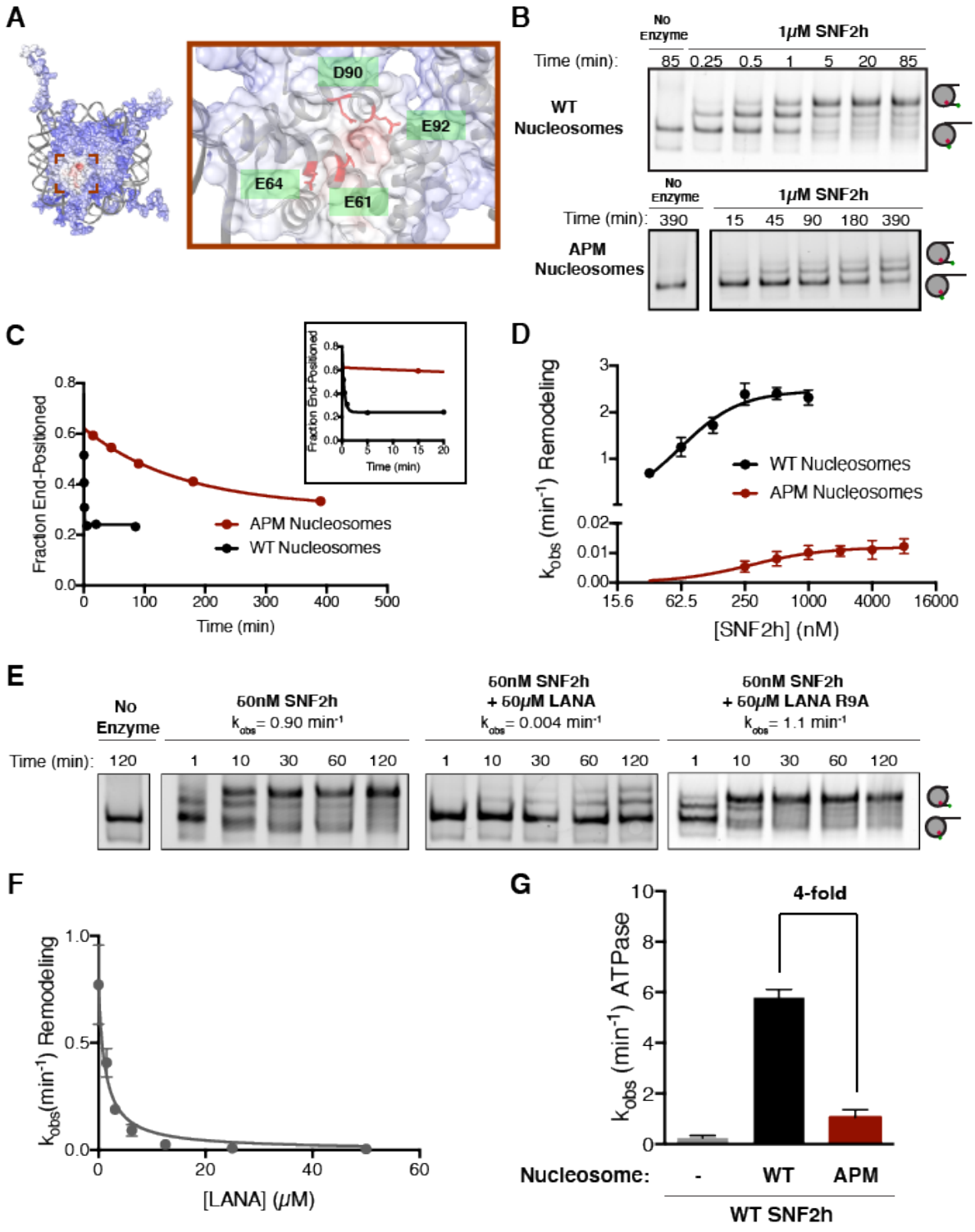

Figure 2.1 The acidic patch is an important epitope for remodeling post-binding. A. Charge profile of the nucleosome (left) and magnification of the acidic patch region (right) (PDBID: 1KX5, charge profile generated using ABPS and UCSF Chimera [58]. Residues of the acidic patch mutated in this study are shown in red. B. Example of a Cy5-fluorescent scan of a gel-based remodeling assay with 0/60 WT and acidic patch mutant (APM) nucleosomes (1μM SNF2h, 20nM nucleosomes, saturating ATP). C. Quantification of the gel in B and fits to a single exponential decay. Inset is zoomed to show faster time points with WT nucleosomes. D. Gel remodeling rate as a function of enzyme concentration, plotted on a log(2) scale. APM nucleosomes are remodeled substantially slower even at saturating concentrations of enzyme. Data were fit to a cooperative binding model (WT nucleosomes: K_M^{app} = 61 nM, k_{max} =2.5 min^{-1}, h=1.5; APM nucleosomes: K_M^{app} = 280 nM, k_{max} =.012 min^{-1}, h=1.2). E. Remodeling is inhibited by competition for the acidic patch. WT nucleosomes were remodeled with sub-saturating SNF2h and in the presence of KSHV LANA peptide. Remodeling is inhibited by the peptide but not when the arginine anchor is mutated to alanine. F. Inhibition curve with the LANA peptide (K_I=1.21 μM). Error bars represent standard errors on the mean for 3 replicates, except for the no-peptide condition in F, which had 2 replicates. G. ATPase activity of WT SNF2h. Nucleosomes were in excess of SNF2h and at saturating concentrations. APM nucleosomes stimulated ATPase activity 4-fold weaker than WT.

FIGURE 2.2

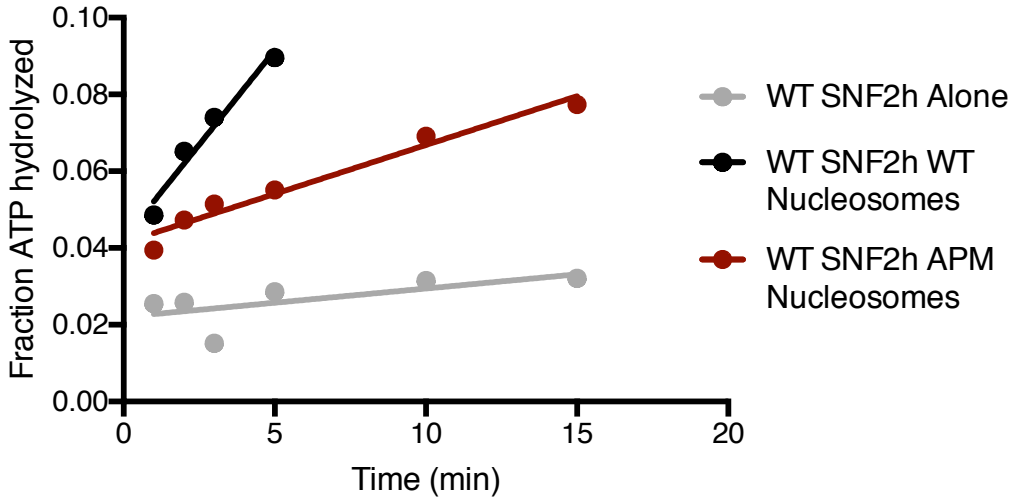

Figure 2.2. Representative ATPase assay fits.
Saturating concentrations of nucleosomes (200nM WT nucleosomes, 187 nM APM nucleosomes) were incubated with 12.5 nM enzyme and 7.5 µM ATP•Mg, and trace amounts of γ-P^{32} ATP. Reactions were analyzed by thin layer chromatography followed by radiography. Initial rates were determined by a linear fit to the first 10% of ATP hydrolyzed in the reaction.

FIGURE 2.3

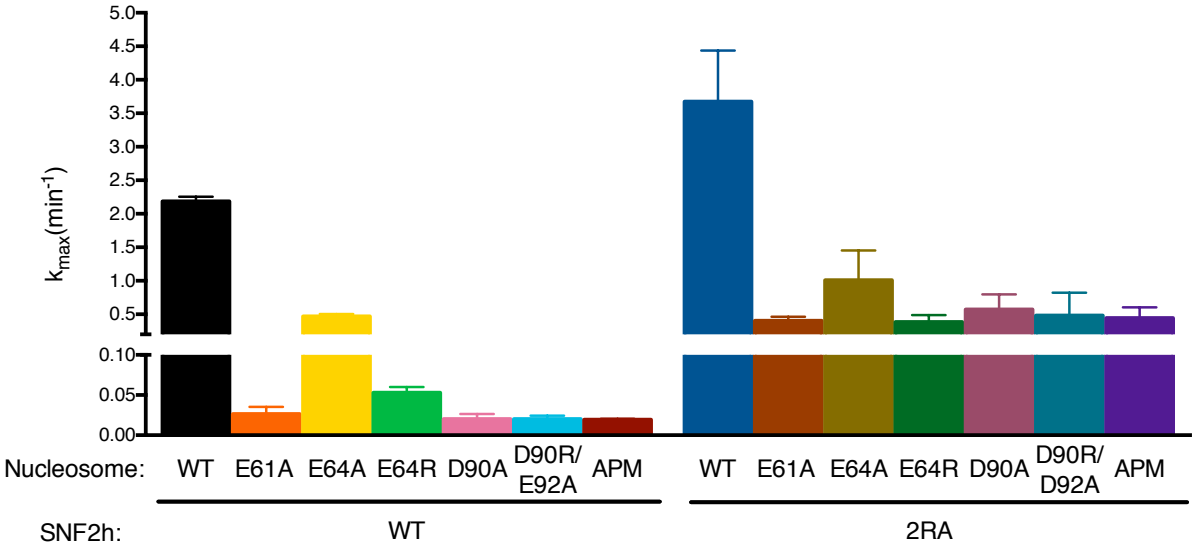

Figure 2.3. Maximal remodeling rates for various acidic patch mutations.
0/60 Cy3-DNA labeled nucleosome constructs were remodeled with saturating concentrations of either WT or 2RA SNF2h (N=3). The mean and standard error are shown for the maximal remodeling rates. Residues in the "arginine anchor" binding site of the nucleosome (E61, D90, E92) produce the same defect when mutated individually or in combination, suggesting a cooperative role for these residues in SNF2h remodeling. Mutating residues in the acidic patch but outside the arginine anchor site (E64) has a weaker effect than mutating the arginine anchor residues. However, all acidic patch mutations have a weaker defect in the context of 2RA mutant SNF2h.

FIGURE 2.4

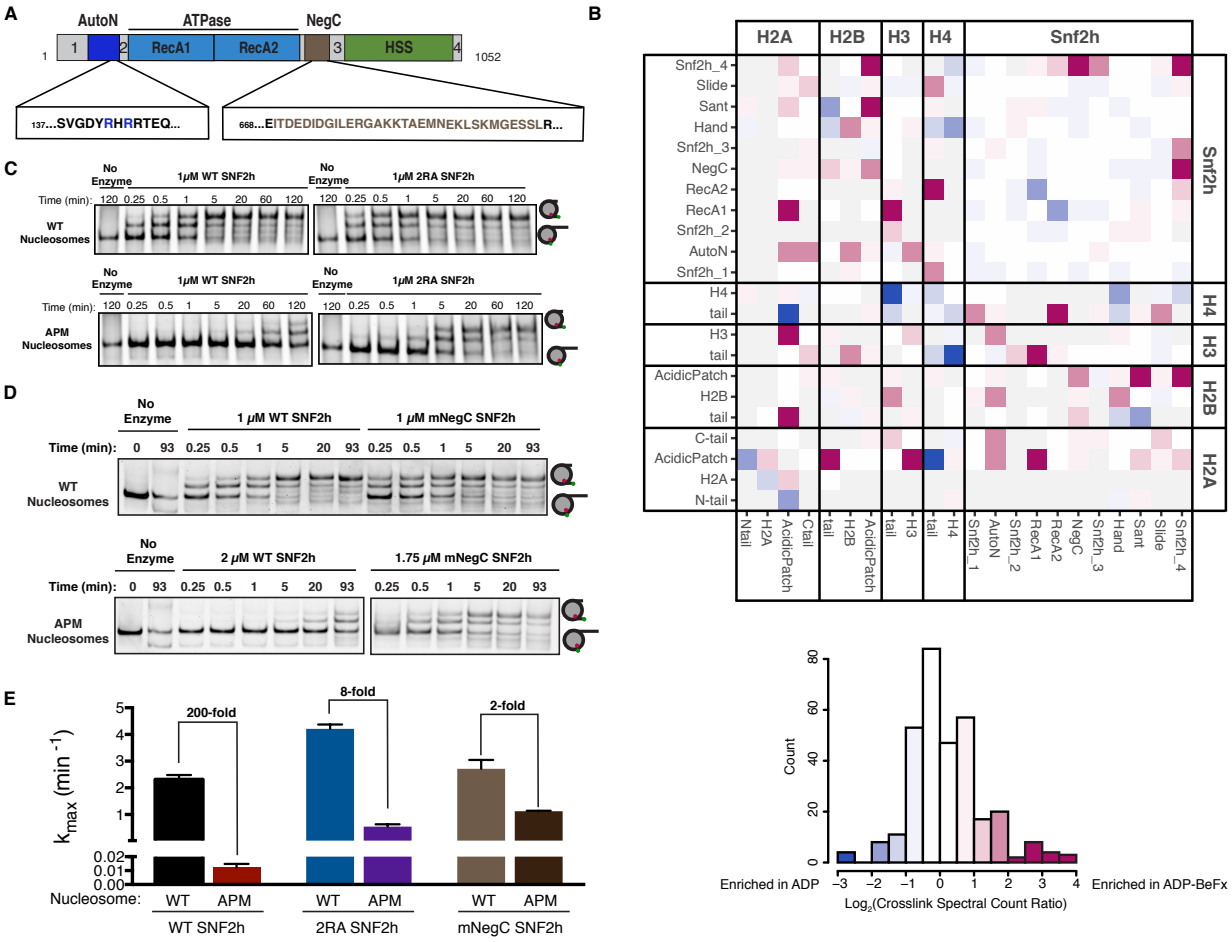

Figure 2.4 Dependence on the nucleosome acidic patch is linked to relief of autoinhibition

A. Domain architecture of SNF2h. The 2 critical arginines (R142, R144) of AutoN are highlighted in blue, while the NegC region replaced with a flexible GGS linker [17] is highlighted in brown. Intervening sequences with no known domain annotations are numbered as in B. B. Direct domain-domain interactions of SNF2h nucleosomes probed by crosslinking mass spectrometry. SNF2h mononucleosomes were crosslinked with the zero-length reagent EDC in the presence of either the ATP transition state analog ADP•BeF_x or ADP. Residue-residue crosslink data were aggregated into domain-domain level spectral counts. The fold change between ADP•BeF_x and ADP conditions is displayed as the log2 of the spectral count ratio. The data were centered to the median value and the color scale depicts the interactions most enriched in ADP•BeF_x in magenta, and ADP in blue. Light grey tiles indicate no crosslinks observed in either condition. Domains are listed from N- to C- term within each protein. The distribution of fold changes in domain-domain spectral counts is plotted as a histogram below. It should also be noted that due to the structure of the histone octamer and the 2:1 stoichiometry of the SNF2h-Nucleosome complex, we cannot distinguish between intramolecular and intermolecular SNF2h-SNF2h or Histone-Histone crosslinks. C and D. Mutation of AutoN

or NegC increases remodeling rate with WT and APM nucleosomes. Cy5 fluorescent scans of native gel remodeling assays. E. Saturating remodeling rates (k_{max}) for WT and APM nucleosomes with WT, 2RA, and mNegC SNF2h. Mutation of the acidic patch has a substantially lower effect on the k_{max} for 2RA and mNegC SNF2h than for WT SNF2h (8-fold and 2-fold respectively vs. 200-fold). Error bars represent standard errors on the mean for N=3 replicates.

FIGURE 2.5

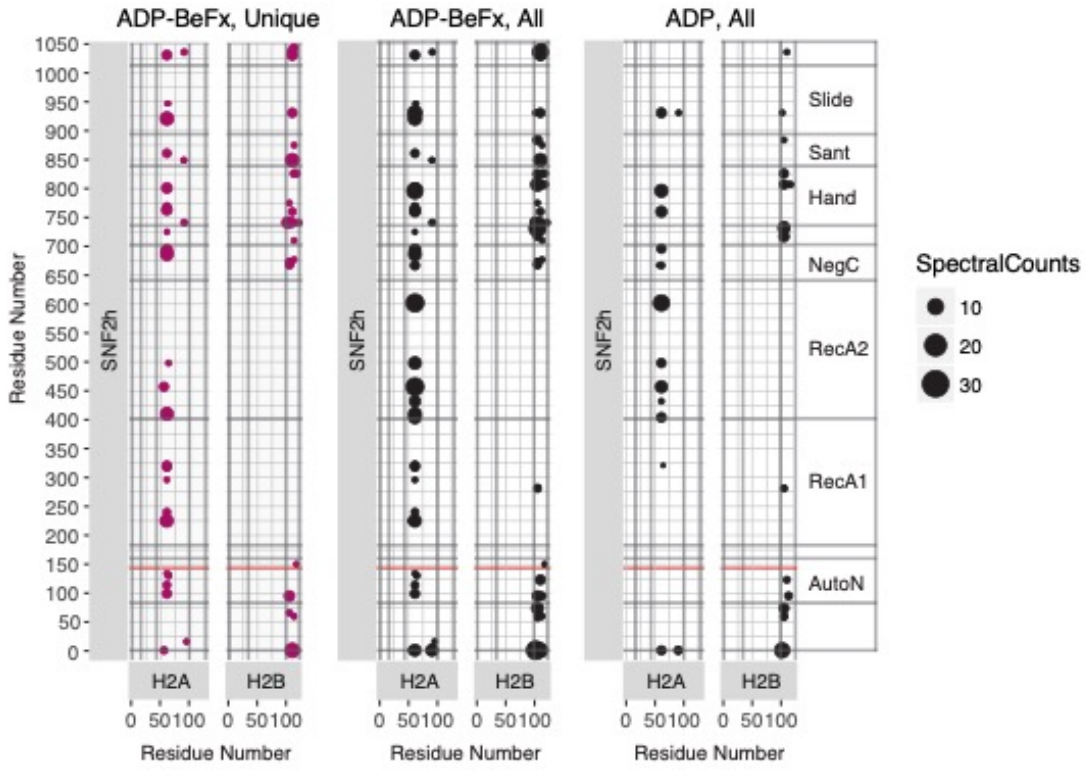

Figure 2.5 Acidic Patch-SNF2h Crosslinks Unique to the ADP•BeF$_x$ condition
Residue level cross-links between SNF2h and the H2A/H2B acidic patch. Each dot represents a pair of amino acid residues that were identified in either the ADP-BeFx experiment or the ADP experiment (right two panels, black). The left panel displays only the cross-links uniquely identified in the presence of ADP-BeFx (magenta). The area of each dot is scaled to the number of spectral counts identified. Domain boundaries are indicated by bold grey lines and labeled for SNF2h. Only cross-links to the H2A and H2B acidic patches (defined as H2A:44-100 and H2B:100-122) are plotted here for clarity. Crosslinks between H2A acidic patch and SNF2h AutoN domain are only observed with ADP-BeFx. Likewise crosslinks between the H2B acidic patch and the SNF2h NegC domain are only observed with ADP-BeFx. Positions of the 2RA mutants (R142, R144) are marked by horizontal red lines.

FIGURE 2.6

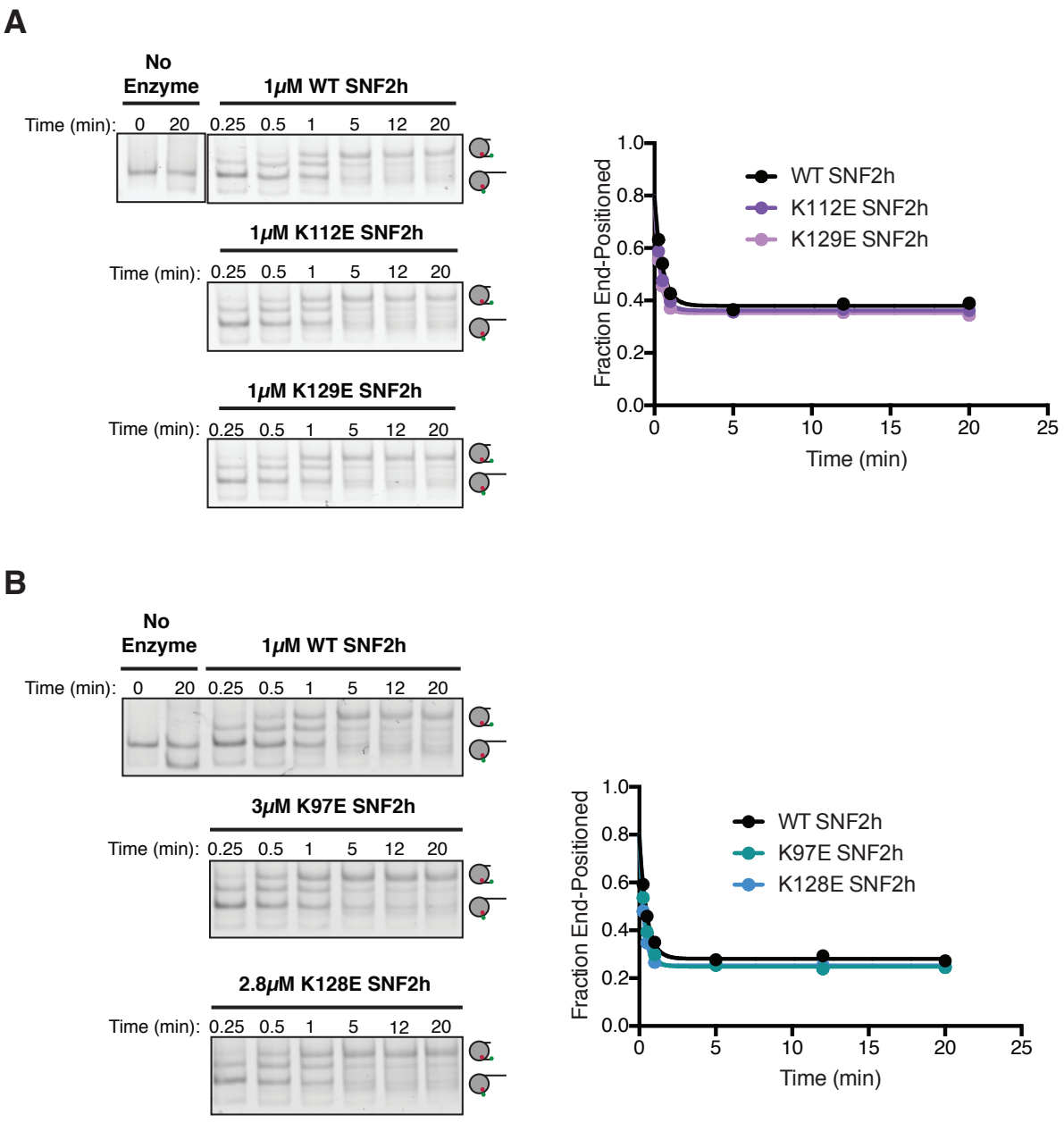
A
No Enzyme
1μM WT SNF2h
Time (min): 0 20 0.25 0.5 1 5 12 20
1μM K112E SNF2h
Time (min): 0.25 0.5 1 5 12 20
1μM K129E SNF2h
Time (min): 0.25 0.5 1 5 12 20
Fraction End-Positioned
Time (min)
WT SNF2h
K112E SNF2h
K129E SNF2h
B
No Enzyme
1μM WT SNF2h
Time (min): 0 20 0.25 0.5 1 5 12 20
3μM K97E SNF2h
Time (min): 0.25 0.5 1 5 12 20
2.8μM K128E SNF2h
Time (min): 0.25 0.5 1 5 12 20
Fraction End-Positioned
Time (min)
WT SNF2h
K97E SNF2h
K128E SNF2h

Figure 2.6 Mutations to the N-terminus have minimal effects on remodeling
A and B. Left. Cy3-fluorscence scan of native gel remodeling assays with WT nucleosomes and either WT or mutant SNF2h. Saturating concentrations of SNF2h were used for all constructs. Right. Quantifications of the gel images shown at the left. The residues chosen are lysines in AutoN that crosslinked to the acidic patch in only the ADP•BeF_x state. In all cases, the mutations showed no appreciable effect on remodeling (<2-fold difference).

FIGURE 2.7

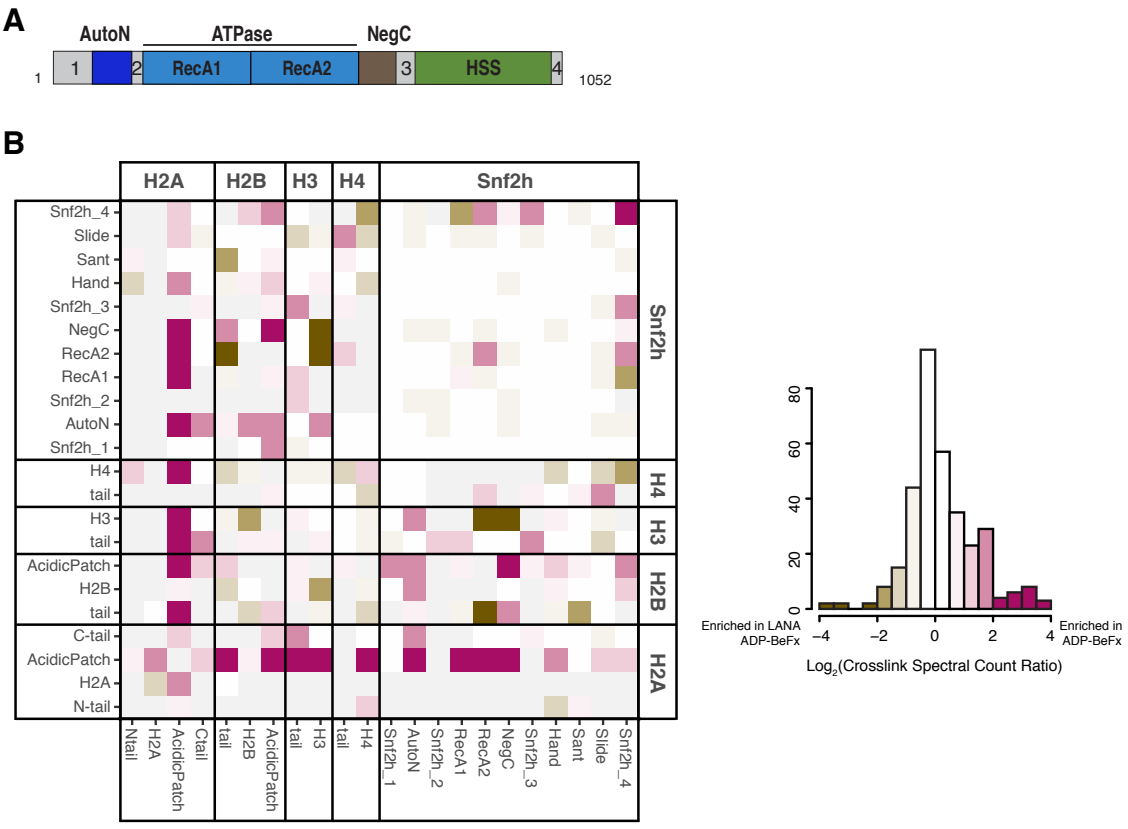

Figure 2.7 Comparison of crosslinks in the ADP•BeFx state with and without LANA peptide

A. Domain diagram of SNF2h B. Direct domain-domain interactions of SNF2h and Nucleosomes with ADP•BeFx in the presence or absence of the LANA peptide. The LANA peptide is expected to compete with domains on SNF2h that bind the acidic patch resulting in reduced crosslinking to this region of the nucleosome. Residue-residue crosslink data were aggregated into domain-domain level spectral counts and plotted as in Figure 2B. The fold change between ADP•BeF_x with and without LANA peptide is displayed as the log2 of the spectral count ratio with the data centered to the median fold change. The domain interactions most enriched in the presence of the LANA peptide are colored in brown, while the interactions promoted in the absence of the peptide are colored in magenta. Light grey tiles indicate no crosslinks observed in either condition. Crosslinks between the H2A acidic patch and both the RecA lobes and the autoinhibitory domains are strongly reduced, while crosslinks to the HSS domain are less affected. The distribution of fold changes in domain-domain spectral counts is plotted as a histogram to the right.

FIGURE 2.8

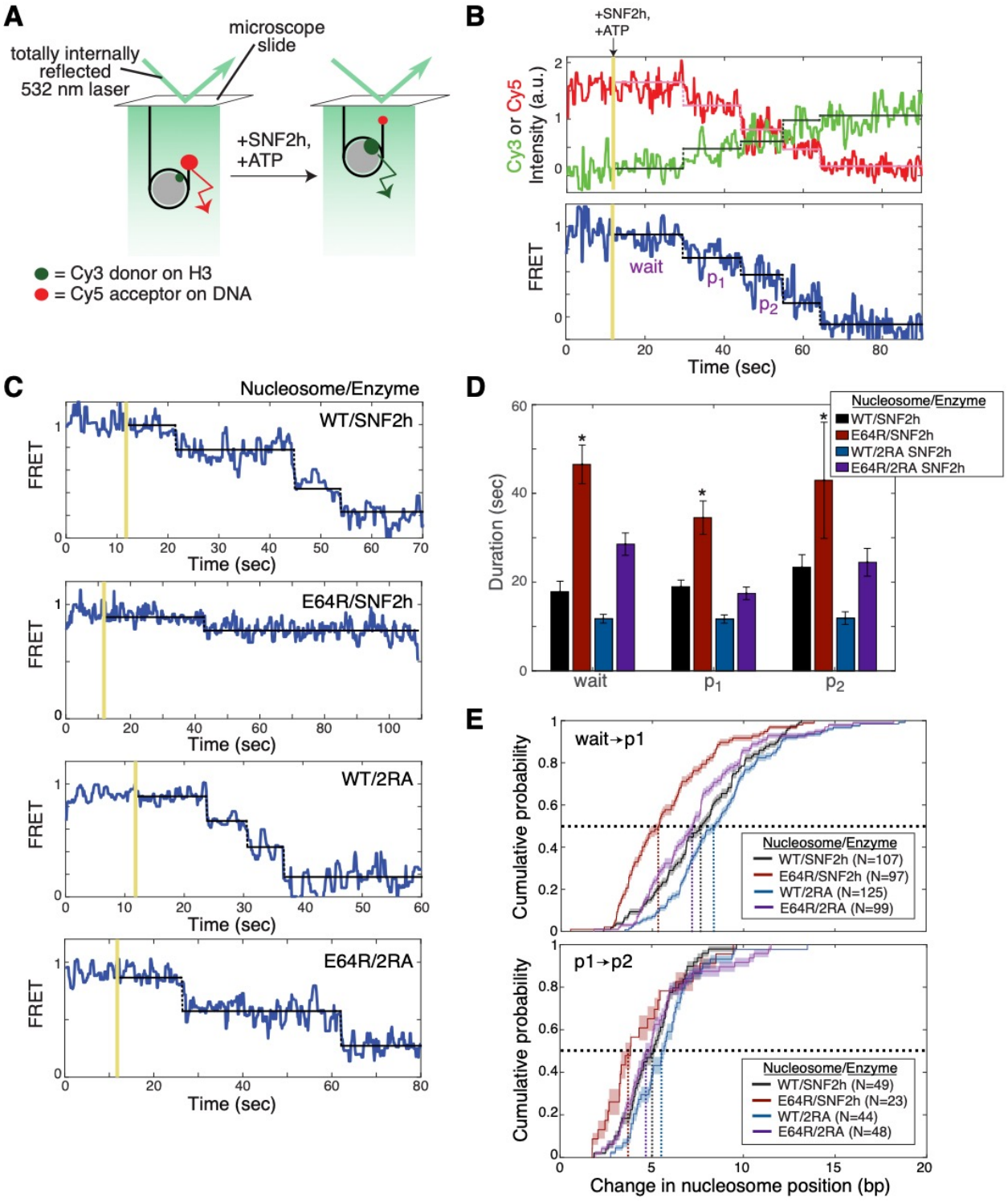
A
totally internally reflected 532 nm laser
microscope slide
+SNF2h, +ATP
= Cy3 donor on H3
= Cy5 acceptor on DNA
B
+SNF2h, +ATP
Cy3 or Cy5 Intensity (a.u.)
FRET
wait
p1
p2
Time (sec)
C
Nucleosome/Enzyme
WT/SNF2h
E64R/SNF2h
WT/2RA
E64R/2RA
FRET
Time (sec)
D
Nucleosome/Enzyme
WT/SNF2h
E64R/SNF2h
WT/2RA SNF2h
E64R/2RA SNF2h
Duration (sec)
wait
p1
p2
E
wait→p1
p1→p2
Cumulative probability
Nucleosome/Enzyme
WT/SNF2h (N=107)
E64R/SNF2h (N=97)
WT/2RA (N=125)
E64R/2RA (N=99)
WT/SNF2h (N=49)
E64R/SNF2h (N=23)
WT/2RA (N=44)
E64R/2RA (N=48)
Change in nucleosome position (bp)

Figure 2.8 The acidic patch interacts antagonistically with AutoN to promote pause exit and persistent translocation

A. Schematic of the smFRET setup. Nucleosomes labeled on histone H3 with a Cy3 donor dye and on one end of the DNA with a Cy5 acceptor dye are immobilized on the surface of a slide and imaged with a prism-based TIRF microscope. The end-positioned nucleosomes used here have an initial high FRET efficiency (see also Figure 3-Supplement 2). As remodeling proceeds and the nucleosome is moved away from the DNA end, the FRET efficiency is reduced. B. Example time-course of remodeling of a single surface-attached, WT nucleosome in the presence of saturating SNF2h and ATP (400 nM and 1 mM, respectively). Vertical yellow line indicates addition of enzyme and ATP; horizontal pink, green, and black lines are the output of an HMM fit used to quantify pause durations and locations (see Methods). Note the alternating "pause" and "translocation" phases of the remodeling reaction; in keeping with the ISWI literature, we call the first pause the "wait" pause, the second pause "p1", the third "p2", etc. Intensity and FRET data here and in C have been smoothed with a 0.95-second median filter for visualization only. C. Example time-courses of remodeling of, from top to bottom, WT nucleosomes by SNF2h, APM nucleosomes by SNF2h, WT nucleosomes by 2RA SNF2h, and APM nucleosomes by 2RA SNF2h. Saturating enzyme (400 nM enzyme with WT nucleosomes; 2 μM enzyme with APM nucleosomes) and ATP (1 mM) were used in all cases. Additional examples are shown in Figure 3-supplement 6. D. Quantification of the first three pause durations. *Indicates a lower limit; as shown in Figure 3-Supplement 2B, remodeling of APM nucleosomes by SNF2h is too slow to capture by smFRET, due to the competition between photobleaching of the dyes and remodeling by SNF2h. Errors were bootstrapped (see Methods). E. Empirical cumulative distribution functions (cdfs) of the change in nucleosome position during the first translocation event (top panel) and the second translocation event (bottom panel) for different combinations of nucleosome constructs and enzymes. Roughly 50% of the initial translocation events by SNF2h on WT nucleosomes move the nucleosome 7 bp or fewer (black dashed lines); in contrast, nearly 80% of initial translocation events by SNF2h on E64R nucleosomes move the nucleosome 7 bp or fewer. Similarly, during the second translocation event, SNF2h moves WT nucleosomes roughly 5 bp or fewer 50% of the time, whereas again nearly 80% of second translocation events for SNF2h with E64R nucleosomes result in step sizes 5 bp or fewer. Shaded areas represent bootstrapped error estimates (see Methods). See also Figure 3-Supplement 6 for additional representations of these data and a further discussion of step sizes.

FIGURE 2.9

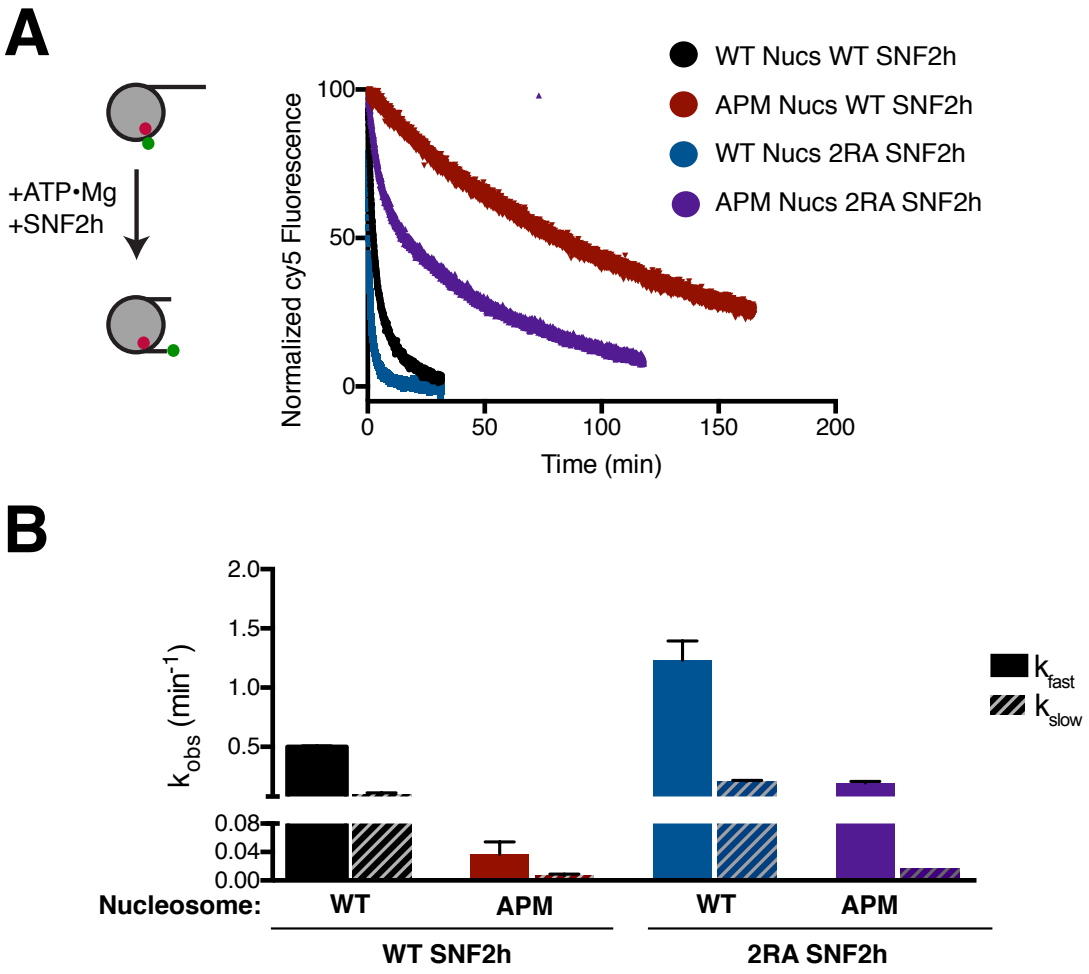

Figure 2.9 Ensemble FRET remodeling shows similar effects as the gel-based assay
A. FRET remodeling assay. Saturating concentrations of enzyme were added to 8 nM FRET-labeled nucleosomes. Cy5 fluorescence was monitored over time and fit to a two-phase exponential decay. Reactions were normalized to the initial (maximal) and plateau (minimal) fluorescence from the fit. B. Remodeling rates of the two phases. Error bars represent standard error of the mean for N=3 replicates.

FIGURE 2.10

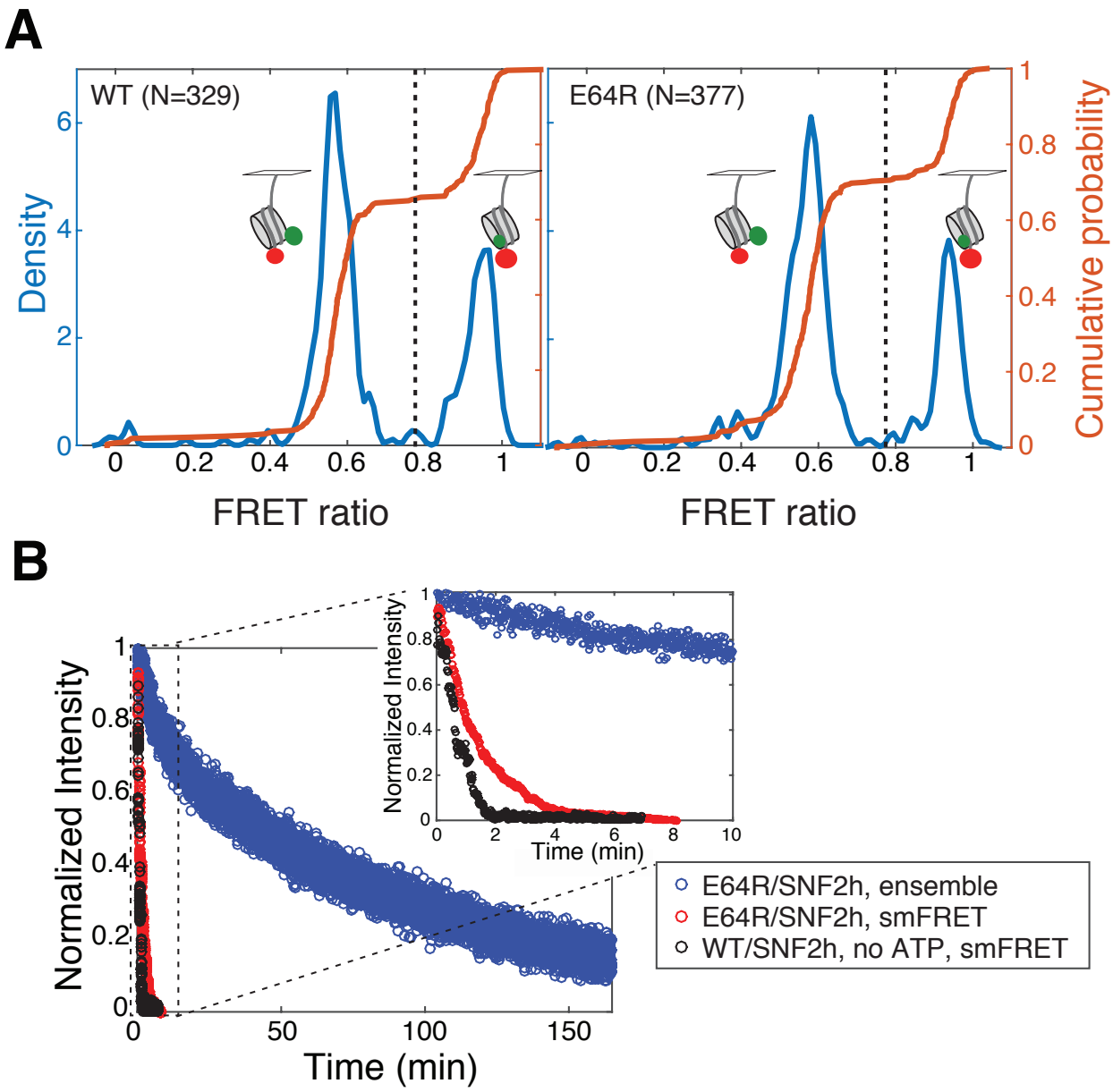
A
WT (N=329)
E64R (N=377)
Density
Cumulative probability
FRET ratio
FRET ratio
B
Normalized Intensity
Time (min)
Normalized Intensity
Time (min)
E64R/SNF2h, ensemble
E64R/SNF2h, smFRET
WT/SNF2h, no ATP, smFRET

Figure 2.10 smFRET controls
A. Kernel density estimation plots (KDE, blue) and empirical cumulative density functions (cdfs, orange) of initial FRET values for 3/78 nucleosomes alone (in the presence of 1 mM ATP, but in the absence of remodeler; previous work with ISWI family remodelers has shown the addition of remodeler does not affect these initial FRET [26,27]. Left panel, wild-type H2A-containing nucleosomes; right panel, H2A/E64R-containing nucleosomes. *N* indicates the number of nucleosomes included in the cdf. KDEs are more intuitive—the y-axis is analogous to the frequency axis of a histogram—but cdfs have the advantage of not requiring any smoothing or binning. Note that here nucleosomes were imaged at a significantly higher laser power (20 mW) than for measuring remodeling (11.5 mW), to ensure that the majority of both donor and acceptor dyes photobleached within the 5 minute imaging interval, so that dyes with two-step photobleaching events could be excluded. Only nucleosomes with an initial FRET value greater than 0.775 (black dashed lines) were included for further analysis. KDEs have Gaussian kernels with bandwidths ~0.01. B. Our ability to measure remodeling of E64R nucleosomes by SNF2h is limited by the photobleaching rate. Previous work has shown remodeling in ensemble FRET assays to be comparable to remodeling in surface-immobilized smFRET assays [26,29], as well as to that of surface-attached dinucleosome constructs [29]. However, as shown here, remodeling of surface-attached E64R nucleosomes (red data) appears to go to completion in about 4 minutes (inset), whereas remodeling of these same nucleosomes in ensemble FRET assays (blue data) takes over two hours to go to completion. This discrepancy is not due to an effect of the surface immobilization, but rather to the competition between remodeling and photobleaching. In the presence of SNF2h alone, without ATP (black data), nucleosomes photobleach on roughly the same timescale as the apparent remodeling of surface-attached E64R nucleosomes. Thus we are able to put only a lower bound on pause durations for remodeling of E64R nucleosomes, because slower remodeling events are undetected due to the relatively fast photobleaching of the dyes. The smFRET data shown here corresponds to the summed Cy5 intensities of all individual nucleosomes in the indicated data set, binned in 1-second intervals to simulate an ensemble measurement.

FIGURE 2.11

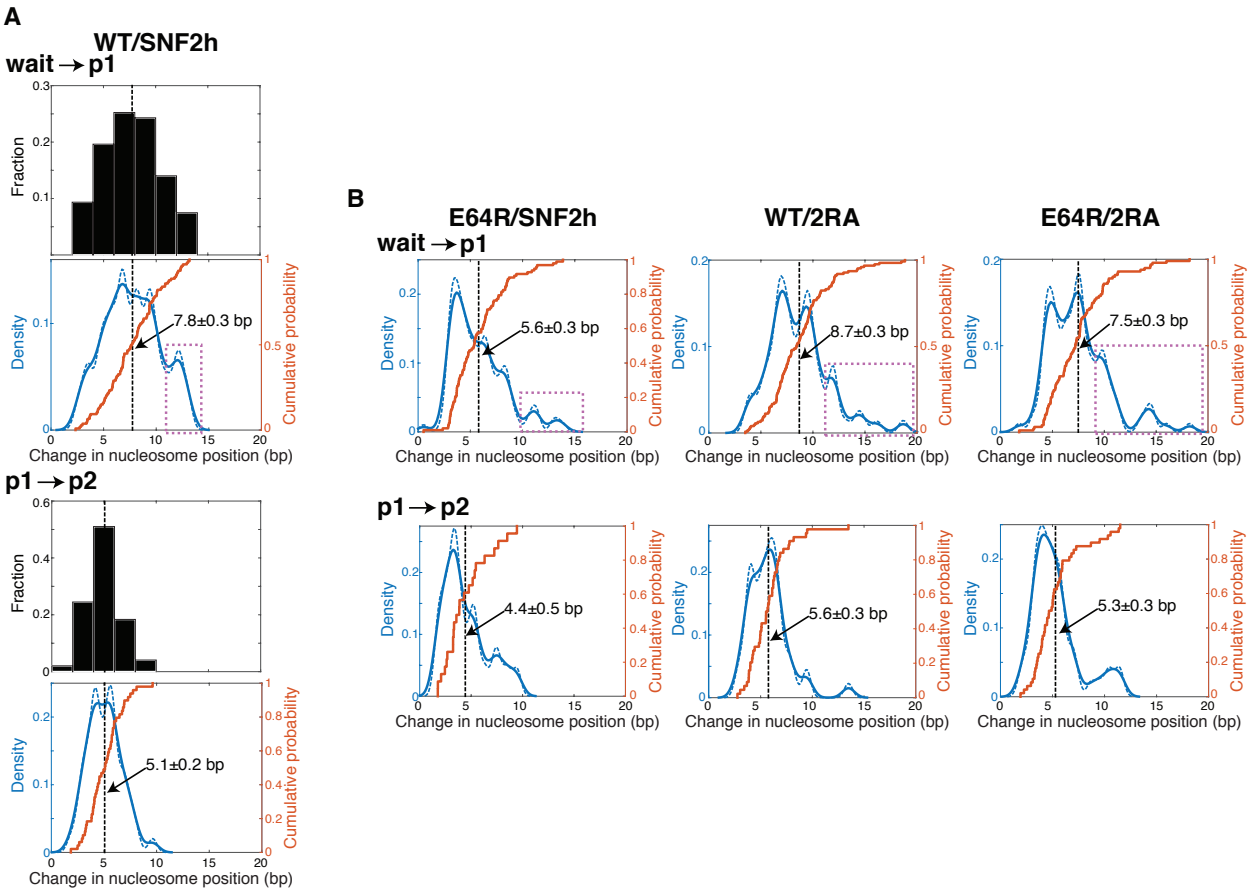

Figure 2.11 The step size of WT SNF2h with WT nucleosomes is comparable to step sizes previously described for ISWI family remodelers.
A. Three different representations of the change in nucleosome position (that is, the step size) during the first (top) or second (bottom) translocation event observed by smFRET, for the ≥100 remodeling trajectories collected with WT nucleosomes and WT SNF2h. The three representations are: histograms in black; kernel density estimations (KDEs) with two different bandwidths (0.6, solid blue lines; 0.4, dashed blue lines) in blue; and cumulative distribution functions (cdfs) in orange. Vertical black dashed lines indicate the mean value, with the value of this mean step size ± S.E.M. given on the KDE/cdf plot. The histograms in black illustrate how the step sizes for SNF2h generally form a cluster, consistent with previous reports for other ISWI-family remodelers (Blosser et al., 2009; Deindl et al., 2013; Hwang et al., 2014). However, the other two representations of the same data reveal additional structure that is difficult to discern from the histograms alone. For example, the purple box over the top KDE indicates steps that likely represent nucleosomes that skipped the p1 pause, or whose p1 pause was too short to detect, such that the nucleosome was moved ~(8 bp+5 bp) = 13 bp during the first translocation. For WT ISWI-family remodelers remodeling WT nucleosomes, the initial step has been reported to range from 6.9 ± 0.1 bp to 7.4 ± 0.1 bp, and the second step from 3.0±0.1 to 3.7±0.2 (Blosser et al., 2009; Deindl et al., 2013; Hwang et al., 2014). The difference of ~ 1 bp in the size of the second step between our work and that in the literature likely

results from the different approaches used to obtain the mean step size. B. KDE and cdf plots as in A, but for the other three combinations of nucleosomes and SNF2h constructs shown in Figure 3. Due to their lack of binning or smoothing parameters, cdfs represent the best quantitative comparison *between* data sets. However, for assessing the step size within a single data set, KDEs can provide a more intuitive picture. Cdfs here are the same as in Figure 3E (though shown here without the error estimate).

FIGURE 2.12

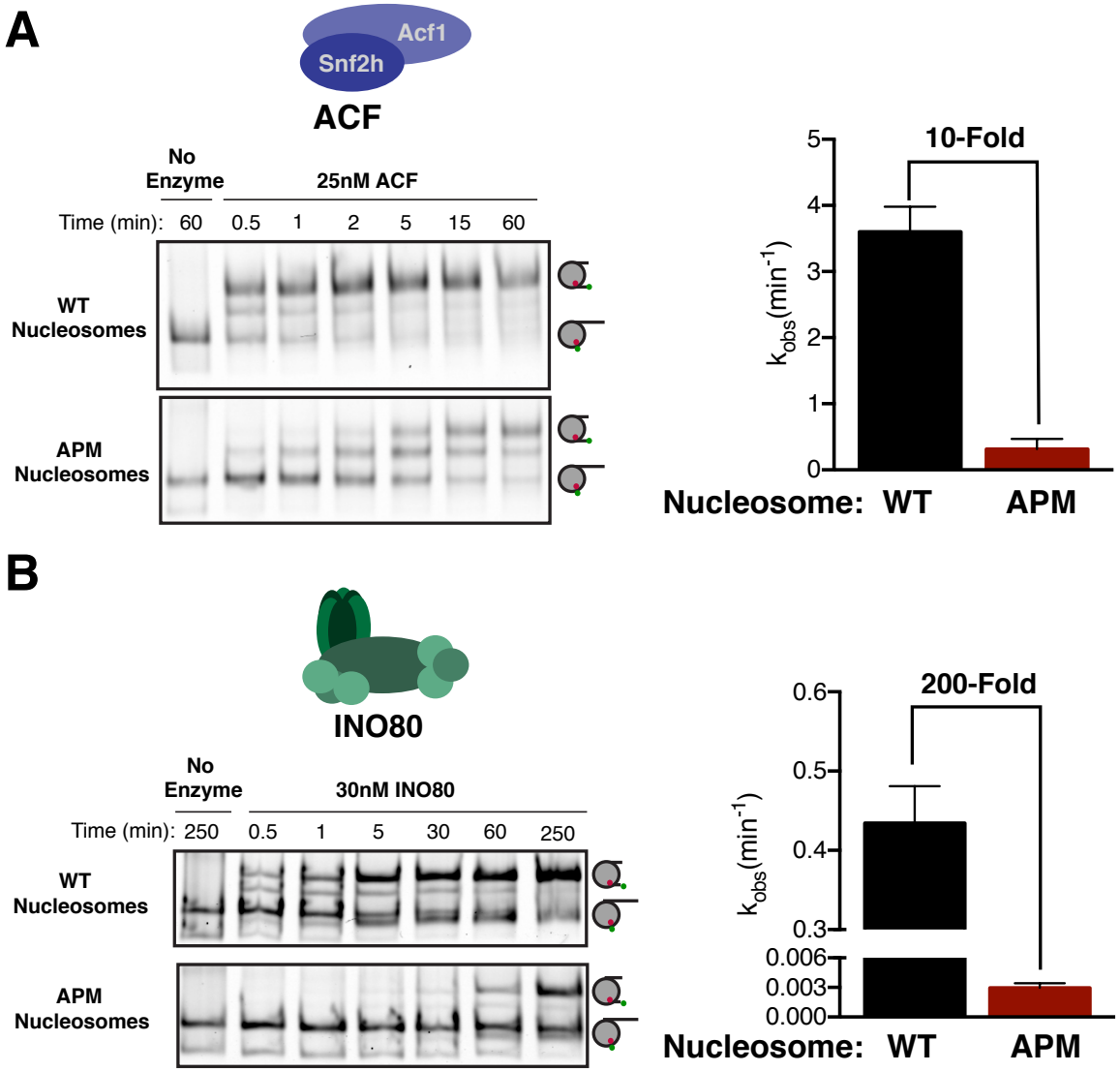

Figure 2.12 The acidic patch is used by ACF and INO80
A. Gel remodeling assay with human ACF and 0/60 nucleosomes. Saturating concentrations of enzyme and ATP were used. B. Gel remodeling with the yeast INO80 complex and 0/60 nucleosomes. Reactions were performed with saturating enzyme and ATP. Error bars represent standard error of the mean for N=3 replicates.

FIGURE 2.13

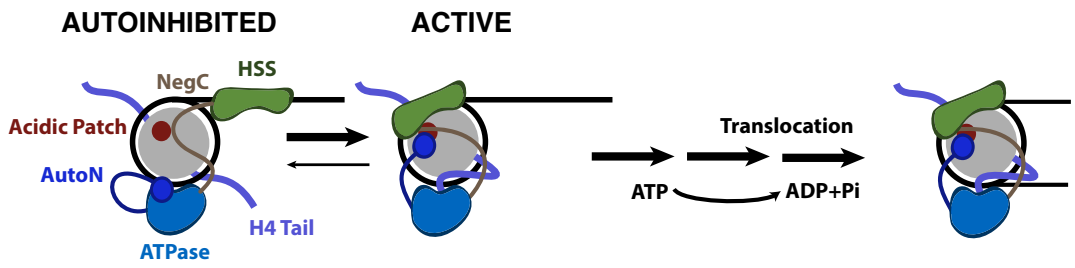

Figure 2.13 Model for nucleosome remodeling by SNF2h
After binding the nucleosome, SNF2h is in equilibrium between an active and autoinhibited state. In the autoinhibited state AutoN and NegC hold the remodeler in an inactive state. The active state is promoted by AutoN and NegC binding near the acidic patch and by H4 tail binding the ATPase domain resulting in conformational changes that bring HSS in close proximity to the acidic patch. From this active state, SNF2h can translocate DNA around the octamer. Although SNF2h remodels nucleosomes as a dimer at saturating enzyme concentrations [26,59], in this model we display only one of the protomers for simplicity.

FIGURE 2.14

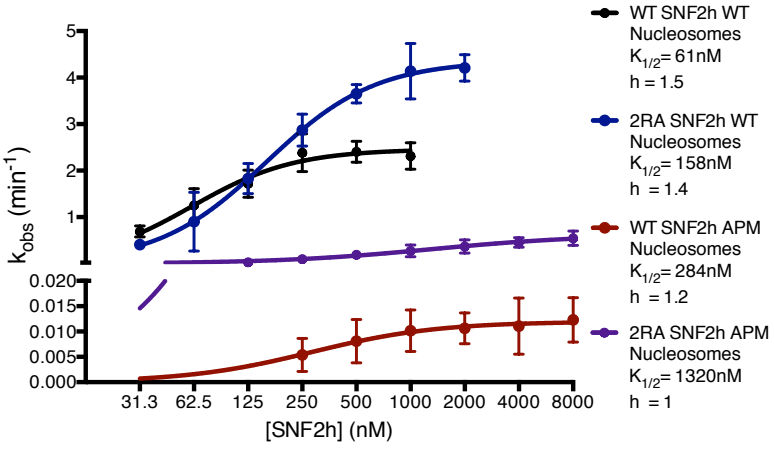
WT SNF2h WT Nucleosomes
K1/2= 61nM
h = 1.5
2RA SNF2h WT Nucleosomes
K1/2= 158nM
h = 1.4
WT SNF2h APM Nucleosomes
K1/2= 284nM
h = 1.2
2RA SNF2h APM Nucleosomes
K1/2= 1320nM
h = 1
kobs (min-1)
0.020
0.015
0.010
0.005
0.000
1
2
3
4
5
31.3 62.5 125 250 500 1000 2000 4000 8000
[SNF2h] (nM)

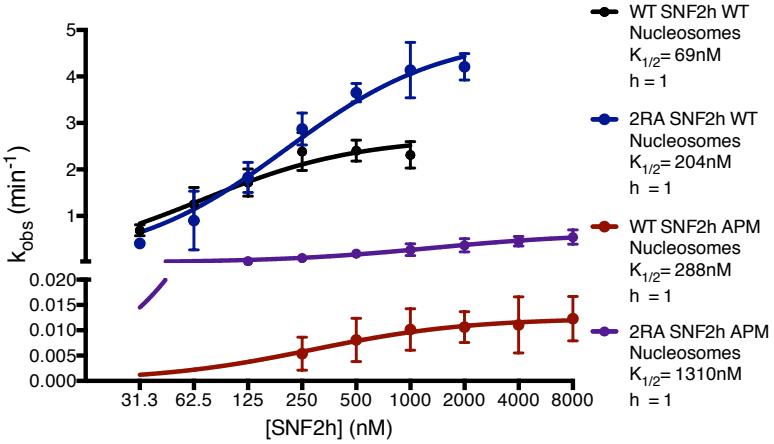
WT SNF2h WT Nucleosomes
K1/2= 69nM
h = 1
2RA SNF2h WT Nucleosomes
K1/2= 204nM
h = 1
WT SNF2h APM Nucleosomes
K1/2= 288nM
h = 1
2RA SNF2h APM Nucleosomes
K1/2= 1310nM
h = 1
kobs (min-1)
0.020
0.015
0.010
0.005
0.000
1
2
3
4
5
31.3 62.5 125 250 500 1000 2000 4000 8000
[SNF2h] (nM)

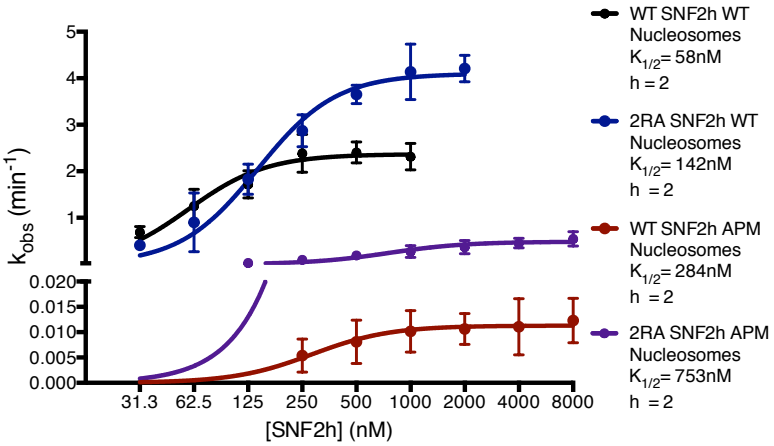
WT SNF2h WT Nucleosomes
K1/2= 58nM
h = 2
2RA SNF2h WT Nucleosomes
K1/2= 142nM
h = 2
WT SNF2h APM Nucleosomes
K1/2= 284nM
h = 2
2RA SNF2h APM Nucleosomes
K1/2= 753nM
h = 2
kobs (min-1)
0.020
0.015
0.010
0.005
0.000
1
2
3
4
5
31.3 62.5 125 250 500 1000 2000 4000 8000
[SNF2h] (nM)

Figure 2.14 Saturation Kinetics Experiments
Fits of the dependence of remodeling rates on enzyme concentration for each enzyme-substrate pair. Previous work indicates that SNF2h cooperatively remodels nucleosomes as a dimer, suggesting the data should fit to a hill coefficient greater than 1[59]. However, we cannot rule out that mutations may affect the cooperative association of SNF2h. To address this, reactions were fit with either a floating hill coefficient (top) or constrained to hill coefficient of 1 (middle) or 2 (bottom). Both K_m^{app} and k_{max} change less than 2-fold regardless of whether the data are fit to a fixed hill coefficient or fit to a floating coefficient.

FIGURE 2.15

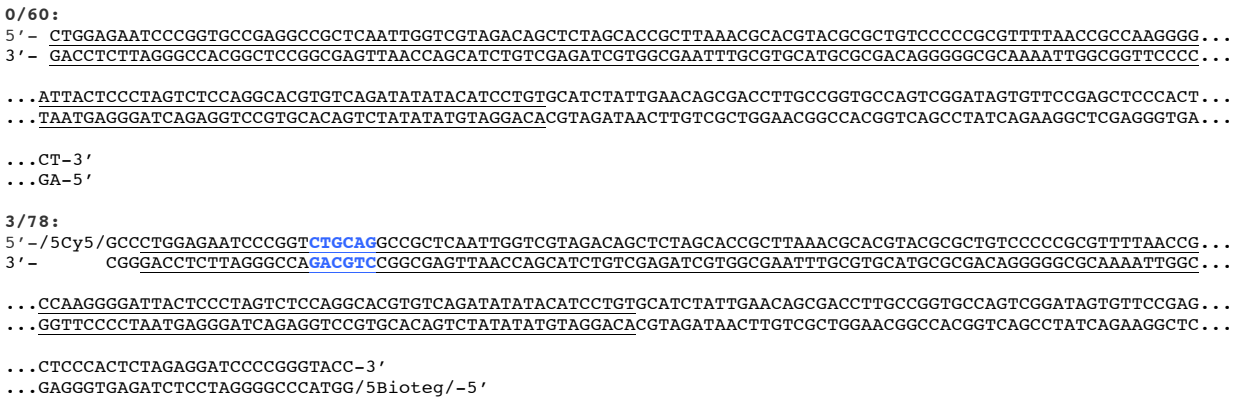

Figure 2.15 Sequences of DNA constructs used in this work
601 nucleosome positioning sequence is underlined; Pst18 restriction site (where present) is in blue. The sequence of the 3/78 construct is the same as the “n=3” construct in Blosser et al., and the 3/78 construct in Zhou et al. 2018 [26,31].

FIGURE 2.16

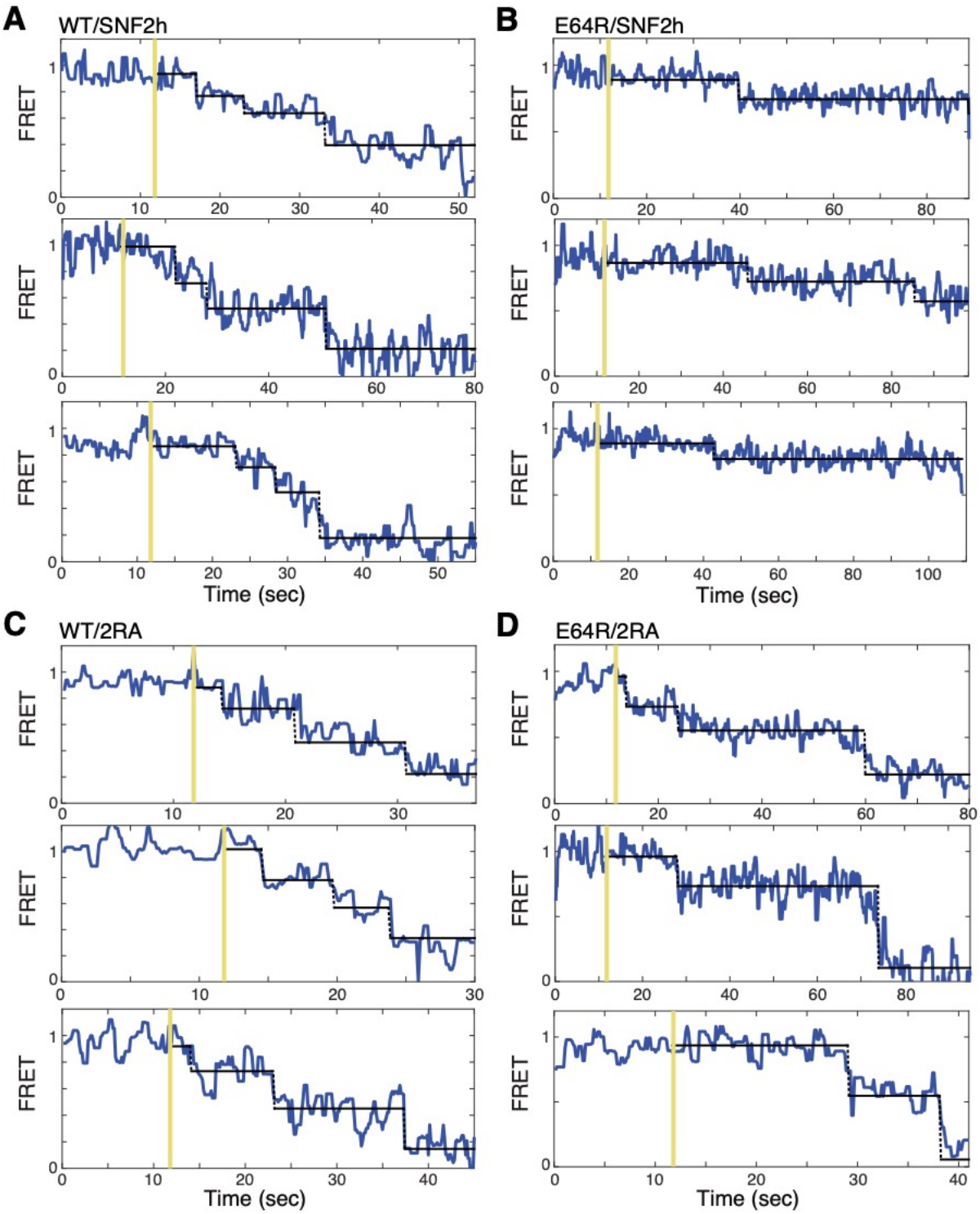

Figure 2.16 Additional example traces of SNF2h or SNF2h/2RA remodeli ng single nucleosomes, plotted as in Figure 3C.

SUPPLEMENTAL FIGURE 2.1

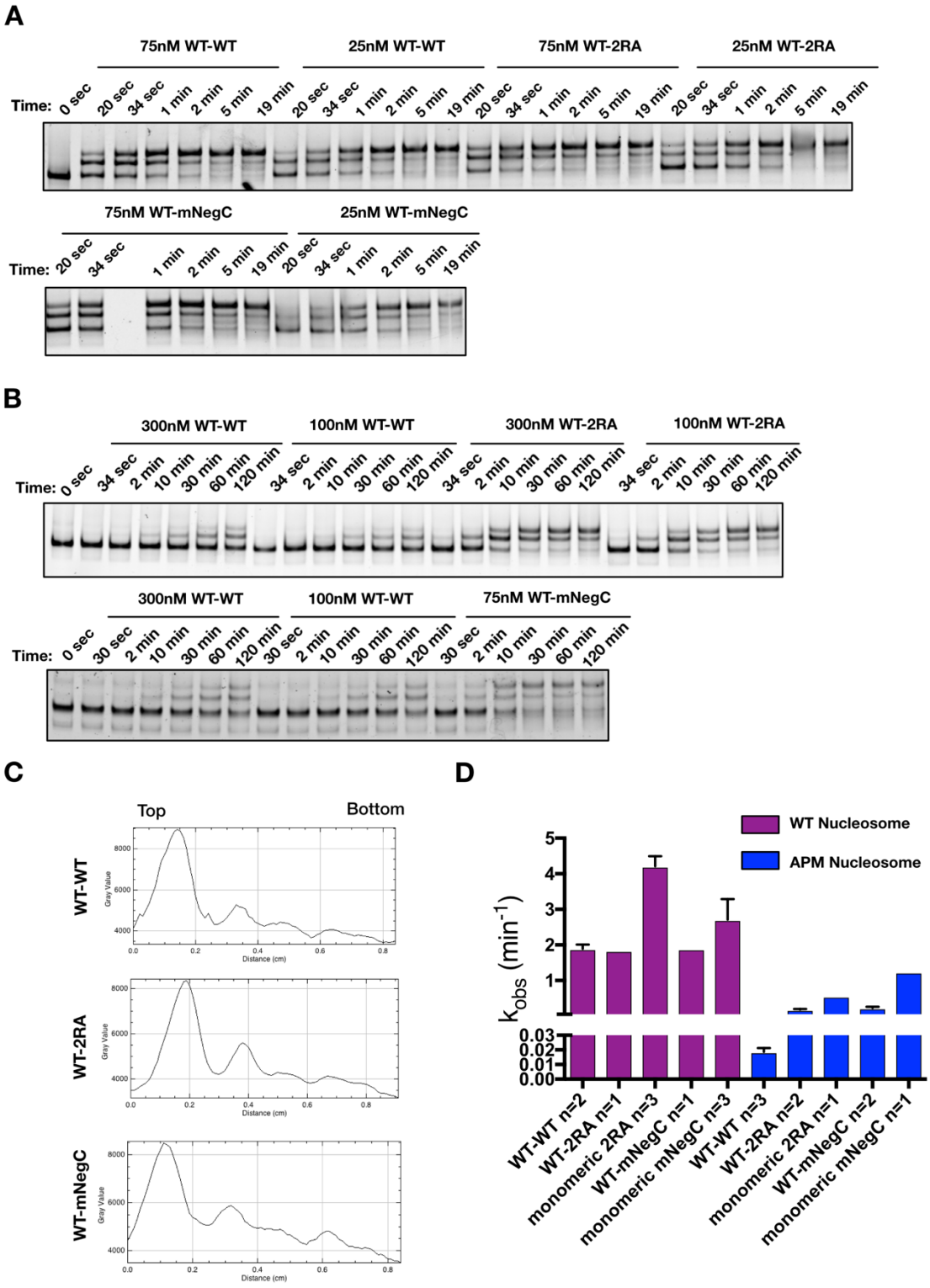

Supplemental Figure 2.1. Remodeling with SNF2h connected dimers with autoinhibition mutants

Native gel sliding assay with A. WT or B. APM nucleosomes with saturating concentrations (values indicated) of connected SNF2h dimer. C. Line scan profiles of the final time points of native gel sliding assays with WT nucleosomes and the indicated connected SNF2h dimer. D. Observed rate constants for connected dimer SNF2h remodeling of 0/60 nucleosomes with the indicated number of replicates. Error bars reflect the SEM.

SUPPLEMENTAL FIGURE 2.2

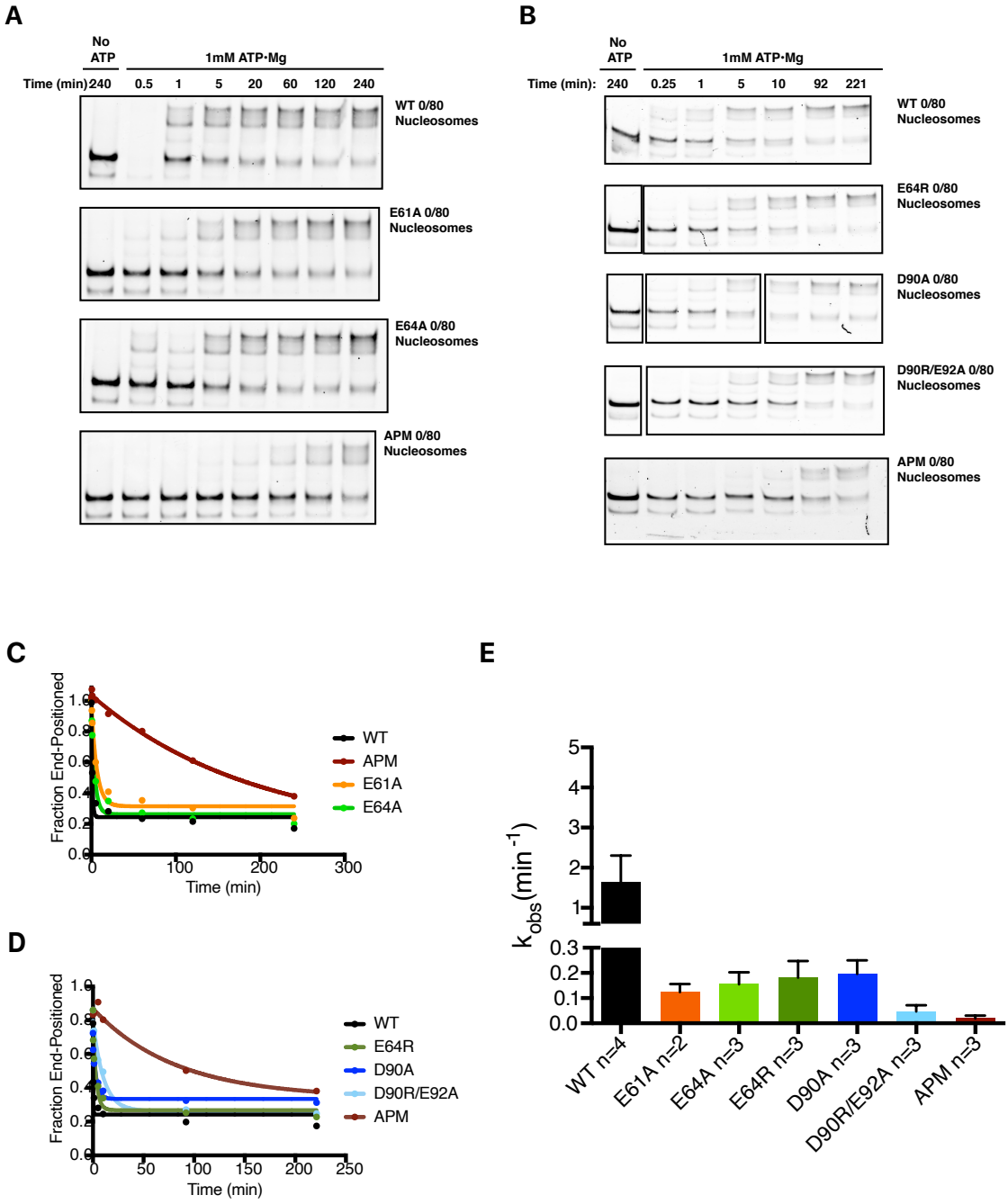

Supplemental Figure 2.2. Residues of the acidic patch contribute additively to INO80 remodeling

A-B. Native gel remodeling assay with saturating concentrations of INO80 (>30nM). C-D. Quantification of data presented in A-B fit to a single exponential decay. E. Observed rate constants for INO80 remodeling of 0/80 nucleosomes with the indicated number of replicates. Error bars reflect the SEM.

References

[1] K. Luger, A.W. Mäder, R.K. Richmond, D.F. Sargent, T.J. Richmond, Crystal structure of the nucleosome core particle at 2.8 A resolution., Nature. 389 (1997) 251–260. https://doi.org/10.1038/38444.

[2] K. Luger, M.L. Dechassa, D.J. Tremethick, New insights into nucleosome and chromatin structure: an ordered state or a disordered affair?, Nature Reviews Molecular Cell Biology. 13 (2012) 436–447. https://doi.org/10.1038/nrm3382.

[3] C.Y. Zhou, S.L. Johnson, N.I. Gamarra, G.J. Narlikar, Mechanisms of ATP-Dependent Chromatin Remodeling Motors, Annual Review of Biophysics. 45 (2016) 153–181. https://doi.org/10.1146/annurev-biophys-051013-022819.

[4] K.B. Falbo, X. Shen, Chromatin remodeling in DNA replication, Journal of Cellular Biochemistry. 97 (2006) 684–689. https://doi.org/10.1002/jcb.20752.

[5] S.K. Hota, B.G. Bruneau, ATP-dependent chromatin remodeling during mammalian development, Development (Cambridge, England). 143 (2016) 2882–2897. https://doi.org/10.1242/dev.128892.

[6] B.D. Price, A.D. D'Andrea, Chromatin Remodeling at DNA Double-Strand Breaks, Cell. 152 (2013) 1344–1354.

[7] C.R. Clapier, G. Längst, D.F. Corona, P.B. Becker, K.P. Nightingale, Critical role for the histone H4 N terminus in nucleosome remodeling by ISWI., Molecular and Cellular Biology. 21 (2001) 875–883. https://doi.org/10.1128/mcb.21.3.875-883.1901.

[8] J.G. Yang, T.S. Madrid, E. Sevastopoulos, G.J. Narlikar, The chromatin-remodeling enzyme ACF is an ATP-dependent DNA length sensor that regulates nucleosome spacing., 13 (2006) 1078–1083. https://doi.org/10.1038/nsmb1170.

[9] J.R. Guyon, G.J. Narlikar, S. Sif, R.E. Kingston, Stable remodeling of tailless nucleosomes by the human SWI-SNF complex., Molecular and Cellular Biology. 19 (1999) 2088–2097.

[10] C.R. Clapier, B.R. Cairns, Regulation of ISWI involves inhibitory modules antagonized by nucleosomal epitopes, Nature. 492 (2012) 280–284. https://doi.org/10.1038/nature11625.

[11] G. Hauk, J.N. McKnight, I.M. Nodelman, G.D. Bowman, The chromodomains of the Chd1 chromatin remodeler regulate DNA access to the ATPase motor., Molecular Cell. 39 (2010) 711–723. https://doi.org/10.1016/j.molcel.2010.08.012.

[12] X. Xia, X. Liu, T. Li, X. Fang, Z. Chen, Structure of chromatin remodeler Swi2/Snf2 in the resting state., Nature Structural & Molecular Biology. 23 (2016) 722–729. https://doi.org/10.1038/nsmb.3259.

[13] L. Yan, L. Wang, Y. Tian, X. Xia, Z. Chen, Structure and regulation of the chromatin remodeller ISWI, Nature. 540 (2016) 466–469. https://doi.org/10.1038/nature20590.

[14] R.K. McGinty, S. Tan, Recognition of the nucleosome by chromatin factors and enzymes., Current Opinion in Structural Biology. 37 (2016) 54–61. https://doi.org/10.1016/j.sbi.2015.11.014.

[15] G.P. Dann, G.P. Liszczak, J.D. Bagert, M.M. Müller, U.T.T. Nguyen, F. Wojcik, Z.Z. Brown, J. Bos, T. Panchenko, R. Pihl, S.B. Pollock, K.L. Diehl, C.D. Allis, T.W. Muir, ISWI

chromatin remodellers sense nucleosome modifications to determine substrate preference, Nature. 548 (2017) 607–611. https://doi.org/10.1038/nature23671.

[16] A.J. Barbera, J.V. Chodaparambil, B. Kelley-Clarke, V. Joukov, J.C. Walter, K. Luger, K.M. Kaye, The nucleosomal surface as a docking station for Kaposi's sarcoma herpesvirus LANA., Science (New York, N.Y.). 311 (2006) 856–861. https://doi.org/10.1126/science.1120541.

[17] J.D. Leonard, G.J. Narlikar, A Nucleotide-Driven Switch Regulates Flanking DNA Length Sensing by a Dimeric Chromatin Remodeler, Molecular Cell. (2015). https://doi.org/10.1016/j.molcel.2015.01.008.

[18] L.R. Racki, N. Naber, E. Pate, J.D. Leonard, R. Cooke, G.J. Narlikar, The histone H4 tail regulates the conformation of the ATP-binding pocket in the SNF2h chromatin remodeling enzyme., Journal of Molecular Biology. 426 (2014) 2034–2044. https://doi.org/10.1016/j.jmb.2014.02.021.

[19] K.K. Sinha, J.D. Gross, G.J. Narlikar, Distortion of histone octamer core promotes nucleosome mobilization by a chromatin remodeler., Science (New York, N.Y.). 355 (2017) eaaa3761. https://doi.org/10.1126/science.aaa3761.

[20] A. Hamiche, R. Sandaltzopoulos, D.A. Gdula, C. Wu, ATP-Dependent Histone Octamer Sliding Mediated by the Chromatin Remodeling Complex NURF, Cell. 97 (1999) 833–842. https://doi.org/10.1016/s0092-8674(00)80796-5.

[21] W. Dang, B. Bartholomew, Domain architecture of the catalytic subunit in the ISW2-nucleosome complex., Molecular and Cellular Biology. 27 (2007) 8306–8317. https://doi.org/10.1128/mcb.01351-07.

[22] M.N. Kagalwala, B.J. Glaus, W. Dang, M. Zofall, B. Bartholomew, Topography of the ISW2-nucleosome complex: insights into nucleosome spacing and chromatin remodeling., The EMBO Journal. 23 (2004) 2092–2104. https://doi.org/10.1038/sj.emboj.7600220.

[23] R. Schwanbeck, H. Xiao, C. Wu, Spatial contacts and nucleosome step movements induced by the NURF chromatin remodeling complex., The Journal of Biological Chemistry. 279 (2004) 39933–39941. https://doi.org/10.1074/jbc.m406060200.

[24] M. Zofall, J. Persinger, S.R. Kassabov, B. Bartholomew, Chromatin remodeling by ISW2 and SWI/SNF requires DNA translocation inside the nucleosome., Nature Structural & Molecular Biology. 13 (2006) 339–346. https://doi.org/10.1038/nsmb1071.

[25] C.R. Clapier, K.P. Nightingale, P.B. Becker, A critical epitope for substrate recognition by the nucleosome remodeling ATPase ISWI., Nucleic Acids Research. 30 (2002) 649–655. https://doi.org/10.1093/nar/30.3.649.

[26] T.R. Blosser, J.G. Yang, M.D. Stone, G.J. Narlikar, X. Zhuang, Dynamics of nucleosome remodelling by individual ACF complexes., Nature. 462 (2009) 1022–1027. https://doi.org/10.1038/nature08627.

[27] S. Deindl, W.L. Hwang, S.K. Hota, T.R. Blosser, P. Prasad, B. Bartholomew, X. Zhuang, ISWI remodelers slide nucleosomes with coordinated multi-base-pair entry steps and single-base-pair exit steps., Cell. 152 (2013) 442–452. https://doi.org/10.1016/j.cell.2012.12.040.

[28] B.T. Harada, W.L. Hwang, S. Deindl, N. Chatterjee, B. Bartholomew, X. Zhuang, Stepwise nucleosome translocation by RSC remodeling complexes., ELife. 5 (2016) 3653. https://doi.org/10.7554/elife.10051.

[29] W.L. Hwang, S. Deindl, B.T. Harada, X. Zhuang, Histone H4 tail mediates allosteric regulation of nucleosome remodelling by linker DNA., Nature. 512 (2014) 213–217. https://doi.org/10.1038/nature13380.

[30] S. Johnson, M. Johnson, L. Breuer, G. Narlikar, Traces: Traces first release, Zenodo, 2018. https://doi.org/10.5281/zenodo.1211233.

[31] C.Y. Zhou, S.L. Johnson, L.J. Lee, A.D. Longhurst, S.L. Beckwith, M.J. Johnson, A.J. Morrison, G.J. Narlikar, The Yeast INO80 Complex Operates as a Tunable DNA Length-Sensitive Switch to Regulate Nucleosome Sliding., Molecular Cell. 69 (2018) 677-688.e9. https://doi.org/10.1016/j.molcel.2018.01.028.

[32] X. He, H.-Y. Fan, G.J. Narlikar, R.E. Kingston, Human ACF1 alters the remodeling strategy of SNF2h., The Journal of Biological Chemistry. 281 (2006) 28636–28647. https://doi.org/10.1074/jbc.m603008200.

[33] M. Oppikofer, T. Bai, Y. Gan, B. Haley, P. Liu, W. Sandoval, C. Ciferri, A.G. Cochran, Expansion of the ISWI chromatin remodeler family with new active complexes., EMBO Reports. 18 (2017) 1697–1706. https://doi.org/10.15252/embr.201744011.

[34] T. Tsukiyama, C. Daniel, J. Tamkun, C. Wu, ISWI, a member of the SWI2/SNF2 ATPase family, encodes the 140 kDa subunit of the nucleosome remodeling factor, Cell. 83 (1995) 1021–1026. https://doi.org/10.1016/0092-8674(95)90217-1.

[35] P.D. Varga-Weisz, P.B. Becker, M. Wilm, P.D. Varga-Weisz, M. Wilm, E. Bonte, E. Bonte, K. Dumas, K. Dumas, M. Mann, M. Mann, Chromatin-remodelling factor CHRAC contains the ATPases ISWI and topoisomerase II, Nature. 388 (1997) 598–602. https://doi.org/10.1038/41587.

[36] N. Collins, R.A. Poot, I. Kukimoto, C. García-Jiménez, G. Dellaire, P.D. Varga-Weisz, An ACF1-ISWI chromatin-remodeling complex is required for DNA replication through heterochromatin., Nature Genetics. 32 (2002) 627–632. https://doi.org/10.1038/ng1046.

[37] D.V. Fyodorov, M.D. Blower, G.H. Karpen, J.T. Kadonaga, Acf1 confers unique activities to ACF/CHRAC and promotes the formation rather than disruption of chromatin in vivo., Genes & Development. 18 (2004) 170–183. https://doi.org/10.1101/gad.1139604.

[38] L. Lan, A. Ui, S. Nakajima, K. Hatakeyama, M. Hoshi, R. Watanabe, S.M. Janicki, H. Ogiwara, T. Kohno, S.-I. Kanno, A. Yasui, The ACF1 complex is required for DNA double-strand break repair in human cells., Molecular Cell. 40 (2010) 976–987. https://doi.org/10.1016/j.molcel.2010.12.003.

[39] R.F. Levendosky, A. Sabantsev, S. Deindl, G.D. Bowman, The Chd1 chromatin remodeler shifts hexasomes unidirectionally., ELife. 5 (2016) 3302. https://doi.org/10.7554/elife.21356.

[40] M. Udugama, A. Sabri, B. Bartholomew, The INO80 ATP-dependent chromatin remodeling complex is a nucleosome spacing factor., Molecular and Cellular Biology. 31 (2011) 662–673. https://doi.org/10.1128/mcb.01035-10.

[41] N. Krietenstein, M. Wal, S. Watanabe, B. Park, C.L. Peterson, B.F. Pugh, P. Korber, Genomic Nucleosome Organization Reconstituted with Pure Proteins, Cell. 167 (2016) 709-721.e12. https://doi.org/10.1016/j.cell.2016.09.045.

[42] A. Hamiche, J.G. Kang, C. Dennis, H. Xiao, C. Wu, Histone tails modulate nucleosome mobility and regulate ATP-dependent nucleosome sliding by NURF., Proceedings

of the National Academy of Sciences. 98 (2001) 14316–14321. https://doi.org/10.1073/pnas.251421398.

[43] R. Sundaramoorthy, A.L. Hughes, V. Singh, N. Wiechens, D.P. Ryan, H. El-Mkami, M. Petoukhov, D.I. Svergun, B. Treutlein, S. Quack, M. Fischer, J. Michaelis, B. Böttcher, D.G. Norman, T. Owen-Hughes, Structural reorganization of the chromatin remodeling enzyme Chd1 upon engagement with nucleosomes., ELife. 6 (2017) 1405. https://doi.org/10.7554/elife.22510.

[44] H. Ferreira, A. Flaus, T. Owen-Hughes, Histone modifications influence the action of Snf2 family remodelling enzymes by different mechanisms., Journal of Molecular Biology. 374 (2007) 563–579. https://doi.org/10.1016/j.jmb.2007.09.059.

[45] C. Stockdale, A. Flaus, H. Ferreira, T. Owen-Hughes, Analysis of nucleosome repositioning by yeast ISWI and Chd1 chromatin remodeling complexes., The Journal of Biological Chemistry. 281 (2006) 16279–16288. https://doi.org/10.1074/jbc.m600682200.

[46] D.P. Ryan, R. Sundaramoorthy, D. Martin, V. Singh, T. Owen-Hughes, The DNA-binding domain of the Chd1 chromatin-remodelling enzyme contains SANT and SLIDE domains., The EMBO Journal. 30 (2011) 2596–2609. https://doi.org/10.1038/emboj.2011.166.

[47] J.A. Goldman, J.D. Garlick, R.E. Kingston, Chromatin remodeling by imitation switch (ISWI) class ATP-dependent remodelers is stimulated by histone variant H2A.Z., The Journal of Biological Chemistry. 285 (2010) 4645–4651. https://doi.org/10.1074/jbc.m109.072348.

[48] S. Brahma, M.I. Udugama, J. Kim, A. Hada, S.K. Bhardwaj, S.G. Hailu, T.-H. Lee, B. Bartholomew, INO80 exchanges H2A.Z for H2A by translocating on DNA proximal to histone dimers., Nature Communications. 8 (2017) 15616. https://doi.org/10.1038/ncomms15616.

[49] J.W.J. Kerssemakers, E.L. Munteanu, L. Laan, T.L. Noetzel, M.E. Janson, M. Dogterom, Assembly dynamics of microtubules at molecular resolution., Nature. 442 (2006) 709–712. https://doi.org/10.1038/nature04928.

[50] J.D. Aalfs, G.J. Narlikar, R.E. Kingston, Functional differences between the human ATP-dependent nucleosome remodeling proteins BRG1 and SNF2H., The Journal of Biological Chemistry. 276 (2001) 34270–34278. https://doi.org/10.1074/jbc.m104163200.

[51] X. Shen, Preparation and analysis of the INO80 complex., Methods in Enzymology. 377 (2004) 401–412. https://doi.org/10.1016/s0076-6879(03)77026-8.

[52] K. Luger, T.J. Rechsteiner, T.J. Richmond, Expression and Purification of Recombinant Histones and Nucleosome Reconstitution, in: Humana Press, 1999: pp. 1–16. https://doi.org/10.1385/1-59259-681-9:1.

[53] C.Y. Zhou, G.J. Narlikar, Analysis of Nucleosome Sliding by ATP-Dependent Chromatin Remodeling Enzymes., Methods in Enzymology. 573 (2016) 119–135. https://doi.org/10.1016/bs.mie.2016.01.015.

[54] P.T. Lowary, J. Widom, New DNA sequence rules for high affinity binding to histone octamer and sequence-directed nucleosome positioning., Journal of Molecular Biology. 276 (1998) 19–42. https://doi.org/10.1006/jmbi.1997.1494.

[55] C.Y. Zhou, C.I. Stoddard, J.B. Johnston, M.J. Trnka, I. Echeverria, E. Palovcak, A. Sali, A.L. Burlingame, Y. Cheng, G.J. Narlikar, Regulation of Rvb1/Rvb2 by a Domain within the INO80 Chromatin Remodeling Complex Implicates the Yeast Rvbs as Protein Assembly Chaperones., Cell Reports. 19 (2017) 2033–2044. https://doi.org/10.1016/j.celrep.2017.05.029.

[56] M.J. Trnka, P.R. Baker, P.J.J. Robinson, A.L. Burlingame, R.J. Chalkley, Matching cross-linked peptide spectra: only as good as the worse identification., Molecular & Cellular Proteomics. 13 (2014) 420–434. https://doi.org/10.1074/mcp.m113.034009.

[57] A. Edelstein, N. Amodaj, K. Hoover, R. Vale, N. Stuurman, Computer Control of Microscopes Using μManager, John Wiley & Sons, Inc., 2010. https://doi.org/10.1002/0471142727.mb1420s92.

[58] E.F. Pettersen, T.D. Goddard, C.C. Huang, G.S. Couch, D.M. Greenblatt, E.C. Meng, T.E. Ferrin, UCSF Chimera—A visualization system for exploratory research and analysis, 25 (2004) 1605–1612. https://doi.org/10.1002/jcc.20084.

[59] L.R. Racki, J.G. Yang, N. Naber, P.D. Partensky, A. Acevedo, T.J. Purcell, R. Cooke, Y. Cheng, G.J. Narlikar, The chromatin remodeller ACF acts as a dimeric motor to space nucleosomes., Nature. 462 (2009) 1016–1021. https://doi.org/10.1038/nature08621.

Chapter 3: Electron cryo-microscopy structures of remodeler-nucleosome intermediates suggest allosteric control through the nucleosome.

Abstract

The SNF2h remodeler slides nucleosomes most efficiently as a dimer, yet how the two protomers avoid a tug-of-war is unclear. Furthermore, SNF2h couples histone octamer deformation to nucleosome sliding, but the underlying structural basis remains unknown. Here we present cryo-EM structures of SNF2h-nucleosome complexes with ADP-BeFx that capture two reaction intermediates. In one structure, histone residues near the dyad and in the H2A-H2B acidic patch, distal to the active SNF2h protomer, are disordered. The disordered acidic patch is expected to inhibit the second SNF2h promoter, while disorder near the dyad is expected to promote DNA translocation. The other structure doesn't show octamer deformation, but surprisingly shows a 2bp translocation. FRET studies indicate that ADP-BeFx predisposes SNF2h-nucleosome complexes for an elemental translocation step. We propose a model for allosteric control through the nucleosome, where one SNF2h protomer promotes asymmetric octamer deformation to inhibit the second protomer, while stimulating directional DNA translocation.

Introduction

ATP-dependent chromatin remodeling motors play central roles in regulating access to the genome [1,2]. Much has been learnt about remodeling mechanisms through the study of four classes of remodeling motors: the SWI/SNF class, the ISWI class, the CHD class and the combined INO80 and SWR class [3]. The ATPase subunits of the SWI/SNF, ISWI and CHD classes have been shown to carry out most of the biochemical activities of their parent complexes. Despite sharing sequence homology within their ATPase domains, these motors play distinct roles *in vivo* and differ significantly in their

biochemical activities [2–4]. For example, SWI/SNF motors can generate products ranging from translationally repositioned to fully evicted histone octamers (nucleosome sliding and disassembly, respectively). In contrast, the ISWI and CHD family of motors appear to only slide nucleosomes but differ in how their activity is regulated by the extra-nucleosomal DNA flanking a nucleosome and the N-terminal histone H4 tail [3]. Finally, while the human ISWI remodeler, SNF2h, functions most optimally as a dimer, SWI/SNF and CHD family remodelers are proposed to mainly function as monomeric ATPases [5–9]. We note that recent cryo-EM structures of yeast Chd1 showed some states with two Chd1 molecules bound to a nucleosome, but the mechanistic significance of this dimeric architecture is not known [10].

Despite fundamental mechanistic advances over the past two decades, the structural basis for how remodeling motors work and why different remodeler families differ in mechanism remains poorly understood. Recent advances in electron cryo-microscopy (cryo-EM) methodology have allowed direct visualization of SWI/SNF, CHD, INO80 and SWR remodeling motors bound to the nucleosome at high resolution [10–14]. Here we present cryo-EM structures of the full-length form of the human ISWI remodeler, SNF2h bound to a nucleosome. Carrying out cryo-EM without any cross-linking and using the ATP analog ADP-BeF_x enabled us to trap three different conformational states of the SNF2h-nucleosome complex: a state with an unexpectedly translocated nucleosome (Figure 3.1, Figure 3.2), a state with two SNF2h protomers bound to a nucleosome (Figure 3.3, Figure 3.4) and a state with one protomer bound to a nucleosome that shows increased disorder within the histone core (Figure 3.3B). The locations of histone disorder strongly suggest a role for octamer deformation in protomer coordination and directional DNA translocation. In addition, we detect new ISWI-histone contacts that make significant

contributions to nucleosome sliding and help explain why ISWI may in differ in mechanism from Swi2/Snf2 (Figure 3.5) [13].

Results

Overview of SNF2h-nucleosome structures

Like most ISWI remodelers, SNF2h slides mono-nucleosomes assembled on short stretches of DNA towards the center of the DNA [1–3]. In previous studies we have found that while a monomer of SNF2h can slide nucleosomes, SNF2h functions most optimally as a dimer [6,9]. In these studies, we were able to visualize both singly bound and doubly bound SNF2h using negative stain EM [9]. Previous studies have further shown that binding of the ATP analog, ADP-BeF_x, promotes a restricted conformation of the ATPase active site in a manner that is dependent on the H4 tail [15]. The restricted conformation is consistent with observations showing an activating role for the H4 tail [16–18]. Further, binding of ADP-BeF_x to SNF2h promotes conformational flexibility of buried histone residues [19]. This conformational flexibility is functionally important because restricting the flexibility via disulfide bonds inhibits nucleosome sliding [19]. Based on these observations we have previously reasoned that the ADP-BeF_x state mimics an activated reaction intermediate. With the goal of obtaining high-resolution structures of this intermediate, we assembled SNF2h-nucleosome complexes in the presence of ADP-BeF_x. The nucleosomes contain 60 base-pairs (bp) of flanking DNA on one end (0/60 nucleosomes). SNF2h-nucleosome complexes were assembled using conditions similar to those used in our previous negative stain EM experiments with the additional variable of salt concentration as discussed below [9]. Cryo-EM grids were prepared without using cross-linking.

During the course of this study, we collected two cryo-EM datasets using two different salt conditions for optimization of cryo-EM grid preparation. Electron micrographs and two-dimensional (2D) class averages calculated from a cryo-EM dataset collected earlier using lower salt (70 mM KCl) on a scintillator-based camera show a relatively high percentage of doubly bound SNF2h-nucleosome complexes (Figure 3.3A, Figure 3.4, 3.6A). In contrast, a more recent dataset collected using higher salt (140 mM KCl) on a K2 direct electron detection camera shows that the majority of the particles have one SNF2h bound to a nucleosome rather than two (Figure 3.1, Figure 3.6B-C, Figure 3.8). The reason for this difference is not fully understood. While higher salt reduces SNF2h affinity for nucleosomes, we believe the increase in salt by itself is not sufficient to cause complex dissociation as by negative stain EM we observe a high proportion of doubly bound complexes under these conditions (Figure 3.9). The higher salt concentration may, however, have a bigger impact when combined with other destabilizing factors during the process of plunge freezing cryo-EM grids, some of which are discussed in the Methods and further below.

With the goal of achieving the highest resolution possible we initially focused on the dataset obtained from the K2 direct electron detection camera. Using this dataset we determined a 3D reconstruction with a single SNF2h bound to a nucleosome at a resolution of 3.4 Å (Figure 3.1). The majority of particles contributed to this reconstruction having SNF2h bound to the flanking DNA at Super Helical Location (SHL) -2, judging from the density of flanking DNA. The locations of SHL +2 and -2 as well as the entry and exit site DNA are defined in Figure 3.1C. This map is of sufficient quality for model building of nucleosomal DNA, core histones and the ATPase domain of SNF2h (Figure 3-supplement 1). The nucleotide binding pocket shows clear density of bound ADP (Figure 3.1D, Figure 3.10), but we cannot unambiguously confirm the presence of

BeFx. The ATP binding site was also functionally confirmed by mutagenesis (Figure 3-supplement 2). In addition to the ATPase domain, SNF2h has a C-terminal domain termed HAND-SANT-SLIDE (HSS), which binds flanking DNA, and an N-terminal region termed AutoN, which plays an autoihibitory role (Figure 3.5A) [2,4,20,21]. These regions are not visible at high resolution, suggesting conformational flexibility of these regions in this state. By comparison to the K2 dataset, the earlier dataset was collected from a scintillator-based camera, which impeded the achievable resolution of the maps. From this dataset we determined two three-dimensional (3D) reconstructions, one of a nucleosome with doubly bound SNF2h and the other with singly bound SNF2h, both at 8.4 Å resolution with most histone helices fully resolved (Figure 3.3A-B, Figure 3.4, Figure 3.6A). The atomic models derived from the 3.4Å reconstruction fit well into the density for the doubly bound SNF2h-nucleosome complex as rigid bodies (Figure 3.3A).

To assess whether the main difference between the two structures was simply resolution or whether we had trapped different states of the SNF2h-nucleosome complex, we carried out further analysis and comparisons as described below.

A SNF2h-nucleosome complex with an asymmetrically deformed histone octamer

For the detailed analysis we first focused on the older data set as this contained a larger set of doubly bound particles. Particles contributing to this reconstruction were aligned unambiguously using flanking DNA as a fiducial marker to break the pseudo symmetry (Figure 3.3A, Figure 3.6A). The density of the SNF2h bound at SHL+2 is weaker than that of SNF2h bound at SHL-2 (Figure 3.3A, Figure 3.6A). This difference suggests that the SNF2h bound to the nucleosome at SHL+2 is conformationally more flexible. Substantial previous work has suggested that when ISWI enzymes move end-positioned nucleosomes towards the center, the active protomer initiates translocation from SHL+2

and engages the entry site flanking DNA via its HSS domain (See Figure 3.1C for nomeclature) [6,20,22–24]. The increased conformational flexibility of the SNF2h protomer bound at SHL+2 is consistent with this protomer being the active one.

Some regions of the histone octamer in the doubly bound structure were less well resolved than other regions, suggesting specific regions of disorder within the octamer (Figure 3.6G). The apparent disorder was somewhat symmetric, and without an internal control for comparison, we could not unambiguously interpret the lower resolution as resulting from increased disorder as opposed to achievable resolution. However, we noticed that in the singly bound structures, with SNF2h bound at SHL+2, the disorder is asymmetric providing a chance to use the non-disordered half of the octamer as an internal control for achievable resolution. With this internal control the reconstruction obtained from the singly bound particles unambiguously shows asymmetric deformation of the histone core (Figure 3.3B-C, compare canonical Face B to disordered Face A). These results suggested that (i) the less well resolved local regions in the doubly bound structure also likely result from increased local disorder and (ii) a given SNF2h protomer causes octamer disorder on only one side of the nucleosome. Specifically, two regions of the folded histones show increased disorder (helix α2 in H3 and the H2A/H2B acidic patch, Figure 3.3C). The disorder is easily apparent when the intact density for the blue, red and yellow helices in face B is compared to the missing or altered density for these helices in face A (Figure 3.3C, black arrows). These locations of octamer disorder are mechanistically informative as detailed below.

The region of increased disorder at helix α2 in H3 is proximal to the nucleosomal dyad. This region also interfaces with buried residues in H4 that showed increased dynamics in our previous NMR studies [19]. What could be the significance of this allosteric deformation? While DNA translocation by SNF2h initiates from SHL+2,

nucleosome sliding requires the disruption of histone-DNA contacts to allow propagation of DNA around the octamer. Histone deformation near the dyad could create a relaxed local environment that facilitates disruption and propagation of DNA around the nucleosome. Further, asymmetry in this disruption may facilitate directionality in the sliding reaction. Consistent with this possibility, our previous work shows that constraining the H3 α2 helix by disulfide cross-linking alters the directionality of nucleosome sliding [19]. Additionally, recent studies by others have suggested asymmetric rearrangements of helix α2 in H3 at 150 mM NaCl and have found that the same disulfide crosslinks inhibit thermally driven nucleosome sliding [25]. Based on these comparisons, our findings here suggest that SNF2h amplifies intrinsic nucleosome dynamics during the sliding reaction.

The other region of increased disorder is the acidic patch formed between histone H2A and H2B. Previous work has suggested that interactions between SNF2h and the acidic patch play a critical role in stimulating nucleosome sliding [26,27]. Interestingly, recent biochemical studies using asymmetric acidic patch mutant nucleosomes indicate that the activity of a SNF2h protomer bound at SHL+2 (as defined in Figure 1C) requires the acidic patch on the undistorted octamer face (Face B) [28]. All of these observations raise the intriguing possibility that binding of one SNF2h protomer allosterically deforms the acidic patch that is required by the second protomer on the other side of the nucleosome. Such an allosteric effect could serve to inhibit the second protomer from initiating sliding in the opposite direction, thus preventing a tug-of-war between the two protomers.

A SNF2h-nucleosome complex with a translocated nucleosome

The analysis above led us to ask if we could also detect octamer deformation in the newer data set. We first explored if there were particles suggesting increased dynamics in the K2 dataset that we could have missed in the drive for homogeneity and the highest resolution. Including particles with substantial octamer dynamics would by definition increase local disorder in the reconstruction and affect the resolution both locally and globally. However, we failed to extract any subset from the excluded particles that shows signs of octamer dynamics, suggesting that this dataset may not contain particles with deformed octamers.

However, as part of our analysis for detecting octamer dynamics, we re-picked the particles and separated them into two different classes of single SNF2h-bound nucleosomes: a larger one of 3.9 Å resolution with a single enzyme bound at SHL-2 (Figure 3.6B, 3.7E, 3.8B,) and a smaller one of 6.9 Å with a single enzyme bound at SHL+2 (Figure 3.6B, 3.6F, 3.7A). The lower resolution of 6.9 Å is primarily due to the small number of particles in this conformation. The atomic models of nucleosomal DNA, core histones and the ATPase domain of SNF2h derived from the 3.4 Å map fit well into the density map of the 3.9 Å and 6.9 Å reconstructions as rigid bodies. Unexpectedly, in both the 3.9 Å and 6.9 Å reconstructions, we observed that 2 bp of DNA is translocated from the exit site (Figure 3.11, 3.12A-B). The DNA density at the exit side of the nucleosome is intact and fully resolved, suggesting tight association of DNA with the histone octamer, similar to what is observed in other nucleosome structures [29,30]. The phosphate groups in the double stranded DNA backbone are clearly resolved, which enabled us to precisely locate and count every bp and to confirm the two extra bp on the exit side of the nucleosome (Figure 3.11A-B, 3.12-3.2). We ruled out the possibility that the nucleosome particles were pre-assembled with two bp shifted before forming a

complex with SNF2h, by determining a reconstruction of nucleosomes assembled identically but untreated with SNF2h (Figure 3.6D, 3.12C). These nucleosomes do not display the 2 bp translocation of DNA from the exit side. Further, intriguingly, no extra DNA density was found in the exit side for the structures obtained at 70 mM KCl (Figure 3.12D). These comparisons indicate that the reconstructions obtained using the K2 and scintillator-based cameras at 140 mM and 70 mM KCl respectively represent different states of the SNF2h-nucleosome complex.

What could be the significance of the 2 bp translocation? Recent studies have shown that the Chd1 remodeling motor can shift 1-3 bp of nucleosomal DNA inwards from the entry site in the apo and ADP states [31]. These observations raised the possibility that SNF2h may display an analogous property in the presence of ADP-BeFx, the nucleotide analog used in our EM preparations. To test if the ADP-BeFx bound state causes changes in the conformation of nucleosomal DNA, we used single-molecule FRET (smFRET) experiments to measure changes in the location of exit DNA relative to the histone octamer (Figure 3.13). Under the 140 mM KCl buffer conditions of the EM sample preparation, we observed a change in FRET in the presence of SNF2h and ADP-BeFx (Figure 3.13D). The extent of FRET change is consistent with the change in FRET that would be expected from the translocation of 1-2 bp of DNA out of the nucleosome. This FRET change was not observed in the absence of SNF2h (Figure 3.13D). Complementary ensemble FRET experiments with a different labeling scheme that reports on changes in distance between the DNA at the exit and entry sites of the nucleosome also showed a change in FRET that is consistent with DNA translocation (Figure 3.11C-D). The ensemble FRET change was also dependent on the presence of SNF2h. These results indicate that analogous to Chd1, SNF2h can promote the shifting of ~2bp of DNA in the absence of ATP hydrolysis. However, these observations raised the question of why comparable DNA

translocation was not detected in the EM reconstructions carried out under the 70 mM KCl conditions (Figure 3.12D). We reasoned that the combination of SNF2h binding and the higher salt conditions of 140 mM KCl could increase the lability of the histone-DNA contacts and promote translocation of a few bp of DNA. To test this possibility, we repeated the ensemble FRET experiment at 70 mM KCl (Figure 3.11D). Under these conditions we did not observe a significant change in FRET explaining the absence of translocation in the 70 mM KCl reconstructions.

Unlike the structures at 70 mM KCl, the structures obtained at 140 mM KCl show a higher proportion of singly bound SNF2h at SHL-2 compared to SHL+2. Yet all the nucleosomes show the 2 bp DNA translocation in the same direction. This result seems paradoxical as a SNF2h protomer bound at SHL-2 is opposite to what is expected for the observed direction of DNA translocation [6,20,22–24]. Comparison of the individual protomers in the doubly bound complex obtained at 70 mM KCl indicates that the SNF2h protomer at SHL+2 is conformationally more flexible than that at SHL-2 (Figure 3.3A, 3.6A). This increased flexibility is consistent with the promoter at SHL+2 being the active protomer. We speculate that the increased dynamics of the SNF2h protomer bound at SHL+2 makes it more prone to dissociate during the cryo-EM grid preparation procedure carried out in 140mM KCl. We therefore interpret the structures captured at 140 mM KCl as arising from partial disassembly of a doubly bound translocated complex, in which the protomer bound at SHL+2 has promoted translocation.

Based on the above comparisons, we conclude that the reconstructions obtained at 70 mM KCl, represent reaction intermediates that are poised to translocate by exploiting specific deformations in the octamer conformation, while the reconstructions obtained at 140 mM KCl represent translocated SNF2h-nucleosome states in which the deformed octamer has relaxed to its canonical conformation. We next use the 3.4 Å

reconstruction of the translocated state to identify new SNF2h-nucleosome interactions and assess their role in nucleosome sliding.

The role of SNF2h-nucleosome interactions in nucleosome sliding

Similar to observations for the Swi2/Snf2 ATPase domain and Chd1, our structure implies a large conformational rearrangement in the RecA lobes of SNF2h upon nucleosome binding [10,13,30,32–35]. (Figure 3.5B, Figure 3.10). A large conformational change is also implied for the brace helix extending from lobe 2 (Figure 3.14A, orange helices) [13,35].

We see several interactions between RecA lobe 2 and the H4 tail (Figure 3.5C). Previous work has shown that the basic patch residues (KRHRK) of the H4 tail substantially activate ISWI remodeling, in part by counteracting the auto-inhibitory AutoN region [4,15–18,36]. The crystal structure of *Myceliophthora thermophila* ISWI revealed that AutoN forms a structured domain that binds a cleft between the two RecA lobes (lobe 1 and lobe 2) of the ATPase domain [35]. In our 3.4 Å structure we find that the AutoN domain has moved away from this cleft and one RecA lobe is flipped over the other to form a new cleft for nucleosome binding (Figure 3.5B, Figure 3.14). Most of AutoN is not resolved suggesting conformational flexibility in this state. Some residues of the RecA lobes that were shown to interact with AutoN in the unbound *Myceliophthora thermophila* ISWI structure now engage with the nucleosomal DNA and the H4 tail [35]. Among these residues is an acidic surface on lobe 2 that directly engages the histone H4 tail basic patch (Figure 3.5C, top left). This exchange of interactions provides a structural explanation for how the H4 tail relieves autoinhibition by AutoN [4]. Similar interactions were observed previously in the crystal structure of the isolated ATPase lobe 2 of *Myceliophthora thermophila* ISWI with an H4 tail peptide [35].

In addition to the H4 tail, the structure reveals new interactions between a loop within RecA lobe 2 and the globular region of histone H3 (Figure 3.5C, top right). Two residues K440 and K443 are in close proximity to make these direct contacts. Of these K443 is unique to and conserved across ISWI family members (Figure 3.15). Mutating K440 or K443 to alanine resulted in 4- and 6-fold defects respectively in the maximal rates of remodeling (Figure 3.5D-F). The K443A mutation had a much smaller effect on ATPase activity (≤ 2-fold), suggesting a role in the coupling of ATP hydrolysis to nucleosome sliding (Figure 3.16). Based on these functional effects we speculate that the interactions with H3 may help stabilize octamer deformation during SNF2h remodeling. Another residue in this loop, D442, is in proximity but not close enough to make a direct contact. Mutating it had a small (2-fold) stimulatory effect on remodeling, suggesting this residue plays a modest autoinhibitory role (Figure 3.5D-F). While comparable H3 contacts by SWI/SNF motors have not been observed, similar functionally important interactions between the H3 alpha 1 helix and an insertion in RecA lobe 2 are found in structures of the Chd1-nucleosome complex[10].

In terms of DNA interactions, several residues of the conserved lobe 1 and lobe 2 motifs are in proximity to the DNA at the SHL-2 region (Figure 4A). Two residues conserved between ISWI and SWI/SNF ATPases are W581 and N448 (Figure 3-supplement 4). While mutation of W581 in the *S. cerevisiae* Swi2/Snf2 ATPase domain causes a >10-fold defect in remodeling, mutating this residue within SNF2h caused a 3-fold defect in the maximal rate of nucleosome sliding (Figure 3.15B-D) [13]. Mutating N448 causes a ~7-fold defect in the maximal rate of remodeling (k_{obs}, Figure 3.17B-D) without causing a significant defect in the K_m (data not shown), suggesting that this interaction makes a bigger contribution during catalysis rather than binding. In contrast, both mutations had smaller effects on DNA-stimulated ATPase activity (≤ 2-fold increase,

Figure 3.16), suggesting these residues contribute to coupling of ATP hydrolysis to DNA translocation. A distortion from the normal path of nucleosomal DNA is also observed at SHL-2 (Figure 3.17E). This distortion is consistent with previous biochemical observations that the DNA path is altered at the site where the ATPase domain binds [23,24].

For *S. cerevisiae* Swi2/Snf2, a positively charged patch in RecA lobe 1 is positioned to bind on the DNA gyre below SHL+/-2 near SHL+/-6 [13]. Charge reversal point mutations in this patch modestly reduced remodeling by Swi2/Snf2 (~2-fold), while multiple charge reversal mutations had severe defects[13]. These cross-gyre contacts are not conserved with CHD family remodelers, which instead have this region in RecA lobe 1 replaced with acidic residues resulting in this lobe being positioned farther away from SHL+/-6 than in Swi2/Snf2 [10]. In our 3.4 Å structure, we see RecA lobe 1 positioned near SHL+6 but without the close contacts seen for Swi2/Snf2 (Figure 3.17A). Mutation of a lysine residue that is proximal to SHL+6 to glutamate (K298E), resulted in only a ~2-fold reduction in maximal sliding activity (Figure 3.17B-D) suggesting a modest role for this interaction in remodeling by SNF2h.

Discussion

The histone octamer is often conceptualized as a steric barrier to accessing DNA. In this context ISWI motors have the difficult task of sliding nucleosomes despite the constraints imposed by the histone octamer. Yet these motors are able to cause rapid and directional nucleosome translocation without disassembling the octamer [2]. Our results here suggest that instead of acting as a barrier that needs to be overcome, the histone octamer may actively participate in the reaction by acting as a deformable medium for

allosteric control. Below we discuss the mechanistic significance of these new findings in the context of previous discoveries.

We have previously found that SNF2h binding in the presence of ADP-BeFx increases the dynamics of a subset of buried histone residues [19]. These dynamics play a role in the initiation of nucleosome sliding from SHL+/-2 and the directionality of sliding. Relevant to these observations, several prior studies have provided evidence for intrinsic dynamics within nucleosomes. These include spontaneous unpeeling of nucleosomal DNA [37], the identification by EM of alternative configurations of histone helices within distorted nucleosomes [38] and the identification of histone mutants than increase the spontaneous dynamics [39] of core histone resides. It has been further demonstrated that core histone dynamics enable spontaneous nucleosome sliding [25]. However the scale and nature of the octamer deformations promoted by a remodeler such as SNF2h has been unknown. The EM reconstructions obtained at 70 mM KCl (Figure 3.3) provide the first direct visualization of the SNF2h mediated octamer fluctuations. Two unexpected features stand out. First, unlike the defined alternative helical conformations observed previously in nucleosomes alone, the EM density changes that we observe imply an ensemble of states with increased disorder in the histone conformation [25,38]. Second, the increased disorder is asymmetric and distal from the bound SNF2h protomer suggesting an allosteric mode of octamer deformation.

We propose that the structure captured at lower salt mimics a reaction intermediate in which SNF2h action results in asymmetric disordering of specific histone regions prior to translocation (Figure 3.18). The asymmetric nature of the octamer deformation helps explain a long-standing question about SNF2h protomer coordination. SNF2h assembles on nucleosomes as a face-to face dimer, but what prevents the two protomers from simultaneously translocating DNA in opposite directions, resulting in a

stalled nucleosome? Our findings suggest that the active protomer prevents a tug of war by allosterically altering the acidic patch surface required by the second protomer. In addition, the disorder near the dyad is expected to promote the directional translocation of DNA initiated by the active protomer. We further propose that collapse of the reaction intermediate results in an elemental translocation step, which is mimicked by the structure captured at higher salt (Figure 3.18). Consistent with this possibility, previous single-molecule studies have indicated that the elemental translocation event driven by ISWI enzymes is 1-2 bp [40].

Future studies looking at structures in additional nucleotide states will help advance our understanding of how changes in ISWI conformation are coupled to changes in octamer dynamics. This will allow for a mechanistic understanding of chromatin remodelers that parallels that of molecular motors such as kinesin and myosin.

Acknowledgements

We thank J. Tretyakova for tirelessly purifying histone proteins and help with generating DNA substrates, D. Asarnow for providing the script for variance map calculation and signal subtraction and G. Bowman and R.F. Levendosky for sharing results from unpublished data. This work is supported by grants from the NIH (GM073767 and GM108455 to GJN and R01GM082893 and 1S10OD020054 to YC) and the UCSF Program for Breakthrough Biomedical Research (New Technology Award) to YC. NG is supported by a pre-doctoral fellowship from the NSF. S.L.J. was supported by a Leukemia and Lymphoma Society Career Development Fellow award. Y.C. is an Investigator with the Howard Hughes Medical Institute. The cryo-EM density maps have been deposited in the Electron Microscopy Data Bank (EMDB) under accession numbers EMD-9353 (nucleosome with doubly bound SNF2h), EMD-9351 (nucleosome with singly bound

SNF2h at SHL+2, 8.4Å), EMD-9352 (SNF2h-nucleosome, 3.4Å), EMD-9354 (SNF2h-nucleosome SHL-2, 3.9Å), and EMD-9355 (SNF2h-nucleosome SHL+2, 6.9Å) (Figure 3.19). Corresponding unsharpened map and both half maps were deposited as maps associated with the primary depositions. Particle image stacks of nucleosome with singly bound SNF2h after motion correction have been deposited in the Electron Microscopy Public Image Archive (http://www.ebi.ac.uk/pdbe/emdb/empiar/) under accession number EMPIAR-341. Atomic coordinate of nucleosome with SNF2h bound near entry side has been deposited in the Protein Data Bank (PDB) under the accession number 6NE3 (Figure 3.19). All other data are available from the corresponding authors upon reasonable request.

Appendix to chapter 3

ATP contamination cannot explain the 1-2bp translocation observed

We have shown here data that strongly suggest that ATP hydrolysis is not required for a single 1-2bp translocation event by SNF2h. However, an additional possibility is that the assays performed with ADP contain a trace amount of contaminating ATP that are responsible for the translocation observed. For this to be possible, ATP binding to SNF2h would have to be tight enough that the trace concentrations of ATP•Mg (<1% of free nucleotide estimated by in house HPLC, data not shown) are sufficient to outcompete 0.5 mM ADP•BeFx present in our assays and CryoEM samples. To test this possibility, we measured remodeling of WT nucleosomes using our previously-described ensemble FRET assay [27] under the 140mM KCl condition with different ratios of ATP:ADP-BeFx (Supplemental Figure 3.1A). An equal mixture of ATP and ADP-BeFx remodels nucleosomes ~100-fold slower than an only ATP-containing reaction. This indicates that ADP-BeFx is a potent competitor of ATP, making it highly unlikely that trace concentrations of ATP are responsible for the 1-2bp ATP-independent translocation observed in our studies.

High concentrations of SNF2h slows remodeling in a manner that varies depending on preparation

During the course of our study of SNF2h nucleosome remodeling with WT nucleosomes using a previously described FRET assay [27], we found that high concentrations of SNF2h (>2μM) inhibits remodeling under the 140mM salt condition (Supplemental Figure 3.1 B). This is somewhat the result of slowing the sliding rate of all remodeling species, but largely is due to shifting the population to a slow-remodeling fraction (Supplemental Figure 3.1 A – C). This is not an inherent property of SNF2h as

some preparations did not exhibit this behavior. Although both preparations shown here were highly purified, both preparations contain a small but detectable fraction of degradation products that cannot be separated from full length SNF2h (data not shown). We hypothesize that differences in the abundance of specific degradation products that can compete. Inhibition of sliding activity is SNF2h concentration dependent which is consistent with a contaminating species binding to the nucleosome and inhibiting remodeling.

Prolonged incubation of SNF2h with nucleosomes in the absence of free nucleotide slows remodeling.

During the course of our studies using our FRET-based sliding assay, we also found that if we incubated saturating concentrations of SNF2h for a period of time with nucleosomes and then initiated sliding reactions by adding nucleotide that sliding was slower than if ATP and SNF2h were simultaneously added to nucleosomes. This effect was dependent on the duration of incubation (Supplemental Figure 3.1 D). Because of this information, all remodeling assays were performed without the incubation of SNF2h with nucleosomes without nucleotide.

Materials and Methods

Protein expression, purification and complex preparation for cryo-EM.

Human SNF2h was expressed in *Escherichia coli* BL21(DE3) Rosetta cells and purified as previously described [6]. SNF2h mutations were generated by site directed mutagenesis using the quick change protocol (Stratagene). Recombinant *Xenopus laevis* histones were expressed in *E. coli,* purified from inclusion bodies and assembled into octamers as described previously [41]. Briefly, histone protein octamer was reconstituted from denatured purified histones via refolding in high salt buffer and purified on a Superdex 200 increase 10/300 GL size exclusion column (GE Healthcare). DNA containing the Widom 601 positioning sequence with 60bp of flanking DNA was made by large scale PCR with Taq DNA polymerase and purified by native PAGE as described previously [42]. For remodeling assays, 5′ Cy3 labeled DNA was made by large scale PCR with a primer labeled at the 5′ end with the fluorophore [42]. DNA labeled at two locations for ensemble FRET experiments was prepared by large scale PCR of two DNA templates using labeled primers (IBA Life Sciences). 120µg of each DNA template was digested with AflIII at 37ºC overnight and purified by native PAGE. Purified DNA fragments were then ligated with 8000 units of T4 DNA ligase with 1mM ATP•$MgCl_2$ (New England Biolabs) for 20 min at room temperature and purified again by native PAGE. Nucleosomes were reconstituted by the salt gradient dialysis method and purified by glycerol gradient centrifugation [42]. Purified nucleosomes were flash frozen in liquid nitrogen and stored at -80ºC.

The sequence of the 601 sequence with 60 bp of flanking DNA (207bp DNA) is as follows:

CTGGAGAATCCCGGTGCCGAGGCCGCTCAATTGGTCGTAGACAGCTCTAGCACCGCTTAA
ACGCACGTACGCGCTGTCCCCCGCGTTTTAACCGCCAAGGGGATTACTCCCTAGTCTCCA

GGCACGTGTCAGATATATACATCCTGTGCATGTATTGAACAGCGACCTTGCCGGTGCCAGT
CGGATAGTGTTCCGAGCTCCCACTCT

Pre-assembled nucleosomes were first dialyzed overnight into 25mM HEPES pH 7.5 to remove glycerol before sample preparations for cryo-EM. To prepare the nucleosome-SNF2h complex, nucleosomes were mixed with purified SNF2h on ice, then incubated at room temperature for 10 min before applying to the grids for plunge freezing. Initially, the complex was prepared by mixing 1.45μM 0/60 nucleosomes with 5μM SNF2h in 20mM HEPES pH 7.5, 70mM KCl, 0.5mM ADP-Mg^{2+}, 0.5 mM $MgCl_2$, 0.5 mM BeF_x (1:5 $BeCl_2$:NaF). This sample yielded a reconstruction of nucleosome with two SNF2h bound at 8.4Å resolution by using a scintillator-based camera. Lately, the complex was prepared by mixing 0.625μM 0/60 nucleosomes with 1.25 μM SNF2h in 0.5mM ADP-Mg, 0.5mM BeFx, 140mM KCl, 3mM Tris pH 7.5, 1.25mM HEPES pH 7.5, 1.5% glycerol. This resulted in high-resolution reconstructions using direct electron detection camera. While the resolution difference is mainly caused by the camera technology and unlikely to be related to the differences in sample preparation, the salt concentration could be amplified during the process of blotting and plunge freezing. For the nucleosome alone reconstruction, 1μM nucleosomes were used directly after the dialysis.

When plunge freezing cryo-EM grids, both protein and solutes in buffer are concentrated but to very different extents. The concentration of SNF2h-nucleosome samples on cryo-EM grids are roughly ~100μM, estimated from the number of particles seen in micrographs. This concentration increase is mostly caused by the volume reduction (~10,000 fold) during blotting, in which filter papers preferably absorb water with chemical solutes over proteins. It is not possible to estimate the final concentration of KCl and ADP-BeFx in a frozen cryo-EM grid, but it may also increase several folds from the sample applied to EM grids, because of evaporation between blotting and freezing.

Thus, 70mM KCl could become as high as ~200mM and 140mM KCl become ~400mM before freezing. If so, it would profoundly impact the binding affinity of SNF2h to the nucleosome, and/or the affinity of ADP-BeFx for SNF2h. We also speculate that macromolecular interactions that are destabilized by the higher ionic strength are more susceptible to being disassembled by the air-water interface during plunge freezing.

Negative stain EM. Grids of negatively stained sample were prepared as described [43]. Sample from these grids was then observed on a Tecnai T12 (FEI) operated at 120kV (Figure 2-supplement 3A-D). From collected micrographs, particles were picked manually, windowed out and subjected to template-free 2D classification using RELION (Scheres, 2012). Selected representative classes are show in Figure 2-supplement 3E

Cryo-EM data acquisition. Cryo-EM grids of nucleosome-SNF2h or nucleosome alone samples were prepared following established protocol [44]. Specifically, 2.5 µl of nucleosome-SNF2h complexes (or 3 µl of samples of nucleosome alone) were applied to a glow discharged Quantifoil holey carbon grid (1.2 µm hole size, 400 mesh), blotted in a Vitrobot Mark I (FEI Company) using 6 seconds blotting at 100% humidity, and then plunge-frozen in liquid ethane cooled by liquid nitrogen.

The scintillator-based camera dataset was collected at liquid nitrogen temperature on a Tecnai TF20 (Thermo Fisher Scientific) electron microscope equipped with field emission gun (FEG) electron source and operated at 200kV. Images were recorded on a TemF816 8k x 8k CMOS camera (TVIPS GmbH) at a nominal magnification of 62,000X, corresponding to a pixel size of 1.2 Å/pixel on the specimen, with a defocus in the range from 1.8 to 2.9 µm. Data collection follows the low-dose procedure using UCSFImage4 (X. Li et al., 2015). The K2 camera dataset of nucleosome-SNF2h complex was collected using UCSFImage4 on a TF30 Polara electron microscope (Thermo Fisher Scientific) equipped with a FEG source and operated at 300 kV. Specifically, images were recorded

in super resolution counting mode using a K2 Summit direct electron detection camera (Gatan Inc.) at a nominal magnification of 31,000X, corresponding to a calibrated physical pixel size of 1.22 Å/pixel. The dose rate on camera was set to 8.2 counts (corresponding to 9.9 electrons) per physical pixel per second. The total exposure time was 6 seconds, leading to a total accumulated dose of 41 electrons per $Å^2$ on the specimen. Each image was fractionated into 30 subframes, each with an accumulated exposure time of 0.2 second. Images were recorded with a defocus in the range from 1.5 to 3.0 um. The K2 dataset of nucleosome alone was collected in the same microscope under the identical imaging conditions, except SerialEM was used for automated acquisition [45].

Image processing. For dataset collected with scintillator based camera, there is no movie stack related image processing, such as motion correction and dose weighting. Otherwise, same software packages and procedures were used as for the K2 datasets.

For K2 datasets, movie stacks were corrected for both global and local motions using MotionCor2 v1.0.0., which outputs both dose-weighted and un-weighted sum of corrected subframes [46]. The output images were first visually inspected for particle distribution. The non-dose-weighted images were used for CTF parameter determination using GCTF [47]. The estimated image resolution and quality of Thon ring fitting were inspected manually and images with poor quality were removed from further image processing. For the rest of image processing, only dose-weighted sums were used. For particle picking, an initial ~1,000 particles were manually picked using e2boxer (EMAN2) [48], followed by two-dimensional (2D) reference free alignment and classification by using Relion2 [49]. Six unique 2D class averages were used as template reference for an automated particle picking using Gautomatch (http://www.mrc-lmb.cam.ac.uk/kzhang/). All picked particles were subject to reference free 2D classifications. Particles within 2D classes that show clear nucleosome features were selected and were further inspected

visually to remove any remaining “junk” particles. The total number of particles in each dataset is listed in Figure 2-supplement 2 and Figure 2-supplement 4A-B. For initial model generation and subsequent runs, cryoSPARC "Ab initio", "Homogeneous refinement" and "Heterogeneous refinement" procedures were employed [50]. For masked refinement and classification without alignment, we used RELION 2. The detailed scheme of classifications and refinements are shown in the Figure 2-supplement 2. The refinement follows gold-standard refinement procedure [51], and the final resolutions were estimated using Fourier Shell Correlation (FSC) equals 0.143 criterion [52].

The K2 dataset was used in two independent analyses. In the first analysis, we picked 120,533 particles and classified into 50 2D class averages. Particles within low quality 2D classes were removed. Through sequential classification and refinement, we obtained a 3.8 Å reconstruction of single SNF2h-bound nucleosome. To separate particles with SNF2h bound to SHL+2 and SHL-2, we first used volume subtraction procedure to subtract the SNF2h from all particles followed by unambiguously aligning all nucleosome particles using the flanking DNA as a fiducial mark. We then performed a focused classification on SNF2h, which lead to two main subclasses: one reconstruction at 3.9 Å resolution has SNF2h bound to the SHL-2 position. The other one at 6.9 Å resolution has SNF2h bound to the SHL+2 position (Figure 1-supplement 2). Both reconstructions show a 2bp translocation of DNA (Figure 1-supplement 3).

Independently, we re-processed frame motion correction by using MotionCor2 v1.2.1, with option accounting for in-frame motion enabled (InFmMotion 1). The motion corrected images were subjected again to independent particle picking and CTF estimation. In this reprocess, we started with 333,430 initially picked particles (Figure 2-supplement 2C). We skipped 2D classification for cleaning up the dataset, instead using 3D classification for this purpose. Using cryoSPARC v2 ‘Ab initio reconstruction’ and

'Heterogeneous refinement', in subsequent rounds of subsorting, the final reconstruction contains 43,165 particles, which yielded 3.4 Å reconstruction using 'Non-homogeneous refinement'. We did not attempt to separate particles with SNF2h bound to SHL+2 and SHL-2 positions.

Validation of 2 base-pair translocated nucleosome.

We ruled out the possibility of nucleosome mis-assembly as described in the main text (Figure 1-supplement 5-6). Furthermore, the following additional experiments were carried out to rule out the possibility of any computational artifacts, such as incomplete separation of particles with SNF2h bound to SHL+2 and SHL-2 positions. In addition to the fact that the 3.9 Å reconstruction shows that DNA has a sharp ending without any weak extension, we calculated 20 bootstrapped 3D reconstructions using a subset of particles bootstrapped from the particles that were used to calculate the 3.9 Å map (Figure 1-supplement 6). These bootstrapped reconstructions show no significant variance at the location of this extra density. These observations demonstrate that this extra density is statistically significant and well defined, and cannot be contributed by misaligned particles. Furthermore, we calculated difference maps between all experimental maps determined from datasets recorded with K2-Summit and the map simulated from the atomic model of nucleosome without the two extra base-pairs at the exit side (Figure 1-supplement 5). We also calculated difference maps between the reconstruction of nucleosome alone and the reconstructions of SNF2h bound to either SHL+2 or SHL-2 (Figure 1-supplement 5A-B). These difference maps confirm the existence of extra DNA density at the exit side of our SNF2h-nucleosome complex reconstructions.

To calculate the variance map, we bootstrapped 5,000 particles 20 times from the 3.9 Å SNF2h dataset and backprojected particles within these subsets to produce 20

reconstructions using relion_reconstruct in Relion2. The variance map between all reconstructions was then calculated. All scripts are included in PyEM (https://github.com/asarnow/pyem). The difference maps were calculated using program diffmap.exe (http://grigoriefflab.janelia.org/diffmap).

Model building and refinement. For the nucleosome 0/60 nucleosome, we used Widom 601 structure crystal structure [53] (PDBID: 3LZ1) and mutated the DNA to reflect the exact sequence used for the sample. We then used Coot [54] and Phenix (phenix.realspacerefine) [55]to extend and fit the DNA into our structures, as well as ensure the correctness of the structure.

SNF2h was constructed using homology modeling, based on an ISWI crystal structure from *Myceliophthora thermophile* (PDBID: 5JXR) [35]. We separated each of the domains and used rigid body fitting into the EM density. Subsequently, Coot and Phenix were used to adjust and modify parts of the model. For model cross-validation, the final structure was initially subjected to 0.1 Å random displacement and then refined against one of the two half-maps using Phenix. Subsequently, the refined pdb was converted to a density map and FSC curves were calculated between three maps: half map 1 (the refinement map, 'work'), half map 2 (not used for refinement, 'free') and the summed map. A very small difference between the 'work' and 'free' FSC curves indicates little-to-no effect of over-fitting of the atomic model. Figures were prepared using UCSF Chimera [56].

Native Gel Remodeling Assay.

All remodeling reactions were performed under single turnover conditions (enzyme in excess of nucleosomes) using similar methods as described previously [42]. Reactions with SNF2h were performed at 20ºC with 15nM cy3-labeled nucleosomes, 12.5mM HEPES pH 7.5, 2mM Tris pH 7.5, 70mM KCl, 5 mM ATP-$MgCl_2$, 3mM $MgCl_2$,0.02%

NP40, and ~3%(v/v) glycerol. 5µL time points were quenched with equal volumes of stop buffer containing an excess of ADP and plasmid DNA. Nucleosomes were resolved on a 6% polyacrylamide 0.5X TBE native gel. Reactions were visualized by scanning on a Typhoon variable mode imager (GE Healthcare) and quantified using ImageJ.

Ensemble FRET Assay.

Steady state fluorescence measurements were performed on an ISS K2 fluorometer equipped with a 550 nm short pass and 535 nm long pass filter in front of excitation and emission monochromators respectively. Fluorescence emission spectra were collected by excitation at 515 nm and emission intensities measured between 550-750 nm in 5 nm wavelength increments. FRET efficiency was determined by the following equation:

$$\text{FRET Efficiency} = \frac{Em_{665}}{Em_{665} + Em_{565}}$$

Where Em_{665} and Em_{565} are the maximal acceptor and donor emission intensities at 665 nm and 565 nm respectively. Reactions were carried out with a final volume of 80µL and with final concentrations of 8 nM labeled nucleosomes, 12.5mM HEPES pH 7.5, 2mM Tris pH 7.5, 0.5mM $MgCl_2$, 0.02% NP40, ~4% glycerol at 20ºC. Each reaction was incubated for ~10 min before an initial emission spectrum was obtained. Reactions were then initiated with 3µL 2µM of SNF2h and 0.5mM ADP-BeF_x-$MgCl_2$ (final concentration) or buffer and emission spectra were obtained at various time points after initiating the reactions. Kinetic measurements were normalized to the FRET efficiency of the initial measurement.

Single molecule FRET

Experiments were performed as in [27], except that the imaging buffer was 53 mM HEPES-KOH, pH 7.5 at 22°C, 9.1 mM Tris-acetate, pH 7.5 at 22°C, 140 mM KCl, 0.5 mM $MgCl_2$, 10% glycerol, 0.02% NP-40, 1% glucose, 0.1 mg/mL acetylated BSA, 2 mM Trolox, 0.03 mM β–mercaptoethanol, 2 U/μL catalase, and 0.08 U/μL glucose oxidase. SNF2h and ADP-BeF_x were added simultaneously to a final concentration of 2 μM and 0.5 mM respectively using an automated syringe pump. Nucleosomes were then imaged after a 10 minute incubation to match the EM preparation conditions. 7 minute movies were collected at a sufficiently high laser power that most nucleosomes photobleached before the end of the movie, enabling the exclusion of nucleosomes that did not exhibit single-step photobleaching in both channels. The reported FRET value for each nucleosome is the average over the portion of the movie prior to the first photobleaching event.

ATPase Assays.

DNA stimulated ATPase assays were performed using an NADH coupled assay [57]. Reactions were performed with 800nM SNF2h, saturating concentrations of 207bp DNA (208nM) and ATP-$MgCl_2$ (4mM) with 10U/μL lactate dehydrogenase, 10 U/μL Pyruvate kinase, 180μM NADH, 2mM phosphoenol pyruvate, 12.5 mM HEPES pH 7.5, 70mM KCl, 3mM free $MgCl_2$, and ~1.5% glycerol at 25ºC. Reactions were incubated in a 384 well plate at 25ºC prior to addition of enzyme to initiate the reaction. Absorbance was monitored at 340 nm in a SpectraMax M5e plate reader and the resulting data was background subtracted using absorbance at 420 nm. The linear phase of each reaction was then fit using linear regression using Prism to obtain hydrolysis rates. For nucleosome stimulated ATP hydrolysis, rates were measured using radioactivity as in [27] under saturating concentrations of nucleosomes without flanking DNA and subsaturating concentrations of (20μM) ATP-$MgCl_2$. Reactions were performed in 12.5 mM HEPES pH

7.5, 70mM KCl, 3mM free $MgCl_2$, 0.02% NP-40, and ~1.5% glycerol at 25ºC, initiated by addition of enzyme, and time points quenched with an equal volume 50 mM Tris pH 7.5, 3% SDS, and 100 mM EDTA. Time points were resolved on a PEI-cellulose TLC plate (Select Scientific) using a 0.5M LiCl/1M Formic acid mobile phase, plates were dried and then exposed on a phosphorscreen overnight. The screen was imaged using a Typhoon variable mode imager. Fraction of ATP hydrolyzed was quantified using ImageJ and initial rates were determined by fitting a line through the first 10% of inorganic phosphate generated using Prism.

Figures

FIGURE 3.1

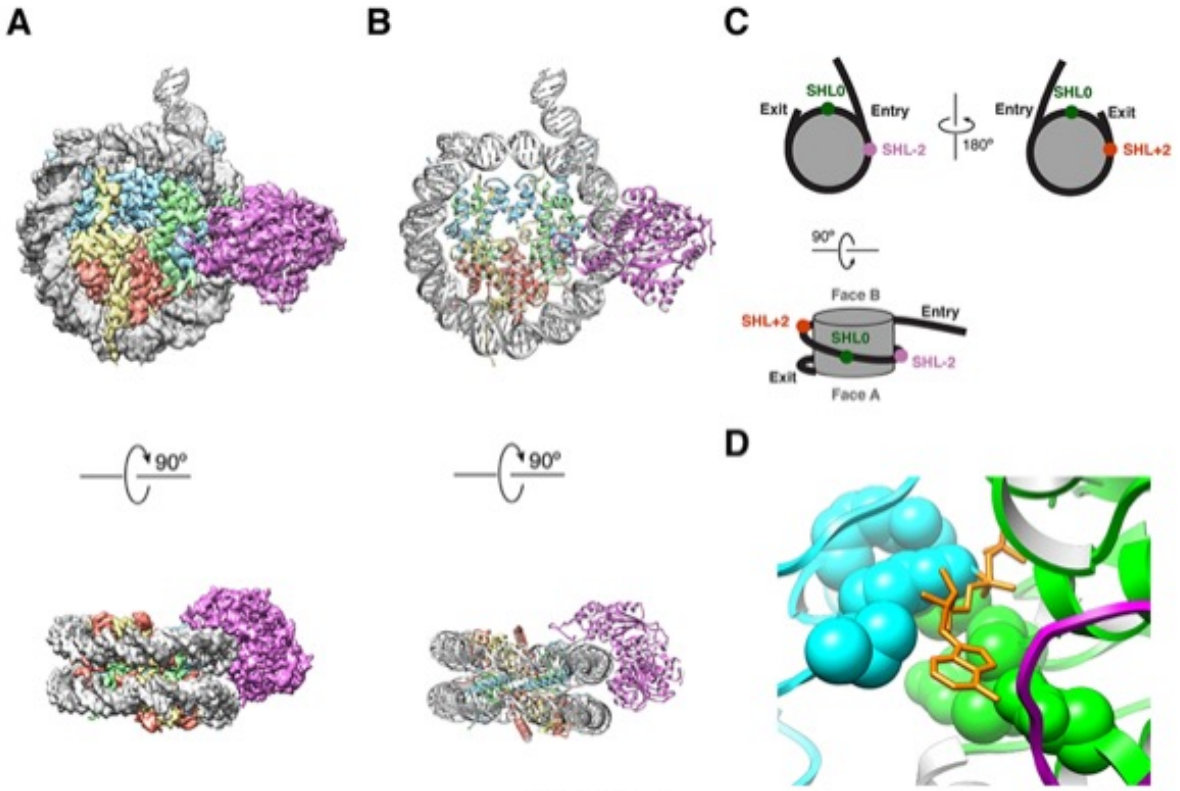

Figure 3.1 High resolution structure of SNF2h bound to a nucleosome with 60bp of flanking DNA in the presence of ADP-BeFx and 140mM KCl
(**A**) Cryo-EM density map of SNF2h bound to the nucleosome at 3.4 Å from data recorded with a K2-summit camera. **(B)** Model built using the density in (A). **(C)** Cartoon representation of a nucleosome with asymmetric flanking DNA as in our structures. Super Helical Location (SHL) +/-2 as well as the entry and exit site DNAs are labeled. The SHL0 location is also labeled and is defined as the dyad. Faces A and B of the histone octamer are labeled in grey. **(D)** Zoom into the ATP-binding pocket of SNF2h with ADP in orange and represented with sticks. In spheres are the SNF2h residues that bind nucleotide with the helicase motif I in green and helicase motif VI in blue (Figure 3-supplement 4).

FIGURE 3.2

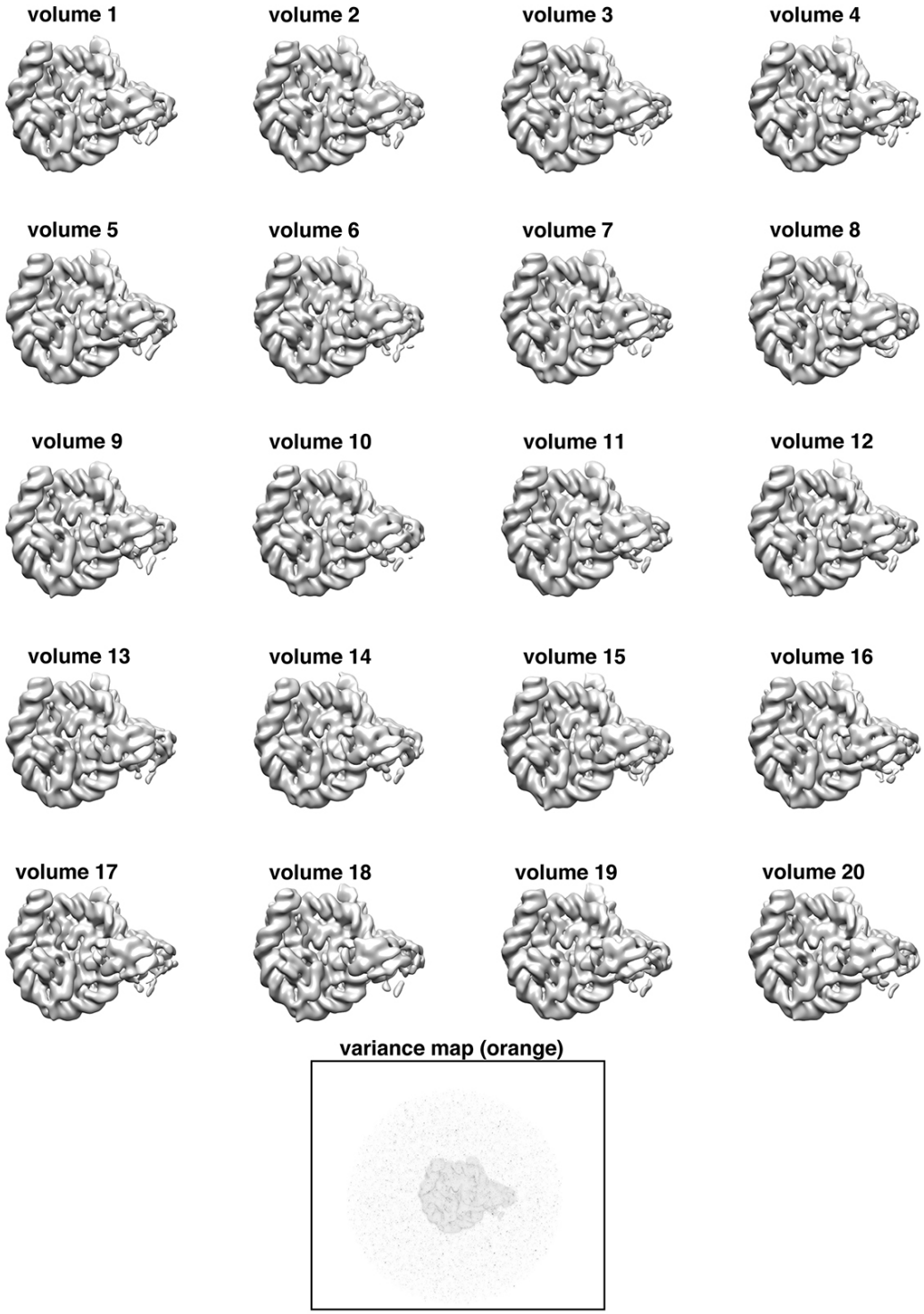
volume 1
volume 2
volume 3
volume 4
volume 5
volume 6
volume 7
volume 8
volume 9
volume 10
volume 11
volume 12
volume 13
volume 14
volume 15
volume 16
volume 17
volume 18
volume 19
volume 20
variance map (orange)

Figure 3.2 Bootstrapped maps of SNF2h-nucleosome complex
20 bootstrapped maps were calculated by using 20 subsets of 5,000 particles bootstrapped from the particles that were used to calculate the 3.9 Å reconstruction. The variance map is shown in the bottom, which shows no significant variance. Transparent overlay of the SHL-2 side 3.9 Å density is shown for orientation.

FIGURE 3.3

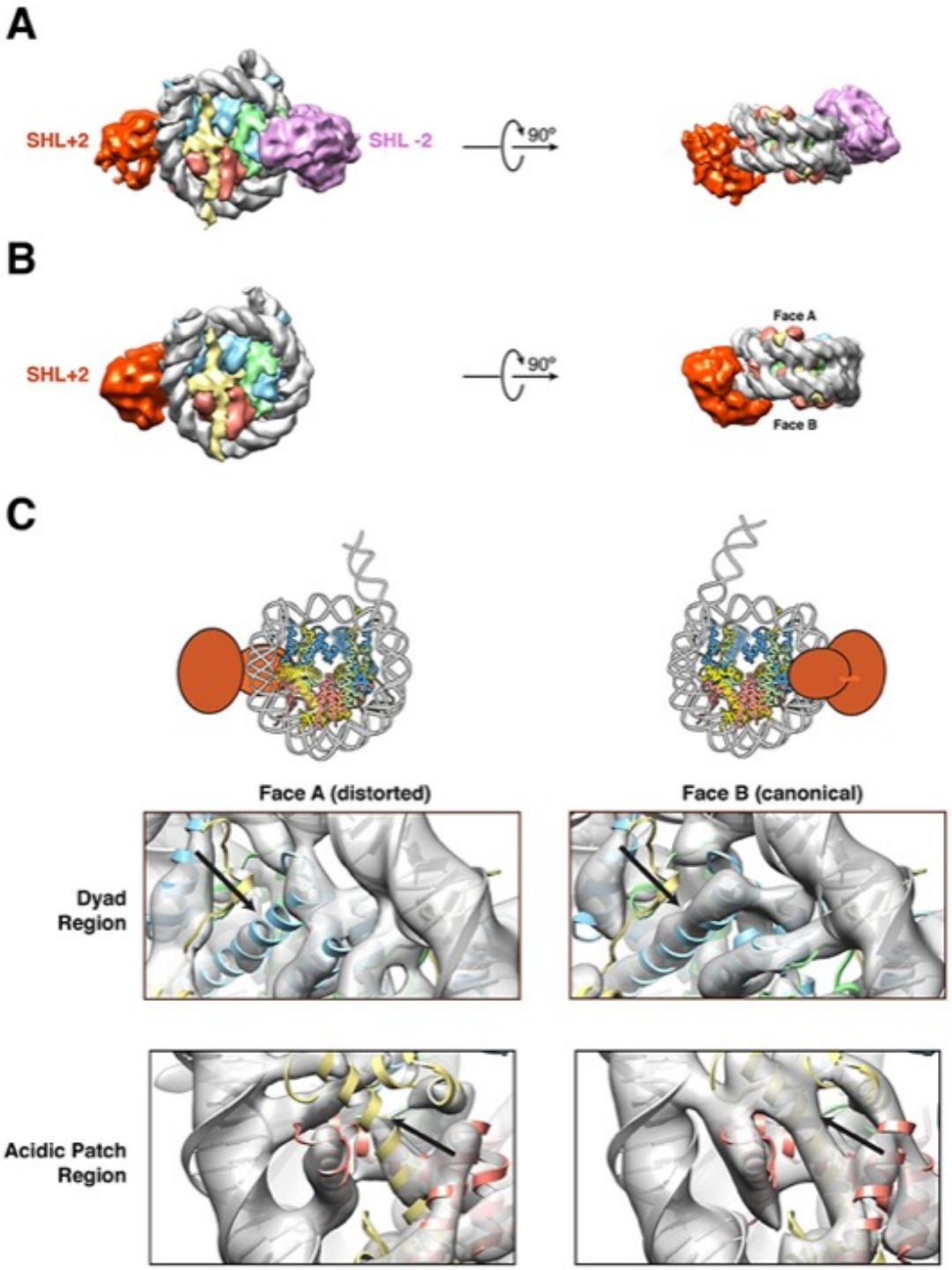
A
SHL+2
SHL -2
90°
B
SHL+2
90°
Face A
Face B
C
Face A (distorted)
Face B (canonical)
Dyad Region
Acidic Patch Region

Figure 3.3 Structures of SNF2h bound to a nucleosome with 60bp of flanking DNA in the presence of ADP-BeFx and 70mM KCl
(A-C) Cryo-EM density maps of SNF2h bound to the nucleosome recorded with a scintillator-based camera (A) Doubly bound SNF2h-nucleosome complex at 8.4 Å resolution. (B) Singly bound SNF2h at SHL+2. (C) Comparison of the Cryo-EM density on the two faces of the nucleosome. Face A of the nucleosome (left column) has weaker EM density at the histone H2A acidic patch (bottom row) and the α2 helix of H3 (top row) when compared to face B (right column) at the same contour level. The black arrows point to the helices that show altered densities in Face A vs. Face B. The regions of increased dynamics are also shown schematically as blurry helices in cartoons of the nucleosome above the densities for Face A and Face B.

FIGURE 3.4

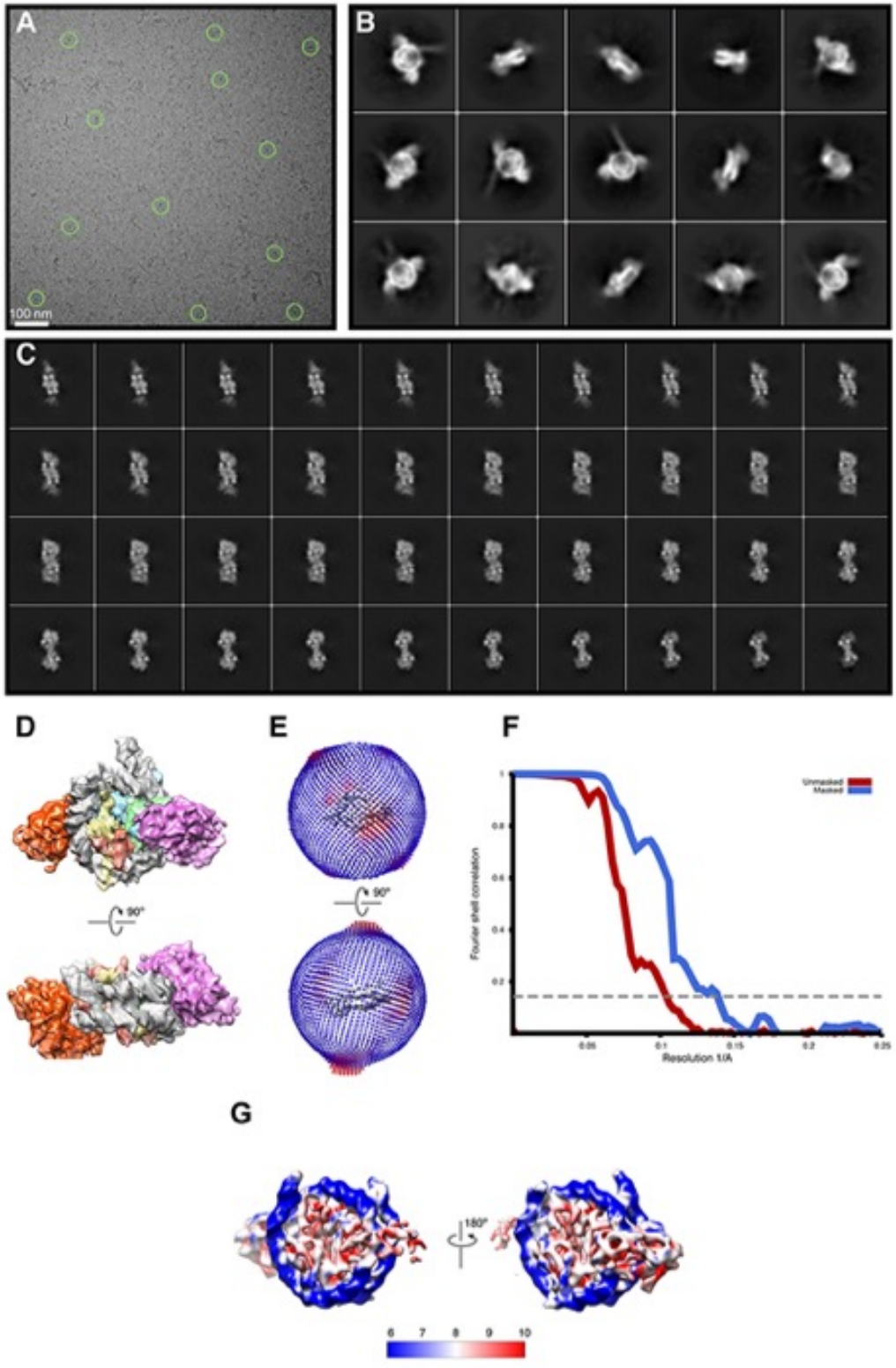
A
100 nm
B
C
D
90°
E
90°
F
Unmasked
Masked
Fourier shell correlation
Resolution 1/Å
G
180°
6 7 8 9 10

Figure 3.4 Cryo-EM analysis of doubly bound SNF2h-nucleosome complexes obtained at 70 mM KCl.
(A) A raw cryo-EM micrograph of doubly bound SNF2h-nucleosome complex recorded as described in Materials and Methods. (B) Typical 2D class averages of selected particles. The box size is 300 pixels. (C) Slices through the unsharpened density at different levels along the side view. (D) Representative views of the doubly bound complex. (E) Euler angle distribution of all particles used for the final 3D reconstruction. The length of each cylinder is proportional to the number of particles visualized from this specific orientation. (F) FSC curves between two independently refined half maps before (red) and after (blue) masking in Cryosparc, indicated with resolutions corresponding to FSC=0.143. (G) Final unsharpened 8.4Å 3D density map of the doubly-bound complex colored with local resolution.

FIGURE 3.5

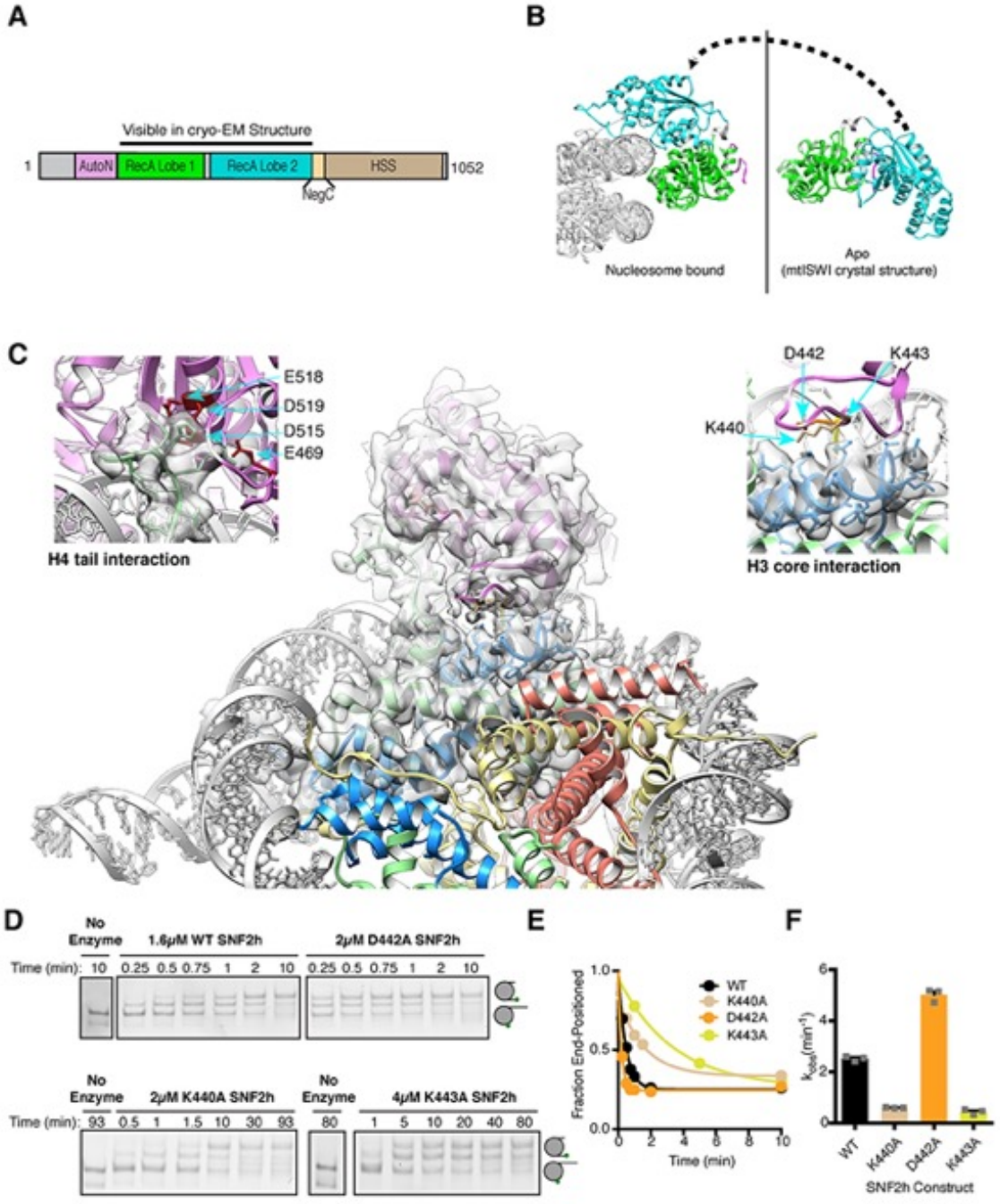
A
Visible in cryo-EM Structure
1
AutoN
RecA Lobe 1
RecA Lobe 2
HSS
1052
NegC
B
Nucleosome bound
Apo
(mtISWI crystal structure)
C
E518
D519
D515
E469
H4 tail interaction
D442
K443
K440
H3 core interaction
D
No Enzyme
1.6μM WT SNF2h
2μM D442A SNF2h
Time (min): 10 0.25 0.5 0.75 1 2 10 0.25 0.5 0.75 1 2 10
No Enzyme
2μM K440A SNF2h
No Enzyme
4μM K443A SNF2h
Time (min): 93 0.5 1 1.5 10 30 93 80 1 5 10 20 40 80
E
Fraction End-Positioned
1.0
0.5
0.0
0 2 4 6 8 10
Time (min)
WT
K440A
D442A
K443A
F
k_{obs} (min^{-1})
6
4
2
0
WT
K440A
D442A
K443A
SNF2h Construct

Figure 3.5 Interactions of SNF2h with the histone proteins
(A) Domain diagram of SNF2h. (B) Conformational changes in SNF2h associated with nucleosome binding. SNF2h is colored according to the domain diagram. The apo structure is the *Myceliophtora thermophila* ISWI crystal structure (PDBID: 5JXR). (C) Middle. High resolution SNF2h-nucleosome structure from Figure 1 enlarged to show details of the interactions with the histone proteins. Colored in red on SNF2h are the acidic residues contacting the histone H4 tail. Colored in orange, tan, and yellow are the residues mutated in this study. Left. Enlarged to show details of the H4 tail interaction. Right. Enlarged to show details of the H3 core interaction. (D) Native gel remodeling assay of SNF2h constructs. Cy3-DNA labeled nucleosomes were incubated with saturating concentrations of enzyme and ATP and resolved on a native 6% polyacrylamide gel. (E) Quantifications of the data in (D) zoomed on the x-axis to show effects more clearly and fit to a single exponential decay. Un-zoomed plots are in Figure 3-supplement 6. (F) Rate constants derived from remodeling assays. Bars represent the mean and standard error from three experiments.

FIGURE 3.6

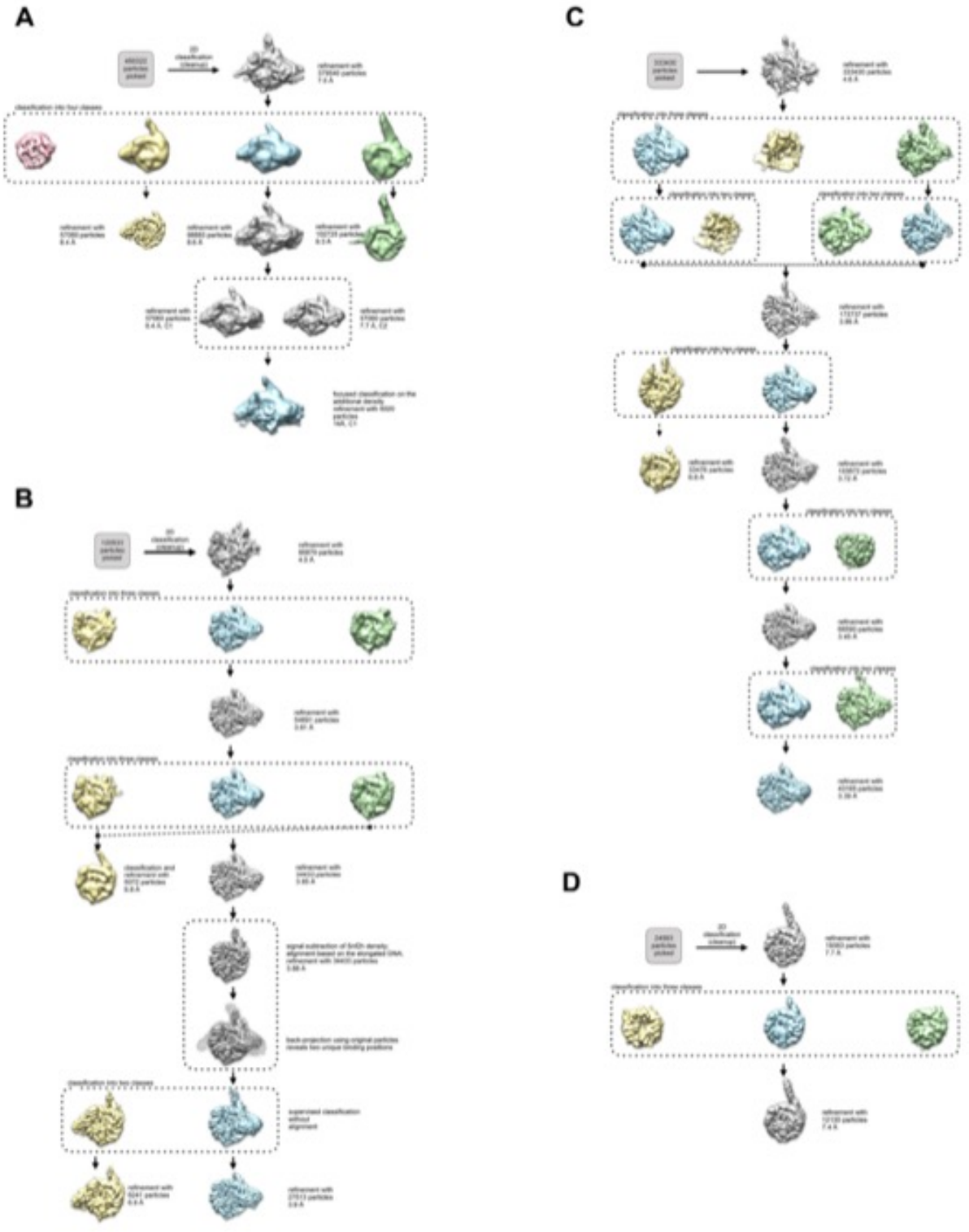

Figure 3.6 3D Classification and refinement
(A-B, D) The flowchart of classification and refinement procedures using RELION and Cryosparc is shown. Following 1 round of 2D classification, each dataset was subjected to 3D refinement and subsequent classification. (A) Scintillator-based doubly-bound dataset. (B) Direct electron detector-based SNF2h-nucleosome complex dataset that resulted in single-bound flanking DNA proximal and distal complexes as well as unbound nucleosomes. (C) Recalculated direct electron detector-based SNF2h-nucleosome complex dataset, resulting in the 3.4 Å consensus Coulomb potential map. (D) Direct electron detector-based data set for core nucleosome with flanking DNA without added SNF2h.

FIGURE 3.7

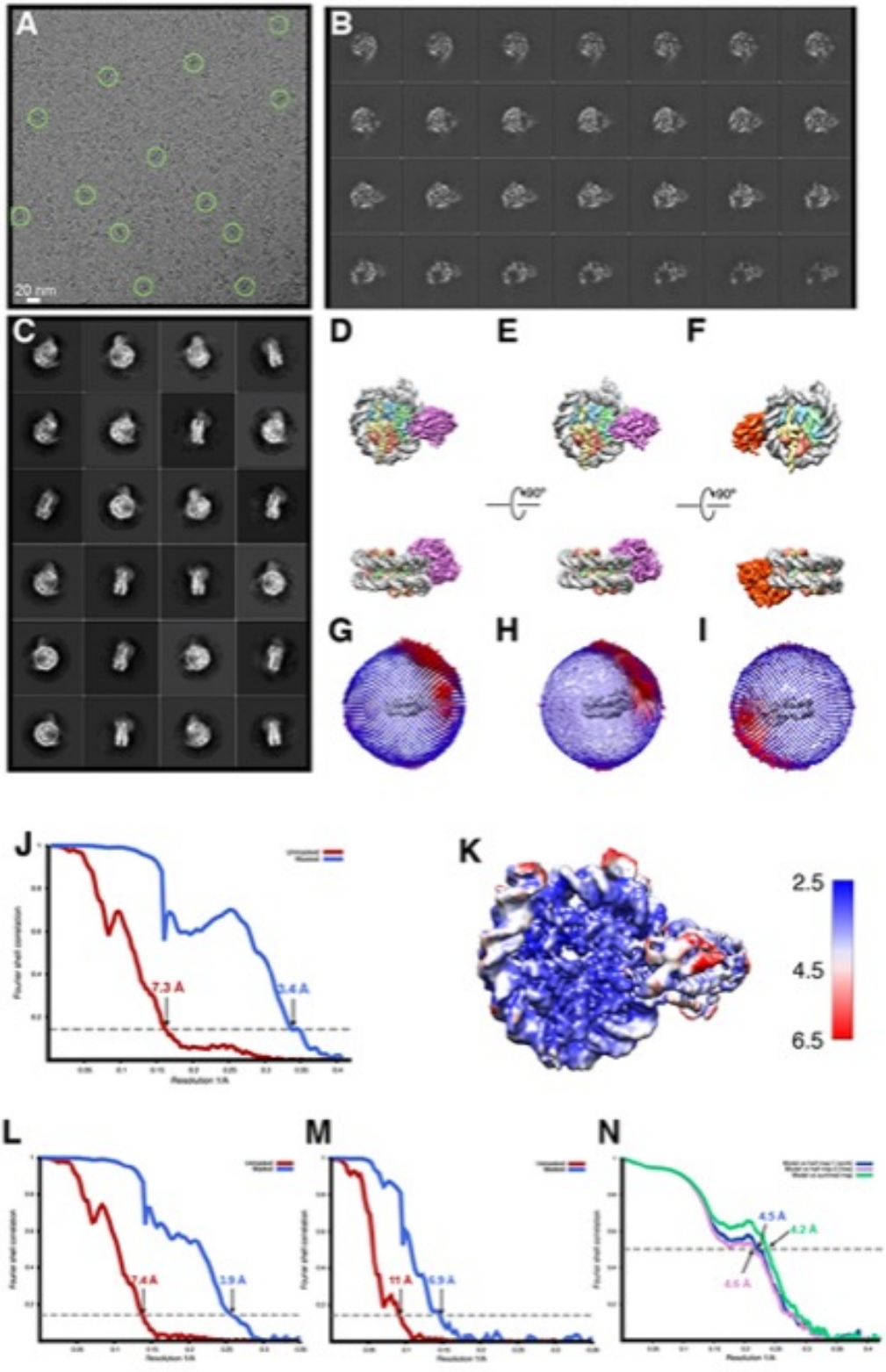
A
20 nm
B
C
D
E
F
G
H
I
J
7.3 Å
5.4 Å
K
2.5
4.5
6.5
L
7.4 Å
3.9 Å
M
11 Å
6.9 Å
N
4.5 Å
4.2 Å
4.6 Å

Figure 3.7 Cryo-EM analysis of singly bound SNF2h-nucleosome complexes (140 mM KCl)
(A) A raw cryo-EM micrograph of single bound SNF2h-nucleosome complex recorded as described in *Materials and Methods*. (B) Slices through the unsharpened density of the 3.9 Å resolution map, which has SNF2h bound to the SHL-2 position, at different levels along the top view. (C) Typical 2D class averages of selected particles. The box size is 256 pixels. (D) Representative views of the 3D reconstruction of the 3.4 Å complex. (E) Representative views of the 3.9 Å resolution map with SNF2h bound to the SHL-2 position. (F) Representative views of the 6.9 Å resolution map with SNF2h bound to the SHL+2 position. (G) Euler angle distribution of all particles used for the final 3D reconstruction of the 3.4 Å complex. The length of each cylinder is proportional to the number of particles visualized from this specific orientation. (H) Euler angle distribution of all particles used for the 3.9 Å 3D reconstruction. The length of each cylinder is proportional to the number of particles visualized from this specific orientation. (I) Euler angle distribution of all particles used for the 6.9 Å resolution 3D reconstruction. (J) FSC curves of the 3.4 Å complex between two independently refined half maps before (red) and after (blue) masking in Cryosparc v2, indicated with resolutions corresponding to FSC=0.143. (K) Final unsharpened 3.4Å 3D density map of SNF2h-nucleosome complex colored with local resolution. (L) FSC curves of the 3.9 Å complex between two independently refined half maps before (red) and after (blue) masking in Cryosparc, indicated with resolutions corresponding to FSC=0.143. (M) FSC curves of the 6.9 Å complex (N) Cross-validation using FSC curves of the density map calculated from the refined model versus half map 1 (‘work’, blue), versus half map 2 (‘free’, pink) and versus summed map (green).

FIGURE 3.8

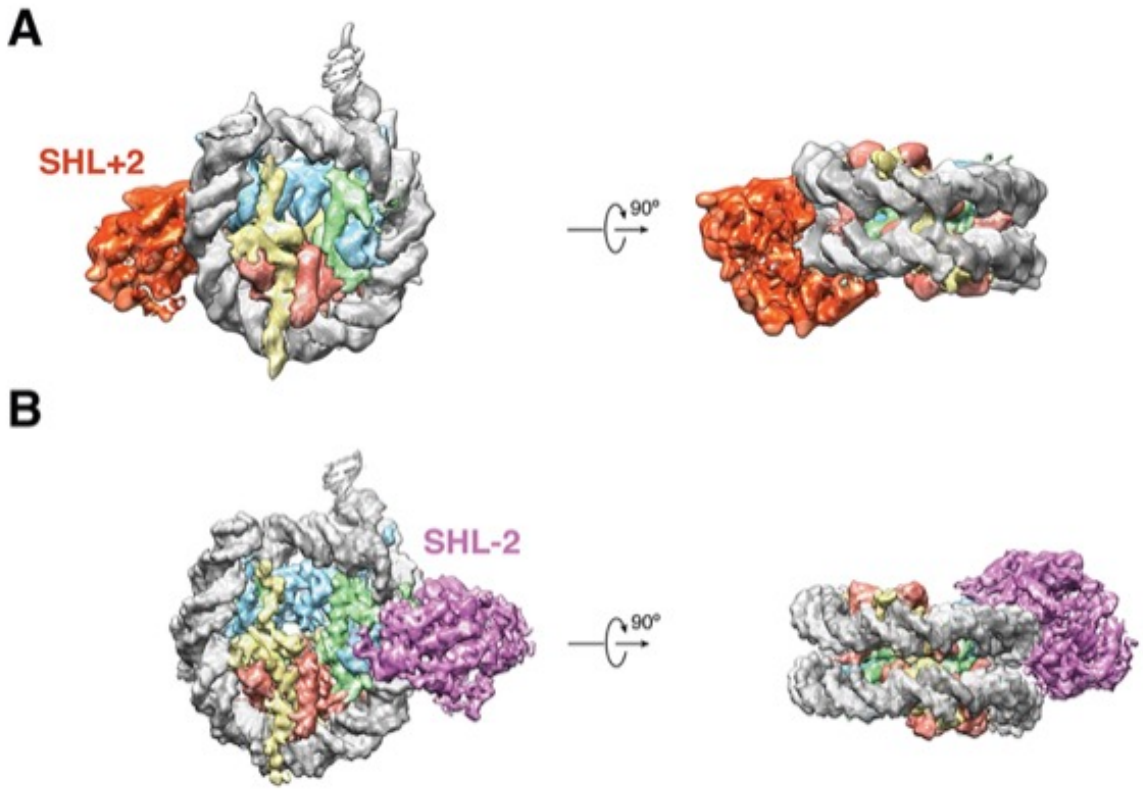

Figure 3.8 Cryo-EM Densities of SHL+2 and SHL-2 SNF2h-Nucleosome complexes obtained at 140mM KCl
Cryo-EM reconstructions of single-SNF2h bound nucleosomes from data recorded on a K2-summit direct electron bound at (A) SHL+2 at 6.9 Å resolution and (B) SHL-2 at 3.9 Å resolution.

FIGURE 3.9

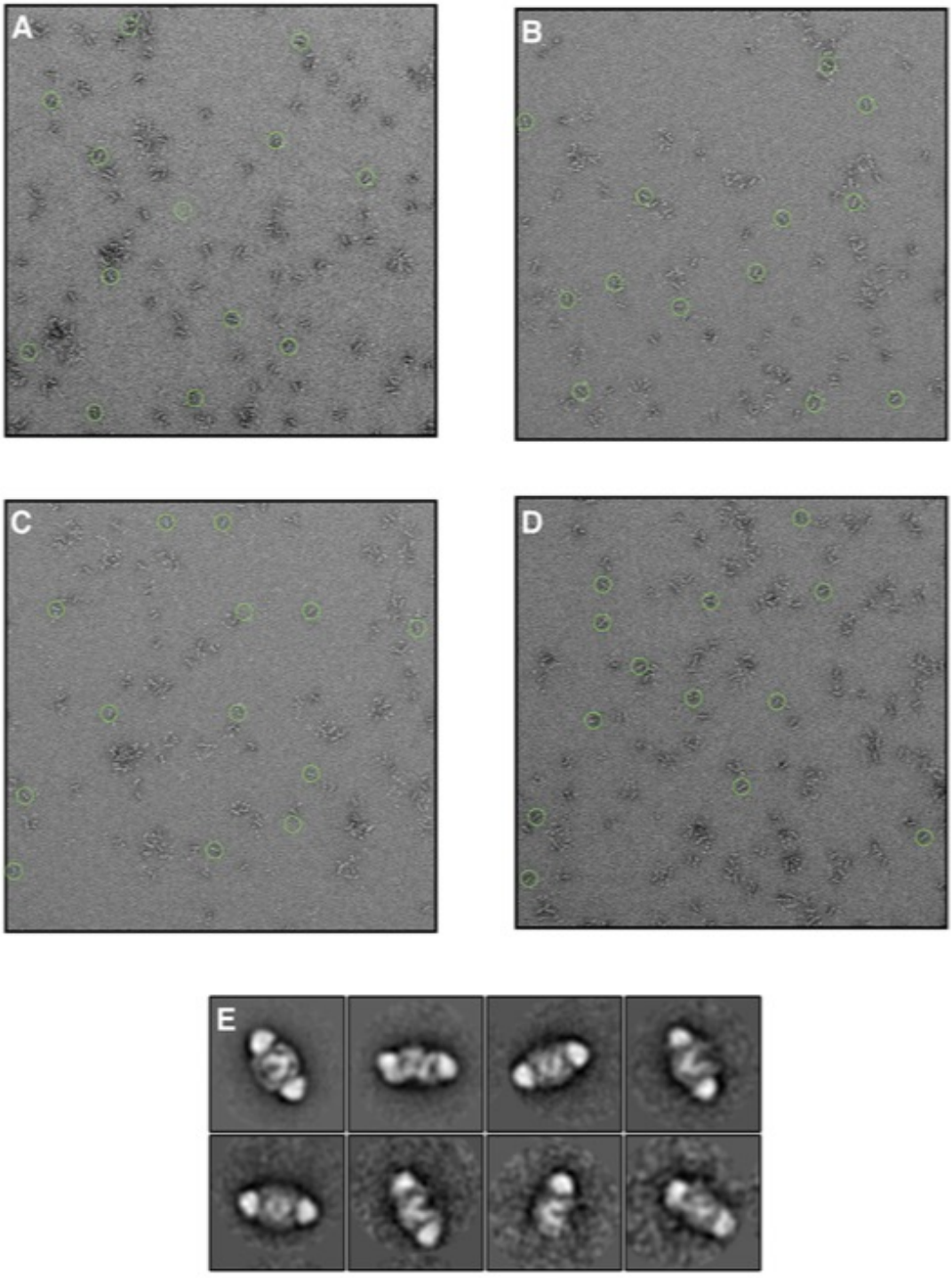

Figure 3.9. Negative stain EM of SNF2h in the presence of ADP-BeFx and 140 mM KCl

(A-D) Raw micrographs of negatively stained sample performed under the same buffer conditions as the dataset in Figure 1. Complexes were assembled identically to the high resolution EM condition and then diluted 40-fold in buffer immediately before applying the sample to the grid to permit visualization by negative stain EM. The final concentration applied to the grid was 15 nM nucleosomes and 31 nM SNF2h. (E) Selected class averages from (A-D) showing that in these conditions, the majority of nucleosomes are doubly-bound

FIGURE 3.10

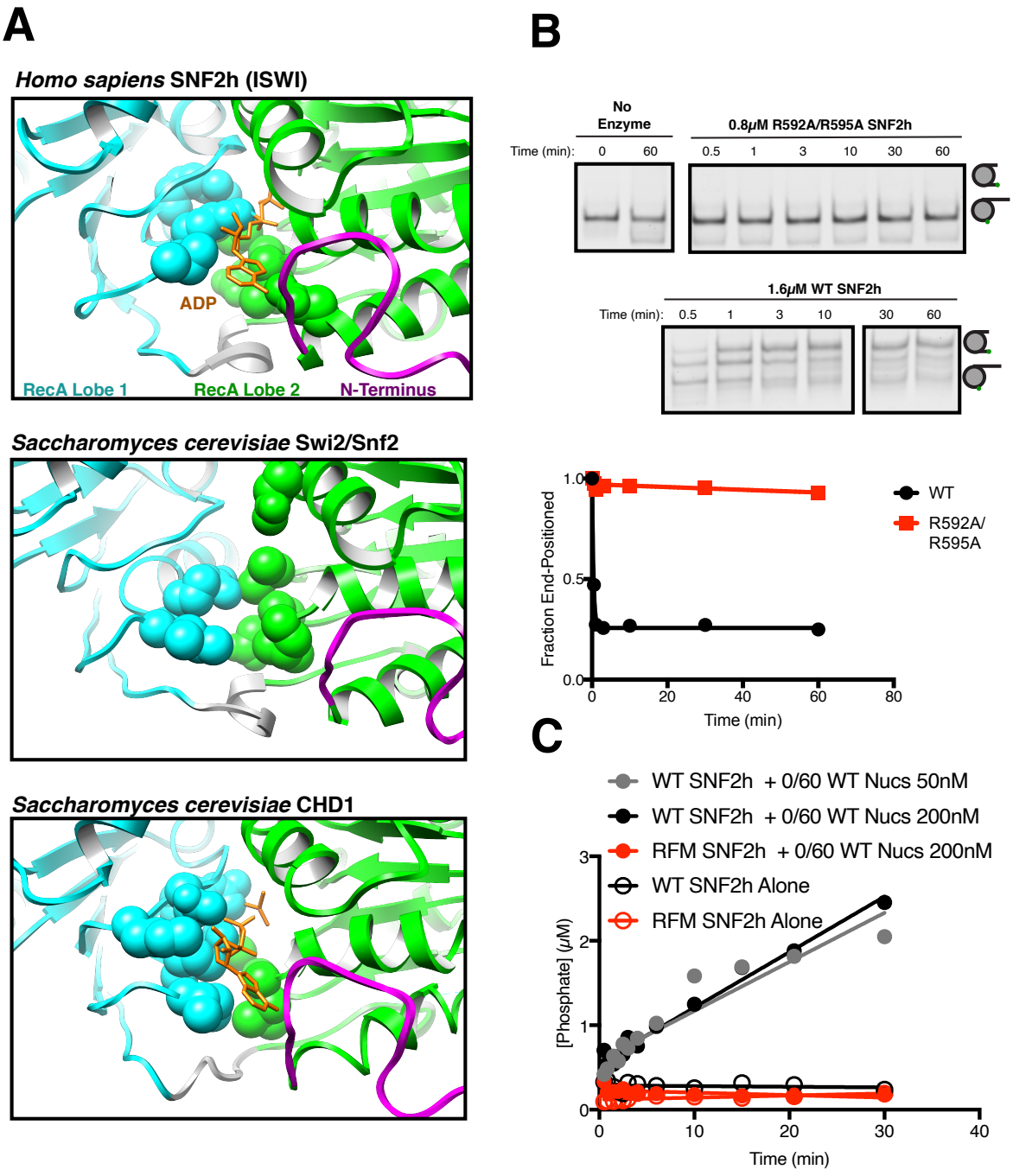
A
Homo sapiens SNF2h (ISWI)
ADP
RecA Lobe 1
RecA Lobe 2
N-Terminus
Saccharomyces cerevisiae Swi2/Snf2
Saccharomyces cerevisiae CHD1
B
No Enzyme
0.8μM R592A/R595A SNF2h
Time (min): 0 60 0.5 1 3 10 30 60
1.6μM WT SNF2h
Time (min): 0.5 1 3 10 30 60
Fraction End-Positioned
Time (min)
WT
R592A/ R595A
C
WT SNF2h + 0/60 WT Nucs 50nM
WT SNF2h + 0/60 WT Nucs 200nM
RFM SNF2h + 0/60 WT Nucs 200nM
WT SNF2h Alone
RFM SNF2h Alone
[Phosphate] (μM)
Time (min)

Figure 3.10 Comparison of ATP-binding pockets of SNF2h with CHD1 and Swi2/Snf2 and functional validation of SNF2h ATP-binding pocket
(A) Top. Close up view of the SNF2h ATP-binding pocket from the 3.4 Å structure with ADP fit in the canonical binding site. Middle. Close up view of the ATP-binding pocket from *S. cerevisiae* Swi2/Snf2 Cryo-EM structure[13]. Bottom. Close up view of the ATP binding pocket from *S. cerevisiae* CHD1 Cryo-EM structure with ADP-BeFx fit in the canonical binding site [10]. The conserved helicase motif I and helicase motif VI that are required for ATP hydrolysis are shown in space fill. (B) Mutation of the putative arginine fingers to alanine abolishes nucleosome sliding activity. Native gel remodeling assay with saturating concentrations of SNF2h. Bottom. Quantification of the gel fit to a single exponential decay. (C) Nucleosome-stimulated ATPase assay comparing WT and R592A/R595A SNF2h (RFM SNF2h). Assay was performed as described in the methods but with 75µM ATP•Mg.

FIGURE 3.11

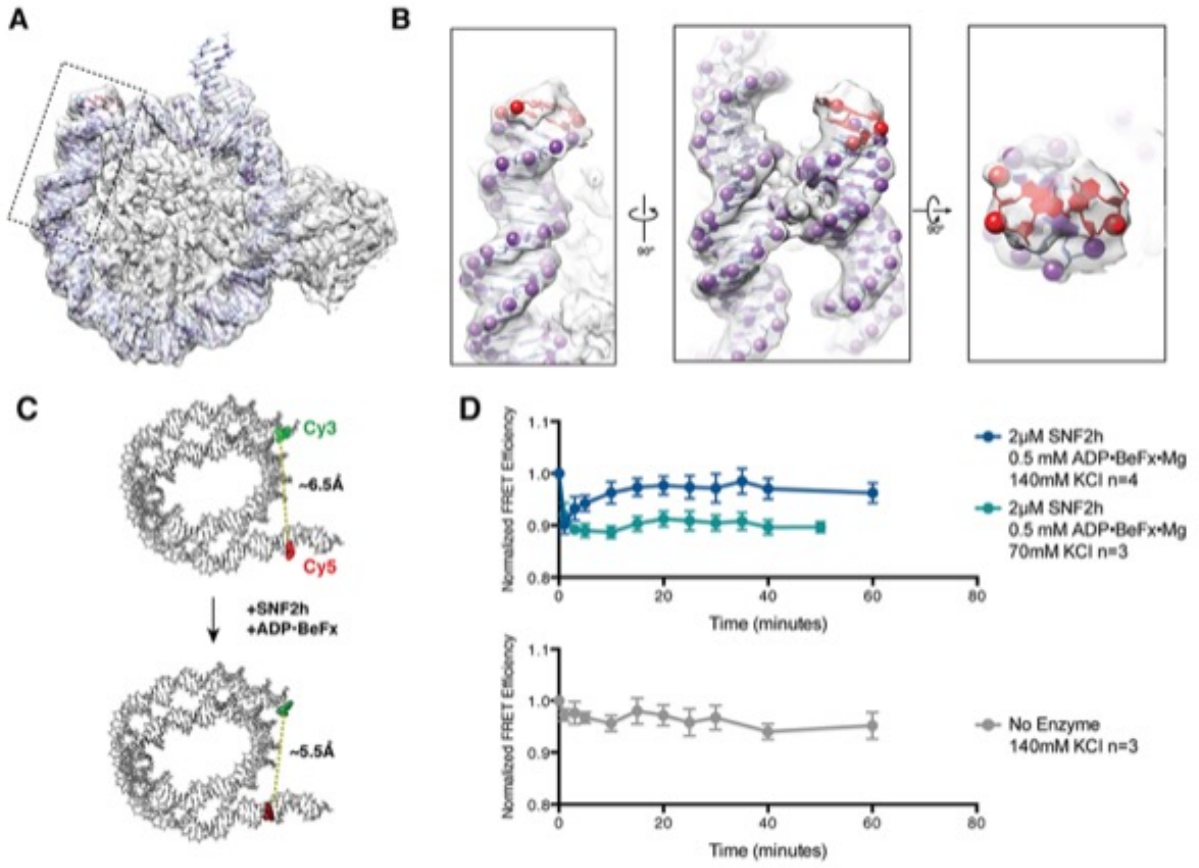

Figure 3.11. Cryo-EM reconstructions of the SNF2h-Nucleosome complexes at 140mM KCl are translocated ~2bp

(A) High resolution structure from Figure 1-supplement 2B with Cryo-EM density fit with an atomic model. The additional 2bp of DNA exiting the canonical nucleosome structure are highlighted in red. The box indicates the region zoomed to show greater detail in (B). (B) Zooms of the boxed region in A to show greater detail. The phosphates of the phosphodiester backbone are shown in spheres and fit precisely into the Cryo-EM density. (C) Schematic of the ensemble FRET experiment performed in (D). Nucleosomes were reconstituted on identical DNA sequence used to obtain Cryo-EM reconstructions and labeled with two fluorophores: cy3 on the 5′ phosphate at the DNA exit side of the nucleosome with a 3 carbon flexible linker and with cy5 on C8 of the cytosine base at position 149 near the entry side of the nucleosome via a 6 carbon flexible linker. Upon addition of SNF2h and ADP-BeFx, if the nucleosome is translocated as in the Cryo-EM reconstruction, the two labeled bases will be brought closer together in 3D space. This change in DNA conformation could be read out as a very small increase in FRET efficiency between the two labels. (D) Ensemble FRET experiment described in (C). FRET efficiency values were normalized to the FRET efficiency of the nucleosome prior to adding SNF2h and nucleotide. Points represent the mean of the indicated number independent experiments and error bars represent the standard error of the mean. Addition of SNF2h and ADP-BeFx produces an instantaneous drop in FRET efficiency that slowly increases in the presence 140mM KCl but not in the presence of 70mM KCl (top). The instantaneous

drop in FRET efficiency may be due to subtle changes in the conformation of DNA immediately upon SNF2h binding or due to previously reported changes in the photophysics of the cy3 dye labeled at this position [9]. Changes in the photophysical properties of the cy5 label were ruled out as contributing to the change in FRET efficiency as there was no change in fluorescence intensity when cy5 was directly excited (data not shown). No increase in FRET signal was seen when only SNF2h buffer was added (bottom).

FIGURE 3.12

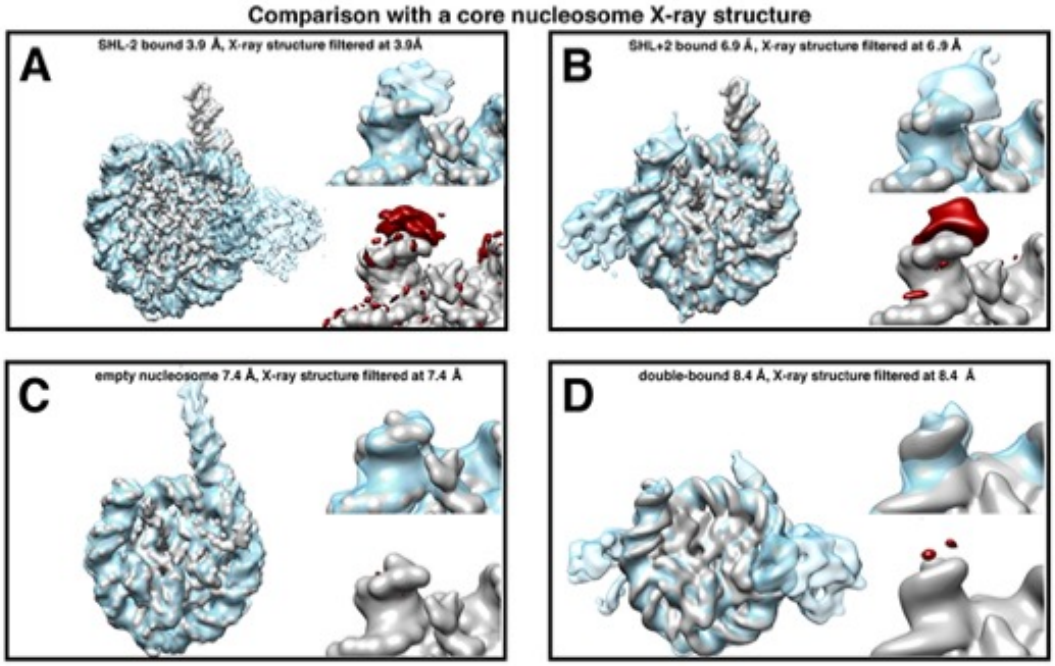

Figure 3.12 Difference maps to test for extra density of DNA at exit side of SNF2h-nucleosome complexes.
(A-C) Cryo-EM density map of the nucleosome either with SNF2h bound at (A) SHL-2 and (B) SHL+2 with 140 mM KCl with the simulated density map of nucleosome without two additional base-pairs filtered to a common resolution (A: 3.9 Å, B: 6.9 Å). (C) Cryo-EM density map of nucleosome without added SNF2h with the simulated density map of nucleosome without two additional base-pairs filtered to a common resolution (7.4 Å). For A-C, left: each panel shows an overview of the EM density (light blue) overlaid onto the simulated nucleosome map. Top right: enlarged view centered on the DNA exit site. Bottom right: enlarged view of the DNA exit site showing the difference density between the simulated map and the EM density at $\sigma = 7$. (D) Left: cryo-EM density map of doubly-bound nucleosome with 70 mM KCl is overlaid with the cryo-EM density map of the simulated nucleosome map. Both maps are filtered to a resolution of 8.4 Å. Top right: an enlarged view of the DNA end. Bottom right: density map of nucleosome alone is overlaid with the difference density calculated between the two, and visualized at $\sigma = 7$.

FIGURE 3.13

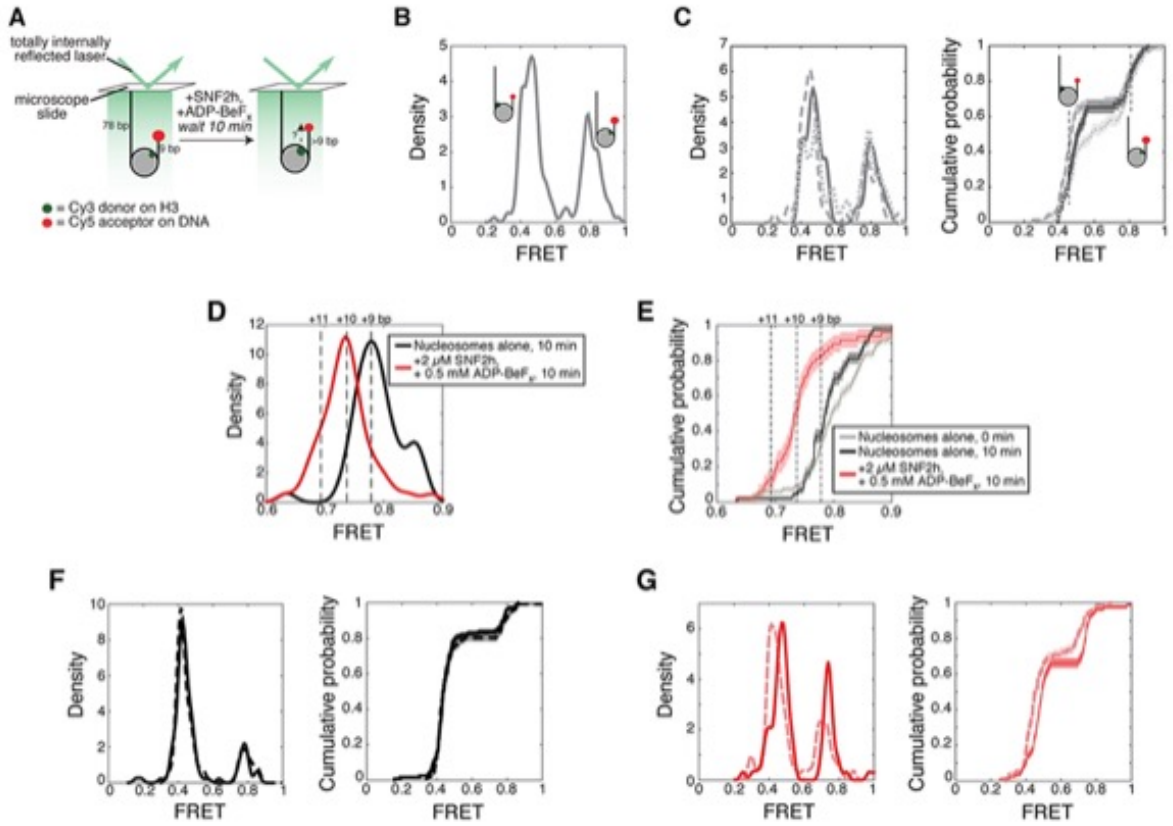

Figure 3.13. By a single molecule assay, SNF2h induces a change in FRET under the 140 mM KCl conditions, consistent with a movement of the nucleosomal DNA.
(A) Setup of the single molecule assay. Nucleosomes with 78 bp flanking DNA on one side are attached to the surface of a microscope slide and imaged using total internal reflection fluorescence microscopy. The nucleosomes have 9 bp flanking DNA on the other side, with a Cy5 dye at the end of the 9 bp. Movement of the DNA will change the distance between the Cy3 and Cy5 dyes, changing the observed FRET. (B) Kernel density estimation (KDE) plot of the starting FRET values of 179 nucleosomes, without SNF2h, combined from the three independent replicates shown in (C). FRET values cluster into two peaks, near 0.8 FRET and 0.45 FRET, corresponding to two possible labeling schemes: a Cy3 dye on the histone H3 closer to the Cy5-labeled DNA end (proximal labeling), or a Cy3 dye on the other copy of histone H3 (distal labeling). As demonstrated in (Zhou et al., 2018), the distally-labeled population is relatively insensitive to changes in the length of the DNA separating the Cy5 from the edge of the nucleosome, and so is not shown in (D) and (E). (C) KDEs (left) and empirical cumulative distribution functions (CDFs; right) of starting nucleosomal FRET values from three independent replicates. Note that the FRET value of the midpoint of a peak in a KDE corresponds to the FRET value where the slope of the CDF is steepest. Thus the distal and proximal peaks in the KDEs appear as two regions of steep slopes in the CDFs. For two data sets with similar peak locations, the FRET value (position along the x-axis) where the slope of the CDF is steepest will be similar. (D) (black) KDE of FRET values for 43 proximally-labeled nucleosomes after 10 minutes of incubation without SNF2h, and (red) 48 proximally-labeled nucleosomes after a 10 minute incubation in the presence of 2 μM SNF2h and 0.5

mM ADP-BeF_x. Dashed lines labeled “+11”, “+10”, and “+9” indicate expected FRET values for nucleosomes with 11, 10, or 9 bp of flanking DNA between the Cy5 and the edge of the nucleosome, based on the calibration curve derived in [58]. (E) Empirical cumulative distribution functions (CDFs) of the data in B and C. (F) Same as (C) but for the two replicates of nucleosomes alone after a 10 minute incubation. The two replicates have 115 and 117 nucleosomes each (with the distally labeled population included). (G) Same as (C) but for the two replicates of nucleosomes plus SNF2h and ADP-BeF_x after 10 minutes. The two replicates have 72 and 83 nucleosomes each. Shaded regions in CDFs in all panels represent an estimate of the error based on a bootstrapping method (see Methods).

FIGURE 3.14

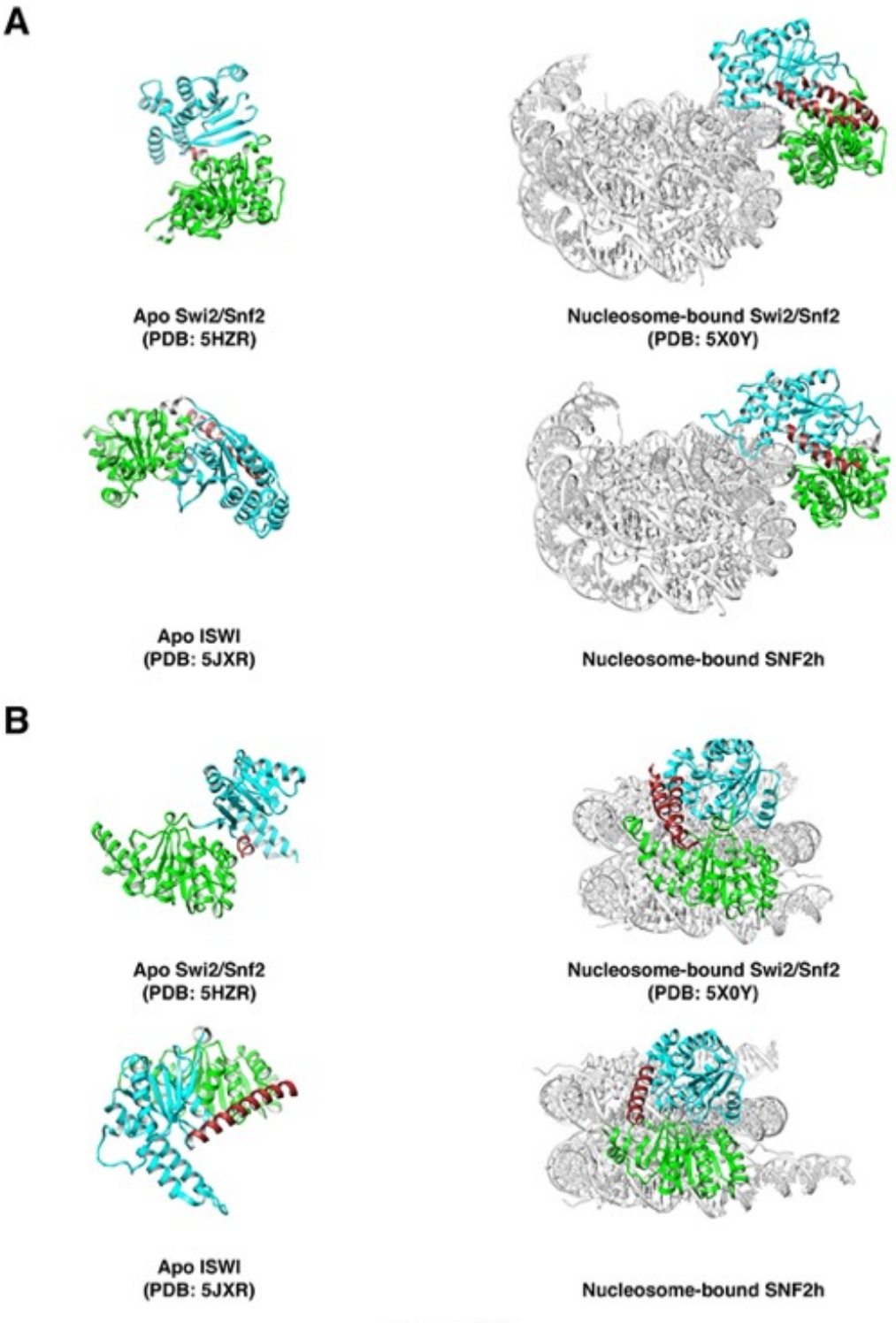
A
Apo Swi2/Snf2
(PDB: 5HZR)
Nucleosome-bound Swi2/Snf2
(PDB: 5X0Y)
Apo ISWI
(PDB: 5JXR)
Nucleosome-bound SNF2h
B
Apo Swi2/Snf2
(PDB: 5HZR)
Nucleosome-bound Swi2/Snf2
(PDB: 5X0Y)
Apo ISWI
(PDB: 5JXR)
Nucleosome-bound SNF2h

Figure 3.14. Brace helix comparisons
(A, B,) Comparison of bound and unbound conformations of Swi2/Snf2 (top A, B) and ISWI (bottom A, B) remodelers in two views. Left: Apo structures of *Myceliophthora thermophila* Swi2/Snf2 ATPase and ISWI ATPase [13,35]. Right: nucleosome-bound *S. cerevisiae* Swi2/Snf2 and *H. sapiens* Snf2h. Brace helix is shown in brown.

FIGURE 3.15

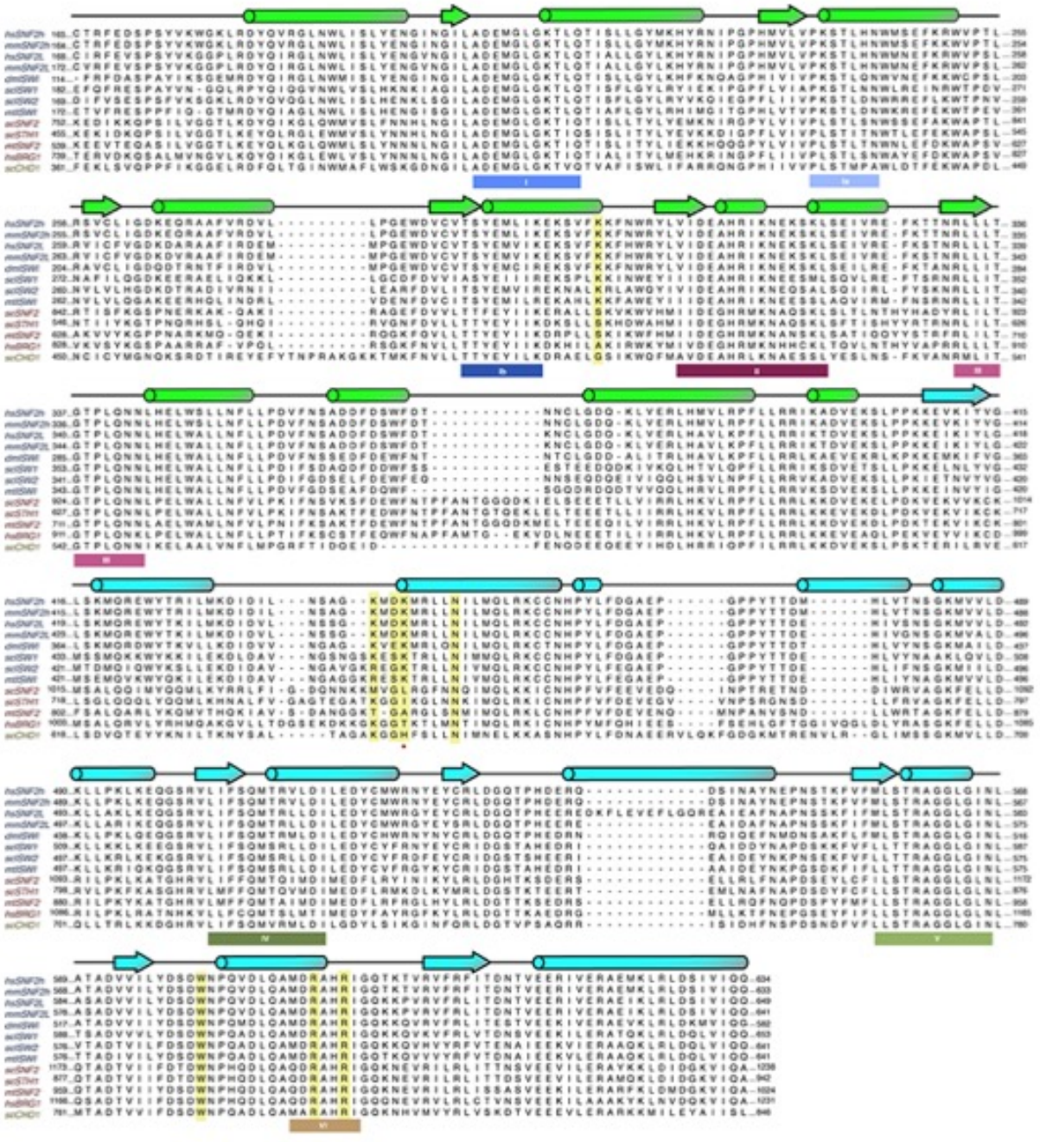

Figure 3.15 Multiple sequence alignment of the ATPase domains of selected members of chromatin remodeling families
Alignment of the ATPase domains of members of the ISWI (blue), SWI/SNF (red), and CHD families (yellow). Below the sequence, canonical SF2 nucleic acid helicase motifs are annotated [59]. Residues mutated in this study are highlighted in yellow. Red (•) denotes K443.

FIGURE 3.16

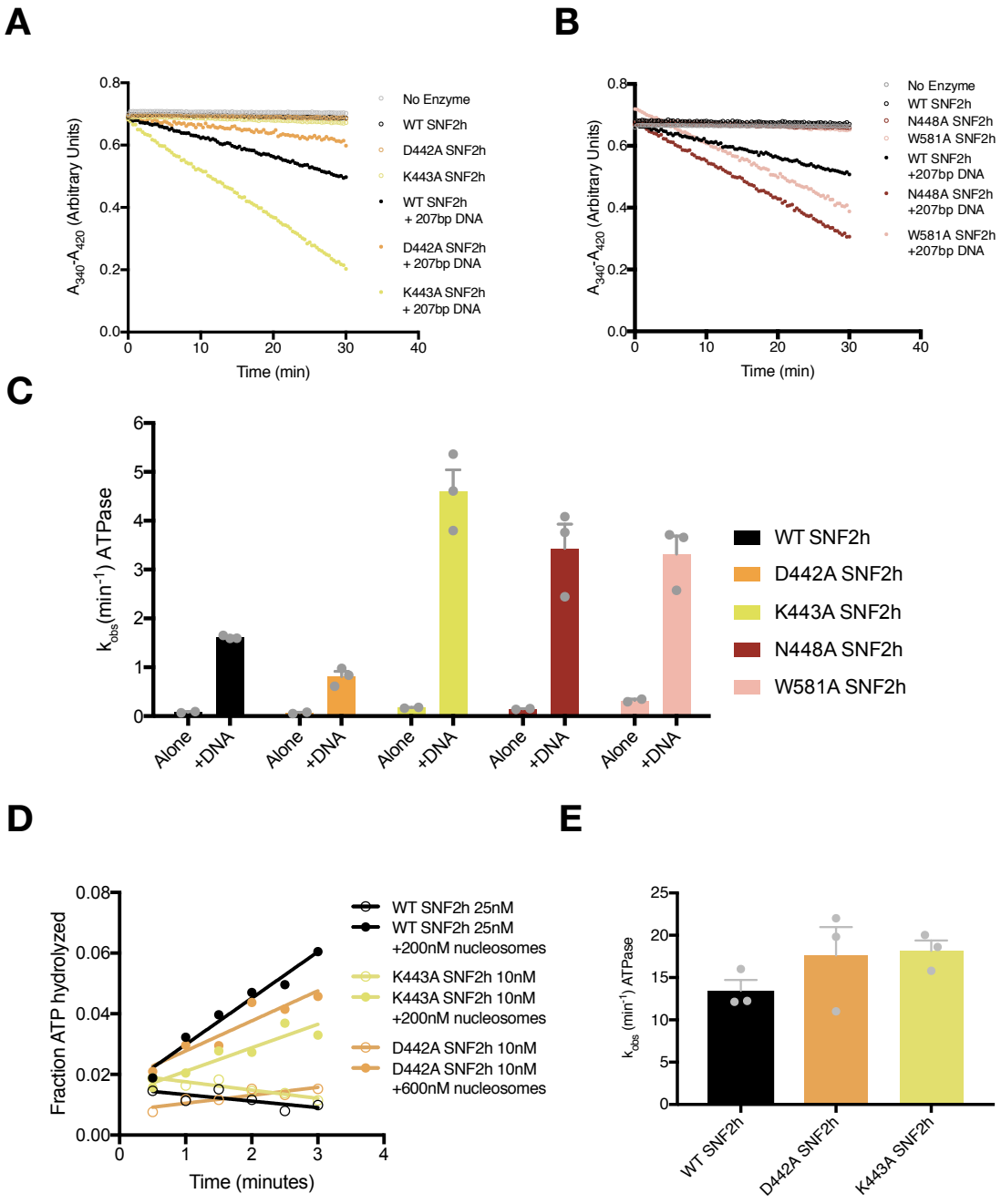
A
B
C
D
E
No Enzyme
WT SNF2h
D442A SNF2h
K443A SNF2h
WT SNF2h + 207bp DNA
D442A SNF2h + 207bp DNA
K443A SNF2h + 207bp DNA
N448A SNF2h
W581A SNF2h
N448A SNF2h +207bp DNA
W581A SNF2h +207bp DNA
A340-A420 (Arbitrary Units)
Time (min)
kobs (min-1) ATPase
Alone
+DNA
Fraction ATP hydrolyzed
Time (minutes)
WT SNF2h 25nM
WT SNF2h 25nM +200nM nucleosomes
K443A SNF2h 10nM
K443A SNF2h 10nM +200nM nucleosomes
D442A SNF2h 10nM
D442A SNF2h 10nM +600nM nucleosomes

Figure 3.16 ATPase activities of point mutants in this study
(A-B) Example absorbance plots of the NADH coupled ATPase assay to measure DNA-stimulated ATPase activity. Reactions were performed with 800nM of the indicated SNF2h constructs either without DNA (open circles) or with saturating concentrations (208nM) of the 207bp DNA used to assemble nucleosomes in our Cryo-EM reconstructions. (C) Mean and standard error of DNA-stimulated ATPase rate measurements for n=3 experiments. All mutations tested had modest effects on DNA-stimulated hydrolysis rates (~2-fold or less). (D) Example plot of radioactive ATP hydrolysis reactions used to measure nucleosome-stimulated ATPase activity. Reactions were performed with the indicated concentrations of SNF2h and nucleosomes without flanking DNA. The concentrations of nucleosomes used were confirmed to be saturating by this assay while the concentration of ATP-MgCl2 used was subsaturating (20μM). (E) Mean and standard error of nucleosome-stimulated ATPase rate measurements from n=3 measurements. All rates measured were within error of each other.

FIGURE 3.17

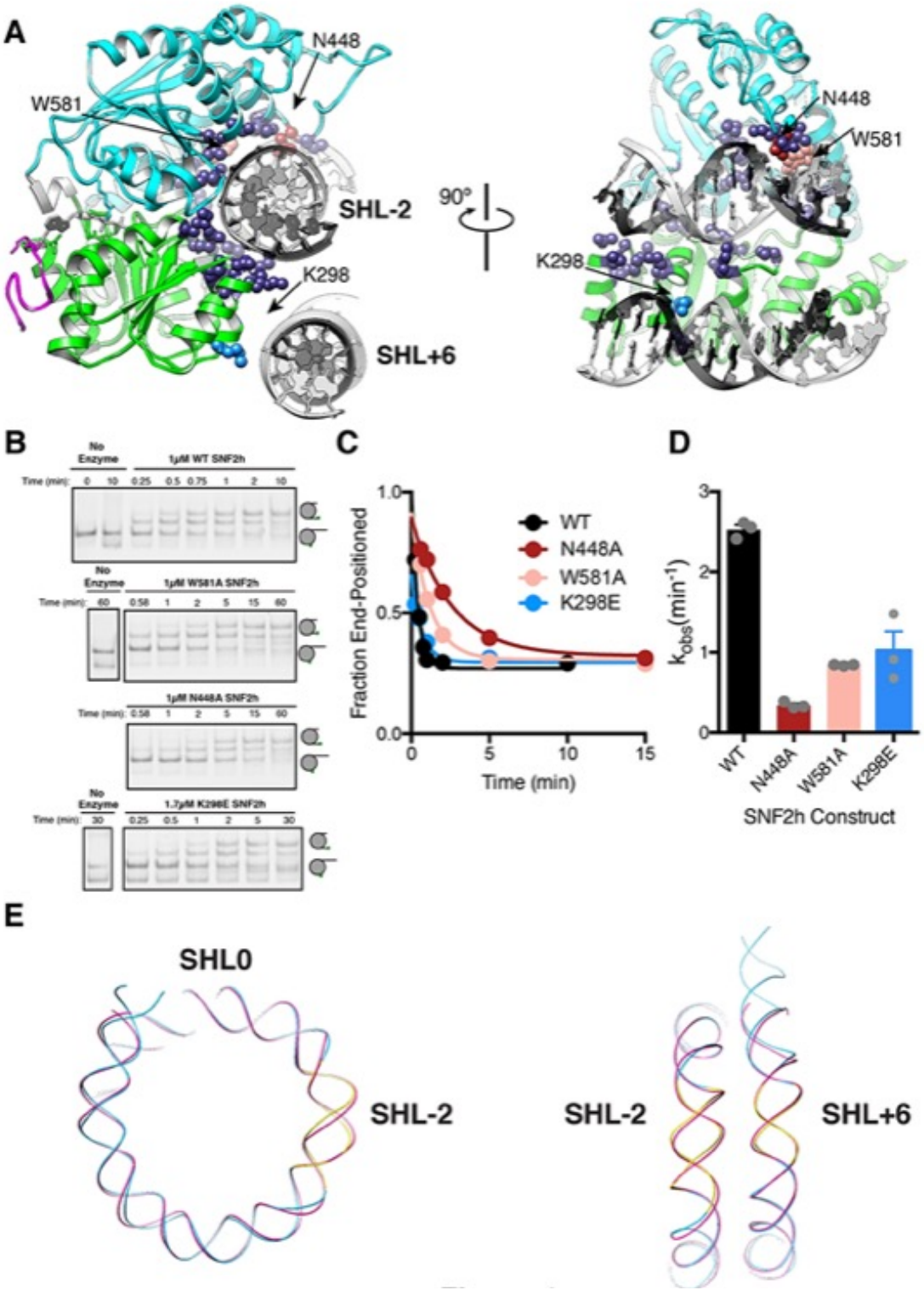
A
N448
W581
SHL-2
K298
SHL+6
90°
N448
W581
K298
B
No Enzyme
1μM WT SNF2h
Time (min): 0 10 0.25 0.5 0.75 1 2 10
No Enzyme
1μM W581A SNF2h
Time (min): 60 0.58 1 2 5 15 60
1μM N448A SNF2h
Time (min): 0.58 1 2 5 15 60
No Enzyme
1.7μM K298E SNF2h
Time (min): 30 0.25 0.5 1 2 5 30
C
Fraction End-Positioned
1.0
0.5
0.0
0
5
10
15
Time (min)
WT
N448A
W581A
K298E
D
k_{obs}(min^{-1})
3
2
1
0
WT
N448A
W581A
K298E
SNF2h Construct
E
SHL0
SHL-2
SHL-2
SHL+6

Figure 3.17. DNA contacts in the SNF2h-Nucleosome structure
(A) SNF2h residues contacting the nucleosome are shown in spheres. In light blue is a contact with the second gyre near SHL+6. In red, pink, and light blue are residues mutated in this study. (B) Native gel remodeling assay of DNA contact mutants. (C) Quantification of gels in (B). The x-axis is zoomed to show detail. The un-zoomed plots are in Figure 3-supplement 6. (D) Mean and standard error of rate constants derived from three experiments. (E) Comparison of the nucleosomal DNA in the SNF2h-nucleosome structure (blue) with the unbound structure (magenta) (PDBID: 1KX5). Contacts with the remodeler at SHL-2 and SHL+6 are highlighted in yellow.

FIGURE 3.18

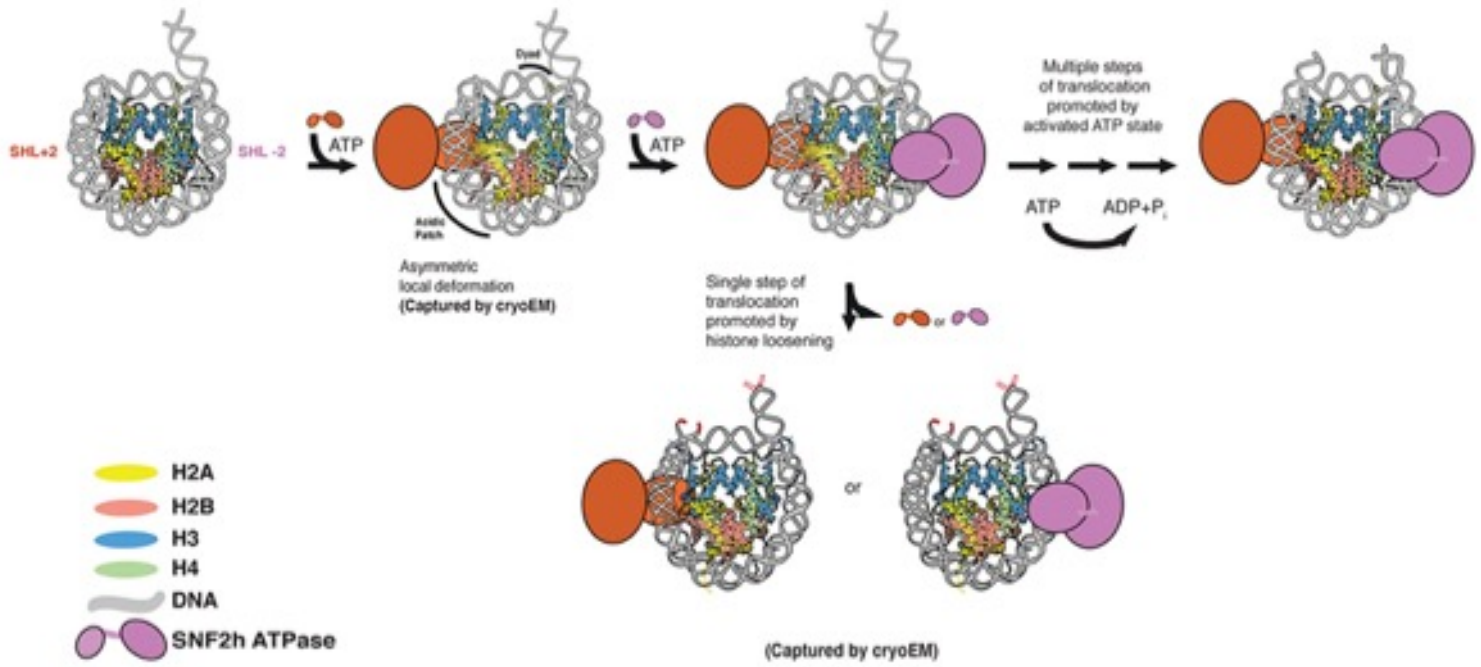
SHL+2
SHL -2
ATP
ATP
Dyad
Acidic Patch
Asymmetric local deformation (Captured by cryoEM)
Multiple steps of translocation promoted by activated ATP state
ATP
ADP+P$_i$
Single step of translocation promoted by histone loosening
or
or
H2A
H2B
H3
H4
DNA
SNF2h ATPase
(Captured by cryoEM)

Figure 3.18 Model that places SNF2h-nucleosome Cryo-EM structures within SNF2h reaction cycle

Two protomers of SNF2h bind to the nucleosome along with ATP. Based on previous work, the directionality of nucleosome sliding is determined by the motor that engages the longer flanking DNA [6]. By this model, the SNF2h motor bound at SHL+2 (orange protomer) will be the active motor and determine the direction of sliding because it would contact the 60 bp flanking DNA with its HSS domain [6]. For simplicity, the HSS domain is not shown. Binding of the SHL+2 protomer asymmetrically and allosterically deforms the acidic patch and histone H3 near the dyad on the opposite face of the histone octamer. The increased dynamics of these specific regions are shown in the cartoon. The second protomer can bind at SHL-2, but cannot act because deformation of the acidic patch inhibits its ability to slide nucleosomes. The SNF2h complex with the deformed octamer represents an intermediate that is poised for translocation. Processive DNA translocation is enabled by successive ATP hydrolysis cycles from this activated intermediate, moving DNA in 1-2bp fundamental increments. We speculate that the cryo-EM structure captured at low salt represents the deformed intermediate, while the structure captured at high salt represents a collapsed product state in which the nucleosome is translocated by 2bp (translocated bases are highlighted in red).

FIGURE 3.19

A

Dataset	Single-bound SNF2h-nucleosome complex at SHL-2	Doubly-bound SNF2h-nucleosome complex at SHL+/-2
Microscope	TF20 (FEI)	
Voltage (kV)	200	
Camera	TemF816 8k x 8k CMOS (TVIPS)	
Magnification	62.000	
Pixel size (Å)	1.2	
Defocus range (μm)	-1.8 : -2.9	
Number of images	766	
Total electron dose ($e^-/Å^2$)	25	
Number of frames	-	
Initial number of particles	450322	
Particles selected after 2D cleanup	379540	
Particles in final reconstruction	32233	57060
Final resolution (Å)	8.4	8.4

B

Dataset	Single-bound SNF2h-nucleosome complex: SHL+2 / SHL-2	Single-bound SNF2h-nucleosome complex, overall	Core nucleosome
Microscope	TF30 (FEI)	TF30 (FEI)	TF30 (FEI)
Voltage (kV)	300	300	300
Camera	K2 Summit (Gatan)	K2 Summit (Gatan)	K2 Summit (Gatan)
Magnification	31.000	31.000	31.000
Pixel size (Å)	1.22	1.22	1.22
Defocus range (μm)	-1.5 : -3.0	-1.5 : -3.0	-1.5 : -3.0
Number of images	720	720	754
Total electron dose ($e^-/Å^2$)	42	42	42
Number of frames	30	30	30
Initial number of particles	120533	333430	24993
Particles selected after 2D cleanup	95879	no cleanup	19363
Particles in final reconstruction	27513 / 6241	43165	12130
Final resolution (Å)	3.9 / 6.9	3.4	7.4

C

PDB	6NE3
EMPIAR	341
EMDB 3.9 Å SNF2h at SHL-2	EMD-9354
EMDB 6.9 Å SNF2h at SHL+2	EMD-9355
EMDB 3.4 Å SNF2h	EMD-9352
EMDB TVIPS 8.4Å singly-bound	EMD-9351
EMDB TVIPS 8.4Å doubly-bound	EMD-9353

Figure 3.19. Summary tables for dataset refinement and deposition
(A-B) Summary table for data collection and refinement on (A) TVIPS 816 scintillator-based camera, (B) Gatan K2-Summit direct electron detector camera. (A) Both single- and double-bound reconstructions originated from the same dataset. (B) Left and middle: Two individual data processing schemes resulted in three individual reconstructions from the same dataset at SHL+/-2; Right: Core nucleosome. (C) Model constructed into consensus 3.4Å map (B: middle) was deposited in the pdb; raw movies that resulted in (B: left and middle) were deposited in EMPIAR; individual maps were also deposited in EMDB under their respective ids

FIGURE 3.20

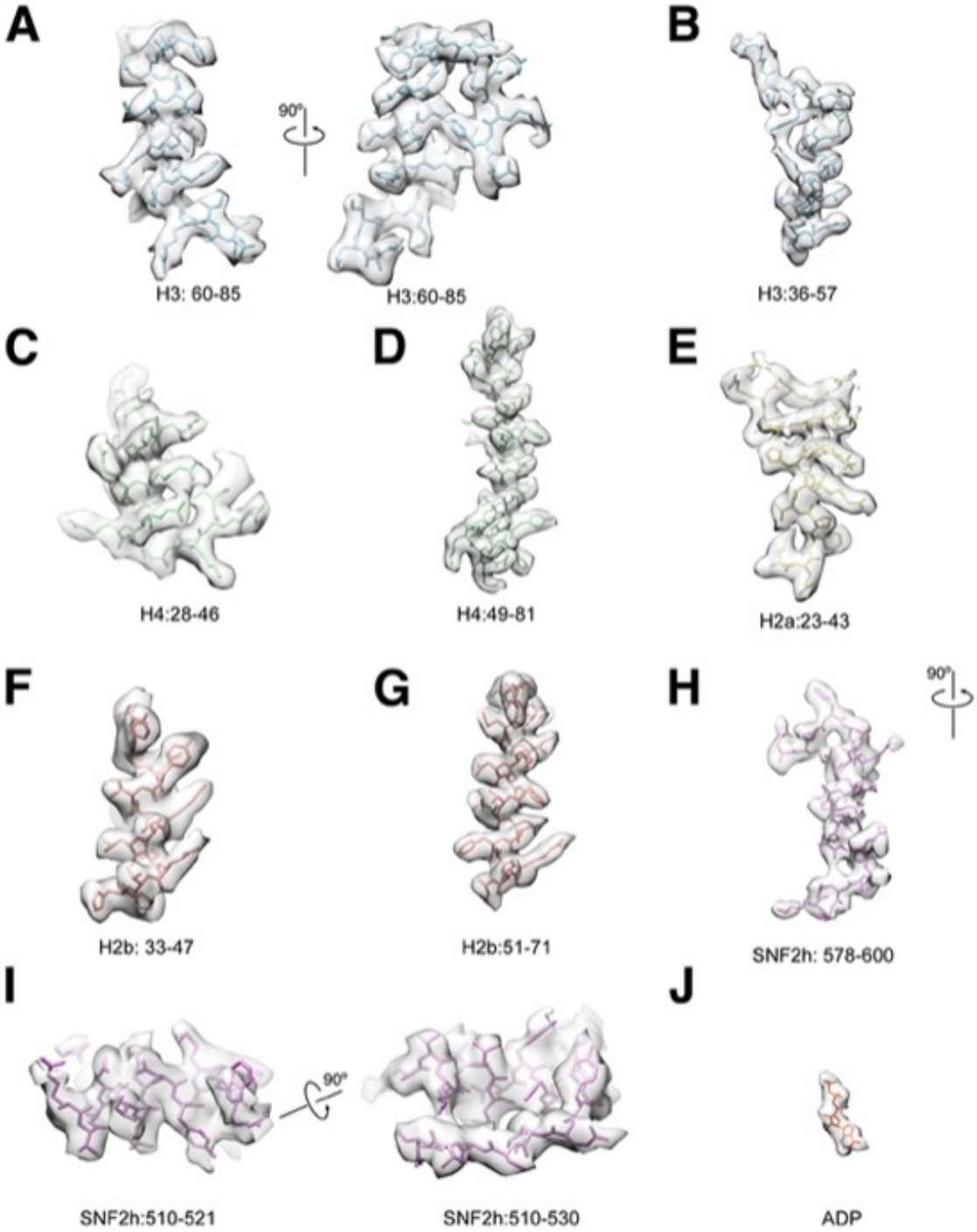
A
90°
H3: 60-85
H3:60-85
B
H3:36-57
C
H4:28-46
D
H4:49-81
E
H2a:23-43
F
H2b: 33-47
G
H2b:51-71
H
90°
SNF2h: 578-600
I
90°
SNF2h:510-521
SNF2h:510-530
J
ADP

Figure 3.20. Selected Cryo-EM protein densities
Representative 3.4Å resolution cryo-EM densities of SNF2h and core histones superimposed on the atomic model. The density maps are shown as semi-transparent, and the model is colored according to the color scheme in the main figures ((A-B) H3: blue, (C-D) H4: green, (E) H2a: yellow, (F-G) H2b: red, (H-I) SNF2h: purple, (J) ADP: orange).

FIGURE 3.21

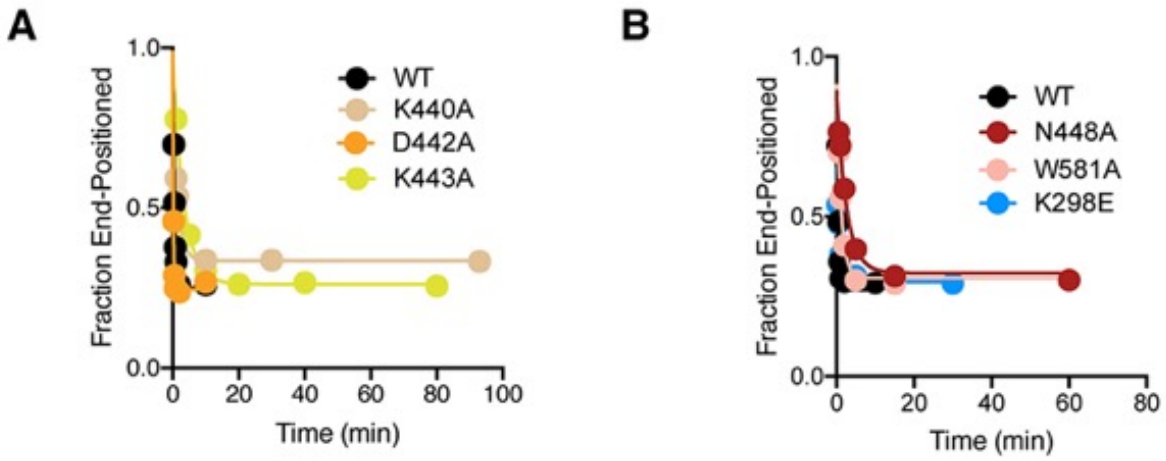

Figure 3.21 Full fits of native gel remodeling assays
Complete time courses from Figure 3D (A) and Figure 4B (B) shown with longer time points.

SUPPLEMENTAL FIGURE 3.1

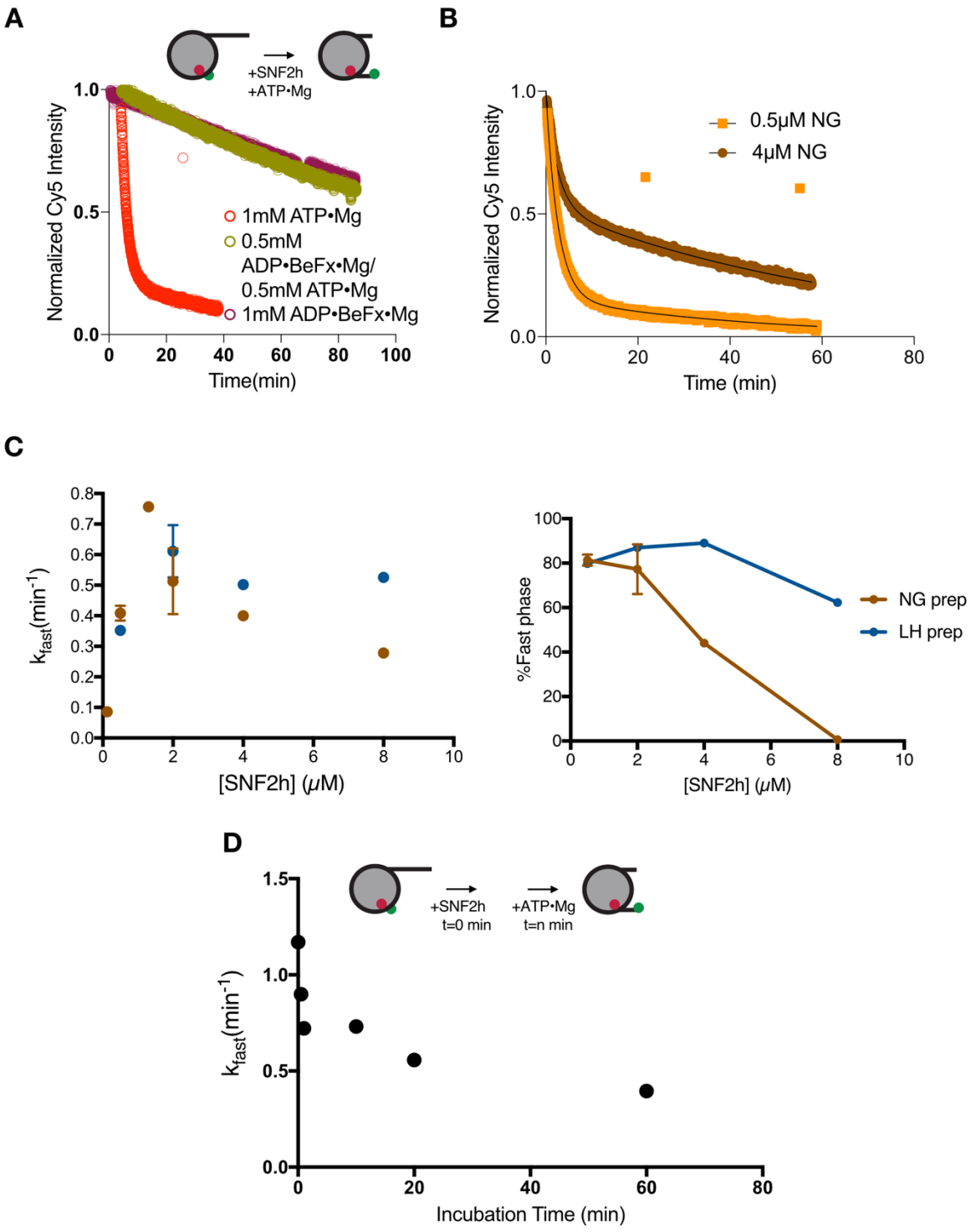

Supplemental Figure 3.1. Remodeling controls using the FRET-based sliding assay
(A) FRET-based remodeling assay with indicated mixture of nucleotide added in the 140mM KCl buffer condition. Decrease in FRET with only ADP-BeFx added reflects nucleosome disassembly and photobleaching [27]. (B) FRET assay performed with indicated concentration of SNF2h in the 140mM KCl buffer condition and fit to a double exponential decay. (C) Left. Rate constant from the fast phase from double exponential fits of remodeling assays as function of SNF2h concentration for two different preparations of SNF2h. Percent in the fast phase of the fit from double exponential fits of remodeling assays as function of SNF2h concentration for two different preparations of SNF2h. Error bars reflect standard error of the mean for n=2 experiments (NG only). (D) Rate constant from the fast phase of the remodeling assay as a function of SNF2h incubation time with nucleosomes without nucleotide added.

References

[1] C.R. Clapier, B.R. Cairns, The Biology of Chromatin Remodeling Complexes, Annu Rev Biochem. 78 (2009) 273–304. https://doi.org/10.1146/annurev.biochem.77.062706.153223.

[2] C.Y. Zhou, S.L. Johnson, N.I. Gamarra, G.J. Narlikar, Mechanisms of ATP-Dependent Chromatin Remodeling Motors, Annual Review of Biophysics. 45 (2016) 153–181. https://doi.org/10.1146/annurev-biophys-051013-022819.

[3] G.J. Narlikar, R. Sundaramoorthy, T. Owen-Hughes, Mechanisms and functions of ATP-dependent chromatin-remodeling enzymes., Cell. 154 (2013) 490–503. https://doi.org/10.1016/j.cell.2013.07.011.

[4] C.R. Clapier, B.R. Cairns, Regulation of ISWI involves inhibitory modules antagonized by nucleosomal epitopes, Nature. 492 (2012) 280–284. https://doi.org/10.1038/nature11625.

[5] F.J. Asturias, C. Ezeokonkwo, R.D. Kornberg, Y. Lorch, Electron microscopic analysis of the RSC chromatin remodeling complex., Methods in Enzymology. 376 (2004) 48–62. https://doi.org/10.1016/s0076-6879(03)76004-2.

[6] J.D. Leonard, G.J. Narlikar, A Nucleotide-Driven Switch Regulates Flanking DNA Length Sensing by a Dimeric Chromatin Remodeler, Molecular Cell. (2015). https://doi.org/10.1016/j.molcel.2015.01.008.

[7] A.E. Leschziner, A. Saha, J. Wittmeyer, Y. Zhang, C. Bustamante, B.R. Cairns, E. Nogales, Conformational flexibility in the chromatin remodeler RSC observed by electron

microscopy and the orthogonal tilt reconstruction method., Proceedings of the National Academy of Sciences. 104 (2007) 4913–4918. https://doi.org/10.1073/pnas.0700706104.

[8] Y. Qiu, R.F. Levendosky, S. Chakravarthy, A. Patel, G.D. Bowman, S. Myong, The Chd1 Chromatin Remodeler Shifts Nucleosomal DNA Bidirectionally as a Monomer., Molecular Cell. 68 (2017) 76-88.e6. https://doi.org/10.1016/j.molcel.2017.08.018.

[9] L.R. Racki, J.G. Yang, N. Naber, P.D. Partensky, A. Acevedo, T.J. Purcell, R. Cooke, Y. Cheng, G.J. Narlikar, The chromatin remodeller ACF acts as a dimeric motor to space nucleosomes., Nature. 462 (2009) 1016–1021. https://doi.org/10.1038/nature08621.

[10] R. Sundaramoorthy, A.L. Hughes, H. El-Mkami, D.G. Norman, H. Ferreira, T. Owen-Hughes, Structure of the chromatin remodelling enzyme Chd1 bound to a ubiquitinylated nucleosome., ELife. 7 (2018) 977. https://doi.org/10.7554/elife.35720.

[11] O. Willhoft, M. Ghoneim, C.-L. Lin, E.Y.D. Chua, M. Wilkinson, Y. Chaban, R. Ayala, E.A. McCormack, L. Ocloo, D.S. Rueda, D.B. Wigley, Structure and dynamics of the yeast SWR1-nucleosome complex, Science (New York, N.Y.). 362 (2018) eaat7716. https://doi.org/10.1126/science.aat7716.

[12] S. Eustermann, K. Schall, D. Kostrewa, K. Lakomek, M. Strauss, M. Moldt, K.-P. Hopfner, Structural basis for ATP-dependent chromatin remodelling by the INO80 complex., Nature. 556 (2018) 386–390. https://doi.org/10.1038/s41586-018-0029-y.

[13] X. Liu, M. Li, X. Xia, X. Li, Z. Chen, Mechanism of chromatin remodelling revealed by the Snf2-nucleosome structure, Nature. 544 (2017) 440–445. https://doi.org/10.1038/nature22036.

[14] R. Ayala, O. Willhoft, R.J. Aramayo, M. Wilkinson, E.A. McCormack, L. Ocloo, D.B. Wigley, X. Zhang, Structure and regulation of the human INO80-nucleosome complex., Nature. 556 (2018) 391–395. https://doi.org/10.1038/s41586-018-0021-6.

[15] L.R. Racki, N. Naber, E. Pate, J.D. Leonard, R. Cooke, G.J. Narlikar, The histone H4 tail regulates the conformation of the ATP-binding pocket in the SNF2h chromatin remodeling enzyme., Journal of Molecular Biology. 426 (2014) 2034–2044. https://doi.org/10.1016/j.jmb.2014.02.021.

[16] C.R. Clapier, G. Längst, D.F. Corona, P.B. Becker, K.P. Nightingale, Critical role for the histone H4 N terminus in nucleosome remodeling by ISWI., Molecular and Cellular Biology. 21 (2001) 875–883. https://doi.org/10.1128/mcb.21.3.875-883.1901.

[17] C.R. Clapier, K.P. Nightingale, P.B. Becker, A critical epitope for substrate recognition by the nucleosome remodeling ATPase ISWI., Nucleic Acids Research. 30 (2002) 649–655. https://doi.org/10.1093/nar/30.3.649.

[18] A. Hamiche, J.G. Kang, C. Dennis, H. Xiao, C. Wu, Histone tails modulate nucleosome mobility and regulate ATP-dependent nucleosome sliding by NURF., Proceedings of the National Academy of Sciences. 98 (2001) 14316–14321. https://doi.org/10.1073/pnas.251421398.

[19] K.K. Sinha, J.D. Gross, G.J. Narlikar, Distortion of histone octamer core promotes nucleosome mobilization by a chromatin remodeler., Science (New York, N.Y.). 355 (2017) eaaa3761. https://doi.org/10.1126/science.aaa3761.

[20] W. Dang, B. Bartholomew, Domain architecture of the catalytic subunit in the ISW2-nucleosome complex., Molecular and Cellular Biology. 27 (2007) 8306–8317. https://doi.org/10.1128/mcb.01351-07.

[21] T. Grüne, J. Brzeski, A. Eberharter, C.R. Clapier, D.F.V. Corona, P.B. Becker, C.W. Müller, Crystal Structure and Functional Analysis of a Nucleosome Recognition Module of the Remodeling Factor ISWI, Molecular Cell. 12 (2003) 449–460. https://doi.org/10.1016/s1097-2765(03)00273-9.

[22] M.N. Kagalwala, B.J. Glaus, W. Dang, M. Zofall, B. Bartholomew, Topography of the ISW2-nucleosome complex: insights into nucleosome spacing and chromatin remodeling., The EMBO Journal. 23 (2004) 2092–2104. https://doi.org/10.1038/sj.emboj.7600220.

[23] R. Schwanbeck, H. Xiao, C. Wu, Spatial contacts and nucleosome step movements induced by the NURF chromatin remodeling complex., The Journal of Biological Chemistry. 279 (2004) 39933–39941. https://doi.org/10.1074/jbc.m406060200.

[24] M. Zofall, J. Persinger, S.R. Kassabov, B. Bartholomew, Chromatin remodeling by ISW2 and SWI/SNF requires DNA translocation inside the nucleosome., Nature Structural & Molecular Biology. 13 (2006) 339–346. https://doi.org/10.1038/nsmb1071.

[25] S. Bilokapic, M. Strauss, M. Halic, Structural rearrangements of the histone octamer translocate DNA., Nature Communications. 9 (2018) 1330. https://doi.org/10.1038/s41467-018-03677-z.

[26] G.P. Dann, G.P. Liszczak, J.D. Bagert, M.M. Müller, U.T.T. Nguyen, F. Wojcik, Z.Z. Brown, J. Bos, T. Panchenko, R. Pihl, S.B. Pollock, K.L. Diehl, C.D. Allis, T.W. Muir, ISWI chromatin remodellers sense nucleosome modifications to determine substrate preference, Nature. 548 (2017) 607–611. https://doi.org/10.1038/nature23671.

[27] N. Gamarra, S.L. Johnson, M.J. Trnka, A.L. Burlingame, G.J. Narlikar, The nucleosomal acidic patch relieves auto-inhibition by the ISWI remodeler SNF2h, ELife. 7 (2018) e35322. https://doi.org/10.7554/elife.35322.

[28] R.F. Levendosky, G.D. Bowman, Asymmetry between the two acidic patches dictates the direction of nucleosome sliding by the ISWI chromatin remodeler., ELife. 8 (2019) 856. https://doi.org/10.7554/elife.45472.

[29] E.Y.D. Chua, V.K. Vogirala, O. Inian, A.S.W. Wong, L. Nordenskiöld, J.M. Plitzko, R. Danev, S. Sandin, 3.9 Å structure of the nucleosome core particle determined by phase-plate cryo-EM., Nucleic Acids Research. 44 (2016) 8013–8019. https://doi.org/10.1093/nar/gkw708.

[30] L. Farnung, S.M. Vos, C. Wigge, P. Cramer, Nucleosome-Chd1 structure and implications for chromatin remodelling., Nature. 550 (2017) 539–542. https://doi.org/10.1038/nature24046.

[31] J. Winger, I.M. Nodelman, R.F. Levendosky, G.D. Bowman, A twist defect mechanism for ATP-dependent translocation of nucleosomal DNA., ELife. 7 (2018) 391. https://doi.org/10.7554/elife.34100.

[32] G. Hauk, J.N. McKnight, I.M. Nodelman, G.D. Bowman, The chromodomains of the Chd1 chromatin remodeler regulate DNA access to the ATPase motor., Molecular Cell. 39 (2010) 711–723. https://doi.org/10.1016/j.molcel.2010.08.012.

[33] R. Sundaramoorthy, A.L. Hughes, V. Singh, N. Wiechens, D.P. Ryan, H. El-Mkami, M. Petoukhov, D.I. Svergun, B. Treutlein, S. Quack, M. Fischer, J. Michaelis, B. Böttcher, D.G. Norman, T. Owen-Hughes, Structural reorganization of the chromatin remodeling enzyme Chd1 upon engagement with nucleosomes., ELife. 6 (2017) 1405. https://doi.org/10.7554/elife.22510.

[34] X. Xia, X. Liu, T. Li, X. Fang, Z. Chen, Structure of chromatin remodeler Swi2/Snf2 in the resting state., Nature Structural & Molecular Biology. 23 (2016) 722–729. https://doi.org/10.1038/nsmb.3259.

[35] L. Yan, L. Wang, Y. Tian, X. Xia, Z. Chen, Structure and regulation of the chromatin remodeller ISWI, Nature. 540 (2016) 466–469. https://doi.org/10.1038/nature20590.

[36] W. Dang, M.N. Kagalwala, B. Bartholomew, Regulation of ISW2 by concerted action of histone H4 tail and extranucleosomal DNA., Molecular and Cellular Biology. 26 (2006) 7388–7396. https://doi.org/10.1128/mcb.01159-06.

[37] G. Li, M. Levitus, C. Bustamante, J. Widom, Rapid spontaneous accessibility of nucleosomal DNA., Nature Structural & Molecular Biology. 12 (2005) 46–53. https://doi.org/10.1038/nsmb869.

[38] S. Bilokapic, M. Strauss, M. Halic, Histone octamer rearranges to adapt to DNA unwrapping., Nature Structural & Molecular Biology. 25 (2018) 101–108. https://doi.org/10.1038/s41594-017-0005-5.

[39] J.L. Kitevski-LeBlanc, T. Yuwen, P.N. Dyer, J. Rudolph, K. Luger, L.E. Kay, Investigating the Dynamics of Destabilized Nucleosomes Using Methyl-TROSY NMR., Journal of the American Chemical Society. 140 (2018) 4774–4777. https://doi.org/10.1021/jacs.8b00931.

[40] S. Deindl, W.L. Hwang, S.K. Hota, T.R. Blosser, P. Prasad, B. Bartholomew, X. Zhuang, ISWI remodelers slide nucleosomes with coordinated multi-base-pair entry steps and single-base-pair exit steps., Cell. 152 (2013) 442–452. https://doi.org/10.1016/j.cell.2012.12.040.

[41] K. Luger, T.J. Rechsteiner, T.J. Richmond, Expression and Purification of Recombinant Histones and Nucleosome Reconstitution, in: Humana Press, 1999: pp. 1–16. https://doi.org/10.1385/1-59259-681-9:1.

[42] C.Y. Zhou, G.J. Narlikar, Analysis of Nucleosome Sliding by ATP-Dependent Chromatin Remodeling Enzymes., Methods in Enzymology. 573 (2016) 119–135. https://doi.org/10.1016/bs.mie.2016.01.015.

[43] M. Ohi, Y. Li, Y. Cheng, T. Walz, Negative Staining and Image Classification - Powerful Tools in Modern Electron Microscopy., Biological Procedures Online. 6 (2004) 23–34. https://doi.org/10.1251/bpo70.

[44] M. Liao, E. Cao, D. Julius, Y. Cheng, Structure of the TRPV1 ion channel determined by electron cryo-microscopy., Nature. 504 (2013) 107–112. https://doi.org/10.1038/nature12822.

[45] D.N. Mastronarde, Automated electron microscope tomography using robust prediction of specimen movements., Journal of Structural Biology. 152 (2005) 36–51. https://doi.org/10.1016/j.jsb.2005.07.007.

[46] S.Q. Zheng, E. Palovcak, J.-P. Armache, K.A. Verba, Y. Cheng, D.A. Agard, MotionCor2: anisotropic correction of beam-induced motion for improved cryo-electron microscopy., Nature Methods. 14 (2017) 331–332. https://doi.org/10.1038/nmeth.4193.

[47] K. Zhang, Gctf: Real-time CTF determination and correction., Journal of Structural Biology. 193 (2016) 1–12. https://doi.org/10.1016/j.jsb.2015.11.003.

[48] G. Tang, L. Peng, P.R. Baldwin, D.S. Mann, W. Jiang, I. Rees, S.J. Ludtke, EMAN2: an extensible image processing suite for electron microscopy., Journal of Structural Biology. 157 (2007) 38–46. https://doi.org/10.1016/j.jsb.2006.05.009.

[49] S.H.W. Scheres, RELION: implementation of a Bayesian approach to cryo-EM structure determination., Journal of Structural Biology. 180 (2012) 519–530. https://doi.org/10.1016/j.jsb.2012.09.006.

[50] A. Punjani, J.L. Rubinstein, D.J. Fleet, M.A. Brubaker, cryoSPARC: algorithms for rapid unsupervised cryo-EM structure determination., Nature Methods. 14 (2017) 290–296. https://doi.org/10.1038/nmeth.4169.

[51] S.H.W. Scheres, S. Chen, Prevention of overfitting in cryo-EM structure determination., Nature Methods. 9 (2012) 853–854. https://doi.org/10.1038/nmeth.2115.

[52] P.B. Rosenthal, R. Henderson, Optimal determination of particle orientation, absolute hand, and contrast loss in single-particle electron cryomicroscopy., Journal of Molecular Biology. 333 (2003) 721–745.

[53] D. Vasudevan, E.Y.D. Chua, C.A. Davey, Crystal structures of nucleosome core particles containing the “601” strong positioning sequence., Journal of Molecular Biology. 403 (2010) 1–10. https://doi.org/10.1016/j.jmb.2010.08.039.

[54] P. Emsley, B. Lohkamp, W.G. Scott, K. Cowtan, Features and development of Coot., Acta Crystallographica. Section D, Biological Crystallography. 66 (2010) 486–501. https://doi.org/10.1107/s0907444910007493.

[55] P.D. Adams, P.V. Afonine, G. Bunkóczi, V.B. Chen, I.W. Davis, N. Echols, J.J. Headd, L.-W. Hung, G.J. Kapral, R.W. Grosse-Kunstleve, A.J. McCoy, N.W. Moriarty, R. Oeffner, R.J. Read, D.C. Richardson, J.S. Richardson, T.C. Terwilliger, P.H. Zwart, PHENIX: a comprehensive Python-based system for macromolecular structure solution., Acta Crystallographica. Section D, Biological Crystallography. 66 (2010) 213–221. https://doi.org/10.1107/s0907444909052925.

[56] E.F. Pettersen, T.D. Goddard, C.C. Huang, G.S. Couch, D.M. Greenblatt, E.C. Meng, T.E. Ferrin, UCSF Chimera—A visualization system for exploratory research and analysis, 25 (2004) 1605–1612. https://doi.org/10.1002/jcc.20084.

[57] J.E. Lindsley, Use of a real-time, coupled assay to measure the ATPase activity of DNA topoisomerase II., Methods in Molecular Biology (Clifton, N.J.). 95 (2001) 57–64.

[58] C.Y. Zhou, S.L. Johnson, L.J. Lee, A.D. Longhurst, S.L. Beckwith, M.J. Johnson, A.J. Morrison, G.J. Narlikar, The Yeast INO80 Complex Operates as a Tunable DNA Length-Sensitive Switch to Regulate Nucleosome Sliding., Molecular Cell. 69 (2018) 677-688.e9. https://doi.org/10.1016/j.molcel.2018.01.028.

[59] A. Flaus, D.M.A. Martin, G.J. Barton, T. Owen-Hughes, Identification of multiple distinct Snf2 subfamilies with conserved structural motifs., Nucleic Acids Research. 34 (2006) 2887–2905. https://doi.org/10.1093/nar/gkl295.

Chapter 4: Histone dynamics within the nucleosome play a critical role in SNF2h-mediated nucleosome sliding

Introduction

Elucidating the mechanisms by which ATP-dependent chromatin remodeling enzymes disrupt nucleosome structure is essential to understanding how chromatin states are established and maintained. We have previously demonstrated that dynamics in the histone core are functionally important for nucleosome sliding by the ISWI-family remodeler SNF2h [1]. Restraining histone octamer dynamics by site-specific disulfide crosslinks engineered in otherwise cysteine-free histones inhibited nucleosome sliding by SNF2h. Using similar approaches, others have also suggested that octamer plasticity is important in nucleosome sliding [2,3]. However, a subsequent study reporting cryo-EM structures of ISWI-family remodeler-nucleosome complexes failed to observe stable conformational rearrangements in the histone octamer [4]. The authors of this study were also unable to replicate the finding that restraining histone dynamics by single H3-H4 crosslinks (H3L82C-H4V81C, called sCX2) impacted nucleosome sliding by SNF2h [1]. Specifically, they found that treatment of disulfide crosslinked nucleosomes with reducing agent failed to rescue SNF2h-dependent nucleosome sliding. This led the authors to conclude that rearrangements in histone conformation are not major contributor to SNF2h-dependent nucleosome sliding and that oxidative damage is responsible the effects seen by Sinha et al. Here we replicate the findings of Sinha et al. that restraining histone dynamics, not oxidative damage, impairs sliding by nucleosome remodeling. Instead, we show specifically that the method used by Yan et al. to reduce nucleosomes fails to break the disulfide bond in H3-H4, explaining the discrepancy.

Results

Site-specific disulfide crosslinking between H3 and H4 impairs SNF2h-mediated nucleosome sliding

Initially, Yan et al. generated sCX2 crosslinks in the background of WT *Xenopus laevis* histone octamers, which bear an endogenous cysteine in histone H3 (H3C110). However, the presence of the additional reactive cysteine, which can readily form disulfides under oxidizing conditions [5], creates the possibility for multiple types of crosslinked species, complicating the interpretation of these results. Yan et al. also created sCX2 crosslinks in an H3C110A mutant octamer and, in this case, found that SNF2h sliding activity was impaired, as seen by Sinha et al., but to a lesser extent than previously observed. Further, when the disulfide bond was apparently reduced by adding 100mM DTT, sliding activity was not restored. Based on these results, Yan et al. suggested, "…that the loss of activity did not result from the disulfide bond but probably from non-specific oxidation damage to the nucleosome, which was prone to precipitate out of the solution under the condition of extensive oxidation. Prolonged treatment might have resulted in damage to the nucleosome and loss of the activity." However, the authors did not directly test this possibility. To address this concern experimentally we first assembled nucleosomes with cysteine-free *Xenopus laevis* H3C110A octamers that were oxidized with CuPhe (Figure 4.1). No precipitates were observed during preparation and the oxidized octamers readily assembled into canonical nucleosomes, suggesting no gross defects. Remodeling of these oxidized nucleosomes with SNF2h after purification by glycerol gradient ultracentrifugation showed no defect compared to nucleosomes assembled from untreated H3C110A octamers (Table 1, Figure 4.2A).

To test whether the oxidation method may impact the results in the context of H3C110A sCX2 octamer, we generated H3C110A sCX2 crosslinked nucleosomes using CuPhe or oxidized glutathione (GSSG), a gentler oxidizing agent that does not generate free radicals and has been used previously to investigate nucleosome dynamics [6]. Oxidation with CuPhe went to near-completion as assessed by a non-reducing SDS-PAGE gel, while GSSG oxidation was less efficient (Figure 4.1A). We then reduced a portion of each H3C110A sCX2 crosslinked octamer by dialysis into buffer containing 100mM DTT (Figure 4.1B). H3C110A sCX2 octamers showed no visible precipitates upon oxidation or after reduction and, like cysteine-free octamers, readily assembled into nucleosome core particles that were purified by glycerol gradient ultracentrifugation. H3C110A sCX2 nucleosomes assembled from octamers oxidized with CuPhe slowed SNF2h nucleosome sliding ~40-fold compared to reduced controls under saturating concentrations of SNF2h, while nucleosomes assembled from octamers oxidized by GSSG slowed sliding ~15-fold (Figures 4.2B and C). This quantitative difference can be attributed to the different crosslinking efficiencies of the two oxidation protocols and cannot be explained by nucleosome disassembly (Figure 4.3 and 4). Reduction of either type of oxidized octamers fully restored SNF2h-dependent sliding activity of nucleosomes assembled from their respective octamers (Figures 4.2B and C). To further test whether the oxidation-dependent impact on SNF2h-dependent sCX2 nucleosome remodeling is due to the formation of a disulfide bond, we also tested remodeling on nucleosomes assembled using oxidized H3C110A octamers containing single cysteines from the sCX2 cysteine pair that were purified by ultracentrifugation (Figure 4.5A). In this side-by-side experiment, SNF2h remodeled CuPhe oxidized H3C110A sCX2 nucleosomes ~30-fold slower than untreated H3C110A nucleosomes in line with our earlier observations, while single cysteine-containing nucleosomes were remodeled only ~2-fold slower. Oxidation-

dependent remodeling defects were also observed with sub-saturating concentrations of enzyme (Figure 4.5B). These results indicate that non-specific oxidative damage to the octamer cannot explain the remodeling defects.

In order to determine whether any differences in the remodeling assay protocols could explain the discrepancies between the two studies, we repeated the remodeling reaction under the conditions used by Yan et al. While the remodeling reactions were faster overall (Figure 4.5C), even under these conditions a disulfide bond between the sCX2 cysteine pair causes a >6-fold reduction in reaction rate (Figure 4.5C). Due to the faster remodeling reaction, nucleosomes are already ~60 % remodeled at the first time point we are able to capture (0.3 min). As a result, the rate constant reported here for non-oxidized nucleosomes is likely an underestimate and the 6-fold defect should be considered a lower limit.

These results (summarized in Table 1), (i) rule out non-specific octamer oxidation causing inhibition of sliding; (ii) reproduce the inhibitory effects seen by Sinha et al. when the H3L82C-H4V81C disulfide bond is formed in an H3C110A nucleosome; and (iii) show that this defect is reversible when the oxidized octamer is reduced prior to nucleosome assembly.

Failure to completely reduce the histone octamer explains reported discrepancies

Yan et al. tested reversibility in a different manner than described above. Specifically, while oxidation was carried out in the context of an octamer, the reduction reaction was carried out in the context of a nucleosome. In our experience, reducing buried disulfides in the context of a fully assembled nucleosome is difficult, likely because the disulfide crosslink is less solvent accessible in a nucleosome compared to an octamer. When we reduced crosslinked H3C110A sCX2 nucleosomes following the same

protocol as Yan et al. (treatment of crosslinked nucleosomes with 100mM DTT at 37ºC for 1hr), we found that SNF2h sliding activity was not restored, consistent with their report (Figure 4.6A). Although Yan et al. showed these conditions were sufficient to completely break the disulfide bond when assayed by non-reducing SDS-PAGE, we reasoned that if the sample was not buffer exchanged to remove excess DTT prior to denaturation in SDS-PAGE loading buffer, once-buried disulfides could become exposed upon denaturation and rapidly reduced by the residual DTT. This would cause an overestimation of the degree of reduction by SDS-PAGE. To test this possibility, we reduced H3C110A sCX2 crosslinked nucleosomes with 100mM DTT for 1hr at 37ºC and either directly added the sample to SDS loading buffer or quenched the residual DTT with 5-fold excess N-ethyl maleimide before SDS treatment. While in the unquenched sample the disulfide bond is completely reversed, quenching the sample prior to SDS treatment causes retention of the disulfide bond (Figure 4.6C). This retention cannot be explained by re-oxidation of the disulfide bond upon quenching as N-ethyl maleimide would also react with cysteine thiols, blocking new disulfide bond formation. In addition, oxidation of the cysteines within octamers in the absence of catalysts such as CuPhe or GSSG is extremely slow (≥48 hours) [1]. It is thus possible that the apparent inability by Yan et al. to reverse the nucleosome sliding defects associated with octamer crosslinking may have been due to an inability to completely reverse crosslinking in fully assembled nucleosomes, and that the reduction they observe occurs while processing the samples for analysis by SDS-PAGE. The results underscore the importance of performing both oxidation and reduction reactions in the context of the histone octamer when attempting to generate or reverse crosslinks to investigate the role of histone dynamics.

Discussion

In summary, we replicate our earlier findings that restraining histone dynamics with disulfide crosslinks interferes with SNF2h-mediated nucleosome sliding. We further show that this finding is robust to the method of crosslinking and cannot be explained by non-specific oxidative damage to the nucleosome. The inability to replicate this finding by Yan et al. might be due to incomplete reduction of the disulfide bond in the context of the nucleosome. Our results are consistent with an important role for histone octamer plasticity during SNF2h-mediated nucleosome sliding.

Importantly, our results do not invalidate the other conclusions drawn in the article by Yan et al. nor do they cast doubt on the quality and accuracy of the structural data presented. Cryo-EM structures represent only the fraction of states that can be reconstructed to high resolution. Lowly-populated or highly dynamic states would likely be lost during the averaging required for high resolution analysis. Consistent with this possibility, a recent cryo-EM study captured multiple stable ISWI-nucleosome states [7]. While the highest resolution structures showed no clear evidence of conformational dynamics, lower resolution structures showed local reduction in the cryo-EM density that overlaps both with dynamic regions captured by NMR [1] and with the crosslinked residues tested here and in Sinha et al. These results are consistent with SNF2h promoting the formation of an ensemble of highly dynamic conformations that cannot be directly visualized by cryo-EM averaging. The absence of a stable deformed histone octamer in the cryo-EM density reported by Yan et al. is compatible with the finding that histone deformation is important for nucleosome sliding. Further study of the structural states adopted during the remodeling reaction are required to clarify the nature of the deformations in histone structure required for sliding.

Acknowledgements

We thank Kalyan Sinha for help generating the disulfide crosslinked nucleosome and Julia Tretyakova for preparing histones. We also thank Serena Sanulli, John Gross, Joseph Lobel, and Yifan Cheng for helpful feedback in preparing this manuscript and all members of the Narlikar lab for helpful discussions. This work was supported by a grant from the NIH to GJN (R35GM127020) and an NSF predoctoral and UCSF discovery fellowship to NG.

Appendix to chapter 4

Dynamics in H2A-H2B are also important for nucleosome remodeling by SNF2h

CryoEM reconstructions of SNF2h-nucleosome complexes have suggested that SNF2h binding increases dynamics of the acidic patch on the opposite face of the nucleosome [7]. We wondered whether these conformational dynamics might be functionally relevant for nucleosome sliding by SNF2h. To do this, we engineered a disulfide bond in the acidic patch by mutating two residues close in proximity and within the acidic patch (H2A 63C, H2B 42C). Crosslinks were generated at the octamer stage by treatment with CuPhe and removed by dialysis with excess reducing agent. APX nucleosomes were then subject to remodeling by SNF2h. Restraining histone dynamics by disulfide bond formation in APX nucleosomes dramatically slowed remodeling (quantifications not determined). This effect was almost completely reversed by disulfide bond scission with reducing agent. Since it has not yet been determined whether the conditions with crosslinked APX nucleosomes were performed under saturating conditions, it is unclear whether this effect represents a defect in SNF2h binding or specifically nucleosome remodeling. However, it is likely that these represent saturating conditions as they were performed at concentrations sufficient to saturate acidic-patch mutant nucleosomes.

Restraining histone dynamics uncouples ATP hydrolysis from remodeling

Restraining conformational dynamics in the histone octamer at locations in H2A-H2B and H3-H4 slows nucleosome sliding by SNF2h [1]. This could be due to a defect in stimulating ATP hydrolysis and/or in the coupling of ATP hydrolysis to nucleosome sliding. To better understand how restraining histone dynamics slows remodeling, we measured nucleosome-stimulated ATP hydrolysis of 0/60 nucleosomes containing a disulfide bond

in APX or sCX2 (Oxidized) and compared them to nucleosomes without the bond (Reduced) using previously described methods [7]. These were performed under multiple turnover conditions (Nucleosomes in excess of SNF2h) and with saturating concentrations of both ATP and nucleosomes. Oxidized APX or sCX2 nucleosomes both stimulated ATP hydrolysis by SNF2h ~4-fold worse than WT nucleosomes. This is substantially less than the >10-fold effect of disulfide bond formation on nucleosome sliding. This indicates that restraining histone dynamics at these locations disrupts both modestly disrupts stimulation ATP hydrolysis and more substantially the coupling of ATP hydrolysis to nucleosome sliding. Reduction of APX nucleosomes fully restored nucleosome stimulated ATP hydrolysis but reduced sCX2 nucleosomes stimulated ATP hydrolysis about ~2-fold weaker than WT nucleosomes also treated with reducing agent. This result is somewhat surprising, as the same preparation of reduced sCX2 nucleosomes is slid by SNF2h at a rate comparable to WT nucleosomes. It is possible then that reduced sCX2 nucleosomes improve the coupling of ATP hydrolysis to remodeling, which enables them to slide nucleosomes at rates comparable to WT nucleosomes.

Dynamics in H2A-H2B are required for nucleosome stability

Previously it has been demonstrated that nucleosome dynamics in the H2A-H2B dimer are critical for the assembly and stability of the nucleosome [8]. This was demonstrated, in part, by the observation that non-specific crosslinking of H2A-H2B with glutaraldehyde prevents dimer incorporation into hexasomes (nucleosomes missing a single H2A-H2B dimer) [8]. During the process of generating APX nucleosomes, a series of nucleosomes with cysteine mutant pairs in H2A-H2B were made. When oxidized, nucleosomes containing one cysteine pair (H2A 67C/H2B 46C) disassembled to

hexasomes when diluted for remodeling assays. Removal of the disulfide bond in H2A 67C/H2B 46C nucleosomes by reduction, showed no dissociation upon dilution. These results are consistent with the notion that conformational plasticity in the H2A-H2B dimer is required for nucleosome stability.

Materials and Methods

SNF2h was purified from E. coli as described previously [7]. Recombinant *Xenopus laevis* histones were expressed and purified from E. coli as previously described [9]. Cysteine mutant histones were purified in the presence of excess DTT. Mutant histones were also purified using only the gel-filtration step because cyanate formed in the urea buffers required for ion exchange reacts with the cysteine thiols [1]. Cy3-labeled nucleosome DNA was generated by PCR with HPLC-purified, labeled primers (IDT, Coralville, IA) and Phusion DNA polymerase using the strong, synthetic 601 nucleosome positioning sequence [10]. Nucleosome DNA was purified by native PAGE.

Histone octamer refolding was performed as described previously [7]. H3C110A sCX2 octamer was refolded in the presence of 10mM DTT to prevent disulfide formation. Refolded histone octamer and H2A/H2B dimer was purified by size exclusion chromatography with 10mM DTT. For oxidation, histone octamers and dimers were diluted to 5µM and ~200µL of sample was dialyzed twice into 1L high salt buffer without reducing agent (10mM HEPES pH 8.5, 2M NaCl, 1mM EDTA) each time overnight at 4ºC.

For the CuPhe oxidation protocol, histone octamer and dimer was dialyzed overnight into 10 mM HEPES pH 7.25, 2 M NaCl. Histones were treated with 25µM Cu(II)SO4 and 100µM o-phenanthroline for 75 min at room temperature in the dark before being quenched with 10mM EDTA. Stocks of Cu(II)SO4 and o-phenanthroline used for oxidation were freshly dissolved in 10 mM HEPES pH 7.25, 2 M NaCl on the day of reaction. For the glutathione oxidation, histones were mixed 4:1 by volume histone:glutathione buffer (250mM Tris pH 9.0, 2M NaCl, 7.5mM Oxidized Glutathione, 2.5mM Reduced Glutathione, 5mM Benzamidine, 0.5mM Leupeptin) at room temperature in the dark for 4 nights. To check the progress of oxidation, aliquots of each reaction

were quenched with 50mM iodoacetamide and run on a non-reducing SDS-PAGE gel. Disappearance of the H3 and H4 bands and appearance of a higher molecular weight species was used to determine the progress of oxidation. Quantification of crosslinking was done by measuring the intensity of the H3-H4 crosslinked band and normalizing it to the intensity of the H2A/H2B band. After oxidation, histones were dialyzed into 1L of 10mM HEPES pH 8.5, 2M NaCl, 1mM EDTA overnight at 4ºC.

To reduce oxidized histones, samples were dialyzed overnight into 10mM HEPES pH 8.5, 2M NaCl, 1mM EDTA, 100mM DTT at 4ºC. Reduced samples were checked using non-reducing SDS-PAGE. Loss of the high molecular weight species and reappearance of the H3 and H4 bands indicated complete reduction.

All nucleosomes except reduced APX nucleosomes were assembled using salt gradient dialysis and purified by glycerol gradient centrifugation as described previously [11]. Oxidized nucleosomes were assembled using buffers without reducing agent while reduced nucleosomes were assembled using buffers with 3mM TCEP. Because they are more sensitive to oxidation, reduced APX nucleosomes were assembled by step dialysis as described previously, with freshly dissolved 100mM DTT present in each buffer.

All remodeling reactions were performed under single turnover conditions (enzyme in excess of nucleosomes) with saturating concentrations (1µM) or subsaturating (50nM) concentrations of SNF2h at 20°C with 15 nM nucleosomes, 12.5 mM HEPES pH 7.5, 2 mM Tris pH 7.5, 70 mM KCl, 5 mM ATP•MgCl2, 3 mM MgCl2 , 0.02% NP40, and ~3%(v/v) glycerol. To assess the effects of the different buffer and temperature conditions used by Yan et al., we also measured remodeling using 50 nM SNF2h and 15 nM nucleosomes at 37ºC with 20mM HEPES pH 7.5, 50mM KCl, 2 mM ATP•MgCl2, 3 mM MgCl2, 0.1mg/mL BSA, and 5%(v/v) glycerol. Reactions were started with addition of nucleosomes and time points were quenched with excess ADP and plasmid DNA. Time points were then resolved

by native PAGE (6% acrylamide, 0.5XTBE) and scanned on a Typhoon variable mode imager (GE Life Sciences, Pittsburgh, PA) by scanning for fluorescent labels. Gels were then quantified by densitometry using ImageJ. The fraction of nucleosomes end-positioned (i.e. unremodeled) at a given time point was determined by the ratio of fast-migrating nucleosomes to the total nucleosome intensity. This was fit to a single exponential decay using Prism 6 (GraphPad, La Jolla, CA).

Figures

FIGURE 4.1

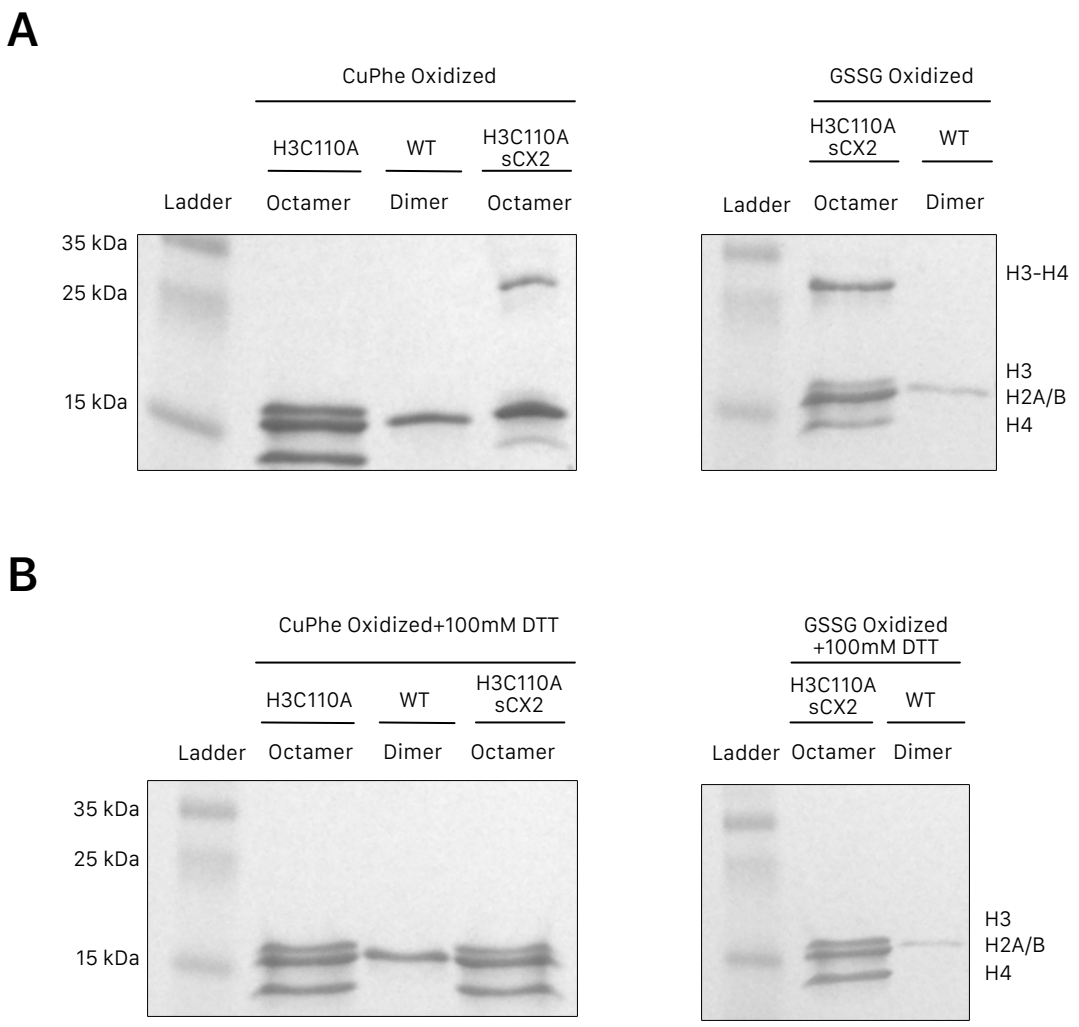

Figure 4.1 Preparation of crosslinked and reduced histone octamers
SDS-PAGE gels of *Xenopus laevis* of histones used to prepare nucleosomes in this study. (A) H3C110A histone octamer and H3C110A sCX2 (H3 L82C, H4 V81C) histone octamer oxidized using copper phenanthroline (CuPhe) or oxidized glutathione (GSSG). (B) The same samples used in (A) treated with 100mM DTT in order to reduce the disulfide bond. Uncropped images for panels A-B are available in Supplementary Figure 8.

FIGURE 4.2

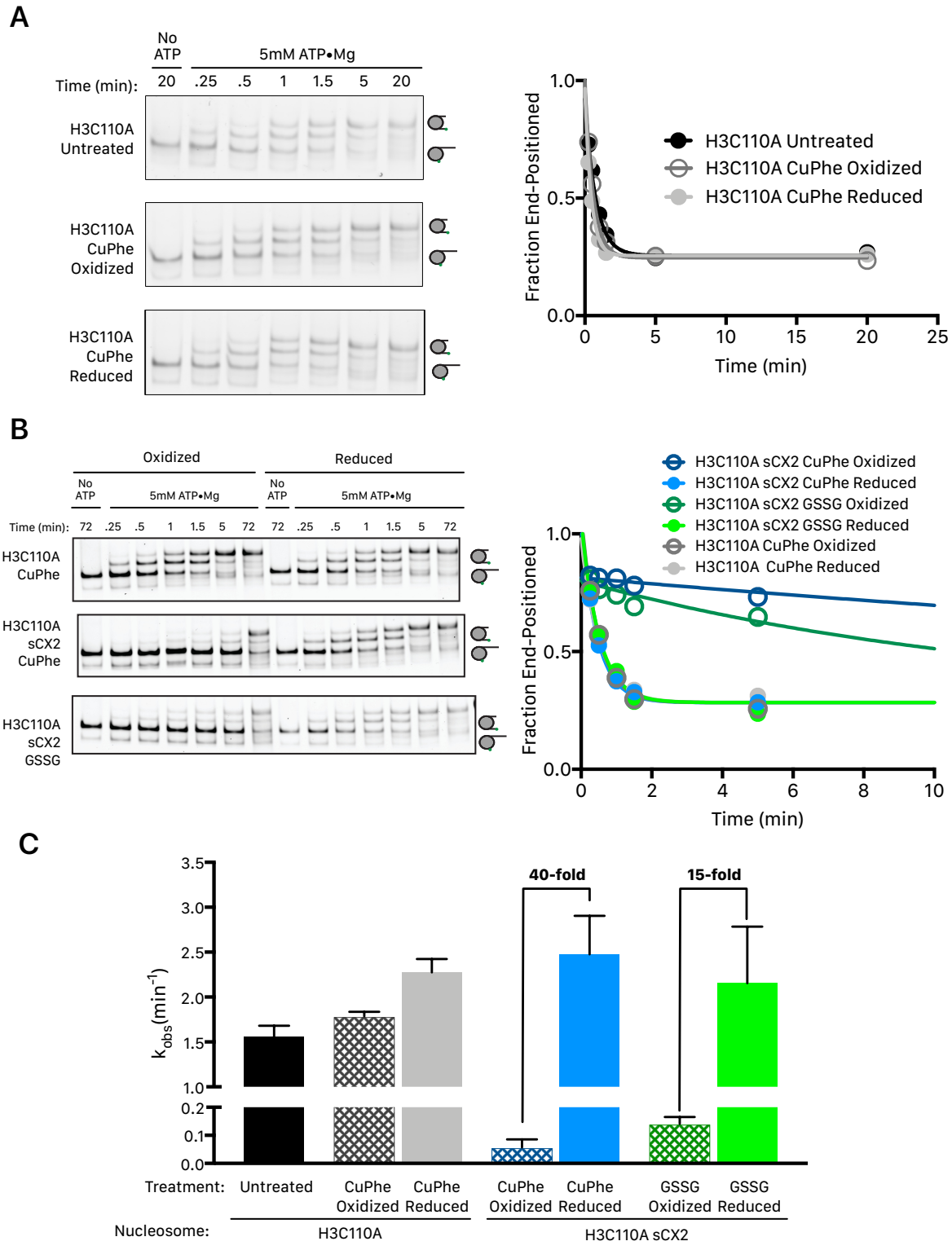
A
No ATP
5mM ATP•Mg
Time (min):
20 .25 .5 1 1.5 5 20
H3C110A Untreated
H3C110A CuPhe Oxidized
H3C110A CuPhe Reduced
Fraction End-Positioned
Time (min)
B
Oxidized
Reduced
H3C110A CuPhe
H3C110A sCX2 CuPhe
H3C110A sCX2 GSSG
H3C110A sCX2 CuPhe Oxidized
H3C110A sCX2 CuPhe Reduced
H3C110A sCX2 GSSG Oxidized
H3C110A sCX2 GSSG Reduced
C
40-fold
15-fold
Treatment:
Untreated
CuPhe Oxidized
CuPhe Reduced
GSSG Oxidized
GSSG Reduced
Nucleosome:
H3C110A
H3C110A sCX2

Figure 4.2. Site-specific cysteine crosslinking, and not general oxidative damage, inhibits remodeling regardless of oxidation method
(A) Treatment of H3C110A histone octamer with CuPhe or GSSG does not affect nucleosome sliding by SNF2h. Left. Native gel sliding assay with saturating concentrations of SNF2h (1μM) with or without saturating ATP and 15nM cy3-labeled nucleosomes using the indicated histone octamer. Time points were quenched with excess ADP and plasmid DNA and resolved on a 6% (29:1 bis) acrylamide gel. Higher migrating species are more centrally-positioned nucleosomes. Right. Quantification of the gel data shown at the left plotted as the fraction of end-positioned nucleosomes over time. The experiment was performed 3 times independently with similar results. (B) Left. Native gel remodeling assay as in A. Right. Quantification of the gel data shown at the left plotted as the fraction of end-positioned nucleosomes over time with the plot zoomed in to the first 10 minutes of the reaction to better evaluate fits. This experiment was performed 3 times independently with similar results. (C) Mean observed rate constants (k_{obs}) from 3 independent experiments. Error bars reflect the standard error of the mean (SEM). In all figure panels "Reduced" nucleosomes refer to nucleosomes that were assembled from octamers oxidized using the indicated method and then subjected to reducing conditions before nucleosome assembly.

FIGURE 4.3

A

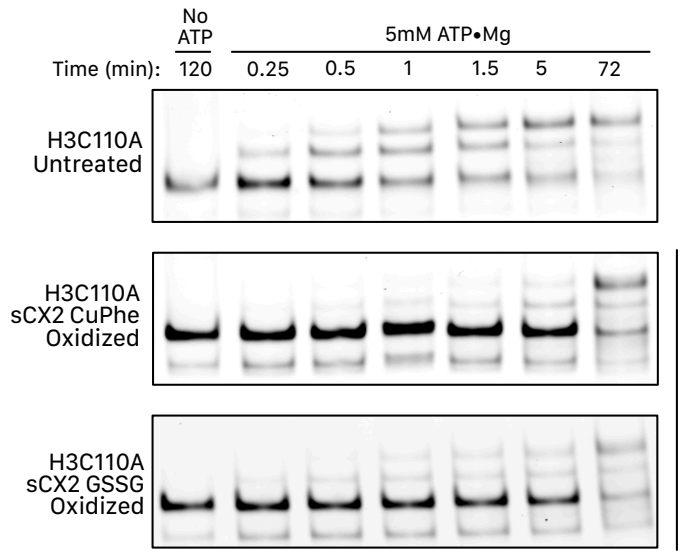

Figure 1B

B

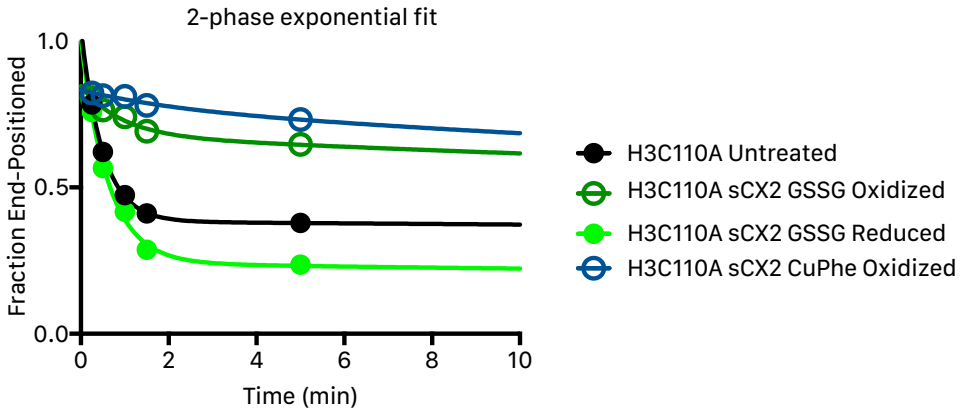

C

Octamer used to assemble nucleosome	k_{fast}	k_{slow}	Percent fast	Percent slow
H3C110A Untreated	2.0 min^{-1}	0.006 min^{-1}	78%	22%
H3C110A sCX2 CuPhe Oxidized	0.5 min^{-1}	0.02 min^{-1}	10%	90%
H3C110A sCX2 GSSG Oxidized	1.1 min^{-1}	0.01 min^{-1}	26%	74%
H3C110A sCX2 GSSG Oxidized and then reduced	1.6 min^{-1}	0.07 min^{-1}	95%	5%

Figure 4.3 Variation in remodeling rate between oxidation methods can be explained by crosslinking efficiency

(A) Native gel remodeling assay from Figure 1B zoomed to better see the early phase of the remodeling reaction. (B) The same quantification shown in Figure 1B but instead fit to a two-phase exponential decay. (C) Best-fit parameters of the two-phase fit of the data in B. The rate constants for the fast and slow phase are similar between GSSG and CuPhe oxidized H3C110A sCX2 nucleosomes but differ in the fraction in the fast and slow phase. Uncropped images for panels A-B are available in Supplementary Figure 6 and values obtained in quantifications are in Table 1.

FIGURE 4.4

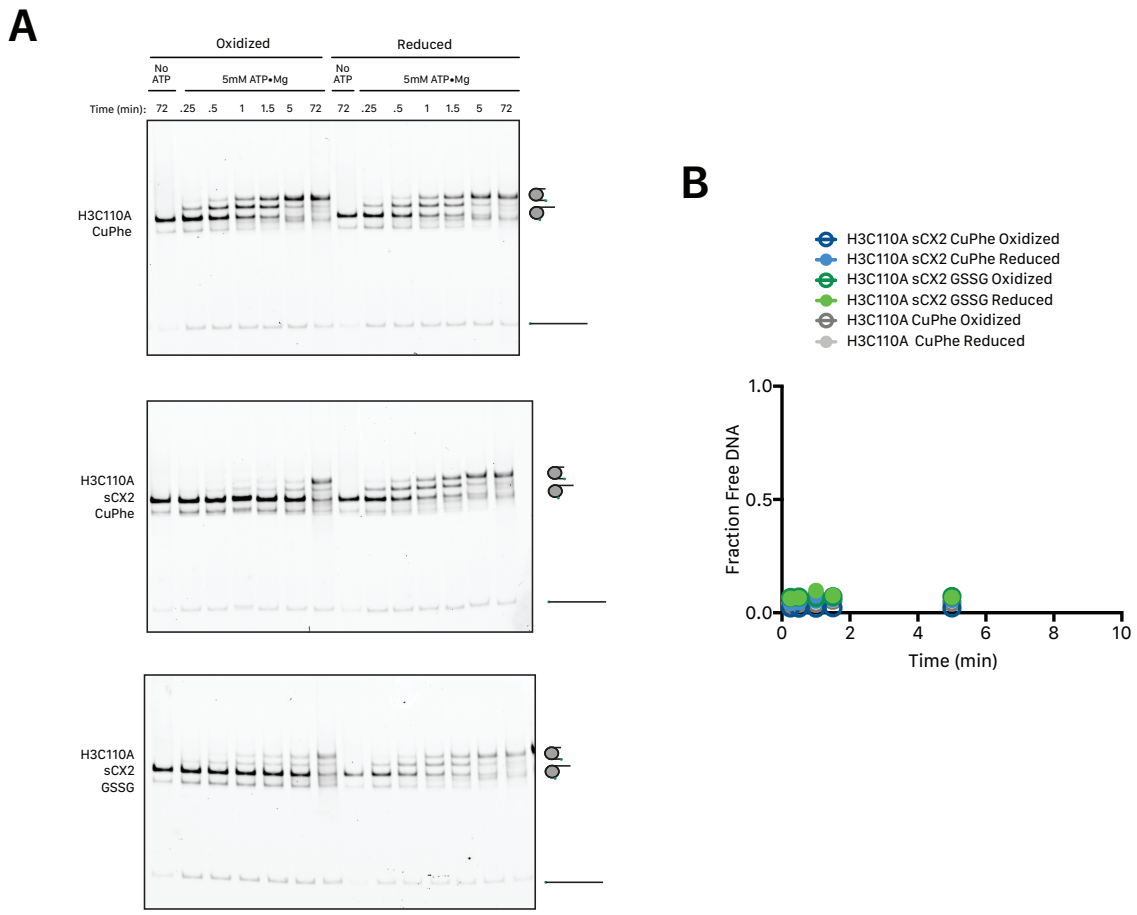

Figure 4.4 Nucleosome disassembly does not contribute to nucleosome remodeling by SNF2h

(A) Native gel remodeling data from Figure 1B of the main text presented again, but with a bigger part of the gel included to show the free DNA band on the native gel. (B) Quantification of the fraction free DNA over time (quantified as the intensity of the free DNA band over all bands). Uncropped images for panel A are available in Supplementary Figure 6 and values obtained in quantifications are in Table 1.

FIGURE 4.5

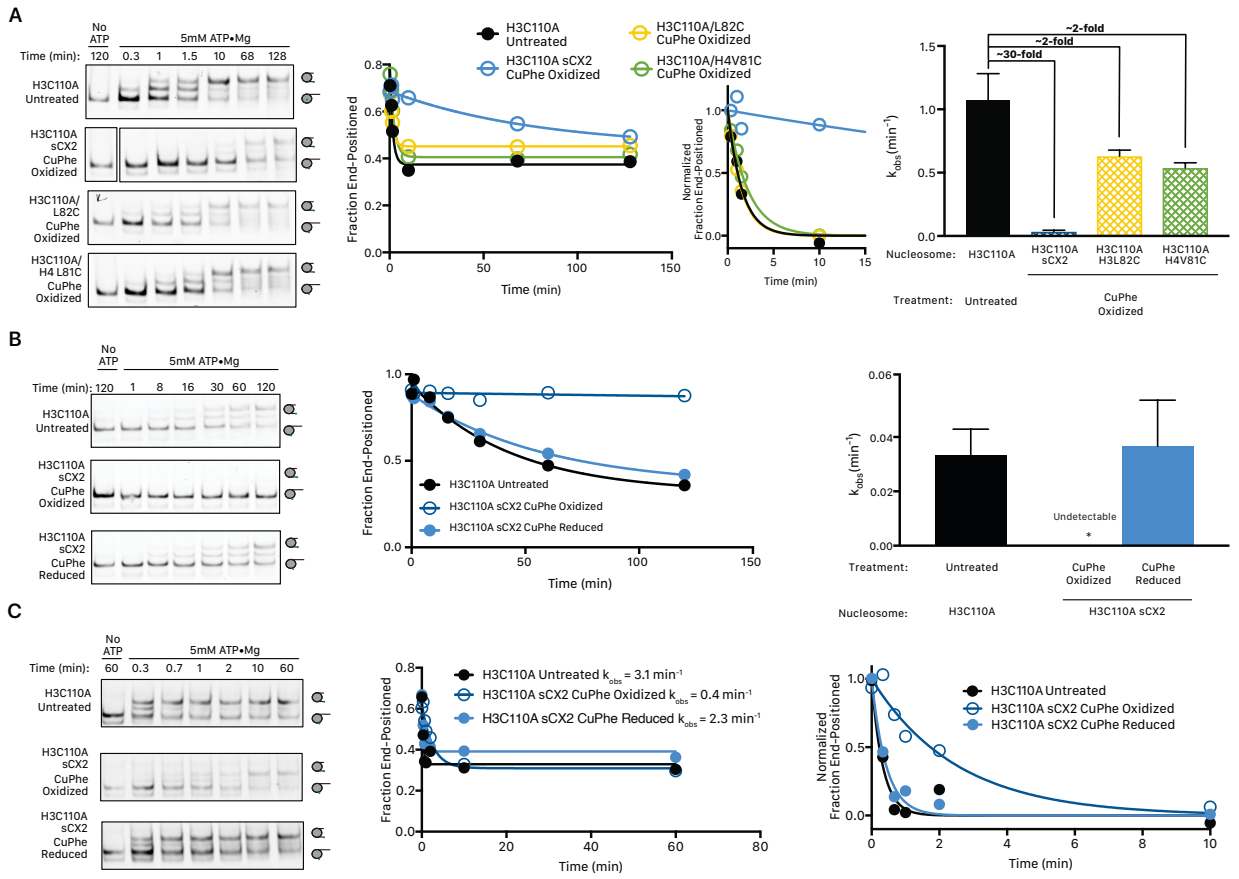

Figure 4.5 Remodeling of oxidized nucleosomes is slowed specifically due to disulfide bond formation and is robust to remodeling conditions.
(A) Left. Native gel remodeling assay with saturating SNF2h (1μM), saturating ATP, and 15nM cy3-nucleosomes as in Figure 1. Middle. Quantification of the experiment at the left including a plot of all time points; and for ease of comparison a plot of the first 15 minutes of the reaction normalized to the best-fit parameters for Y_0 and plateau. This experiment was performed 3 times with similar results. Right. Mean observed rate constants (k_{obs}) from 3 independent experiments. Error bars reflect the standard error of the mean (SEM). (B) Left. Native gel remodeling assay with sub-saturating SNF2h (50nM), saturating ATP, and 15nM cy3-nucleosomes as in Figure 1. Middle. Quantification of the experiment on the left. This experiment was performed 3 times with similar results. Right. Mean and SEM of the observed rate constants (k_{obs}) from 3 independent experiments. The asterisk denotes that the rate constant for the oxidized reaction condition was too slow to reliably quantify with the time points taken. (C) Left. Native gel remodeling assay under the conditions of Yan et al.[2] using 50nM SNF2h, saturating ATP, and 15nM cy3-nucleosomes. Remodeling overall is substantially faster likely because of the different conditions used (higher temperature, lower salt concentration, the absence of .02% (v/v) NP40, and the presence of 0.1mg/mL BSA). Middle. Quantification of the gel on the left along with the indicated observed rate constants. This experiment was performed once. Right. Time-

courses shown in the middle panel normalized to the best fit parameters for Y_0 and Plateau of the exponential decay and zoomed in to the first 10 minutes of the reaction to better evaluate the fits. Values obtained in quantifications are in Table 1.

FIGURE 4.6

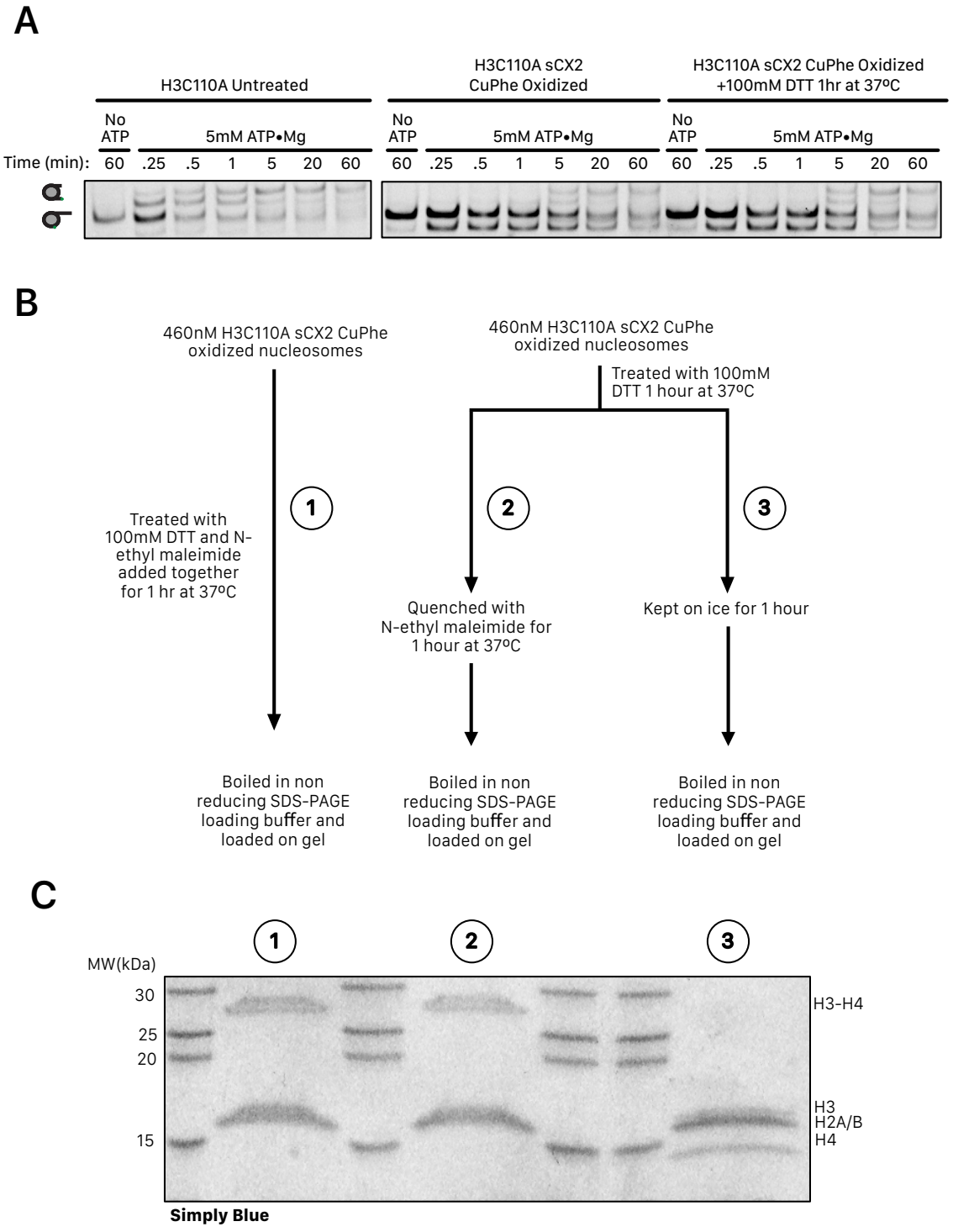
A
H3C110A Untreated
H3C110A sCX2 CuPhe Oxidized
H3C110A sCX2 CuPhe Oxidized +100mM DTT 1hr at 37ºC
No ATP
5mM ATP•Mg
Time (min): 60 .25 .5 1 5 20 60
B
460nM H3C110A sCX2 CuPhe oxidized nucleosomes
460nM H3C110A sCX2 CuPhe oxidized nucleosomes
Treated with 100mM DTT 1 hour at 37ºC
Treated with 100mM DTT and N-ethyl maleimide added together for 1 hr at 37ºC
1
2
3
Quenched with N-ethyl maleimide for 1 hour at 37ºC
Kept on ice for 1 hour
Boiled in non reducing SDS-PAGE loading buffer and loaded on gel
Boiled in non reducing SDS-PAGE loading buffer and loaded on gel
Boiled in non reducing SDS-PAGE loading buffer and loaded on gel
C
MW(kDa)
30
25
20
15
H3-H4
H3
H2A/B
H4
Simply Blue

Figure 4.6 Disulfide reduction is impaired in the context of the nucleosome
(A) Native gel remodeling assay with saturating SNF2h (1μM), saturating ATP, and 15nM cy3-nucleosomes as in Figure 1. Nucleosomes containing the oxidized sCX2 bonds were generated by oxidizing the H3C110A sCX2 octamer using CuPhe, and then assembling nucleosomes. (B) Scheme for the samples run in C. Nucleosomes treated with DTT were either directly added to non-reducing SDS-PAGE loading buffer or quenched with 500mM N-Ethyl Maleimide freshly dissolved in DMSO (final [DMSO]≈10%(v/v)). Additionally, a condition where N-Ethyl Maleimide and DTT were added simultaneously is included to evaluate the efficacy of the quench. (C) SDS-PAGE of samples treated as in B. Samples with reducing agent quenched prior to running on the gel are near-completely oxidized.

SUPPLEMENTAL FIGURE 1

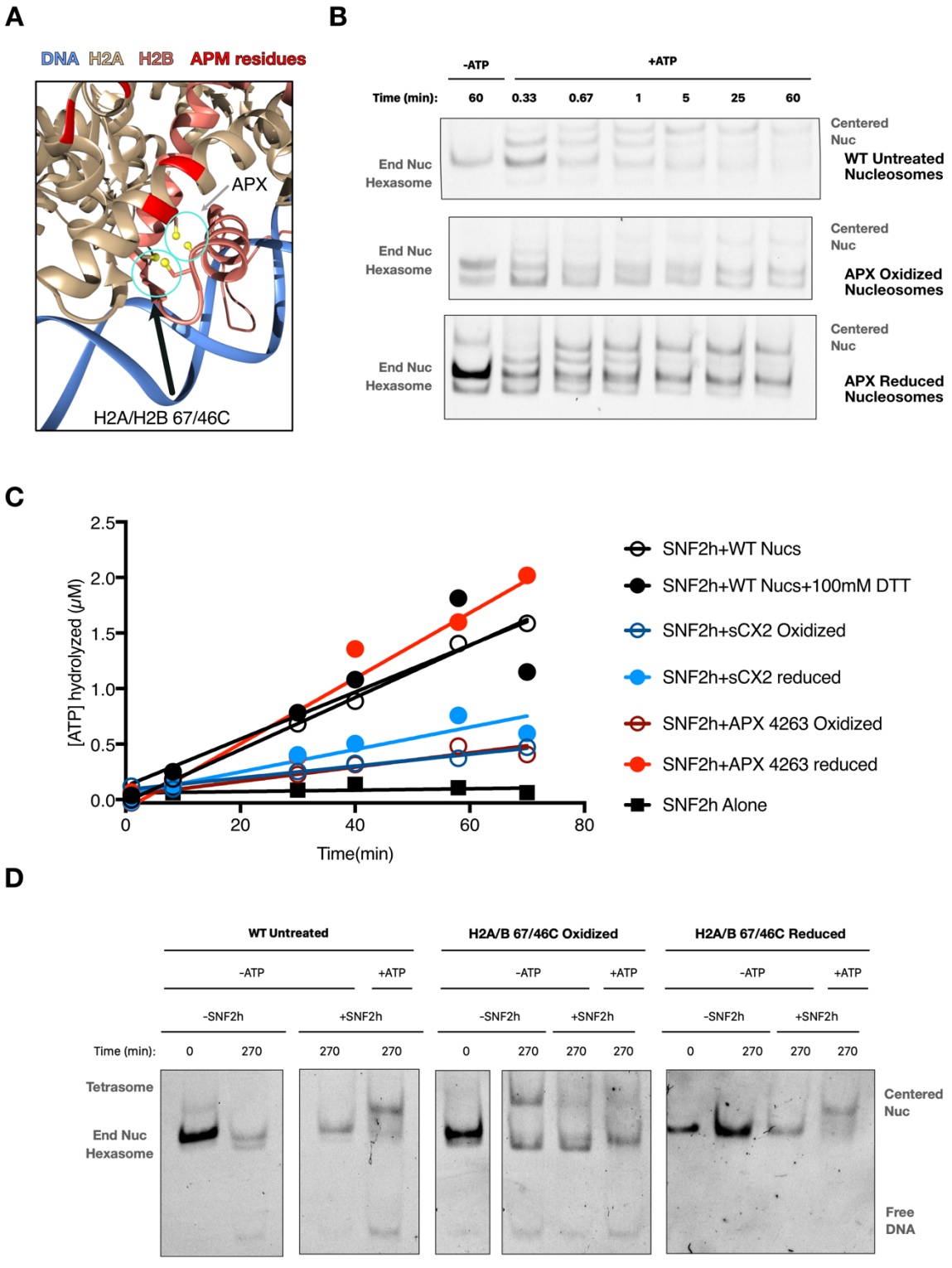

Supplemental Figure 1. Dynamics in the H2A-H2B dimer are also important for SNF2h remodeling

A. Zoom into the acidic patch of the nucleosome in the crystal structure of the nucleosome (PDB ID: 1KX5). Residues mutated in APM nucleosomes are shown in red. Cysteine mutations tested here are shown as ball and stick with the mutant pair labeled. B. Native gel remodeling assay performed with 1μM SNF2h with the indicated nucleosomes. C. Nucleosome stimulated ATPase assay performed as in Chapter 2 with saturating ATP•Mg (100μM), 25nM SNF2h, and with or without the addition of 100nM 0/60 nucleosomes. Reactions were fit to a straight line using linear regression. Native gel analysis of nucleosomes incubated for the indicated time and then quenched with excess ADP and stop plasmid before running.

Tables

Table 1. Observed rate constants for nucleosome sliding with cysteine mutant nucleosomes

Octamer used to assemble nucleosome	k_{obs}, number of replicates	
[SNF2h]	**1µM**	**50nM**
H3C110A Untreated	1.3±0.2 min^{-1}, n=6	0.03±0.01 min^{-1}, n=3
H3C110A CuPhe Oxidized	1.8±0.1 min^{-1}, n=3	Not Determined
H3C110A CuPhe Oxidized and then reduced	2.3±0.1 min^{-1}, n=3	Not Determined
H3C110A/L82C CuPhe Oxidized	0.63±0.05 min^{-1}, n=3	Not Determined
H3C110A/H4L81C CuPhe Oxidized	0.54±0.04 min^{-1}, n=3	Not Determined
H3C110A sCX2 CuPhe Oxidized	0.05±0.01 min^{-1}, n=6	Undetectable, n=3
H3C110A sCX2 CuPhe Oxidized and then reduced	2.5±0.4 min^{-1}, n=3	0.03±0.02 min^{-1}, n=3
H3C110A sCX2 GSSG Oxidized	0.14±.02 min^{-1}, n=3	Not Determined
H3C110A sCX2 GSSG Oxidized and then reduced	2.2±0.6 min^{-1}, n=3	Not Determined

References

[1] K.K. Sinha, J.D. Gross, G.J. Narlikar, Distortion of histone octamer core promotes nucleosome mobilization by a chromatin remodeler., Science (New York, N.Y.). 355 (2017) eaaa3761. https://doi.org/10.1126/science.aaa3761.

[2] A. Hada, S.K. Hota, J. Luo, Y. Lin, S. Kale, A.K. Shaytan, S.K. Bhardwaj, J. Persinger, J. Ranish, A.R. Panchenko, B. Bartholomew, Histone Octamer Structure Is Altered Early in ISW2 ATP-Dependent Nucleosome Remodeling, Cell Reports. 28 (2019) 282-294.e6. https://doi.org/10.1016/j.celrep.2019.05.106.

[3] S. Bilokapic, M. Strauss, M. Halic, Structural rearrangements of the histone octamer translocate DNA., Nature Communications. 9 (2018) 1330. https://doi.org/10.1038/s41467-018-03677-z.

[4] L. Yan, H. Wu, X. Li, N. Gao, Z. Chen, Structures of the ISWI–nucleosome complex reveal a conserved mechanism of chromatin remodeling, Nature Structural & Molecular Biology. 26 (2019) 258–266. https://doi.org/10.1038/s41594-019-0199-9.

[5] J. Ausio, D. Seger, H. Eisenberg, Nucleosome core particle stability and conformational change, J Mol Biol. 176 (1984) 77–104. https://doi.org/10.1016/0022-2836(84)90383-8.

[6] S. Sanulli, M.J. Trnka, V. Dharmarajan, R.W. Tibble, B.D. Pascal, A.L. Burlingame, P.R. Griffin, J.D. Gross, G.J. Narlikar, HP1 reshapes nucleosome core to promote phase separation of heterochromatin, Nature. 575 (2019) 390–394. https://doi.org/10.1038/s41586-019-1669-2.

[7] J.P. Armache, N. Gamarra, S.L. Johnson, J.D. Leonard, S. Wu, G.J. Narlikar, Y. Cheng, Cryo-EM structures of remodeler-nucleosome intermediates suggest allosteric control through the nucleosome, ELife. 8 (2019) e46057. https://doi.org/10.7554/eLife.46057.

[8] S. Bilokapic, M. Strauss, M. Halic, Histone octamer rearranges to adapt to DNA unwrapping., Nature Structural & Molecular Biology. 25 (2018) 101–108. https://doi.org/10.1038/s41594-017-0005-5.

[9] K. Luger, T.J. Rechsteiner, T.J. Richmond, Expression and Purification of Recombinant Histones and Nucleosome Reconstitution, in: Humana Press, 1999: pp. 1–16. https://doi.org/10.1385/1-59259-681-9:1.

[10] P.T. Lowary, J. Widom, New DNA sequence rules for high affinity binding to histone octamer and sequence-directed nucleosome positioning., Journal of Molecular Biology. 276 (1998) 19–42. https://doi.org/10.1006/jmbi.1997.1494.

[11] C.Y. Zhou, G.J. Narlikar, Analysis of Nucleosome Sliding by ATP-Dependent Chromatin Remodeling Enzymes., Methods in Enzymology. 573 (2016) 119–135. https://doi.org/10.1016/bs.mie.2016.01.015.

Publishing Agreement

It is the policy of the University to encourage open access and broad distribution of all theses, dissertations, and manuscripts. The Graduate Division will facilitate the distribution of UCSF theses, dissertations, and manuscripts to the UCSF Library for open access and distribution. UCSF will make such theses, dissertations, and manuscripts accessible to the public and will take reasonable steps to preserve these works in perpetuity.

I hereby grant the non-exclusive, perpetual right to The Regents of the University of California to reproduce, publicly display, distribute, preserve, and publish copies of my thesis, dissertation, or manuscript in any form or media, now existing or later derived, including access online for teaching, research, and public service purposes.

DocuSigned by:

3F3A98E2A861412...

Author Signature

12/9/2020

Date